Synthesis of Biodegradable Microparticles for Controlled Active Ingredient Release

By

Annette Louise Christie

Submitted for the degree of Doctor of Philosophy

Department of Chemistry

University of Warwick

August 2017

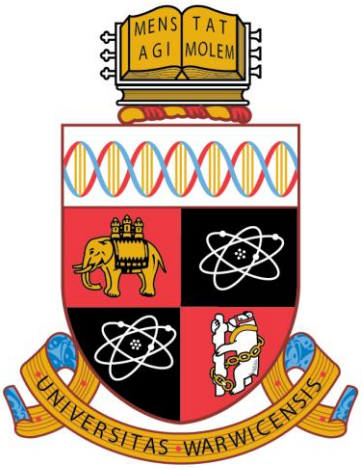

Table of Contents

List of Figures, Schemes and Tables

Figures

Schemes

Tables

Acknowledgements

Firstly, I would like to thank my supervisor, Professor Andrew Dove, for all his help and guidance throughout my PhD. I am especially grateful and will forever remember your continued support and knowledgeable advice on science, careers and general life. I would also like to express my gratitude to Syngenta for funding my PhD, in particular, James Burns, Martine DeHeer, Rosa Dominguez Espinosa and Chris Lindsay for all of your direction and advice throughout.

Secondly, I would like to thank all the Dove and O'Reilly group members past and present for their continuous help, proof-reading and for making the lab a fun place to work, especially Vinh, Bo, Anaïs, Anne, Marianne, James, Ruairí, Josh and spicy Wei. Thanks are also due to the coffee club: Zoe, Anthony, Laura, Chiara and my 'lab twin' Ed, I will definitely miss all of the daily entertaining chats over coffee (or prosecco…). Special thanks go to my fellow Fakashian members; my lab 'husband' and chief proof-reader Guillaume and my Uni Wife Alice, for always providing unconditional support and encouragement!

A massive thank you to my housemate Karen, 99 Hallgarth and the Durham dream girls, Meg, Ange and Kat for helping me dance away any problem. Thanks to Jonny, Rory, Helen and my original lab partner Charlotte for their unconditional long-term support. Special thanks to Sarah for her constant positivity, I am looking forward to hearing about your future adventures and life-saving abilities!

My biggest thanks goes to all my family members. In particular I would like to thank my Aunty Fiona for helping me move the whole Trafford Centre from one flat to another. To my sister Helen, for showing me that the Christie girls can do anything. Finally, an enormous thanks to my mum and dad for persevering through reading my entire Thesis and for being my inspirations in life and in work, without you I would not have been able to complete this degree, Thank You!

Declaration of Authorship

This thesis is submitted to the University of Warwick in support for the degree of Doctor of Philosophy. It has been composed by myself and has not been submitted in any previous applications for any degree. The work presented (including data generated and data analysis) was carried out by the author except in the cases outlined below:

- The confocal microscopy images in Chapter 2 were obtained by Dr James Burns and Mr Tim Powell (Syngenta, Jealott's Hill).
- TEM images were obtained in Chapter 3 by Dr Graeme Cambridge and in Chapter 7 by Dr Maria Chiara Arno (University of Warwick).
- EtMA, and NO_2BnMA in Chapter 5 were synthesised and polymerised by Mr Edward Cant (University of Warwick).
- DSC characterisation in Chapter 5 was performed by Mr Panagiotis Bexis, Miss Zoe Roberts and Dr Anaïs Pitto-Barry (University of Warwick).
- Fluorescence optical microscopy images in Chapter 5 were obtained by Dr Maria Chiara Arno (University of Warwick).
- MDO monomer in Chapter 6 was synthesised by Dr Guillaume Hedir (University of Warwick).
- Quantitative ^{13}C NMR spectra in Chapter 7 were obtained by Dr Ivan Prokes and Mr Robert Perry (University of Warwick).

Abstract

This thesis investigates the degradation and release of a fluorescent dye from biodegradable microparticles. Particular attention is given to determining the effect of polymeric properties on the subsequent microparticle degradation and release rate. Chapter 1 reviews the current polymerisation techniques for the synthesis of polyesters and introduces the synthetic procedures and degradability currently attainable for biodegradable microparticles. The concept of 'smart' release technology is introduced and the potential for using biodegradable 'smart' particles for enhanced agricultural formulations is explored.

In Chapter 2, the ring-opening polymerisation (ROP) of a variety of polyesters is demonstrated, including an investigative study on the ROP of poly(3-hydroxybutyrate) (PHB) using magnesium 2,6-di-tert-butyl-4-methylphenoxide ($Mg(BHT)_2(THF)_2$). The polyesters are used to prepare microparticles *via* a single oil-in-water solvent evaporation technique, a range of formulation parameters are studied to enable optimisation of the subsequent particle size and stability.

Chapter 3 investigates the encapsulation of a model fluorescent dye into poly(*L*-lactide) (PLLA) microparticles and the subsequent PLLA particle degradation and dye release under simulated environmental conditions is reported.

Chapter 4 describes the degradation and release of 3-bromo-4-(butylamino)-2,5-dihydro-1H-pyrrole-2,5-dione (ABM) from a range of polyester microparticles, investigating the effect of polymer properties (*e.g.*, molecular weight, crystallinity, *etc*.) on the particle degradation and release rate.

In Chapter 5, the incorporation of a stimulus responsive polymer using optimised particle synthesis and degradation conditions (detailed in Chapter 2 and 3) is investigated. The successful tuneable microparticle degradation and release is described by incorporation of a light-responsive poly(nitrobenzyl malic acid) (PNO_2BnMA) into homopolymer blends of PLLA microparticles.

Chapter 6 explores the synthesis of degradable poly(vinyl acetate) (PVAc) microparticles by the incorporation of 2-methylene-1,3-dioxepane (MDO) degradable ester linkages into the polymer backbone *via* free radical ring-opening polymerisation (rROP) and post-polymerisation microparticle synthesis (using the optimised solvent evaporation technique detailed in Chapter 2). The successful encapsulation of ABM into P(MDO-*co*-VAc) microparticles is reported and compared to encapsulation into PVAc microparticles.

In Chapter 7, the synthesis of poly(ω-pentadecalactone) (PPDL) microparticles using the optimised single oil-in-water emulsion technique (Chapter 2) is reported. Investigation into the synthesis and degradation of films prepared from random copolymers of PPDL and poly(ε-caprolactone) (PCL) is described. An attempt at polymerisation-induced self-assembly (PISA) using block copolymers of PPDL and poly(ε-decalactone) (PeDL) is demonstrated.

In chapter 8, a general summary of Chapters 2-7 is presented and key findings and conclusions highlighted. Chapter 9 provides the experimental methods used throughout this thesis and Chapter 10 provides supporting degradation studies for Chapter 3 and 4.

Abbreviations

ABM	3-Bromo-4-(butylamino)-2,5-dihydro-1H-pyrrole-2,5-dione
AI	Active ingredient
AIBN	2,2'-Azobis(isobutyronitrile)
ATRP	Atom transfer radical polymerisation
BA	Benzyl alcohol
CDSA	Crystallisation-driven self-assembly
CKA	Cyclic ketene acetal
CRP	Controlled radical polymerisation
d	Doublet
***D,L*LA**	*D,L*-Lactide
DBU	1,8-Diazabicyclo[5.4.0]undec-7-ene
DI Water	Deionised water
DIC	*N,N*'-diisopropylcarbodiimide
DLS	Dynamic light scattering
$Đ_M$	Dispersity
DP	Degree of polymerisation
DPP	Diphenylphosphate
DPTS	4-(Dimethylamino) pyridinium 4-toluenesulfonate
DSC	Differential scanning calorimetry
E	Encapsulation efficiency
EtMA	Ethyl malic acid
ε-CL	ε-Caprolactone
FRP	Free radical polymerisation
GC	Gas chromatography

I	Initiator
J	Coupling constant
$\boldsymbol{k_d}$	Rate of depolymerisation
$\boldsymbol{k_p}$	Rate of polymerisation
LA	Lactide
LDPE	Low-density polyethylene
***L*LA**	*L*-Lactide
Ln	Ligand
m	Multiplet
M	Monomer
MA	Malic acid
MDO	Poly(2-methylene-1,3-dioxepane)
MeMA	Methyl malic acid
$\boldsymbol{M_n}$	Number average molecular weight
$\boldsymbol{M_w}$	Weight average molecular weight
NMP	Nitroxide-mediated polymerisation
NMR	Nuclear magnetic resonance
NO_2BnMA	Nitrobenzyl malic acid
P(MDO-*co*-VAc)	Poly(2-methylene-1,3-dioxepane-*co*-vinyl acetate)
P(PDL-*co*-CL)	Poly(ω-pentadecalactone-*co*-ε-caprolactone)
P(PDL-*co*-DL)	Poly(ω-pentadecalactone-*co*-ε-decalactone)
PBS	Phosphate buffered saline solution
PCL	Poly(ε-caprolactone)
PDL	Poly(ε-decalactone)
PDLLA	Poly(*D*,*L*-lactide)

PDMS	Poly(dimethylsiloxane)
PeDL	Poly(ε-Decalactone)
PEtMA	Poly(ethyl malic acid)
PHB	Poly(3-hydroxybutyrate)
PICDSA	Polymerisation-induced crystallization-driven self-assembly
PISA	Polymerisation-induced self-assembly
PLGA	Poly(lactic-*co*-glycolic acid)
PLLA	Poly(*L*-lactide)
PMA	Poly(malic acid)
PMDO	Poly(2-methylene-1,3-dioxepane)
PMeMA	Poly(methyl malic acid)
PNO_2BnMA	Poly(nitrobenzyl malic acid)
PPDL	Poly(ω-pentadecalactone)
PVA	Poly(vinyl alcohol)
PVAc	Poly(vinyl acetate)
R.T.	Room temperature
RAFT	Reversible addition-fragmentation chain-transfer
RI	Refractive index
ROP	Ring-opening polymerisation
rROP	Radical ring-opening polymerisation
s	Singlet
SEC	Size exclusion chromatography
SEM	Scanning electron microscopy
t	Triplet
T_c	Crystallisation temperature

TEM	Transmission electron microscopy
TFAA	Trifluoroacetic anhydride
T_g	Glass transition temperature
THF	Tetrahydrofuran
T_M	Melting temperature
UV	Ultraviolet
UV-vis	Ultraviolet/visible
VAc	Vinyl acetate
β-BL	β-Butyrolactone
δ	Chemical shift
δ-VL	δ-Valerolactone
λ	Wavelength
ω-DL	ω-Decalactone

1. Introduction

1.1 Polymers in Agriculture

1.1.1 *Current Challenges Facing Agriculture*

Agriculture provides the backbone to successful international health and economic development. The term agrochemical applies to a chemical that aims to protect, manage or enhance an agricultural environment and thus encompasses a wide range of materials (such as pesticides, fungicides, herbicides, *etc*.). Since the first reported use of an insecticide over 4,500 years ago, the application of agrochemicals has become essential to the provision of efficient crop production observed today.[1] Consequently, there is currently a broad array of available agrochemicals, each with distinct desired abilities, such as, fertiliser, pest management and disease prevention and control.[2] In particular, the 1940's-1960's were termed the 'Green Revolution', resulting from extensive research and development which has led to major advances in the fields of fertilisers, water quality, pesticides, new crop strains and other technologies (Figure 1.1).[3] The human population is expected to grow by 80 million people per annum, with a projected total reaching 9.2 billion by 2050.[4] Therefore, there is a rapidly growing demand for increased plant and crop production.

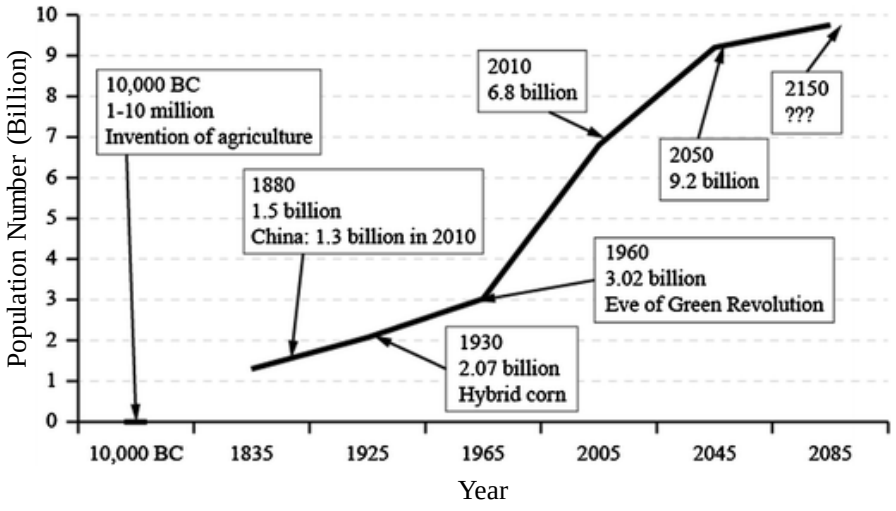

Figure 1.1: Graphical representation of the world population's growth from 10,000 BC to the predicted population in 2150 by Popp *et al*.[4]

Agrochemicals are generally applied through spraying, broad casting and other techniques.[4,5] However, depending on the distribution method and climatic conditions, the agrochemicals can easily be lost as a consequence of leaching, volatilization and degradation. In the worst case, up to 90% of the applied agrochemicals never reach their intended target (Figure 1.2).[5] Consequently, to achieve the desired agrochemical concentration for optimum plant protection, an excess of agrochemical is required to be applied at regular intervals. A large proportion of agrochemicals are known to be toxic, therefore, a high concentration of loss can lead to detrimental ecological side effects on plant life, animals, public health and the surrounding environment.[6] Undoubtedly, the beneficial outcomes observed through the application of agrochemicals will continue to be a pivotal tool in the ever-advancing diverse agricultural technologies that help to maintain and improve living standards worldwide. Nevertheless, with the increasing population, there is a continued need to reduce the amount of agrochemical required to achieve safe and efficient crop growth.[6]

Controlled release technology using polymeric materials has emerged as a promising pathway to successfully reduce the predicted strain on the agricultural industry.[7] This Chapter highlights the advancements observed within conventional polymerisation techniques. The concept of controlled release using biodegradable microparticles is introduced, with specific focus on the current and future progress for microparticle synthesis *via* a solvent-evaporation technique and the subsequent microparticle degradation and controlled release. The innovative advancements observed using stimuli-responsive drug delivery vehicles are discussed and the potential benefits afforded by utilising these devices within agriculture assessed and reviewed.

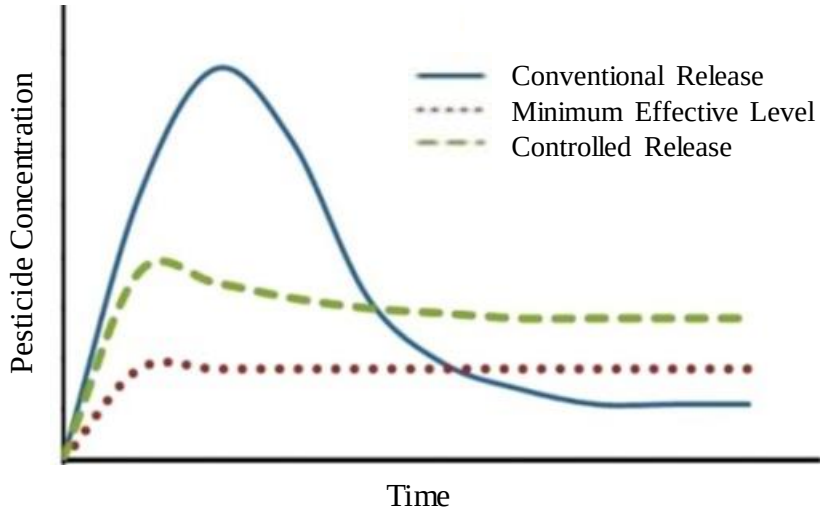

Figure 1.2: Graphical representation of desired pesticide concentration *vs*. actual pesticide concentration as a function of time from conventional and controlled release systems by Roy *et al*.[5]

1.1.2 ***Polymer Synthesis***

To date, a vast library of synthetic polymers are available. Currently, polymers have found use and are indispensable within almost all aspects of modern day life, (*e.g.*, packaging, drug delivery, paint, protective coatings *etc*.). In general, polymer synthesis can be grouped into two classifications; chain-growth and step-growth polymerisation. The type of reaction can be determined according to the dependence on the degree of polymerisation (DP) or molecular weight on the monomer conversion (Figure 1.3).[8] Chain growth polymerisation usually requires an initial reaction between the monomer and an initiator to start the growth of the chain. The polymerisation can then proceed through direct reaction of the monomer with the reactive end-group of the growing polymer chain. Consequently, for a chain-growth polymerisation, it is characteristic to observe an initial rapid consumption of monomer followed by slower growth of all the initiated chains. On the other hand, step-growth polymerisation proceeds *via* only one process, the reaction between two reactive functionalities (a dicarboxylic acid and a diol, a dicarboxylic acid and a diamine, *etc*.). The reaction has

been shown to occur *via* the reaction of two functionalities within one monomer, (*e.g.*, amino acids), or between two separate molecules (*e.g.*, diisocyanates and diols to form polyurethanes). As a consequence of the single step-reaction mechanism, the resultant polymer chain builds up slowly *e.g.*, reaction of two functionalities to create a dimer, dimer reacts with dimer to form a tetramer *etc.* However, typically, the polymerisation pathway is less defined *e.g.*, a tetramer can react with a dimer or trimer, *etc*., hence, the polymerisation is uncontrolled and as such, the technique is limited to the formation of simple architectures.

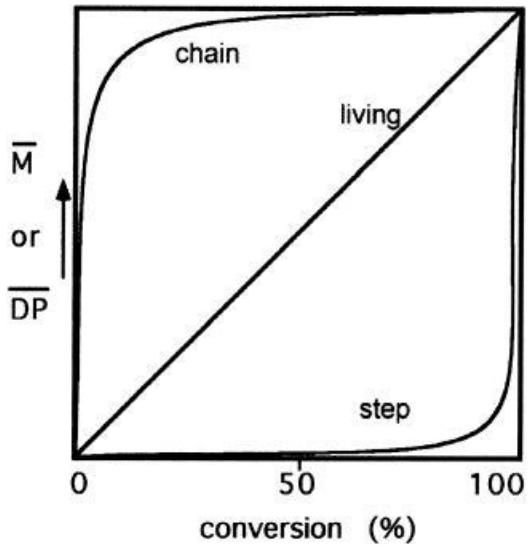

Figure 1.3: Graphical representation of the difference in molecular weight evolution against conversion for chain-growth, step-growth and living polymerisation procedures by Darling *et al*.[8]

Living polymerisation is a modified form of chain-growth, where again rapid initiation is proceeded by chain propagation. In an ideal living polymerisation, termination reactions are supressed.[9] Therefore, all of the polymer chains grow linearly and can retain their end group functionality, thus enabling the production of higher ordered structures, (*e.g.*, di-, tri- and multi-block copolymers).[10]

1.1.2.1 Free Radical Polymerisation

Free radical polymerisation (FRP) contributes an integral role in commercial polymerisation processes.[11] Since the first report of radical polymerisation by Simon *et al*. in 1839, who observed light-induced polymerisation of styrene, interest in radical polymerisation has escalated rapidly.[12] In fact, approximately 50% of all commercially available synthetic polymers are prepared by this fundamental synthetic technique.[13] Furthermore, the mild reaction conditions have enabled a pivotal pathway to the successful polymerisation of an extensive range of monomers, including acrylates, methacrylates, styreneic monomers and vinyl acetates. FRP has been shown to be tolerant to a wide range of functional groups (for example, OH, COOH, NR_2, $CONR_2$ *etc*.), as well as being compatible with protic solvents, such as water.

FRP proceeds *via* a chain-growth polymerisation procedure and can generally be divided into three sections; initiation, propagation and termination.[14] The technique has been shown to be successfully applied to a range of reaction conditions (*e.g*., bulk, suspension, emulsion, *etc*.). These attractive properties make FRP simple to implement and inexpensive in relation to competitive technologies, thus enabling its successful incorporation into industrial procedures. Nevertheless, the high reactivity of the radicals present during polymerisation often results in a high proportion of chain termination and side reactions. Hence, polymers prepared *via* conventional FRP characteristically have broad dispersities and uncontrolled molecular weights.

1.1.2.2 Controlled Polymerisation

The discovery of controlled polymerisation techniques (such as reversible addition-fragmentation chain-transfer (RAFT), ring-opening polymerisation (ROP), nitroxide-mediated polymerisation (NMP) and atom-transfer radical-polymerisation (ATRP)) have the potential to revolutionize polymer science. Controlled polymerisations aim

to achieve quantitative initiation and supress termination reactions occurring during polymerisation, thus yielding well-defined polymers with narrow molecular weight distributions ($Đ_M$). Indeed, controlled polymerisation techniques enable good control over the chain-end fidelity, thus enabling the synthesis of complex architectures, such as multiblock copolymers and hyperbranched materials, which have found use in a broad array of applications, (including pharmaceutical, agrochemical, packaging *etc*.).[15, 16]

1.1.3 *Ring-Opening Polymerisation of Polyesters*

Since the pioneering discovery of the first synthetic polyester in 1930 by Carothers *et al*., a diverse range of polyesters have been synthesised and applied for a broad array of applications.[15] As a consequence of the ever-growing demand for sustainable resources, biodegradable polyesters such as poly(lactic acid) (PLA), poly(δ-valerolactone) (PVL) and poly(ε-caprolactone) (PCL) have received particular attention.[17-19] Polyesters have been synthesised by several methods, including; step growth polymerisation, ring-opening polymerisation (ROP) and free radical polymerisation.[20-22] ROP has received specific interest as a consequence of the high control afforded throughout polymerisation. Therefore, this allows the accurate targeting and tuneable control over the molecular weight, thus enabling the production of more refined macromolecular architectures (*e.g.*, block copolymers, star-shaped polymers, hyperbranched materials *etc*.).[23-25] In general, polymerisation of a cyclic monomer proceeds *via* a chain-growth mechanism and as such, ROP can allow the production of high molecular weight polymers.

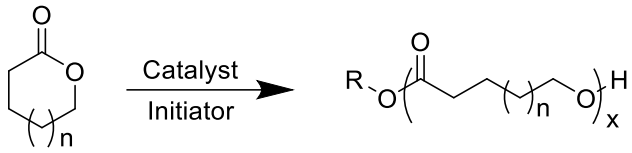

Scheme 1.1: Schematic representation of ROP of a cyclic lactone

For small ring lactones (4-, 6- and 7- membered rings), the relief of bond-angle strain and steric repulsions between atoms of the ring acts as the driving force for ROP.[26] However, the structure of the monomer has a large impact on the polymerisation behaviour, in fact not all rings are susceptible to being ring-opened.[27] The availability for a cyclic monomer to be ring-opened and the optimum polymerisation conditions can be determined using the change in Gibbs free energy upon transformation (Equation 1), *e.g.*, if $\Delta G < 0$, the reaction is favoured, whereas if $\Delta G > 0$, the reaction will not proceed. For instance, the 5-membered γ-butyrolactone experiences very little ring-strain and as such displays a positive enthalpy and Gibbs free energy, hence polymerisation is not favoured.[27] On the other hand, for the majority of lactones the relief of ring strain results in an exothermic release that subsequently generates a highly negative enthalpy, thus permitting polymerisation to occur.[26]

$$\Delta G_0 = \Delta H_0 - T\Delta S_0$$

Equation 1: Gibbs free energy equation

In general, for 6- and 7-membered rings, ring strain is less prominent than for smaller rings, hence, if reliant on ring strain alone the polymerisation would proceed at a relatively slow rate. The polymerisation rate would be dependent upon factors including the monomer type, monomer concentration and reaction temperature. Therefore, to enhance the polymerisation rate, a catalyst is usually applied to the system. A wide range of catalysts have been investigated for ROP of cyclic lactones

(Figure 1.4).[28-32] Typically, the type of catalyst can be broadly categorised into organic, inorganic or enzymatic catalysts.[33] Most inorganic catalysts consist of a metal centre with surrounding ligands, thus enabling tuneable catalytic properties depending on the metal and ligands used. However, removal of the inorganic catalyst after polymerisation is expensive and often leads to toxic catalytic residues within the final polymer. Conversely, organocatalysts are usually either acidic or basic, so can easily be removed through simple washing.[34] Moreover, organocatalysts can display good stability during storage and polymerisation, which has been observed to be problematic when using an enzymatic catalyst.[35, 36]

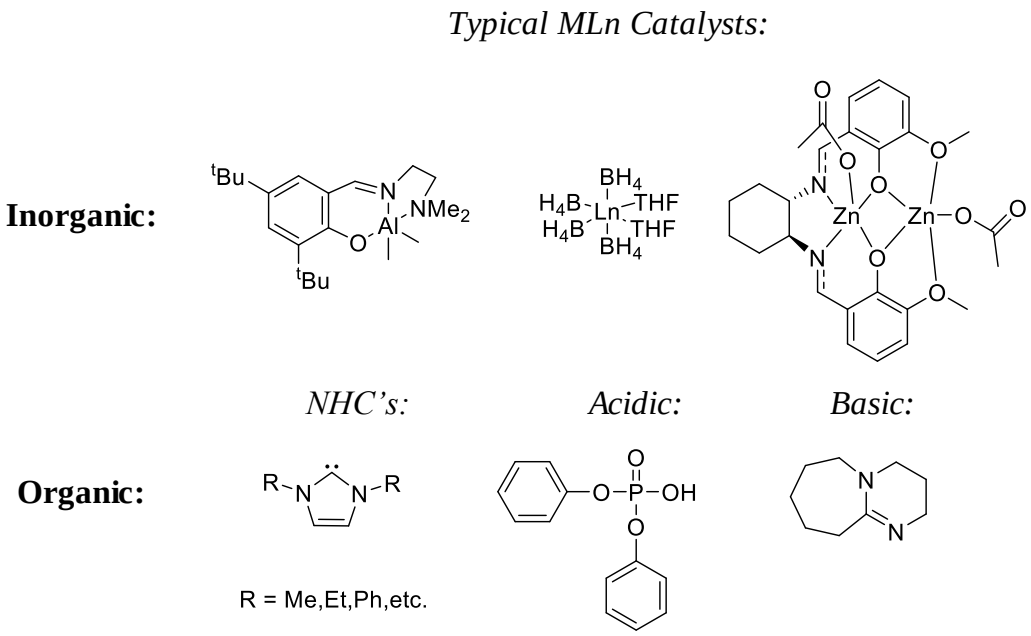

Figure 1.4: Selection of representative catalysts applied for the ROP of cyclic lactones, M = metal centre, Ln = Ligand[34, 37-41]

Macrolactones (14-, 15- and 16-membered lactones) are a particularly interesting class of monomers as a consequence of their potential to provide an efficient synthetic pathway to the production of high molecular weight polymers.[42-44] Unlike conventional lactone rings, the large structure observed with macrolactones increases the flexibility within the monomer and consequently decreases the observed ring strain.[45] Nevertheless, even with the decreased ring strain, ROP can be achieved through the introduction of an entropic gain. This is usually achieved *via* the use of more strenuous reaction conditions (*e.g.* high temperature) and as such macrolactones have been less widely studied.

1.2 Controlled Release Using Polymeric Materials

The inspirational work accomplished in materials science encouraged the innovative production and development of controlled release technology. Indeed, since the first reports of controlled release from silicone rubber and polyethylene in the 1960's, substantial research has been focussed on designing novel drug delivery vehicles, methodologies and equipment.[46-48] To this date, a multitude of delivery devices have successfully achieved controlled release, such as thin films, hydrogels, self-assembled structures, nano- and micro-particles.[49-52] Furthermore, the extremely adaptable properties attainable with polymeric devices have enabled their wide spread application for a multitude of diverse applications, *e.g.*, agricultural, medicinal, cosmetics, food products, perfume, printing, *etc*.[19, 53, 54]

1.2.1 *Controlled Release from Microparticles*

The term microparticle is typically defined as a spherical particle with the size varying between 1-1000 μm.[55] In the 1960's, Chang *et al*. reported the first encapsulation of a macromolecular therapeutic protein into a polymeric microcapsule.[56] The particles were semi-permeable, thus enabling diffusion of the encapsulated enzyme to the specific target substrate both *in-vivo* and *in-vitro*. The attractive advantages offered by encapsulation, (such as lower drug doses, protection of the encapsulated substance, decreased toxicity of the encapsulated material, *etc*.) sparked a surge in research into controlled release formulations utilising microparticles.[57] Following from the pioneering work by Chang *et al*., in 1976 Mason *et al*. introduced the concept of degradability by coating a narcotic antagonist, cyclazocine, with degradable poly(*D*,*L*-lactic acid) (PDLLA).[58] Since these revolutionary studies, a wide range of materials have been employed for microparticle synthesis, *e.g.*, polyamides, polyesters,

poly(amino acids), polyorthoesters, ceramics and glass.[59-61] In general, the types of particles synthesised can be split into two categories (Figure 1.5):[62]

1. Reservoir Microcapsules: The desired encapsulated material is encased within a typically water-insoluble material. Reservoir particles can either consist of a main central reservoir containing the encapsulated AI, or the AI can be dispersed in smaller reservoirs within the polymer membrane.
2. Matrix Microparticles: The chemically active substance is combined within a desired matrix material.

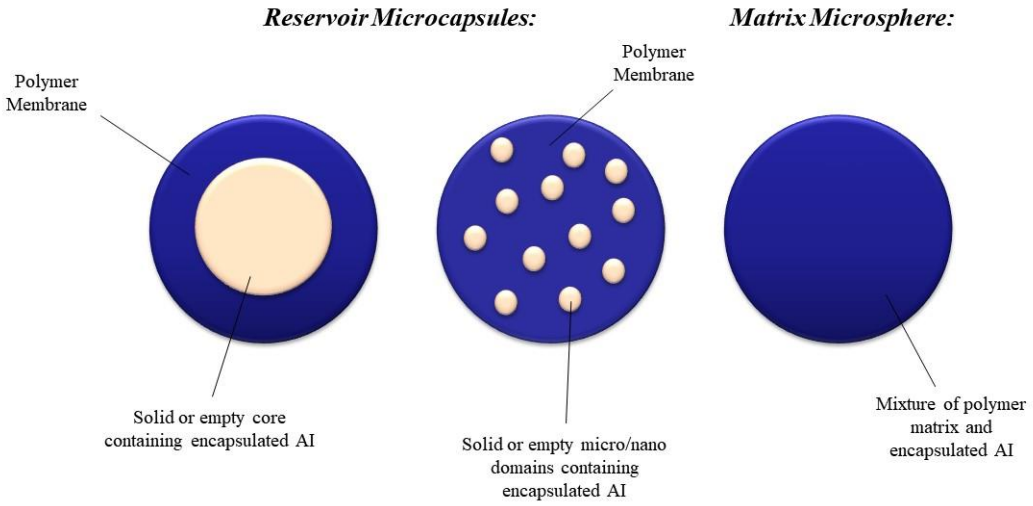

Figure 1.5: Diagrammatic representation of the two main types of microparticles

The type of particle synthesised is highly dependent on the technique applied for particle synthesis, the desired encapsulated active ingredient (AI) and the required release mechanism.[63] Since the initial reports of diffusion controlled release, a variety of release mechanisms have been investigated, which include direct dissolution, erosion, osmotic pump systems and ion-exchange resins.[63-65] Direct dissolution involves either coating or encapsulating the AI within a particle that is partially soluble within the required release medium, thus enabling AI release as the particle

coating/particle matrix dissolves. Application of an osmotic pump system involves the build-up of pressure within the device which acts to push out the AI *via* an orifice, this is usually applied to a reservoir microcapsule. Particle systems using an ion-exchange resin are used commercially, where a drug is bound to the resin and released by exchanging the appropriately charged ions, in contact with the ion exchange groups.

1.2.1.1 Microparticle Synthesis

There are many techniques known, both physical and chemical, that are capable of manufacturing microparticles (*e.g.*, phase separation, precipitation, pan-coating, spray-drying, *etc*.).[59, 66-69] However, the most widely used methods are based on simple emulsion techniques. Solvent evaporation has received particular interest as a consequence of its simple methodology and easily tuneable nature. Furthermore, particle synthesis *via* solvent evaporation is a post-polymerisation technique, therefore, it can be easily adapted and applied using a wide range of materials.[62] Several procedures exist for solvent evaporation, the methodology chosen depends on the selected materials and the desired application.

1.2.1.2 Single Oil-in-Water Solvent Evaporation

Preparation of polymeric particles using a single oil-in-water solvent evaporation technique has been successfully achieved for the encapsulation of an extensive variety of drugs (*e.g.*, anti-cancer drugs, steroids, narcotic agents, *etc*.).[70-72] The technique can be split into two stages; the first step is emulsification, this requires the mixing of an organic phase (usually consisting of the polymer and AI dissolved in a volatile organic solvent) and an aqueous phase (containing a surfactant).[73] The second stage is known as particle hardening and involves evaporation of the volatile organic solvent (Figure 1.6).[74]

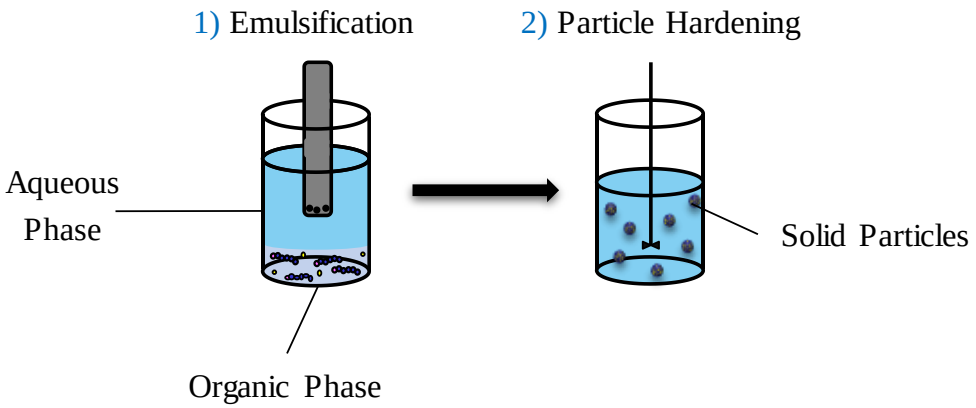

Figure 1.6: Schematic representation of microparticle synthesis *via* single oil-in-water solvent evaporation

To generate the emulsion, the organic and aqueous phases are mixed before physically applying a force to make the organic phase disperse as droplets within the aqueous phase. This is usually achieved through high shear mixing, *e.g.*, using a Silverson mixer or by sonication. Hence, varying the emulsification length and intensity can be used to control the particle size and particle size distribution.[75] After emulsification, the solution is slowly stirred enabling the successful removal of the organic solvent. The high volatility of the solvent enables diffusion of the organic solvent into the continuous water phase and its evaporation at the water-air interface.[73] This in turn results in polymer precipitation and subsequent particle hardening.

1.2.1.2.1 Factors Affecting Particle Composition

Numerous variables are known to affect the particle formation and AI encapsulation and release when using a single oil-in-water emulsion technique, both within emulsification and particle hardening. During emulsification, process parameters, such as emulsification time and intensity are well known to affect the resultant microparticle size.[75] The type of material used for particle synthesis is a key factor in predicting the AI release rate. A diverse range of materials have been applied as the

particle matrix. However, as a consequence of the good biocompatibility and biodegradability observed with biodegradable polymers, polyesters, such as PLA, PCL and poly(lactic-*co*-glycolic acid) (PLGA) continue to be the pivotal materials selected for the design and synthesis of innovative microparticle delivery vehicles.[76-78] Several reports have distinguished a clear influence of the polymer molecular weight on the AI release rate, for instance, Makino *et al*., investigated the release of the steroid, estradiol, from PLGA particles at three different PLGA molecular weights.[79] Characterisation of the drug release by fluorescence spectroscopy revealed that as the molecular weight increased, the release rate decreased as a consequence of the decreased surface area: volume ratio (Figure 1.7).[79] Furthermore, the release of estradiol was considered to be a consequence of diffusion between the device interior and the bulk solution, polymer degradation and change in water content within the particle. Further investigations into emulsification parameters have shown that the polymer concentration, microparticle size and the encapsulated AI can all have a significant effect on the particle release rate.[80-82] Therefore, overall, it can be surmised that the rate of AI release from particles synthesised *via* a single oil-in-water technique is foremostly governed by the properties of the polymer and the encased AI.

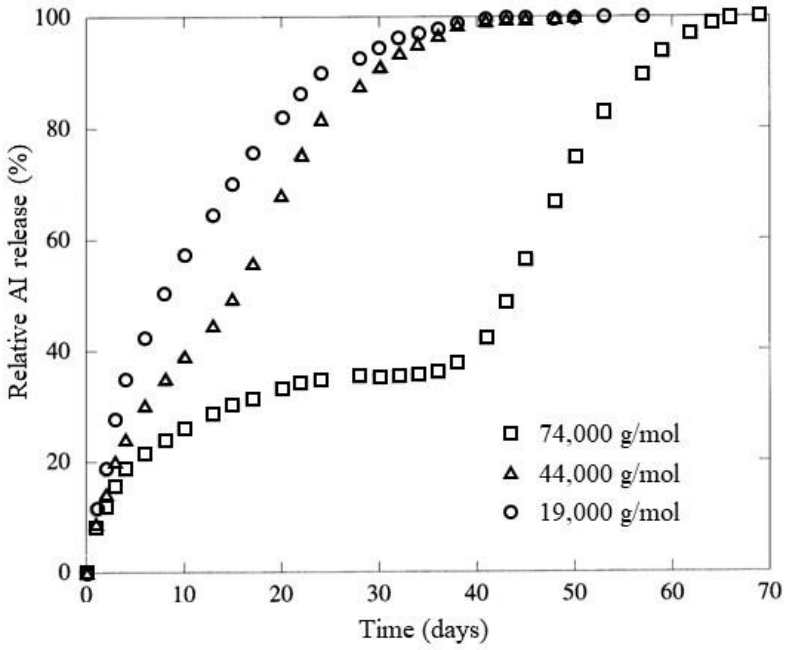

Figure 1.7: Graph displaying the difference in release rate obtained from PLGA microparticles with varying PLGA molecular weight[79]

To achieve the optimum conditions for successful particle hardening, the organic droplets are required to remain dispersed and stable to coalescence, within the continuous aqueous phase. Moreover, the particles must remain stable long enough for evaporation of the organic solvent to occur, thus permitting the formation of stable, solidified microparticles. Therefore, to prevent droplet coalescence, the aqueous phase typically contains a surfactant that can stabilise the dispersed phase droplets.[75] Indeed, the surfactant aligns at the droplet surface, thus acting to lower the free energy at the water-oil droplet interface and subsequently increasing the particle stability.[83] Multiple surfactants have been applied, however, as a consequence of its good biocompatibility, the non-ionic poly(vinyl alcohol) (PVA) has been the most widely investigated.[84, 85] Furthermore, investigations by Sansdrap *et al.*, have reported that an increase in surfactant concentration can decrease the particle size.[86] The decreased particle size can result in an increased rate of AI release as a consequence of the

decreased total volume of the particle. Hence, the applied stabiliser and stabiliser concentration can significantly influence the AI release profile.

The organic solvent has an integral role in both emulsification and particle hardening.[87] In general, the organic solvent should be able to easily solubilise the polymer and drug, be immiscible with the continuous phase and have a relatively low boiling point. Several solvents have been applied for the synthesis of microparticles *via* solvent evaporation emulsion technique, however, as a consequence of its high volatility, low boiling point and high immiscibility in water, most reports have focussed on dichloromethane.[84] The rate of solvent removal is a key factor in controlling the particle morphology and AI encapsulation and release rate. Many factors are known to affect the time required for solvent extraction, for example, the ratio of the continuous phase to the organic phase, temperature, organic solvent volatility, *etc*.[72, 88] Indeed, Jeyanthi *et al*. investigated the effect of increasing the organic solvent extraction rate by transferring the prepared emulsion into a larger continuous phase.[89] However, they discovered the decreased extraction time (less than 30 min) resulted in increased porosity within the particle. Additional reports have noted the increased extraction of the solvent resulted in increased loss of encapsulated AI during particle synthesis and consequently a decreased encapsulation efficiency.[90] In a different approach to enhance the solvent extraction rate, several studies have investigated the effect of the addition of a co-solvent (*e.g.*, methanol) into the aqueous phase.[91] However, even though an initial increase in solvent removal rate was observed, the overall time required for particle solidification did not significantly change.

Solvents used in microencapsulation may be retained in the microsphere as a residual volatile organic impurity.[72] Bitz *et al*. determined the total amount of residual

dichloromethane in a microsphere *via* multiple headspace gas chromatography (GC).[92] A rotary evaporator was used to remove the dichloromethane from the microsphere before storing the particles under vacuum for three days. The researchers found that the level of residual dichloromethane was below the recommended 600 ppm (as outlined by the European Medicines Agency).[93] However, dichloromethane is known to be non-biocompatible, therefore, several reports have focussed on finding and utilising 'greener' solvents.[94-96] As a consequence of its decreased toxicity, in comparison to dichloromethane, and its good volatility, ethyl acetate appeared to be a promising alternative. However, the partial miscibility of ethyl acetate with water (a factor of 4.5 times higher than dichloromethane), resulted in the formation of fibre-like agglomerates as a consequence of the fast precipitation of the polymer which is associated with rapid extraction of the dispersed phase.[95] Several modifications were considered, including pre-saturation of the continuous phase with ethyl acetate and decreasing the polymer concentration. However, the resultant particles appeared to be partly collapsed and displayed low *E* of the respective encapsulated AIs.[96]

Typically, hydrophilic AIs diffuse out of the particle matrix as the organic solvent evaporates, this can result in a very low *E* and a large initial burst release. With the aim to increase the *E* of a hydrophilic AI, several investigations into the formation of a single oil-in-oil emulsion have been reported.[97, 98] To achieve a single oil-in-oil emulsion, the AI and polymer are dissolved in a water miscible oil phase (such as acetonitrile), before being suspended and emulsified with a second immiscible oil continuous phase. The water miscible oil-phase can then be either evaporated or extracted into water, resulting in particle hardening. Investigations into the development of water-in-oil emulsions and double oil-in-water emulsions have also reported increased *E* of encapsulated hydrophilic AI's.[99, 100]

1.2.1.3 Double Oil-in-Water Solvent Evaporation

The double oil-in-water emulsion technique has attracted particular attention as a consequence of its simple methodology and ability to successfully encapsulate hydrophilic AI's with increased *E* compared to the single oil-in-water emulsion. To create a double emulsion, initially a water-in-oil emulsion is prepared (Figure 1.8); the drug is dissolved within an aqueous phase before emulsifying with an excess of organic solvent. The emulsion is then added to an excess of a second aqueous phase, thus resulting in the formation of a water-in-oil-in-water emulsion. The second aqueous phase typically contains an oil soluble surfactant, which is usually a fatty acid ester *e.g.*, polyoxyethylene or sorbitan to stabilise the particles.

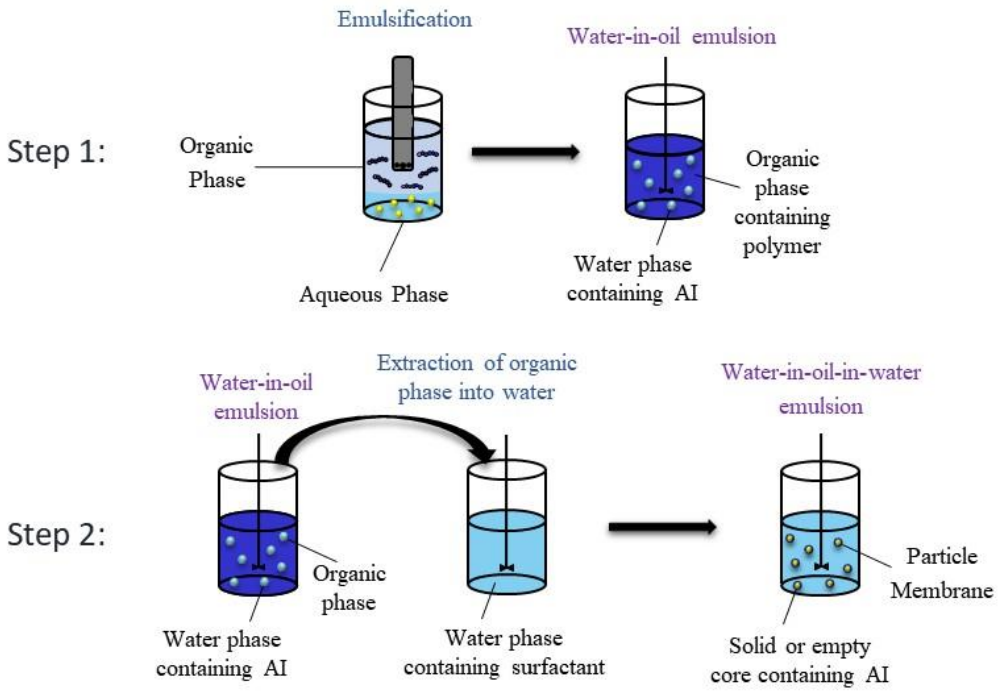

Figure 1.8: Schematic representation of microparticle synthesis *via* double oil-in-water solvent evaporation technique

Similar to a single oil-in-water technique, a wide array of parameters are known to influence the particle formation and subsequent AI release when using a double emulsion technique.[100] Specifically, Siepmann *et al.*, investigated the effect of the size

of biodegradable microparticles on the release rate of the encapsulated drug.[81] To achieve this, Siepmann *et al*. prepared microparticles of PLGA loaded with the drug 5-Fluorouracil (5-FU) *via* the double emulsion technique. Analysis of the degradation behaviour of the polymer and morphological changes of the microparticles upon exposure to the release medium *via* DSC, SEM and SEC revealed that the release rate of the drug increased as the microparticle size increased.[81]

The double emulsion technique has proven to be a great alternative for the encapsulation of drugs that are insoluble in organic solvents. However, similarly to a single oil-in-water emulsion system, the particle size and morphology obtained using a double emulsion is highly dependent on the emulsification parameters.[101, 102] Furthermore, as a consequence of the uncontrolled particle synthesis attained with emulsification of an organic and aqueous phase, both the single and double oil-in-water emulsion procedures display broad particle size distributions, with standard deviations of the distribution equal to 25%-50% of the average size.[67] Even though these characteristic broad particle size distributions are usually reproducible, the lack of control observed with a conventional emulsion technique prevents the controlled synthesis of advanced, hierarchical particle morphologies (*e.g.*, Janus particles), which have been shown to be highly desirable for enhanced drug delivery.[103]

1.2.1.4 Microfluidic Devices

The microparticle size can significantly affect the AI release rate, hence, the large particle size distribution observed with conventional emulsion techniques has been a large limitation in the production of accurate, reproducible controlled release.[104] Consequently, with the ever-advancing research into controlled release technology, increasing attention has been focussed into the synthesis of mono-disperse, custom designed, multi-functional microspheres. In particular, the synthesis of microfluidic

devices has received considerable attention as a consequence of their ability to yield particles with a high *E* and a low particle size distribution, with a standard deviation compared to mean less than 3%.[105] In general, a microfluidic device utilises a modified emulsion technique, where controlled flow technology is applied to introduce a dispersed phase (containing polymer and AI) into a larger continuous phase (usually an aqueous solution containing a surfactant). The dispersed phase is injected through a flow-focussing microchannel (typically tens of micrometers in dimension), hence the diameter of the microchannel can be used to control the particle size (Figure 1.9).[106] The flow of the continuous phase is also controlled as the fluid dynamics at the microchannel controls droplet break up, hence the dispersed phase forms particles as a consequence of the shear force and interfacial tension at the fluid-fluid interface.

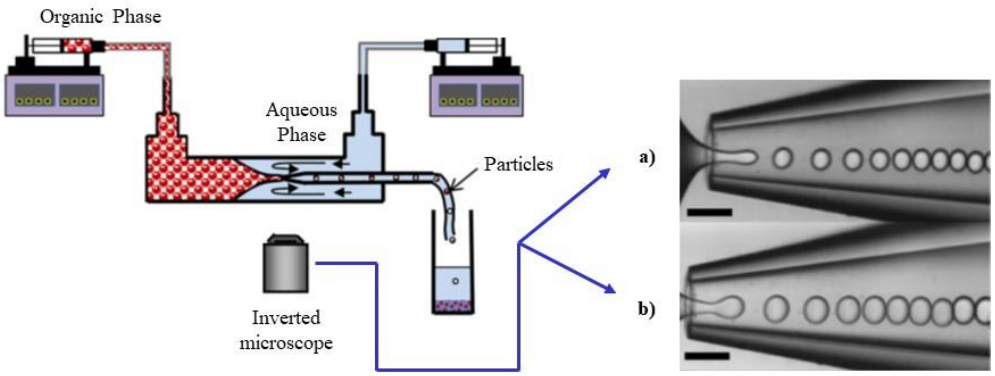

Figure 1.9: Schematic representation of microparticle synthesis using a microfluidic device a) and b) PLA/ nanoclay in dichloromethane organic phase with varied nozzle diameter[105]

As a consequence of its easy synthesis and good bio-compatibility, most research has focussed on using poly(dimethylsiloxane) (PDMS) as the microfluidic droplet generator. However, PDMS does have limitations in this application, as it is well known to swell and deform when in contact with organic solvents.[107] Hence, increasing attention is being directed to the synthesis of novel microfluidic droplet generators. Indeed, Utada *et al*. investigated the use of a glass capillary device, which

offered to minimize wetting, is cheap to fabricate and is more mechanically robust and inert than polymeric devices.[108] Following from this work, Ekanem *et al*., synthesised PLGA microparticles utilising a glass capillary microfluidic device.[105] Utilising their novel counter-current flow focussing glass capillary devices, Ekanem *et al*., revealed they could tune the PLA and PLGA particle size, shape, internal structure and surface roughness morphology (Figure 1.10).

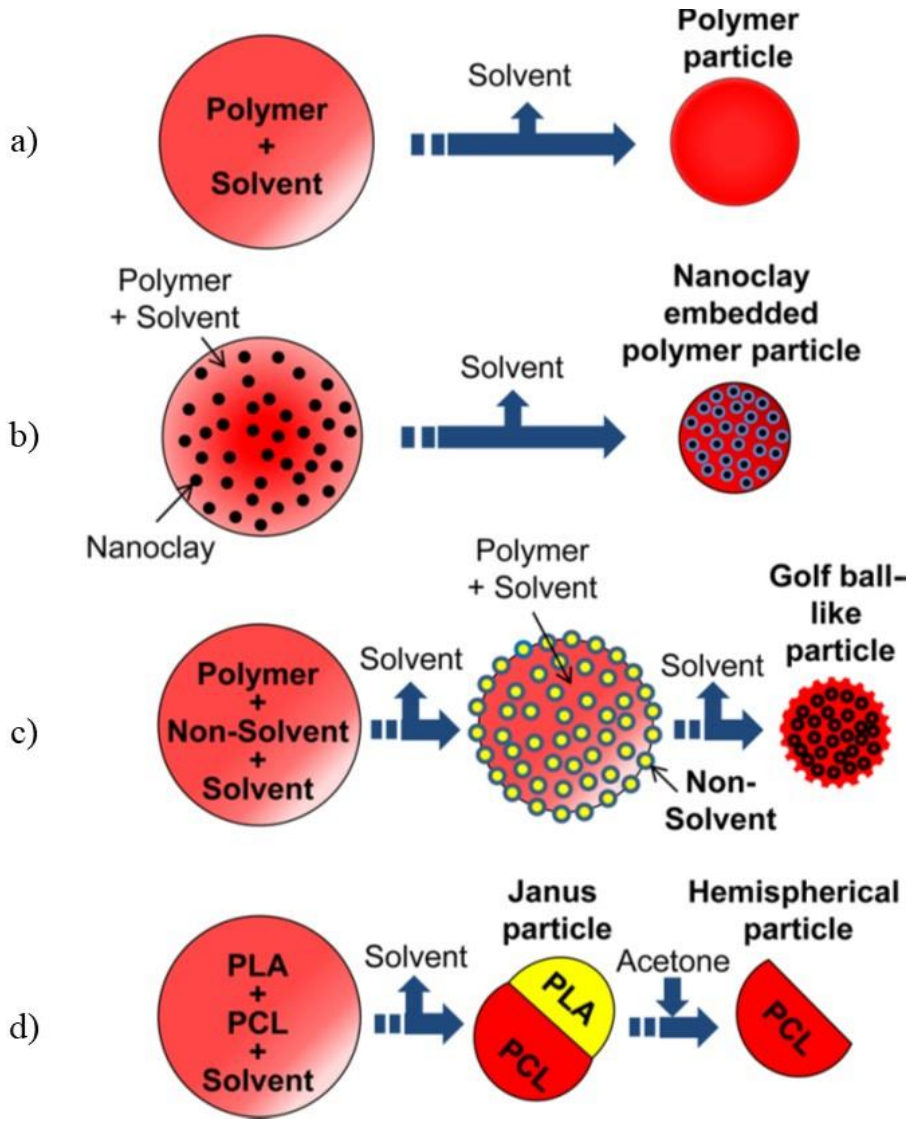

Figure 1.10: Diagrammatic illustration of structures synthesised by Ekanem *et al*. using a glass capillary microfluidic device a) conventional PLA or PCL particle, b) nanoclay embedded polymer particle, c) golf-ball like particle and d) janus and hemispherical particle[105]

Within a microfluidic particle synthesis, the particle size is highly dependent on the size of the microfluidic droplet generating nozzle. As the nozzle size is decreased, the increased shear forces are present at the orifice, therefore, there is high potential for the generation of blockages within the nozzle.[109] Furthermore, the difficulties in operation of the instrumentation along with problematic cleaning makes this process less favourable than conventional processing techniques. However, the ability to obtain control over the particle size along with the promise of the controlled synthesis of advanced morphologies suggests the high future potential for the application of microfluidic devices within multiple disciplines of industrial applications.

1.2.2 ***Controlled Release Using Degradable Microparticles***

1.2.2.1 Biodegradable Polymers

In general, the degradation of polymeric materials can be split into four categories; hydrolytic, enzymatic, oxidative and physical degradation.[110] As a consequence of the heteroatom linkages present within common polymer backbones, hydrolytic and enzymatic degradation are the most frequently observed degradation pathways for polymers. A wide range of enzyme-catalysed degradation reactions are available, however, the only known mechanism of enzyme-mediated degradation of a synthetic polymer is hydrolysis.[111] Moreover, the degradable polymers with hydrolysable bonds can react with water to form two or more lower molecular weight degradation species (Scheme 1.2).

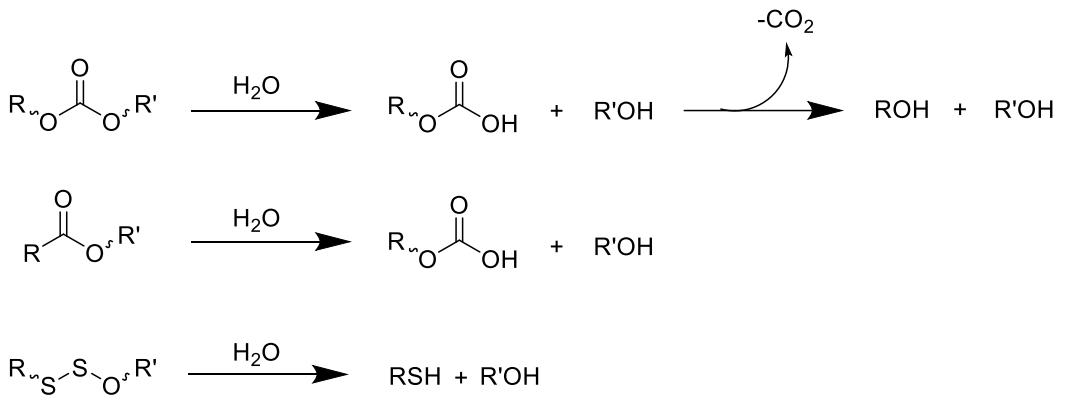

Scheme 1.2: Schematic illustration of the hydrolysis of a) carbonate, b) ester and c) disulfide bonds

1.2.2.2 Biodegradable Microparticles

The increasing legislation regarding the resistance of polymeric waste to degradation and its disposability have resulted in an increased interest for the use of biodegradable polymers for microparticle synthesis. A wide range of both natural and synthetic degradable polymers have been used for microparticle synthesis (Table 1.1). As the polymers decompose, they ideally form non-toxic, low molecular weight species which can be easily metabolised or adsorbed by organisms both within the body and in the environment.[19, 112, 113] Upon degradation, several degradable polymers are known to form toxic species, hence the chemical nature of the degradation products is a key factor of determining the polymer biocompatibility.[114] Polymer biocompatibility is typically characterised by performing cell studies during degradation.

Table 1.1: Table summarising the different types of polyesters, their preferred degradation route and their use when applied as a microparticle

Polymer	Degradable Bond	Degradation Pathway	Polymeric Microparticle	Application
Polyanhydride	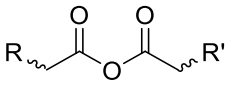	Hydrolysis	Poly(sebaic anhydride-*co*-1,6-bis(*p*-carboxyphenoxy)hexane[115]	Delivery of ovalbumin for enhanced antibody response
Polyorthoester	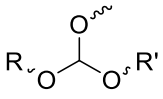	Hydrolysis	Poly(cyclohexane-1,4-diyl acetone dimethylene ketal)[116]	Delivery of superoxide dismutase for the treatment of inflammatory diseases
Polyurethane	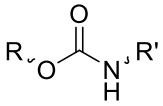	Hydrolysis, enzymatic	Copolymer of toluene-2,4-diisocyanate, bis(4-hydroxybutyl)8,8'-(5,6-dihexylcyclohex-3-ene-1,2-diyl)dioctanoate and 1,4-butanediol[117]	Delivery of isosorbide for anticorrosion/ self-healing coatings
Polyester	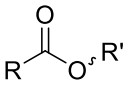	Hydrolysis, enzymatic	PLGA[118]	Controlled release of insulin
Polycarbonate	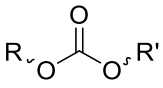	Hydrolysis, enzymatic	Polycarbonate[119]	Release of aspirin, griseofulvin and *p*-nitroaniline to the intestine
Polyamide	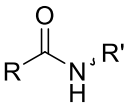	Hydrolysis, enzymatic	Poly(hexamethylene terephthalimide)[120]	Controlled release of ascorbic acid for improved skin treatments

The use of biodegradable polymers for the synthesis of matrix type microparticles has been intensively studied as a consequence of the attractive potential to control the encapsulated AI release rate solely by the polymer degradation rate.[121] In general, microparticles can undergo homogenous (bulk) degradation or heterogeneous

(surface) erosion (Figure 1.11).[122] However, it is not uncommon to observe both degradation profiles within the same microparticle degradation system. In more detail, bulk degradation involves the random hydrolytic scission of hydrolysable bonds throughout the particle matrix.[111] During homogeneous degradation, both the particle mass and density decrease, whereas the total volume of the particle remains constant throughout. Furthermore, as a consequence of the reduced diffusivity observed within a particle matrix, acidic degradation products can be trapped and accumulate within pockets or pores within the particle.[123] Consequently, the observed change in pH within the system can in turn result in autocatalytic degradation of the polymeric matrix.[124, 125] This is usually coupled with a loss of structural integrity and mechanical stability which typically results in the break down and collapse of the particle.

On the other hand, heterogeneous degradation necessitates that hydrolysis at the particle surface is faster than water penetration into the particle matrix.[110] This in turn results in an observable degradation of the particle from the outside towards the core. Surface erosion is typically characterised by a linear decrease in particle volume with mass, which results in the density remaining constant throughout. Unlike bulk degradation, the generated degradation products can rapidly diffuse away from the system.[126] Therefore, no auto-catalytic effects within the particle matrix are observed, hence, degradation is solely based on the polymer degradation rate at the particle surface.

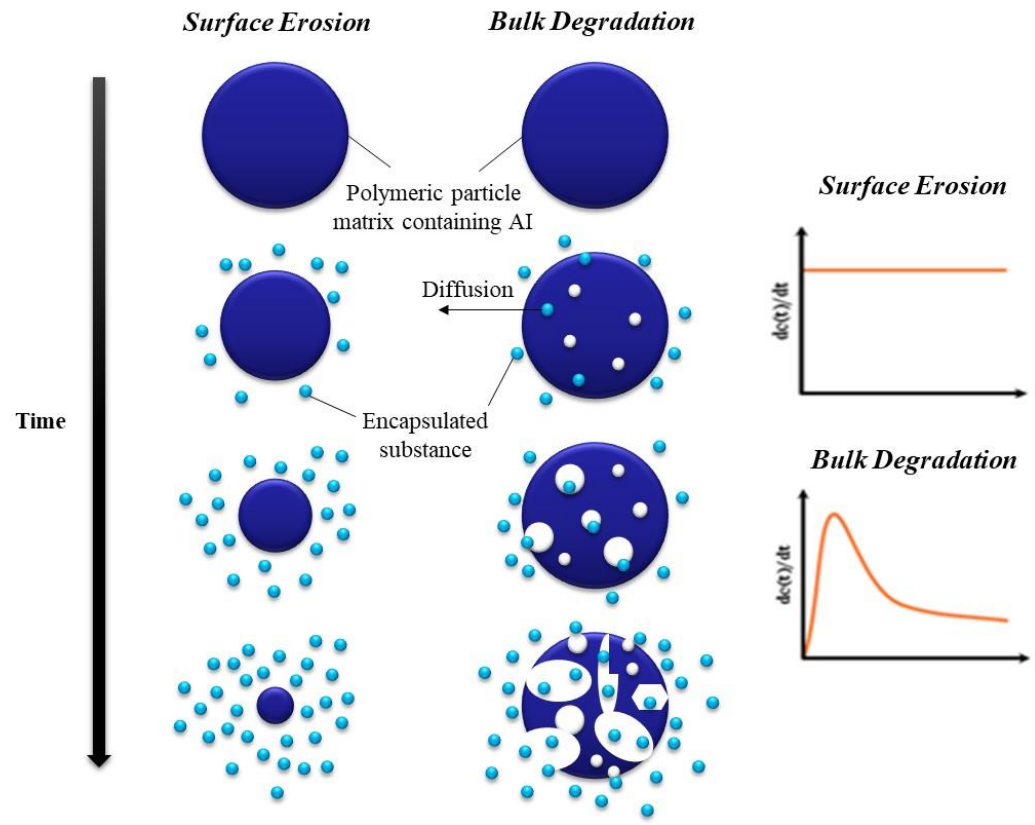

Figure 1.11: Schematic representation of surface and bulk degradation occurring within a matrix microparticle and the corresponding drug release rate

1.2.2.2.1 Polyesters for Biodegradable Microparticles

In this demanding area, as a consequence of their synthetic versatility, good mechanical and thermal properties and their easy degradability under a variety of conditions, polyesters have become the most intensively studied and investigated degradable particles.[64, 127] Indeed, investigations into the synthesis of PLA, PVL, PCL and PLGA microparticles are well known in the literature. Research has shown depending on the polyester used and the degradation conditions, the AI, which can be encased or dispersed within a polyester particle, can be slowly and continuously released over a period of days to years. In particular, Gonzalez *et al.*, investigated the degradation of PLA microparticles incubated at 37 °C in a buffer solution over 8 months (Figure 1.12).[128] SEM characterisation displayed signs of particle degradation

after 9 days. Further characterisation of the PLA particles revealed the formation of large pores within the particle after 143 days in the buffer solution, thus implying that bulk degradation had occurred. Interestingly, characterisation of the particles by X-ray diffraction, Gonzalez *et al*., discovered that the PLA particles displayed an increase in crystallinity during degradation, which fit well with previous PLA characterisation by Migliaresi *et al.*, who termed the behaviour as "degradation-induced crystallisation".[129] Further elucidation of the X-ray diffraction spectrum by Gonzalez *et al*. revealed the formation of a crystalline oligomeric structure formed during particle degradation. Crystallisation is a highly interesting phenomenon and has been shown to influence the resultant polymer degradation rate.[130] Moreover, as a consequence of the increased interactions enabled by tightly packed crystalline polymer chains, an amorphous polymeric matrix will display increased diffusivity within the particle matrix. Therefore, the increased diffusivity enables an increased influx of water and consequently an increased rate of hydrolysis. Therefore, the observed crystallisation of low molecular weight species within PLA particles could act to decrease the particle degradation and subsequent AI release rate.

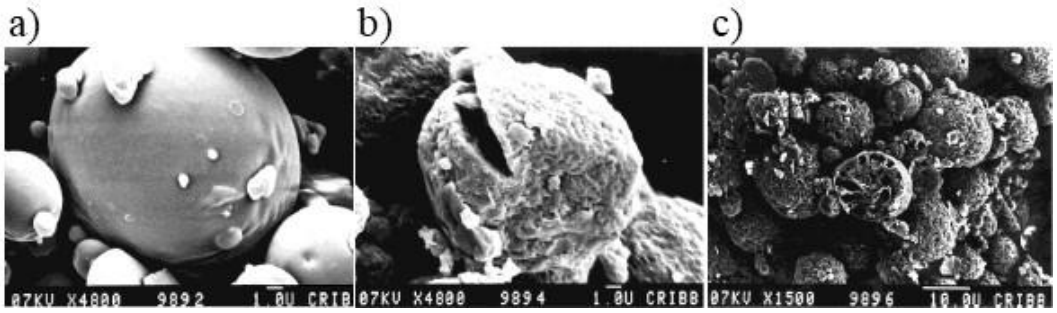

Figure 1.12: SEM characterisation of PLA microparticle degradation in Titrisol buffer solution (pH 7, merck reagent) after a) 0 days, b) 9 days and c) 143 days as observed by Gonzalez *et al.*[128]

The degradability of a particle is primarily determined by the degradation rate associated with the applied polymer.[121] Therefore, with the aim to incorporate tuneable degradability within a microparticle system, particle synthesis using a wide selection of polyester copolymers has been investigated.[71, 131] The use of copolymers for particle synthesis has also been shown to be an ideal pathway for the incorporation of functionality within the system. A second approach to incorporate tuneable degradation profiles has been to create particles from homopolymer blends, thus enabling the combining of the desired polymeric properties without the complexity and time required for copolymerisation.[132, 133]

1.2.2.3 Typical Release Profiles

The overall aim with encapsulation into microparticles is to achieve controlled or sustained release of the encapsulated AI, therefore, significant attention has been focussed on elucidation of the drug release profile. The most desirable drug release behaviour would follow a zero-order profile, showing a constant AI release with time until all of the encapsulated substance has been released.[134] However, it is well acknowledged that the AI can be released *via* diffusion through water filled pores within the particle. The diffusion of the AI through the particle matrix is determined by random movements of the drug and further driven by chemical potential gradients and convection produced by osmotic pressure. Therefore, in most cases, release profiles are more complex and often multiphasic.[100] Simplistically, drug release from a polyester matrix microparticle can be separated into two main expulsion processes; an initial burst release followed by a constant release (Figure 1.13).

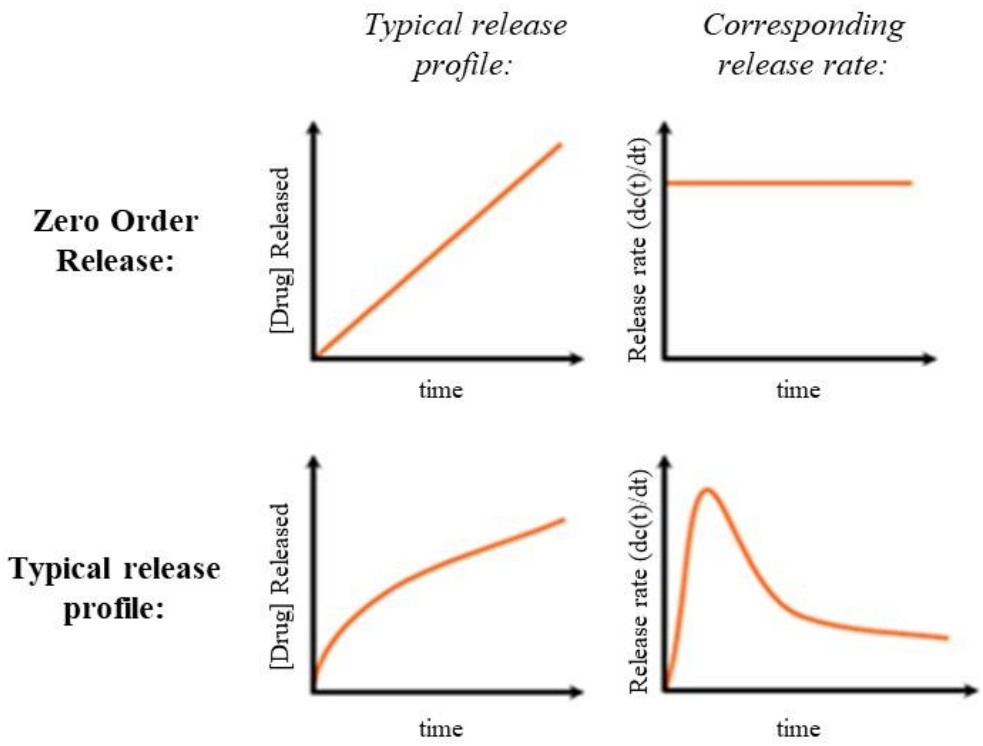

Figure 1.13: Graphical representation of an idealistic zero-order AI release profile *vs*. a conventional biphasic AI release profile

The initial burst observed within a matrix microparticle has been attributed to dye diffusion to the particle surface during the encapsulation process.[87] Typically, the initial burst release can result in the expulsion of 10-50% of the original drug load.[109] In a conventional single oil-in-water emulsion technique, a large quantity of the encapsulated AI will diffuse to the particle surface as the dichloromethane evaporates, hence an initial burst release using a standard solvent evaporation set-up is usually unavoidable. Whilst the initial burst release is not always high, a large release of AI could be toxic to the surroundings and also be irregular between batches. Therefore, several reports have investigated a variety of methodologies which aim to reduce or alleviate the burst release (*e.g.*, addition of excipients to the polymer phase, synthesis of novel polymers and encapsulating a drug in particulate form).[135] Further research into the initial burst release revealed that in general, the concentration of dye released

during the initial burst is thought to be dependent on the compatibility of the particle matrix and AI, the solubility of AI in the processing solvent and the availability of diffusion within the particle matrix.[64] Therefore, the initial burst release can be minimised by carefully optimising and tuning the emulsion conditions before particle synthesis.

After the initial burst, the AI typically follows a constant release rate until complete release has been achieved.[136] During this second stage, the AI release rate is highly dependent on both diffusion of the AI through the polymer matrix and the polymer degradation rate. Hence, the AI release rate during constant release can be controlled by the degradation rate of the polymeric material used for the particle matrix.[137] Bulk degradation of the particle matrix increases the porosity of the particle, which in turn increases the availability for dye diffusion and release. Nevertheless, the autocatalytic degradation observed within polyester particle systems can act to enhance the AI release rate. Therefore, degradation observed within a particle system is typically faster compared to degradation of the free polymer in solution. Consequently, in practice, enhanced drug release after erosion effects is often observed after an initial diffusion controlled lag.[138] On the other hand, some particles are more susceptible to surface degradation, which requires that hydrolysis at the particle surface is faster than water penetration into the matrix. Subsequently, the particle degradation rate can be controlled by varying the particle thickness, rather than by changing the total volume of the particle system. Therefore, for some particle systems, where the predominant erosion mechanism follows surface degradation, (such as polyanhydrides or polyorthoesters) zero-order AI release can be achieved.

1.3 Smart Release Technology

When selecting the optimal degradable release system for a specific application, the most significant criteria is for the material to decompose within a suitable and tuneable time period that is compatible with the desired drug release rate. Within nature, the most important, fundamental substances are macromolecules that can adapt their structure or behaviour depending on their surrounding environment.[139] Inspired by the dynamic versatility and efficiency observed within living systems, research into the synthesis and development of stimuli-responsive (also known as 'smart' or 'intelligent') polymers has been intensively researched.[140-142] Synthetic smart polymers have been designed to undergo either chemical or physical changes within response to small environmental variations.[142] A wide variety of stimuli parameters have previously been investigated, such as, pH, temperature, light and carbon dioxide.[143-149] Furthermore, as a consequence of the high efficiency offered by stimuli-responsive polymers, they have been applied for a broad array of applications with a multitude of controlled release devices (*e.g.*, hydrogels, nano/micro-particles, films, *etc*.).[50, 150-152]

1.3.1 *Stimulus-Responsive Particles*

Incorporating a stimulus-responsive polymer within a particle system enables modulated control over the site-specific AI release. Furthermore, this can be advantageous in both controlling the concentration of AI released and for tailoring the AI release rate. For this reason, multiple approaches have been investigated to develop stimulus-responsive particles; development of novel responsive polymers, copolymerisation of one or more smart polymers with a conventional polymer, blending smart polymers with conventional polymers, *etc*.[153-155]

In general, pH-responsive polymers consist of an ionisable acidic or basic residue, whose ionisation depends on the pH of the surrounding solution.[156] pH-Responsive particles have received a lot of attention especially for drug delivery applications.[60, 157, 158] Indeed, within the medical field, numerous particle systems have been developed specifically targeting delivery to the low pH of the stomach (pH 1.5-3.5) or higher pH observed within the intestine (pH 6.0-7.4).[159, 160] Lin *et al*., discovered that particles synthesised from differing ratios of chitosan and heparin could encapsulate antibiotics for the prevention and treatment of peptic ulcers.[161] In more detail, the degradable particles controlled the localised release of the encapsulated drug whilst acting to protect the incorporated AI from destructive gastric acids. On a similar note, numerous pH-sensitive drug-delivery systems have also taken advantage of the difference in pH observed with healthy tissues (7.4) and the extracellular environment of solid tumours (6.5-7.2), thus enabling site-specific release of anti-cancer drugs to cancerous cells.[162, 163]

Stimuli parameters can often require forcing conditions to trigger an environmental change. However, the excellent exogeneous and non-invasive control attainable using a photo-responsive system has enabled the engineering of light-responsive polymers whose structural modification can be induced under mild conditions for a variety of wavelengths (ultraviolet, visible or near-infrared regions).[164] Consequently, a wide range of photo-responsive systems have been designed and investigated for a broad array of applications.[51, 139] Azobenzene derived materials have received particular attention as a consequence of their easily irradiation-induced switchable isomerisation.[165] Moreover, *cis*-azobenzene is relatively polar with a dipole moment, conversely, *trans*-azobenzene is a stable macromolecule with no dipole moment. The

observed change from *cis-trans* azobenzene can result in a complete change in electronic structure, geometric shape and polarity.[139]

In recent years, to further improve the versatility of drug delivery systems, increasing research into the synthesis and design of multi-responsive polymers has been observed.[155, 166, 167] In certain pathological systems, pH-gradients and oxidative environments co-exist, therefore, the combination of pH and redox responsive particles has been shown to be highly advantageous for the design of drug delivery vehicles.[168] Indeed, Sokolovskaya *et al*. synthesised novel dual responsive Janus microparticles based on a novel poly(ethylene glycol) based polymer.[169] The polymer contained both a redox responsive thioether and a light sensitive nitrobenzyl group, thus enabling selective degradation *via* the application of either oxidative stress or UV light, thus demonstrating their high potential for controlled release.

1.3.2 *Smart Release in Agriculture*

With the increasing population and imminent strain on the agricultural industry, controlled release technology has emerged as a promising alternative to conventional agrochemical delivery with the promise to solve the problems accompanying the use of some agrochemicals, while avoiding possible side effects with others. The agrochemical can be contained within a material, which allows for the controlled release of the AI to the desired target. Therefore, the substance can be slowly and continuously released for up to several years. This can be highly advantageous, leading to fewer repeat applications, reduced agrochemical toxicity levels and increased efficiency of the agrochemical. This can be demonstrated by the recent work by Meyer *et al*., who investigated the controlled release of the pesticide imidacloprid from PLGA microparticles.[170] On its own, imidacloprid is known to cause undesirable toxicity towards and has been found to be especially detrimental to colonies of honey bees.

However, Meyer *et al*., discovered by encapsulating the imidacloprid into PLGA microparticles using a solvent evaporation technique, approximately 200 times less pesticide was required to achieve the same mortality of psyllids as the pesticide on its own.

Currently, several micro-encapsulated products are commercially available that aim to achieve slow release effects within the crop market, in particular Stomp Aqua (BASF), Samurai II CS Insecticide (J. Oliver Products) and Force (Syngenta).[171-174] Syngenta owns a patent that uses base-triggered microparticles which are designed to open in the alkaline environment of insect guts.[174] As a consequence of the high levels of localised control offered by 'smart' release systems, increasing research is being performed to enable stimulus-responsive release of agrochemicals. Indeed, Hill *et al*. investigated the synthesis of biodegradable pH-responsive nanoparticles for site-specific agrochemical delivery.[175] Moreover, the synthesised amphiphilic functionalised polysuccinimide particles displayed controlled release under alkaline conditions, thus enabling the localised release of an AI to the plant phloem (pH 7.3-8.5). Similar work by Chen *et al*., also detailed the localised release of an encapsulated AI to the plant phloem through the novel synthesis and encapsulation into pH-responsive amphiphilic polysuccinimide star copolymers.[176] The next fifty years are predicted to be the most challenging yet with regards to the strain applied on the agricultural industry. Therefore, the exciting opportunities attainable through the application of innovative 'smart' release technologies have the potential to shape and define the successful future for more efficient, enhanced agricultural practices.

1.4 Conclusions

In this Chapter, the diverse array of available polymerisation techniques are introduced, with specific attention given to the advancements observed within the ROP of polyesters. The significant developments within the synthesis of biodegradable particles has revolutionised controlled release technology. In particular the application of biodegradable release systems promises to increase drug efficiency whilst reducing any associated toxicity of the encapsulated AI. The current synthetic procedures for microparticle synthesis using a solvent-evaporation technique are reviewed, including the innovative advancements set to define the future practices within this field for the development of controlled, precision microparticle synthesis. Specific attention is focussed on particle synthesis using a single oil-in-water technique and the effect of process parameters on the subsequent microparticle size, degradation and release rate. The microparticle biodegradation pathways and the proceeding release profiles are discussed and the concept of 'smart' release technology is introduced, with specific focus given to the potential advantages for more efficient agricultural procedures.

1.5 References

1. V. V. Oberemok, K. V. Laikova, Y. I. Gninenko, A. S. Zaitsev, P. M. Nyadar and T. A. Adeyemi, *J. Plant Prot. Res.*, 2015, **55**, 221-226.
2. E. C. Oerke, *J. Agr. Sci.*, 2005, **144**, 31-43.
3. D. Tilman, K. G. Cassman, P. A. Matson, R. Naylor and S. Polasky, *Nature*, 2002, **418**, 671-677.
4. J. Popp, K. Pető and J. Nagy, *Agron. Sustain. Dev.*, 2013, **33**, 243-255.
5. A. Roy, S. K. Singh, J. Bajpai and A. K. Bajpai, *Cent. Eur. J. Chem.*, 2014, **12**, 453-469.
6. V. C. Baligar, N. K. Fageria and Z. L. He, *Commun. Soil Sci. Plant Anal.*, 2001, **32**, 921-950.
7. I. M. Shirley, H. B. Scher, R. M. Perrin, P. J. Wege, M. Rodson, J.-L. Chen and A. W. Rehmke, *Pest Manage. Sci.*, 2001, **57**, 129-132.
8. T. R. Darling, T. P. Davis, M. Fryd, A. A. Gridnev, D. M. Haddleton, S. D. Ittel, R. R. Matheson, G. Moad and E. Rizzardo, *J. Polym. Sci. Part A: Polym. Chem.*, 2000, **38**, 1706-1708.
9. R. P. Quirk and B. Lee, *Polym. Int.*, 1992, **27**, 359-367.
10. N. Hadjichristidis, M. Pitsikalis, S. Pispas and H. Iatrou, *Chem. Rev.*, 2001, **101**, 3747-3792.
11. G. Moad and D. H. Solomon, in *The Chemistry of Radical Polymerization (Second Edition)*, Elsevier Science Ltd, Amsterdam, 2005, pp. 1-9.
12. D. Braun, *Int. J. Polym. Sci.*, 2009, **2009**.
13. M. F. Cunningham and R. Hutchinson, in *Handbook of Radical Polymerization*, John Wiley & Sons, Inc., New York, 2003, pp. 333-359.
14. D. Colombani, *Prog. Polym. Sci.*, 1997, **22**, 1649-1720.

15. C. Zhang, in *Biodegradable Polyesters*, Wiley-VCH Verlag GmbH & Co. KGaA, Weinheim, 2015, pp. 1-24.

16. K. Madhavan Nampoothiri, N. R. Nair and R. P. John, *Bioresour. Technol.*, 2010, **101**, 8493-8501.

17. D. Rasselet, A. Ruellan, A. Guinault, G. Miquelard-Garnier, C. Sollogoub and B. Fayolle, *Eur. Polym. J.*, 2014, **50**, 109-116.

18. F. Faÿ, E. Renard, V. Langlois, I. Linossier and K. Vallée-Rehel, *Eur. Polym. J.*, 2007, **43**, 4800-4813.

19. L. S. Nair and C. T. Laurencin, *Prog. Polym. Sci.*, 2007, **32**, 762-798.

20. M. Sokolsky-Papkov, R. Langer and A. J. Domb, *Polym. Adv. Technol.*, 2011, **22**, 502-511.

21. A.-C. Albertsson and I. K. Varma, *Biomacromolecules*, 2003, **4**, 1466-1486.

22. W. J. Bailey, Z. Ni and S. R. Wu, *Macromolecules*, 1982, **15**, 711-714.

23. S. M. Guillaume, E. Kirillov, Y. Sarazin and J.-F. Carpentier, *Chem. Eur. J.*, 2015, **21**, 7988-8003.

24. U. H. Choi, A. Mittal, T. L. Price, R. H. Colby and H. W. Gibson, *Macromol. Chem. Phys.*, 2016, **217**, 1270-1281.

25. J. Ling, X. Wang, L. You and Z. Shen, *J. Polym. Sci. Part A: Polym. Chem.*, 2016, **54**, 3012-3018.

26. A. Duda and A. Kowalski, in *Handbook of Ring-Opening Polymerization*, Wiley-VCH Verlag GmbH & Co. KGaA, Weinheim, 2009, pp. 1-51.

27. K. N. Houk, A. Jabbari, H. K. Hall and C. Alemán, *J. Org. Chem.*, 2008, **73**, 2674-2678.

28. H.-J. Fang, P.-S. Lai, J.-Y. Chen, S. C. N. Hsu, W.-D. Peng, S.-W. Ou, Y.-C. Lai, Y.-J. Chen, H. Chung, Y. Chen, T.-C. Huang, B.-S. Wu and H.-Y. Chen, *J. Polym. Sci. Part A: Polym. Chem.*, 2012, **50**, 2697-2704.

29. Y. Wang and M. Kunioka, *Macromol. Symp.*, 2005, **224**, 193-206.

30. A. Kumar, K. Garg and R. A. Gross, *Macromolecules*, 2001, **34**, 3527-3533.

31. F. Nederberg, E. F. Connor, M. Möller, T. Glauser and J. L. Hedrick, *Angew. Chem. Int. Ed.*, 2001, **40**, 2712-2715.

32. K. S. Bisht, L. A. Henderson, R. A. Gross, D. L. Kaplan and G. Swift, *Macromolecules*, 1997, **30**, 2705-2711.

33. A. P. Dove, *Chem. Commun.*, 2008, 6446-6470.

34. B. G. G. Lohmeijer, R. C. Pratt, F. Leibfarth, J. W. Logan, D. A. Long, A. P. Dove, F. Nederberg, J. Choi, C. Wade, R. M. Waymouth and J. L. Hedrick, *Macromolecules*, 2006, **39**, 8574-8583.

35. A. Kumar, B. Kalra, A. Dekhterman and R. A. Gross, *Macromolecules*, 2000, **33**, 6303-6309.

36. Y. Mei, A. Kumar and R. Gross, *Macromolecules*, 2003, **36**, 5530-5536.

37. M. Bouyahyi and R. Duchateau, *Macromolecules*, 2014, **47**, 517-524.

38. Y. Nakayama, N. Watanabe, K. Kusaba, K. Sasaki, Z. Cai, T. Shiono and C. Tsutsumi, *J. Appl. Polym. Sci.*, 2011, **121**, 2098-2103.

39. S. Csihony, D. A. Culkin, A. C. Sentman, A. P. Dove, R. M. Waymouth and J. L. Hedrick, *J. Am. Chem. Soc.*, 2005, **127**, 9079-9084.

40. K. Makiguchi, T. Satoh and T. Kakuchi, *Macromolecules*, 2011, **44**, 1999-2005.

41. A. Thevenon, J. A. Garden, A. J. P. White and C. K. Williams, *Inorg. Chem.*, 2015, **54**, 11906-11915.

42. M. Letizia Focarete, M. Scandola, A. Kumar and R. A. Gross, *J. Polym. Sci. B Polym. Phys.*, 2001, **39**, 1721-1729.

43. Z. Jiang, H. Azim, R. A. Gross, M. L. Focarete and M. Scandola, *Biomacromolecules*, 2007, **8**, 2262-2269.

44. M. de Geus, I. van der Meulen, B. Goderis, K. van Hecke, M. Dorschu, H. van der Werff, C. E. Koning and A. Heise, *Polym. Chem.*, 2010, **1**, 525-533.

45. M. P. F. Pepels, P. Souljé, R. Peters and R. Duchateau, *Macromolecules*, 2014, **47**, 5542-5550.

46. S. J. Desai, A. P. Simonelli and W. I. Higuchi, *J. Pharm. Sci.*, 1965, **54**, 1459-1464.

47. J. Folkman and D. M. Long, *J. Surg. Res.*, 1964, **4**, 139-142.

48. A. S. Hoffman, *J. Controlled Release*, 2008, **132**, 153-163.

49. S.-J. Park and S.-H. Kim, *J. Colloid Interface Sci.*, 2004, **271**, 336-341.

50. Y. Gao, G. P. Zago, Z. Jia and M. J. Serpe, *ACS Appl. Mater. Interfaces*, 2013, **5**, 9803-9808.

51. I. Tomatsu, K. Peng and A. Kros, *Adv. Drug Delivery Rev.*, 2011, **63**, 1257-1266.

52. M. J. Derry, L. A. Fielding and S. P. Armes, *Prog. Polym. Sci.*, 2016, **52**, 1-18.

53. E. V. R. Campos, J. L. de Oliveira, L. F. Fraceto and B. Singh, *Agron. Sustain. Dev.*, 2015, **35**, 47-66.

54. M. Okada, *Prog. Polym. Sci.*, 2002, **27**, 87-133.

55. V. R. Sinha, K. Bansal, R. Kaushik, R. Kumria and A. Trehan, *Int. J. Pharm.*, 2004, **278**, 1-23.

56. T. M. S. Chang, *Science*, 1964, **146**, 524-525.

57. J. Siepmann and F. Siepmann, in *Smart Colloidal Materials*, ed. W. Richtering, Springer, Berlin, Heidelberg, 2006, pp. 15-21.

58. N. Mason, C. Thies and T. J. Cicero, *J. Pharm. Sci.*, 1976, **65**, 847-850.

59. J. A. Champion, Y. K. Katare and S. Mitragotri, *J. Controlled Release*, 2007, **121**, 3-9.

60. S. R. Little, D. M. Lynn, Q. Ge, D. G. Anderson, S. V. Puram, J. Chen, H. N. Eisen and R. Langer, *Proc. Natl. Acad. Sci. U. S. A*, 2004, **101**, 9534-9539.

61. B. Lei, X. Chen, Y. Wang, N. Zhao, G. Miao, Z. Li and C. Lin, *Mater. Lett.*, 2010, **64**, 2293-2295.

62. E. Campos, J. Branquinho, A. S. Carreira, A. Carvalho, P. Coimbra, P. Ferreira and M. H. Gil, *Eur. Polym. J.*, 2013, **49**, 2005-2021.

63. U. Sathish, B. Shravani, R. Raghavendra, R. Srikanth and N. Sanjeev, *Int. J. Pharma. Sci*, 2013, **3**, 258-269.

64. N. Kamaly, B. Yameen, J. Wu and O. C. Farokhzad, *Chem. Rev.*, 2016, **116**, 2602-2663.

65. W. L. Webber, F. Lago, C. Thanos and E. Mathiowitz, *J. Biomed. Mater. Res.*, 1998, **41**, 18-29.

66. B. Han, X. Wang, X. Gao, J. Liu, F. Liang, X. Qu and Z. Yang, *J. Biomed. Mater. Res. Part B Appl. Biomater.*, 2011, **99B**, 120-126.

67. C. Berkland, K. Kim and D. W. Pack, *J. Controlled Release*, 2001, **73**, 59-74.

68. C. Berkland, E. Pollauf, D. W. Pack and K. Kim, *J. Controlled Release*, 2004, **96**, 101-111.

69. V.-T. Tran, J.-P. Benoît and M.-C. Venier-Julienne, *Int. J. Pharm.*, 2011, **407**, 1-11.

70. R. Verrijk, I. J. H. Smolders, N. Bosnie and A. C. Begg, *Cancer Res.*, 1992, **52**, 6653.

71. B. Buntner, M. Nowak, J. Kasperczyk, M. Ryba, P. Grieb, M. Walski, P. Dobrzyñski and M. Bero, *J. Controlled Release*, 1998, **56**, 159-167.

72. P. B. O'Donnell and J. W. McGinity, *Adv. Drug Delivery Rev.*, 1997, **28**, 25-42.

73. I. D. Rosca, F. Watari and M. Uo, *J. Controlled Release*, 2004, **99**, 271-280.

74. R. Bodmeier and J. W. McGinity, *Pharm. Res.*, 1987, **4**, 465-471.

75. N. Sharma, P. Madan and S. Lin, *Asian J. Pharm. Sci.*, 2016, **11**, 404-416.

76. P. Stloukal, P. Kucharczyk, V. Sedlarik, P. Bazant and M. Koutny, *J. Agric. Food Chem.*, 2012, **60**, 4111-4119.

77. W.-J. Lin, D. R. Flanagan and R. J. Linhardt, *Polymer*, 1999, **40**, 1731-1735.

78. D. Wang, O. Molavi, M. E. C. Lutsiak, P. Elamanchili, G. S. Kwon and J. Samuel, *J Pharm Pharm Sci*, 2007, **10**, 217-230.

79. K. Makino, T. Mogi, N. Ohtake, M. Yoshida, S. Ando, T. Nakajima and H. Ohshima, *Colloids Surf. B Biointerfaces*, 2000, **19**, 173-179.

80. Y. Capan, B. H. Woo, S. Gebrekidan, S. Ahmed and P. P. DeLuca, *J. Controlled Release*, 1999, **60**, 279-286.

81. J. Siepmann, N. Faisant, J. Akiki, J. Richard and J. P. Benoit, *J. Controlled Release*, 2004, **96**, 123-134.

82. C. Wischke and S. P. Schwendeman, *Int. J. Pharm.*, 2008, **364**, 298-327.

83. M. J. Lawrence and G. D. Rees, *Adv. Drug Delivery Rev.*, 2000, **45**, 89-121.

84. M. Li, O. Rouaud and D. Poncelet, *Int. J. Pharm.*, 2008, **363**, 26-39.

85. G. Paradossi, F. Cavalieri, E. Chiessi, C. Spagnoli and M. K. Cowman, *J. Mater. Sci.: Mater. Med.*, 2003, **14**, 687-691.

86. P. Sansdrap and A. J. Moës, *Int. J. Pharm.*, 1993, **98**, 157-164.

87. J. L. Maia, M. H. A. Santana and M. I. Ré, *Braz. J. Chem. Eng.*, 2004, **21**, 01-12.

88. B. Conti, I. Genta, T. Modena and F. Pavanetto, *Drug Dev. Ind. Pharm.*, 1995, **21**, 615-622.

89. R. Jeyanthi, B. C. Thanoo, R. C. Metha and P. P. Deluca, *J. Controlled Release*, 1996, **38**, 235-244.

90. R. Arshady, *J. Controlled Release*, 1991, **17**, 1-21.

91. H. Sawalha, K. Schroën and R. Boom, *Chem. Eng. J.*, 2011, **169**, 1-10.

92. C. Bitz and E. Doelker, *Int. J. Pharm.*, 1996, **131**, 171-181.

93. I. C. H. Guideline, *Organic Volatile Impurities*, European Medicines Agency, London, 2017.

94. H. Sah, *Int. J. Pharm.*, 2000, **195**, 103-113.

95. T. Freytag, A. Dashevsky, L. Tillman, G. E. Hardee and R. Bodmeier, *J. Controlled Release*, 2000, **69**, 197-207.

96. H. Sah, *J. Controlled Release*, 1997, **47**, 233-245.

97. C. Sturesson, J. Carlfors, K. Edsman and M. Andersson, *Int. J. Pharm.*, 1993, **89**, 235-244.

98. S. Gu, C. Zhai and S. C. Jana, *Langmuir*, 2016, **32**, 5637-5645.

99. H. T. Wang, E. Schmitt, D. R. Flanagan and R. J. Linhardt, *J. Controlled Release*, 1991, **17**, 23-31.

100. Y.-Y. Yang, T.-S. Chung, X.-L. Bai and W.-K. Chan, *Chem. Eng. Sci.*, 2000, **55**, 2223-2236.

101. J. Herrmann and R. Bodmeier, *Int. J. Pharm.*, 1995, **126**, 129-138.

102. C. Schugens, N. Laruelle, N. Nihant, C. Grandfils, R. Jérome and P. Teyssié, *J. Controlled Release*, 1994, **32**, 161-176.

103. A. Choi, K. D. Seo, D. W. Kim, B. C. Kim and D. S. Kim, *Lab Chip.*, 2017, **17**, 591-613.

104. R. K. Shah, H. C. Shum, A. C. Rowat, D. Lee, J. J. Agresti, A. S. Utada, L.-Y. Chu, J.-W. Kim, A. Fernandez-Nieves, C. J. Martinez and D. A. Weitz, *Mater. Today*, 2008, **11**, 18-27.

105. E. E. Ekanem, S. A. Nabavi, G. T. Vladisavljević and S. Gu, *ACS Appl. Mater. Interfaces*, 2015, **7**, 23132-23143.

106. K. Keohane, D. Brennan, P. Galvin and B. T. Griffin, *Int. J. Pharm.*, 2014, **467**, 60-69.

107. S. Ralf, B. Martin, P. Thomas and H. Stephan, *Rep. Prog. Phys.*, 2012, **75**, 016601.

108. A. S. Utada, E. Lorenceau, D. R. Link, P. D. Kaplan, H. A. Stone and D. A. Weitz, *Science*, 2005, **308**, 537-541.

109. K. K. Kim and D. W. Pack, in *BioMEMS and Biomedical Nanotechnology: Volume I Biological and Biomedical Nanotechnology*, eds. M. Ferrari, A. P. Lee and L. J. Lee, Springer, Boston, MA, 2006, pp. 19-50.

110. R. P. Brannigan and A. P. Dove, *Biomater. Sci.*, 2017, **5**, 9-21.

111. S. Lyu and D. Untereker, *Int. J. Mol. Sci.*, 2009, **10**, 4033.

112. G. Gallet, R. Lempiäinen and S. Karlsson, *Polym. Degrad. Stab.*, 2000, **71**, 147-151.

113. H. Pranamuda, Y. Tokiwa and H. Tanaka, *Appl. Environ. Microbiol.*, 1997, **63**, 1637-1640.

114. E. Marin, M. I. Briceño and C. Caballero-George, *Int. J. Nanomedicine*, 2013, **8**, 3071-3091.

115. L. Huntimer, J. H. Wilson Welder, K. Ross, B. Carrillo-Conde, L. Pruisner, C. Wang, B. Narasimhan, M. J. Wannemuehler and A. E. Ramer-Tait, *J. Biomed. Mater. Res. Part B: Appl. Biomater.*, 2013, **101B**, 91-98.

116. S. Lee, S. C. Yang, M. J. Heffernan, W. R. Taylor and N. Murthy, *Bioconjugate Chem.*, 2007, **18**, 4-7.

117. E. Koh, S. Lee, J. Shin and Y.-W. Kim, *Ind. Eng. Chem. Res.*, 2013, **52**, 15541-15548.

118. K. D. Hinds, K. M. Campbell, K. M. Holland, D. H. Lewis, C. A. Piché and P. G. Schmidt, *J. Controlled Release*, 2005, **104**, 447-460.

119. B. C. Thanoo, M. C. Sunny and A. Jayakrishnan, *J. Pharm. Pharmacol.*, 1993, **45**, 21-24.

120. L. Ripoll and Y. Clement, *Cosmetics*, 2016, **3**, 38.

121. F. Y. Han, K. J. Thurecht, A. K. Whittaker and M. T. Smith, *Front. Pharmacol.*, 2016, **7**.

122. A. C. Fonseca, P. Ferreira, R. A. Cordeiro, P. V. Mendonça, J. R. Góis, M. H. Gil and J. F. J. Coelho, in *New Strategies to Advance Pre/Diabetes Care: Integrative Approach by PPPM*, ed. M. S. Mozaffari, Springer Netherlands, Dordrecht, 2013, pp. 399-455.

123. A. Brunner, K. Mäder and A. Göpferich, *Pharm. Res.*, 1999, **16**, 847-853.

124. T. G. Park, W. Lu and G. Crotts, *J. Controlled Release*, 1995, **33**, 211-222.

125. B. S. Zolnik and D. J. Burgess, *J. Controlled Release*, 2007, **122**, 338-344.

126. J. Heller, J. Barr, S. Y. Ng, K. S. Abdellauoi and R. Gurny, *Adv. Drug Delivery Rev.*, 2002, **54**, 1015-1039.

127. R. Grillo, A. d. E. S. Pereira, N. F. S. de Melo, R. M. Porto, L. O. Feitosa, P. S. Tonello, N. L. D. Filho, A. H. Rosa, R. Lima and L. F. Fraceto, *J. Hazard. Mater.*, 2011, **186**, 1645-1651.

128. M. F. Gonzalez, R. A. Ruseckaite and T. R. Cuadrado, *J. Appl. Polym. Sci.*, 1999, **71**, 1223-1230.

129. C. Migliaresi, L. Fambri and D. Cohn, *J. Biomater. Sci., Polym. Ed.*, 1994, **5**, 591-606.

130. W. Zhai, Y. Ko, W. Zhu, A. Wong and C. B. Park, *Int. J. Mol. Sci.*, 2009, **10**, 5381-5397.

131. S. Freiberg and X. X. Zhu, *Int. J. Pharm.*, 2004, **282**, 1-18.

132. U. Edlund and A.-C. Albertsson, *J. Polym. Sci. Part A: Polym. Chem.*, 2000, **38**, 786-796.

133. F.-L. Mi, Y.-M. Lin, Y.-B. Wu, S.-S. Shyu and Y.-H. Tsai, *Biomaterials*, 2002, **23**, 3257-3267.

134. D. H. Lewis and D. R. Cowsar, *Principles of Controlled Release Pesticides*, ACS Symp. Series, Washington, 1977.

135. X. Huang and C. S. Brazel, *J. Controlled Release*, 2001, **73**, 121-136.

136. Y.-Y. Yang, T.-S. Chung and N. Ping Ng, *Biomaterials*, 2001, **22**, 231-241.

137. T. Mogi, N. Ohtake, M. Yoshida, R. Chimura, Y. Kamaga, S. Ando, T. Tsukamoto, T. Nakajima, H. Uenodan, M. Otsuka, Y. Matsuda, H. Ohshima and K. Makino, *Colloids Surf. B*, 2000, **17**, 153-165.

138. D. J. Hines and D. L. Kaplan, *Crit. Rev. Ther. Drug Carrier Syst.*, 2013, **30**, 257-276.

139. D. Roy, J. N. Cambre and B. S. Sumerlin, *Prog. Polym. Sci.*, 2010, **35**, 278-301.

140. H. Yang, H. Zhu, M. M. R. M. Hendrix, N. J. H. G. M. Lousberg, G. de With, A. C. C. Esteves and J. H. Xin, *Adv. Mater.*, 2013, **25**, 1150-1154.

141. M. R. Aguilar and J. San Román, in *Smart Polymers and their Applications*, Woodhead Publishing, Cambridge, 2014, pp. 1-11.

142. A. Aghabegi Moghanjoughi, D. Khoshnevis and A. Zarrabi, *Drug Deliv. Transl. Res.*, 2016, **6**, 333-340.

143. M. I. Gibson and R. K. O'Reilly, *Chem. Soc. Rev.*, 2013, **42**, 7204-7213.

144. D. Roy, W. L. A. Brooks and B. S. Sumerlin, *Chem. Soc. Rev.*, 2013, **42**, 7214-7243.

145. S. Dai, P. Ravi and K. C. Tam, *Soft Matter*, 2008, **4**, 435-449.

146. K. E. B. Doncom, H. Willcock and R. K. O'Reilly, *J. Polym. Sci. Part A: Polym. Chem.*, 2014, **52**, 3026-3031.

147. L. D. Blackman, K. E. B. Doncom, M. I. Gibson and R. K. O'Reilly, *Polym. Chem.*, 2017, **8**, 2860-2871.

148. S. Lin and P. Theato, *Macromol. Rapid Commun.*, 2013, **34**, 1118-1133.

149. K. Ding, L. Shi, L. Zhang, T. Zeng, Y. Yin and Y. Yi, *Polym. Chem.*, 2016, **7**, 899-904.

150. M. Wei, Y. Gao, X. Li and M. J. Serpe, *Polym. Chem.*, 2017, **8**, 127-143.

151. S. Mura, J. Nicolas and P. Couvreur, *Nat. Mater.*, 2013, **12**, 991-1003.

152. S.-J. Jeon, A. W. Hauser and R. C. Hayward, *Acc. Chem. Res.*, 2017, **50**, 161-169.

153. Q. Zhang, T. Sauter, L. Fang, K. Kratz and A. Lendlein, *Macromol. Mater. Eng.*, 2015, **300**, 522-530.

154. M. Brzeziński and S. Seiffert, *Mater. Lett.*, 2015, **161**, 471-475.

155. J. S. Lee, X. Deng, P. Han and J. Cheng, *Macromol. Biosci.*, 2015, **15**, 1314-1322.

156. G. Kocak, C. Tuncer and V. Butun, *Polym. Chem.*, 2017, **8**, 144-176.

157. H. Li, Y. Jia, X. Feng and J. Li, *J. Colloid Interface Sci.*, 2017, **487**, 12-19.

158. Z. Li, F. Xiong, J. He, X. Dai and G. Wang, *Eur. J. Pharm. Biopharm.*, 2016, **109**, 24-34.

159. P. He, Z. Tang, L. Lin, M. Deng, X. Pang, X. Zhuang and X. Chen, *Macromol. Biosci.*, 2012, **12**, 547-556.

160. X. Zhou, Y. Zhao, S. Chen, S. Han, X. Xu, J. Guo, M. Liu, L. Che, X. Li and J. Zhang, *Biomacromolecules*, 2016, **17**, 2540-2554.

161. Y.-H. Lin, C.-H. Chang, Y.-S. Wu, Y.-M. Hsu, S.-F. Chiou and Y.-J. Chen, *Biomaterials*, 2009, **30**, 3332-3342.

162. H. Devalapally, D. Shenoy, S. Little, R. Langer and M. Amiji, *Cancer Chemother. Pharmacol.*, 2007, **59**, 477-484.

163. I. Brigger, C. Dubernet and P. Couvreur, *Adv. Drug Delivery Rev.*, 2002, **54**, 631-651.

164. G. Mayer and A. Heckel, *Angew. Chem. Int. Ed.*, 2006, **45**, 4900-4921.

165. K. G. Yager and C. J. Barrett, *J. Photochem. Photobiol.*, 2006, **182**, 250-261.

166. R. V. Joshi, C. E. Nelson, K. M. Poole, M. C. Skala and C. L. Duvall, *Acta Biomater.*, 2013, **9**, 6526-6534.

167. N. Cheng, Y. Wang and F. Wu, *J. Appl. Polym. Sci.*, 2016, **133**, 1-10.

168. E. A. Mahmoud, J. Sankaranarayanan, J. M. Morachis, G. Kim and A. Almutairi, *Bioconjugate Chem.*, 2011, **22**, 1416-1421.

169. E. Sokolovskaya, S. Rahmani, A. C. Misra, S. Bräse and J. Lahann, *ACS Appl. Mater. Interfaces*, 2015, **7**, 9744-9751.

170. W. L. Meyer, P. Gurman, L. L. Stelinski and N. M. Elman, *Green Chem.*, 2015, **17**, 4173-4177.

171. J. L. Ansiaux, F. Borgo, T. W. Cheung, J. Edmonds, T. E. Kunkel, G. L. Melchior, F. R. Miranda and G. D. Newberry, *Improved processes for the control of undesired vegetative growth in crops*, US 13, 813, 090, 2013.

172. J. Street and A. Jutsum, *Pesticidal mixtures giving synergistic pesticidal effects*, US 20110318272, 2013.

173. F. P. Silverman, J. Zhiguo, P. D. Petracek, D. F. Heiman and P. Warrior, *Herbicidal composition comprising a ps-ii inhibitor and sar inducer*, US 20040116293, 2004.

174. J. E. Van Koppenhagen, H. B. Scher, K. S. Lee, I. M. Shirley, P. Wade and R. Follows, *Base-triggered release microcapsules*, US 6544540, 2003.

175. M. R. Hill, E. J. MacKrell, C. P. Forsthoefel, S. P. Jensen, M. Chen, G. A. Moore, Z. L. He and B. S. Sumerlin, *Biomacromolecules*, 2015, **16**, 1276-1282.

176. M. Chen, S. P. Jensen, M. R. Hill, G. Moore, Z. He and B. S. Sumerlin, *Chem. Commun.*, 2015, **51**, 9694-9697.

2. Synthesis of Microparticles from Biodegradable Polymers

2.1 Introduction

The ever-increasing demand for sustainability, means that there has been a surge of interest in research into biodegradable materials.[1-3] In general, biodegradable polymers can be defined as those who break down into low-molecular weight compounds in the presence of microorganisms.[4-8] Therefore, they have been shown to be ideal materials for use as the polymer matrix to encapsulate a wide range of active ingredients (AI's).[9-11] Furthermore, the low molecular weight species formed during polymer degradation are typically non-toxic and can be easily metabolised or absorbed by organisms within the soil.[12-16] Therefore, this still enables controlled release of an AI, but without causing further harm to the environment. In particular, polyesters such as poly(lactic acid) (PLA), poly(*ε*-caprolactone) (PCL) and poly(3-hydroxybutyrate) (PHB) have received a lot of attention as a consequence of their ability to undergo degradation under environmental conditions.[17-19]

Polyesters are typically synthesised *via* two processes: polycondensation of a diol and dicarboxylic acid or by ring-opening polymerisation (ROP) of a cyclic monomer. ROP of cyclic monomers has been widely studied as a consequence of the good control attainable over the growth of polymer chains during polymerisation (Scheme 2.1).[20] Hence, ROP offers an efficient pathway to the specific and detailed design over polymer composition, molecular weight and microstructure.[21-23] A vast library of catalysts have been studied for the controlled ROP of polyesters, including enzymes, inorganic catalysts and organocatalysts.[24-30]

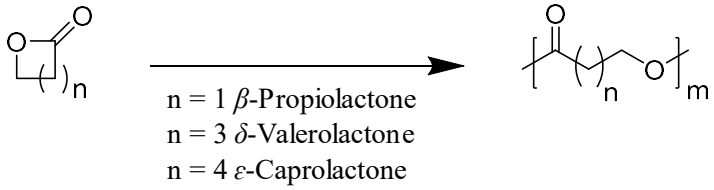

Scheme 2.1: Schematic representation of ring-opening polymerisation of a polyester.[20]

Investigations into the synthesis of PLA, PCL and poly(lactic acid-*co*-glycolic acid) (PLGA) microparticles have been well reported in the literature.[31, 32] Several synthetic techniques have been shown to successfully prepare the biodegradable microparticles, such as single and double oil-in-water emulsions, phase separation or precipitation and spraying methods.[33-37] Particle synthesis using an oil-in-water single emulsion is highly desirable for industrial applications as a consequence of its simple and easily tuneable methodology. However, the production of stable particles using a solvent-evaporation technique is highly dependent on the emulsion set-up and therefore, even small changes in the organic phase evaporation rate can alter the particle morphology and encapsulation efficiency.[38] Additionally, various other factors are known to affect the particle morphology, encapsulation and release rate, such as the particle size, stabiliser concentration, the polymer type and polymeric molecular weight.[39-42]

The vast majority of crops require the protection and beneficial influence of agrochemicals to enable increased crop efficiency.[43] Nevertheless, an excess of agrochemical is currently required to be applied to the crop to achieve the essential quantity for optimum plant protection.[44] A large proportion of agrochemicals are toxic above specific concentrations, therefore, the increased quantity can result in undesirable environmental side effects.[45] Consequently, controlled release technology using biodegradable particles promises an efficient alternative to conventional

agrochemical delivery, providing a route to increased yields with reduced active ingredient (AI) toxicity.

As a consequence of the increased efficacy promised by agrochemical encapsulation, the aim of this thesis was to provide a simple approach to prepare stable and degradable microparticles for controlled AI release. To successfully control the release of an AI, a reproducible methodology of creating stable microparticles with tuneable degradation properties was required. Therefore, this Chapter details the controlled polymerisation of a range of cyclic monomers with different properties and their subsequent use to create biodegradable microparticles. In order to accurately target different molecular weights whilst maintaining a narrow size distribution, the polyesters were prepared *via* ROP. Using the resultant polyesters, a single oil-in-water emulsion technique was used to prepare biodegradable microparticles. The size and stability of the particles was optimised by monitoring the effect of a range of variables during particle synthesis.

2.2 Results and Discussion

2.2.1 Ring-Opening Polymerisation of Cyclic Monomers

2.2.1.1 L-Lactide

The ROP of *L*-LA was carried out using a benzyl alcohol (BA) initiator and 1,8-diazabicycloundec-7-ene (DBU) as catalyst, analogous to the procedure by Lohmeijer *et al*. (Scheme 2.2).[46] Four molecular weights were targeted by varying the initial monomer to initiator ratio (Table 2.1). The concentration of monomer (0.7 M in dichloromethane) and DBU (1 mol%) were kept constant for each targeted DP.

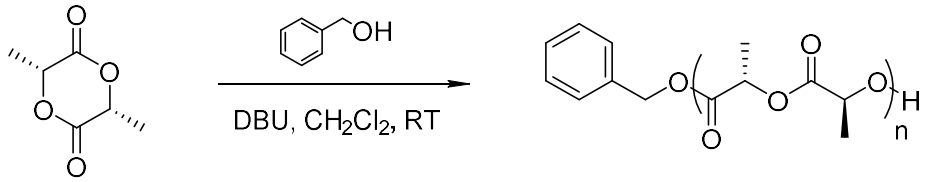

Scheme 2.2: Schematic representation of ROP of *L*-LA at RT with DBU as a catalyst

Table 2.1: ROP of 0.7 M *L*-Lactide in CH_2Cl_2 with varying [*L*-LA]: [BA] using DBU at RT

Polymer	Target [M]/[I]	Time (h)	$M_{n\ theory}$ (g mol^{-1})[a,b]	$M_{n\ NMR}$ (g mol^{-1})[a]	$M_{n\ SEC}$ (g mol^{-1})[c]	$Đ_{M\ SEC}$[c]	DP
PLLA 25	25	0.25	3,700	4,200	4,900	1.18	28
PLLA 75	75	0.75	10,800	11,100	19,000	1.06	77
PLLA 100	100	1	14,400	14,900	17,600	1.07	103
PLLA 250	250	2.5	35,700	35,200	41,000	1.05	244

[a]Determined by ^{1}H NMR spectroscopy, [b]Calculated from ([*L*-LA]$_0$/[BA] x conv. x (Molecular weight of *L*-LA) + (molecular weight of BA), [c]Determined by SEC analysis in $CHCl_3$ against polystyrene standards

Characterisation of PLLA 25 by ^{1}H NMR spectroscopy revealed the typical polymer profile expected for PLLA as seen in the literature by Csihony *et al*., (Figure 2.1).[47] The multiplet peak at δ = 7.33 ppm corresponds to the phenyl group on the chain end, thus confirming the successful polymerisation initiation from benzyl alcohol. The actual DP was calculated by comparison of the integration of the peak at δ = 7.33 ppm

with the integration of the shift for the methine proton next to the carbonyl on the polymer backbone at δ = 5.18 ppm. Varying the monomer: initiator ratio enabled the production of polymers with tuneable molecular weights (Table 2.1) and narrow $Đ_M$, approaching 1, as observed by SEC analysis (Figure 2.2).

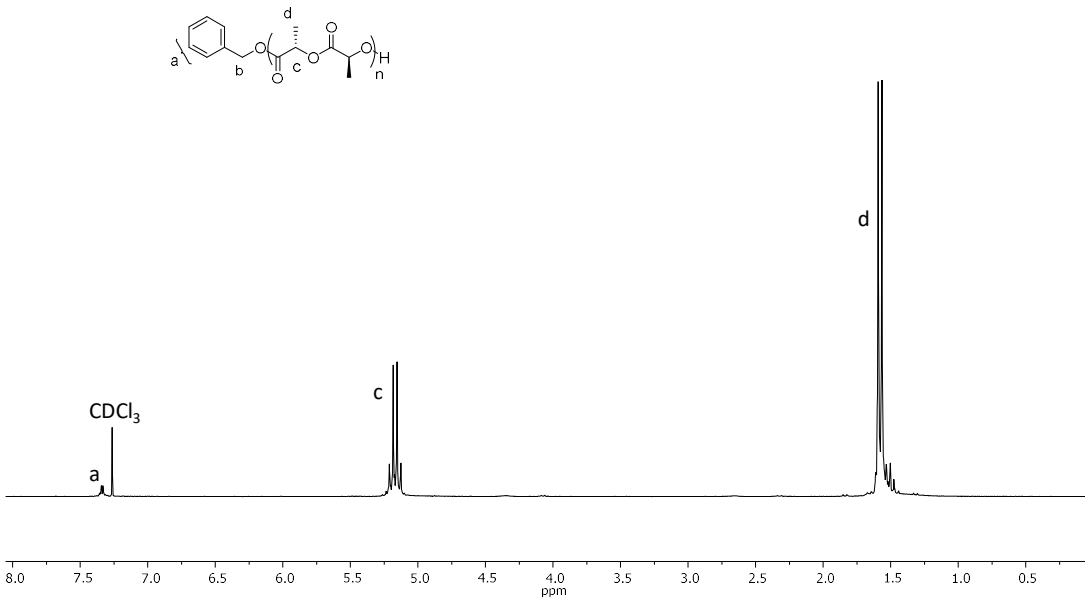

Figure 2.1: ^{1}H NMR spectrum of PLLA 25 ($CDCl_3$, 300 MHz)

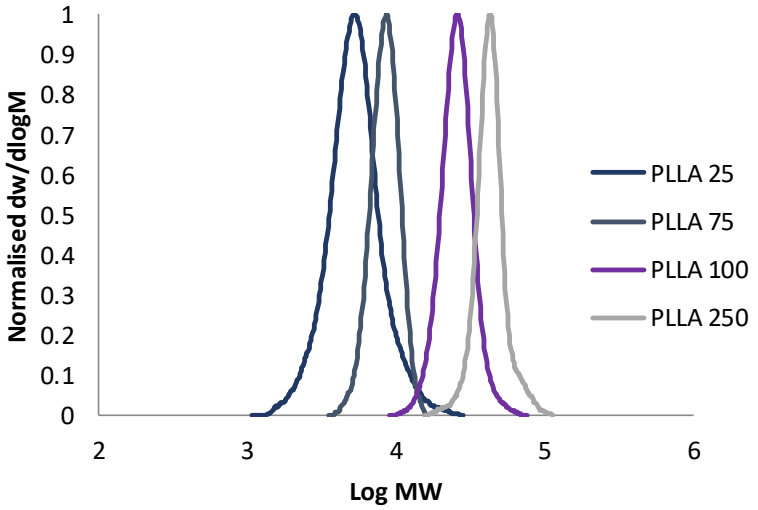

Figure 2.2: Normalised SEC traces for PLLA DP 25, 75, 100 and 250 ($CHCl_3$, polystyrene (PS) standards)

2.2.1.2 D, L-Lactide

The properties of PLA have been shown to be highly dependent on the polymer tacticity.[48] Consequently, it was interesting to investigate the effect of chirality on the resultant microparticle properties. Hence, PDLLA was synthesised using the same ROP conditions as PLLA (Section 2.2.1.1), including using a benzyl alcohol initiator and DBU (1 mol%) as catalyst (Scheme 2.3). As expected, similar polymerisation results were obtained as compared to PLLA (Table 2.2).

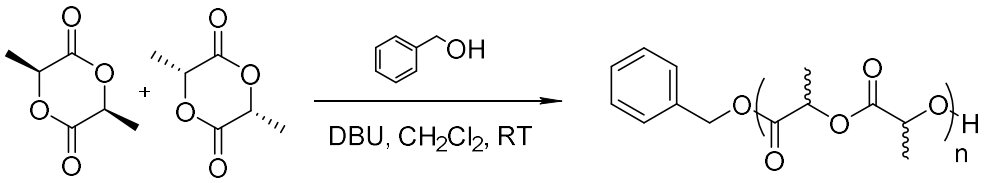

Scheme 2.3: Schematic representation of of ROP of *D, L*-LA at RT with DBU as a catalyst

Table 2.2: Characterisation data for polymerisation of PDLLA with varying [PDLLA]: [BA] ratio

Polymer	Target [M]/[I]	Time (h)	$^{a,b}M_{n\ theory}$ (g/mol)	$^{a}M_{n\ NMR}$ (g/mol)	$^{c}M_{n\ SEC}$ (g/mol)	$^{c}Đ_{M\ SEC}$	DP
PDLLA 25	25	0.25	3,500	3,000	5,600	1.10	21
PDLLA 75	75	0.75	7,700	11,100	13,200	1.06	77
PDLLA 100	100	1	13,800	13,800	21,400	1.08	95
PDLLA 250	250	2.5	35,400	35,700	36,000	1.14	247

[a]Determined by ^{1}H NMR spectroscopy, [b]Calculated from ([*D*, *L*-LA]$_0$/[BA] x conv. x (Molecular weight of *D*, *L*-LA) + (molecular weight of BA), [c]Determined by SEC analysis in $CHCl_3$ against PS standards

Analysis by ^{1}H NMR spectroscopy detailed the successful synthesis of PDLLA 25 (Figure 2.3), confirmed by the presence of the characteristic peaks for PDLLA as seen in literature.[49] The varying chirality observed with PDLLA results in the presence of both syndiotactic and isotactic proton environments, thus leading to an observed overlapping of the ^{1}H NMR resonances. Hence, the increased breadth of the methine resonance on the polymer backbone (δ = 5.18 ppm (Figure 2.3)), compared to the symmetric splitting pattern observed with PLLA (δ = 5.18 ppm (Figure 2.1)) confirms

the production of racemic PLA. Characterisation of the varying DP PDLLA polymers revealed the presence of monomodal traces with narrow $Đ_M$ (Figure 2.4).

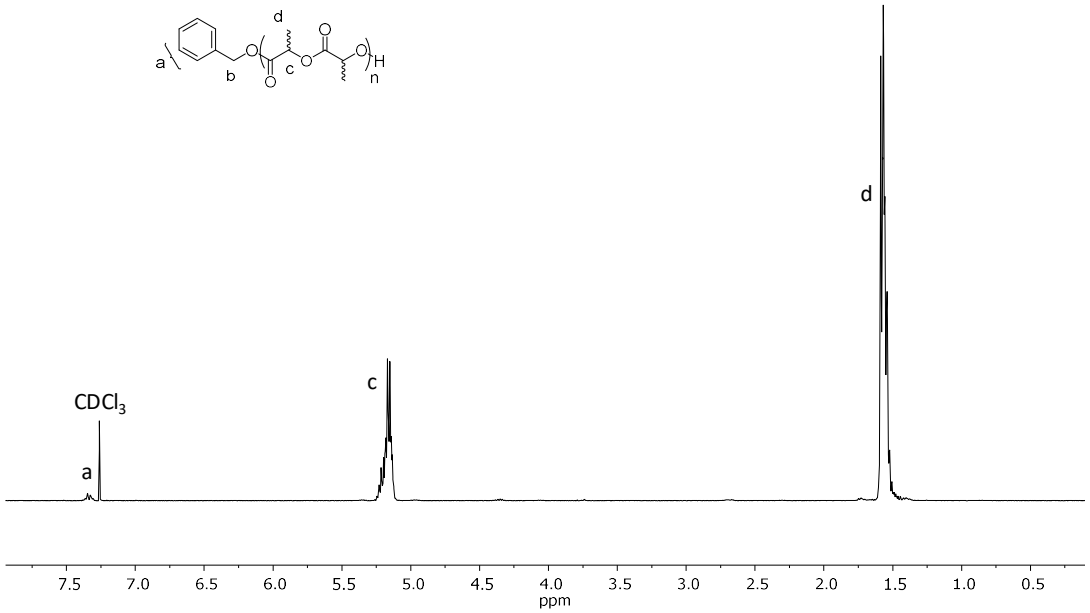

Figure 2.3: ^{1}H NMR spectrum of PDLLA 25 ($CDCl_3$, 300 MHz)

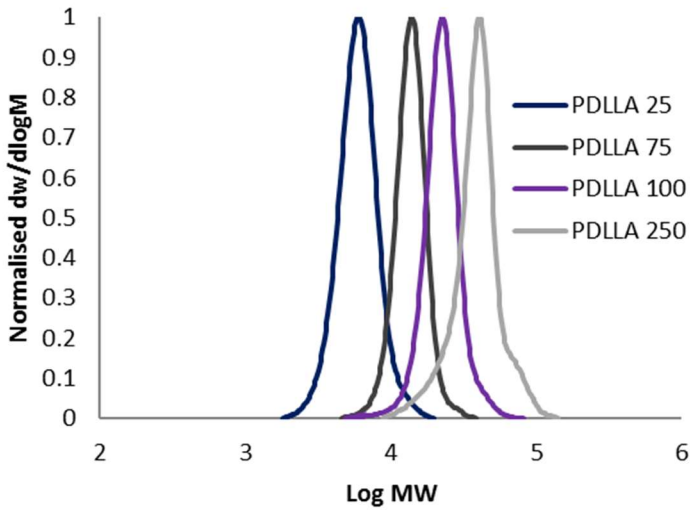

Figure 2.4: Normalised SEC traces for PDLLA DP 25, 75, 150 and 250 ($CHCl_3$, PS standard)

2.2.1.3 ε-Caprolactone

The ROP of ε-CL was performed in line with the procedure by Makiguchi *et al*. using a benzyl alcohol initiator and diphenylphosphate as a catalyst (DPP) in 1 M toluene (Scheme 2.4).[50] In order to fairly compare the effect of different monomers on polymer microparticle degradation and release rate, the same four DPs were targeted as for PLLA and PDLLA (DP 25, 75, 100 and 250) (Table 2.3).

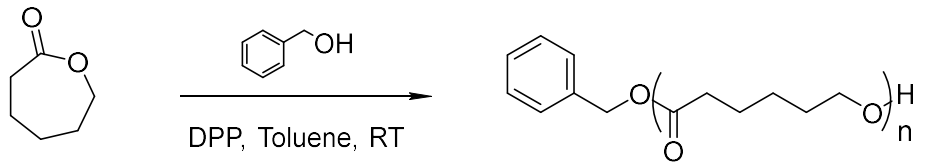

Scheme 2.4: Schematic representation of ROP of ε-CL with a BA initiator and DPP catalyst in 1 M toluene at RT

Table 2.3: Characterisation data for the polymerisation of ε-CL with a varying Monomer: BA initiator ratio in 1 M toluene at RT

Polymer	Target [M]/[I]	Time (h)	$M_{n\ theory}$ (g mol^{-1})[a,b]	$M_{n\ NMR}$ (g mol^{-1})[a]	$M_{n\ SEC}$ (g mol^{-1})[c]	$Đ_{M\ SEC}$[c]	DP
PCL 25	25	4	3,000	3,000	4,700	1.06	25
PCL 75	75	12	8,700	8,100	12,800	1.05	70
PCL 100	100	16	11,000	16,000	17,900	1.10	98
PCL 250	250	24	26,000	27,700	27,000	1.08	242

[a]Determined by ^{1}H NMR spectroscopy, [b]Calculated from ([ε-CL]$_0$/[BA] x conv. x (molecular weight of ε-CL) + (molecular weight of BA), [c]Determined by SEC analysis in $CHCl_3$ against PS standards

All of the polymerisations produced polymers with narrow $Đ_M$ and $M_{n\ NMR}$ close to the expected $M_{n\ theory}$ thus proving that good control over the polymerisation can be achieved for a range of molecular weights yielding polymers with high chain end fidelity. Signals corresponding to the methylene on the PCL polymer backbone were observed at δ = 4.06 ppm in the ^{1}H NMR spectrum, as demonstrated for PCL 25 (Figure 2.5), suggesting the successful polymerisation of the monomer. The singlet at δ = 5.11 ppm, representing the methylene on the chain end, could be easily distinguished and integrated, thus enabling calculation of the polymer DP. Further

characterisation of the polymer by SEC revealed that the polymers all have monomodal traces with narrow $Đ_M$ (Figure 2.6).

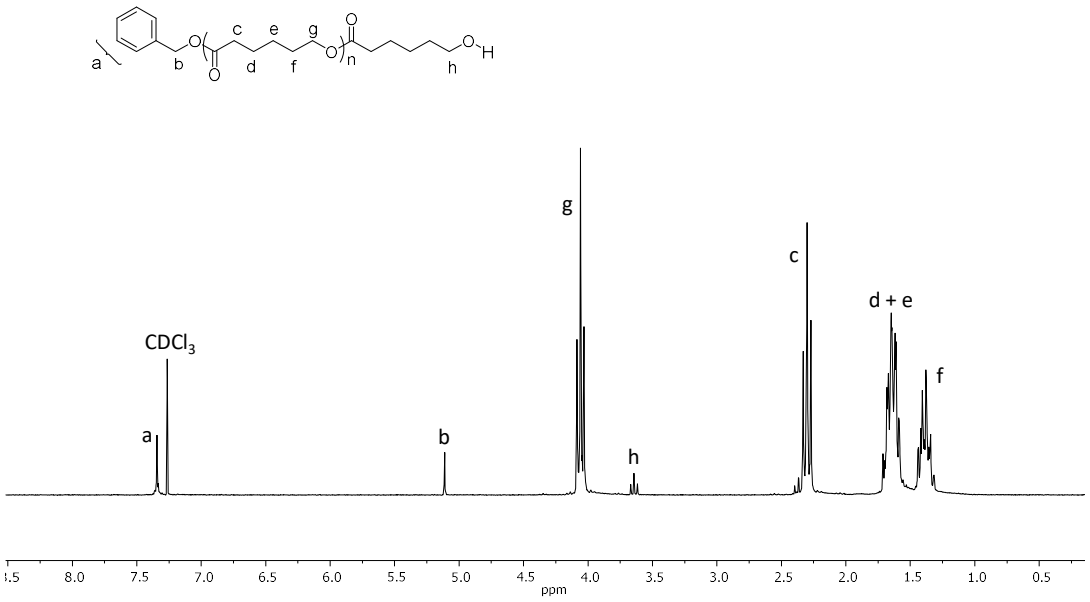

Figure 2.5: ^{1}H NMR spectrum of PCL 25 ($CDCl_3$, 300 MHz)

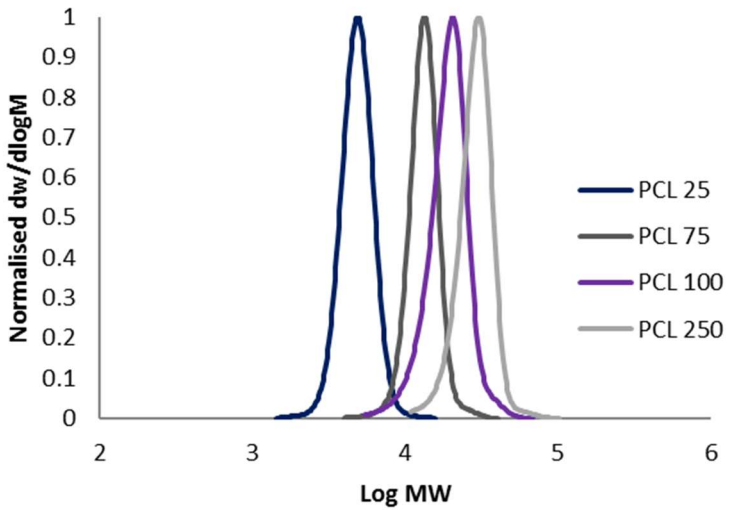

Figure 2.6: Normalised SEC traces for PCL DP 25, 75, 150 and 250 ($CDCl_3$, 300 MHz)

2.2.1.4 β-Butyrolactone

$Mg(BHT)_2(THF)_2$ has previously been studied for the polymerisation of εCL and more recently as a catalyst for the polymerisation of the cyclic macrolactone, ω-pentadecalactone (PDL).[24, 51] Hence, it was interesting to investigate the catalytic ability of $Mg(BHT)_2(THF)_2$ on a smaller, 4-membered ring lactone. The ROP of *β*-BL was performed in a 1 M solution of toluene at 80 ˚C using benzyl alcohol as an initiator and left to react overnight (Scheme 2.5). The polymer was purified by precipitation into excess methanol.

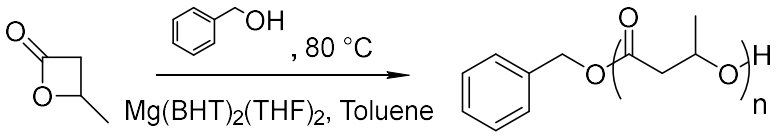

Scheme 2.5: Schematic representation of ROP of *β*-BL with $Mg(BHT)_2(THF)_2$ as a catalyst

The successful polymerisation of PHB was confirmed by ^{1}H NMR spectroscopy (Figure 2.7), thus allowing for the calculation of the DP through the ratio of the benzyl methylene resonance at δ = 5.11 ppm to the methylene resonance of the PHB at δ = 5.26 ppm (Figure 2.7). SEC characterisation of the polymer (Figure 2.8) confirmed the successful controlled polymerisation of PHB using $Mg(BHT)_2(THF)_2$. The dispersity measured by SEC was determined to be 1.15, which fits well with the observed narrow, monodisperse trace (Figure 2.8). Therefore, the catalytic activity of $Mg(BHT)_2(THF)_2$ for polymerisation of *β*-BL was investigated further.

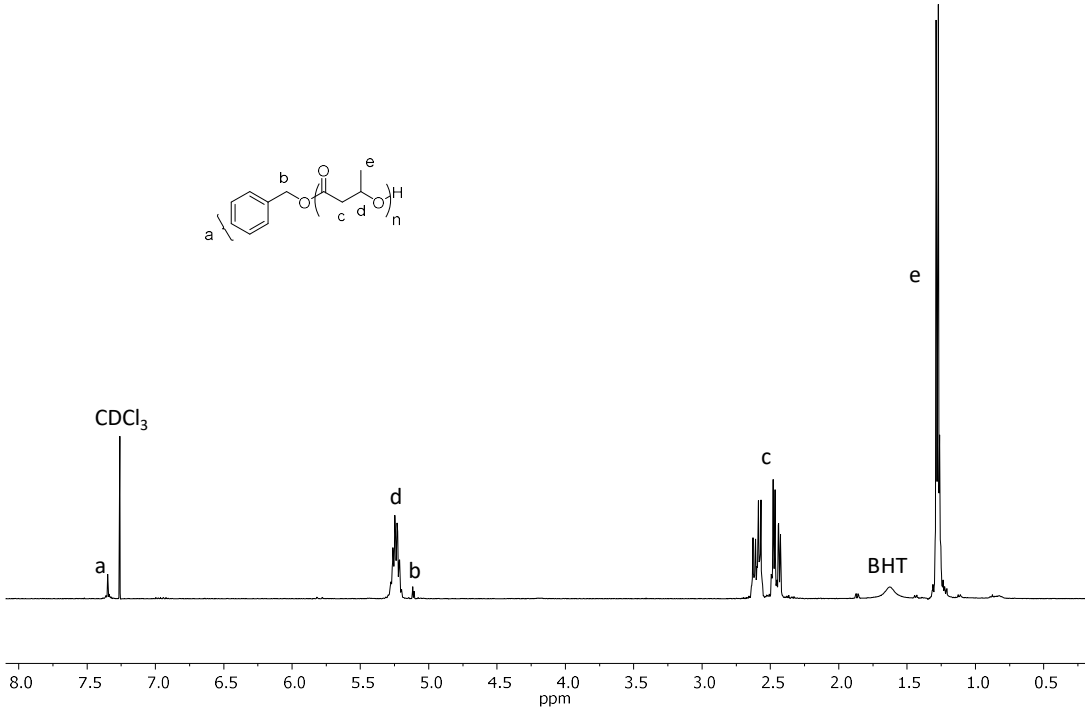

Figure 2.7: ^{1}H NMR spectrum of PHB 75 ($CDCl_3$, 300 MHz)

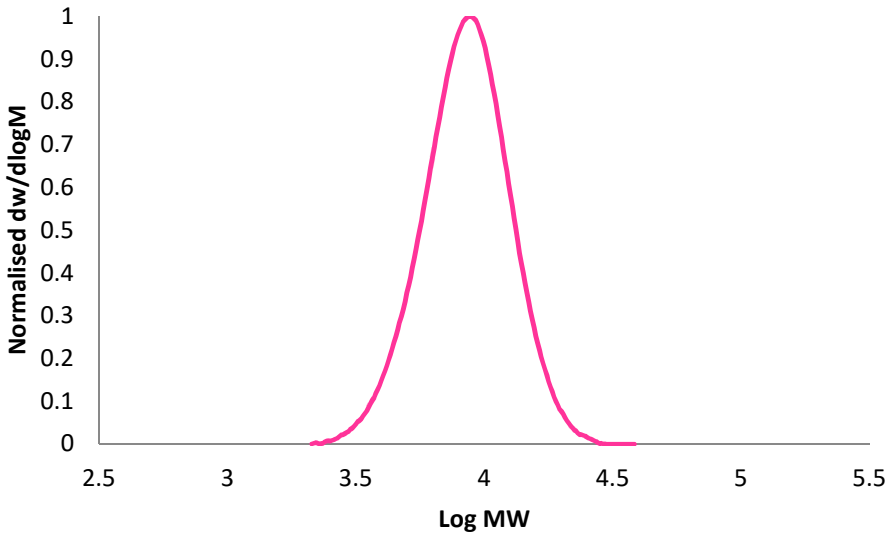

Figure 2.8: SEC characterisation of PHB 75 ($CHCl_3$, PS standards)

2.2.1.4.1 Catalytic Activity of $Mg(BHT)_2(THF)_2$ in the ROP of β-BL

Based on the polymerisation time of poly(ω-pentadecalactone) (PDL) reported by Wilson *et al*., the polymerisation kinetics were observed over a 15 h period.[51] Monomer conversion was monitored during the polymerisation using ^{1}H NMR spectroscopy *via* the disappearance of the methine monomer signal at δ = 4.7 ppm and the occurrence of the methine polymer signal at δ = 5.26 ppm, in good agreement with previous literature.[52]

Whilst monitoring the kinetics of the polymerisation of PHB using $Mg(BHT)_2(THF)_2$, it was observed that after 3 h the polymerisation had reached 40% conversion. However, the conversion did not increase further even after 8 h. The decreased reaction time compared to that observed for PDL was hypothesised to be a consequence of the smaller cyclic structure of *β*-BL compared to PDL. The smaller size of the ring means that *β*-BL has decreased flexibility and therefore, increased ring strain. Consequently, the polymerisation of *β*-BL is driven by the entropic gain of rotation from ring-opening rather than ring strain enthalpy, resulting in shorter reaction times. Therefore, the kinetic run was repeated over a shorter time period of 30 minutes and characterised by ^{1}H NMR spectroscopy and SEC (Table 2.4 and Figure 2.9).

Table 2.4: Kinetic analysis of polymerisation of PHB 100 with $Mg(BHT)_2(THF)_2$ with a 1:1 monomer:initiator ratio, at 1M in toluene over 30 min

Polymer	Time (min)	$M_{n\ theory}$[a,b] (g/mol)	$M_{n\ SEC}$[c] (g/mol)	$Đ_M$[c]	Conversion[a] (%)
1	6	2,300	3,600	1.17	26
2	12	2,800	4,500	1.16	31
3	18	3,000	4,400	1.17	34
4	24	3,400	4,900	1.15	38
5	30	3,600	5,600	1.14	40

[a]Determined by ^{1}H NMR spectroscopy, [b]Calculated from ($[\beta\text{-BL}]_0/[BA]$ x conv. x (molecular weight of β-BL) + (molecular weight of BA), [c]Determined by SEC analysis in $CHCl_3$ against PS standards

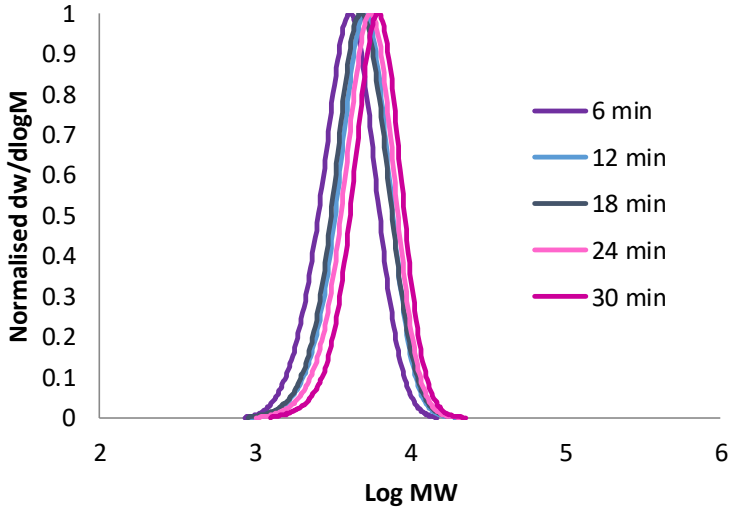

Figure 2.9: SEC of 2 M β-BL over 30 min at 80 ºC ($CHCl_3$, PS standards)

^{1}H NMR spectroscopy and SEC analysis revealed that the polymerisation had stopped within 30 minutes. The resultant SEC traces showed monodisperse traces, with no evidence of unwanted transesterification reactions. However, it was observed that the polymerisation only proceeded to a low monomer conversion of 40%. Therefore, with the aim to increase the total monomer conversion, the polymerisation conditions, such as temperature and the initial concentration of monomer and catalyst were varied systematically (Table 2.5).

Table 2.5: Characterisation data of PHB 100 after 30 min with varied polymerisation conditions

PHB	[M]	[M]:[I]:[Cat]	Temperature (°C)	Conversion[a] (%)	M_n (g/mol)[b]	$Đ_M$[b]
1	2 M	100:1:1	80	40	4,800	1.15
2	4 M	100:1:1	80	58	5,600	1.22
3	Bulk	100:1:1	80	48	2,800	1.45
4	2 M	100:0:1	80	2	-	-
5	2 M	100:1:5	80	40	1,800	1.37
6	2 M	100:1:1	RT	29	2,100	1.81
7	2 M	100:1:1	60	31	2,800	1.14
8	2 M	100:1:1	70	59	6,400	1.27
9	2 M	100:1:1	85	59	5,700	1.27

[a]Determined by ^{1}H NMR spectroscopy, [b]Determined by SEC analysis in $CHCl_3$ against PS standards

^{1}H NMR spectroscopy and SEC analysis of PHB with a range of polymerisation conditions revealed that even with increased monomer concentration and temperature, the conversion still only reached 40-60%. It was hypothesised that the catalyst could be competing with the benzyl alcohol to act as initiator, thus hindering its catalytic capabilities. However, ^{1}H NMR spectroscopy determined that only minimal conversion was evident after 30 minutes. Furthermore, even with an increased initial catalyst loading, (in the presence of benzyl alcohol initiator) a monomer conversion of 40% was attained with a broader dispersity of 1.37. Therefore, it was postulated that the catalyst was quenched during the polymerisation. To confirm this hypothesis, an extra aliquot of catalyst was added to PHB 1 (Table 2.5) after polymerisation for 30 min at 80°C. Subsequent ^{1}H NMR spectroscopy and SEC analysis revealed that the monomer conversion increased by 20%, whilst still maintaining the monodisperse SEC trace. Further investigation of the subsequent ^{1}H NMR spectrum revealed the characteristic shift for the alkenyl group of a crotonate at $\delta = 5.7$ ppm (Figure 2.10).[53] The crotonate occurs *via* α-deprotonation of the monomer during initiation, thus releasing water as a side product. It was hypothesised that the water released during

crotonate formation interacts with the Mg catalyst, thus diminishing its catalytic ability.

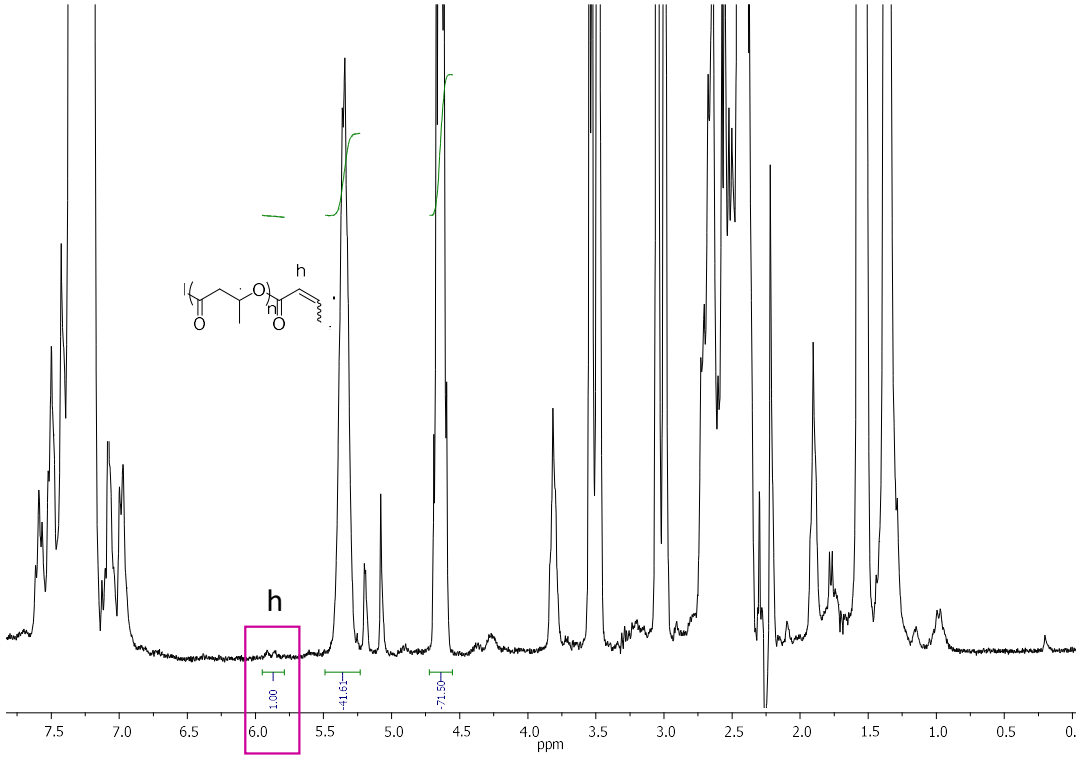

Figure 2.10: ^{1}H NMR spectrum showing crotonate formation during PHB 100 polymerisation with $Mg(BHT)_2(THF)_2$

2.2.1.4.2 Elucidation of the Mechanism of ROP of β-BL using $Mg(BHT)_2(THF)_2$

Ring opening of *β*-BL can occur *via* either acyl cleavage or alkyl cleavage (Scheme 2.6). Acyl cleavage results in the formation of an alkoxide chain end and is characteristic of a coordination-insertion mechanism. Conversely, alkyl cleavage is typical of an anionic mechanism and produces a carboxylate. Penczek *et al*. and Brulé *et al*. reported that diphenyl phosphoryl chloride (DPPCl) can be reacted with the ring opened polymer to yield a tetraphenoxydiphosphate with a carboxylate chain end or a phosphate in the presence of an alkoxide chain end. Subsequently, characterisation *via* ^{31}P NMR spectroscopy enables elucidation of the polymerisation mechanism.

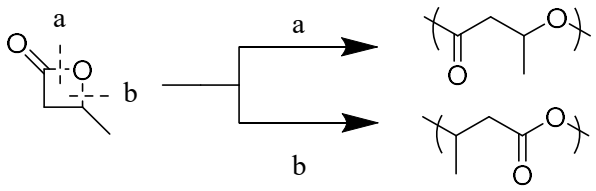

Scheme 2.6: Schematic representation of the two possible pathways for ring opening of β-BL

The polymerisation was performed at 2 M β-BL and was left at 80 °C for 30 minutes before adding an excess of DPPCl. ^{31}P NMR analysis revealed a shift at δ = -13 ppm, thus suggesting that the DPPCl had reacted with an alkoxide chain end to produce a phosphate (Figure 2.11). Therefore, it was postulated that the polymerisation proceeds *via* acyl cleavage, thus implying a coordination insertion mechanism.

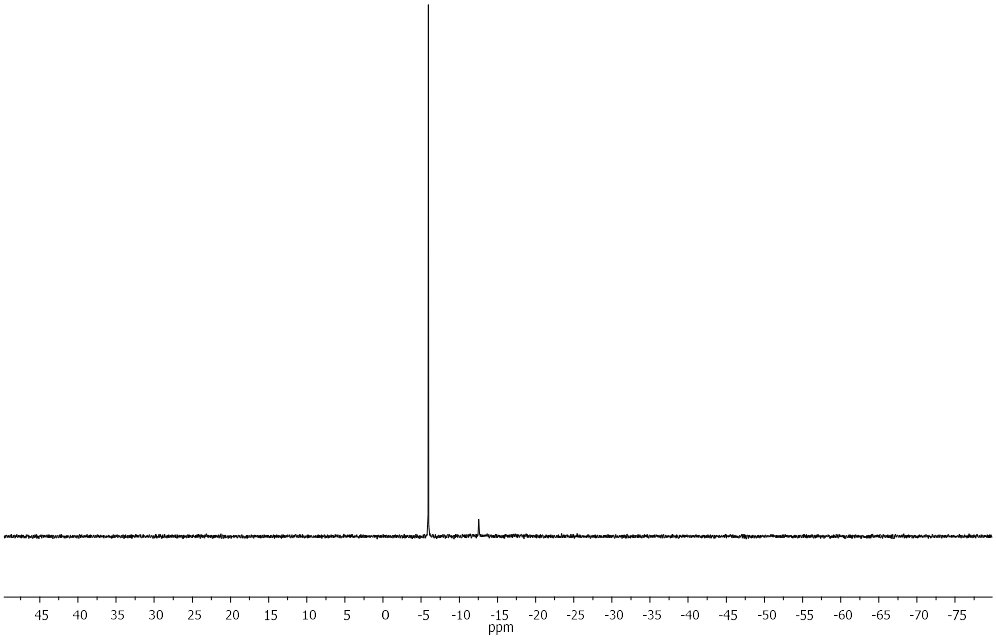

Figure 2.11: ^{31}P NMR spectrum of PHB after polymerisation with $Mg(BHT)_2(THF)_2$ for 30 minutes at 80 °C obtained after addition of excess DPPCl (δ = -5.94)

2.3 Microparticle Formation

The microparticles were synthesised using a simple solvent evaporation technique that requires the formation of a single oil in water emulsion. The creation of the emulsion was achieved *via* homogenisation of an organic phase, consisting of the polymer and active ingredient (AI) dissolved in dichloromethane and an aqueous phase containing Mowiol 488 (80% hydrolysed polyvinyl alcohol (PVA)) and water. In order to produce a high enough shear rate to create a stable emulsion, a Silverson high shear mixer was used. Many factors can affect the formation of the particles, therefore, before choosing the best polymer and molecular weight, the optimum parameters for particle preparation were investigated.

2.3.1 Varying Shear Time vs Particle Size

The application of a high shear mixer allows for the production of a fine emulsion. In order to do this, the active workhead contains rotor blades, which can undergo high speed rotation. The high speed rotation results in a powerful suction, which aims to pull solution from the base of the beaker into the centre of the workhead. The material is then forced to the periphery of the workhead by centrifugal force, where the solution is milled between rotor blades and the stator. This in turn forces the solution radially out of the workhead at high velocity, resulting in intense hydraulic shear. The radial motion allows for suction of fresh material, creating a circulating mixing cycle, thus minimising aeration by reducing the amount of turbulence felt by the surface of the liquid.

The shearing action produced by the mixer controls the particle size. Therefore, the particle size is highly dependent on solution viscosity, the concentration of polymer, the shear speed and the shear time. Consequently, the concentration of the polymer, the shear speed (7000 rpm) and the ratio of organic to aqueous phase were kept

constant, which enabled the investigation of shear time on particle size for PCL 25 microparticles with 1% PVA stabilizer.

a)

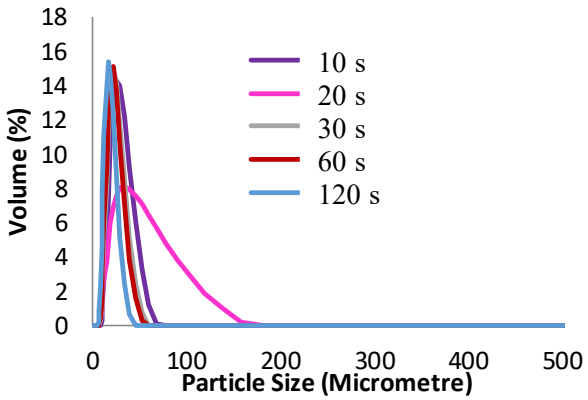

b)

Shear time (s)	Particle size (μm)	Dispersity
10	27	0.3
20	41	0.6
30	23	0.2
60	21	0.3
120	17	0.3

Figure 2.12: Light scattering characterisation of particle size versus shear time a) Plot of volume against particle size and b) Table showing resultant volume weighted mean particle size and dispersity

In order to investigate the effect of shear time on particle size, several batches of particles were prepared with varying shear times from 10 to 120 seconds. Dichloromethane was evaporated from the suspensions before characterising the particle size using a Malvern Mastersizer (Figure 2.12). As expected, the particle size decreases with increasing shear time. It was also observed that the lower shear times did not produce stable emulsions and furthermore, the particles formed after 10 seconds of shear seemed to settle and aggregate. This was postulated to be a consequence of the increased pull of gravity felt by the increased weight of the larger particles, at which point they are too heavy/ insufficiently stabilised by the concentration of PVA, that they either aggregate or break apart. Consequently, 30 seconds of shear was found to be the ideal conditions to create a stable emulsion, without over-shearing the particles.

2.3.2 Shear Speed Versus Time

Shear speed heavily influences the particle size and emulsion stability, therefore, four different shear speeds were investigated and the resultant microparticle suspensions were analysed *via* light scattering and optical microscopy. Each set of particles were prepared using 1 wt% PVA as stabiliser and were subjected to 30 s of shear before analysis.

a)

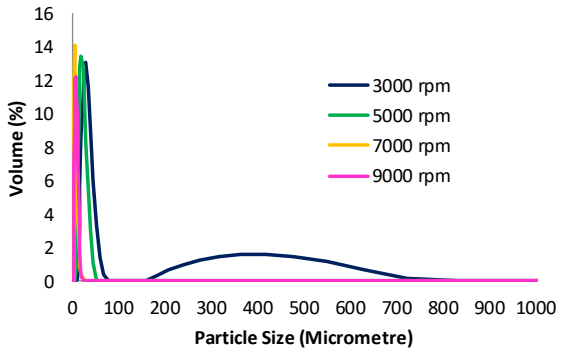

b)

Shear speed (rpm)	Particle size (μm)	Dispersity
3000	65	1.58
5000	20	0.3
7000	11	0.4
9000	7.4	0.4

Figure 2.13: Mastersizer analysis showing the size distribution of PCL 25 microparticles at varying shear speeds

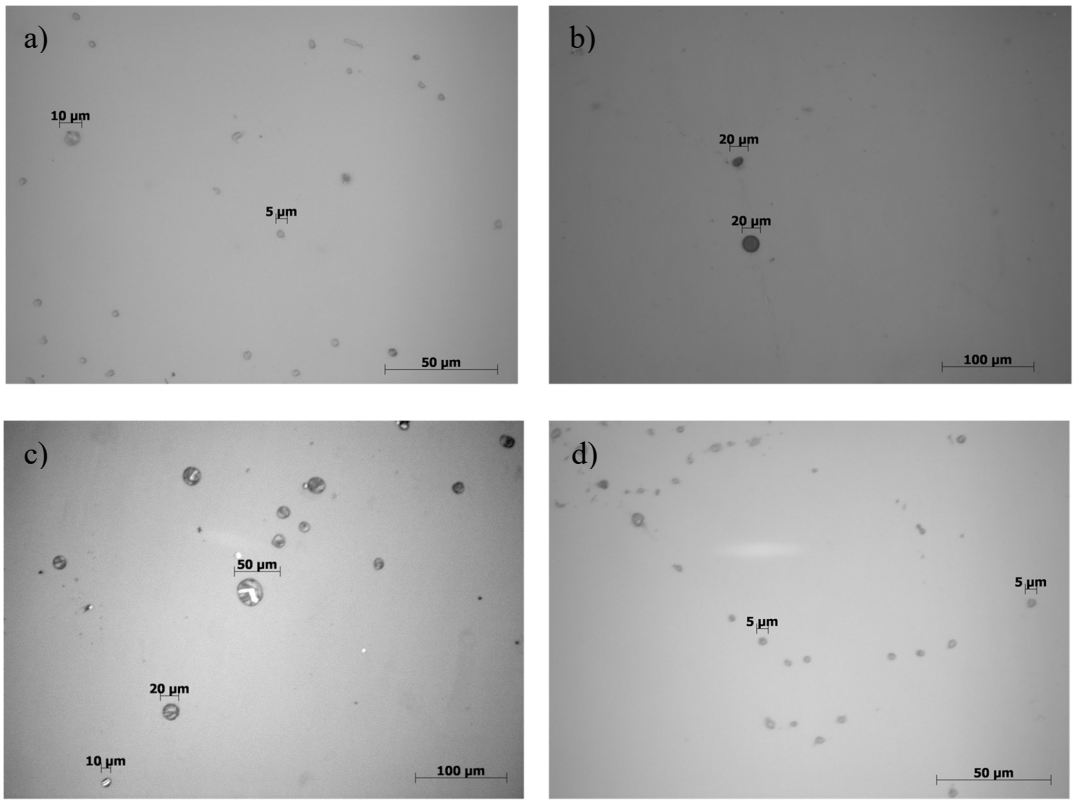

Figure 2.14: Optical microscopy images for PCL 25 microparticles after 30 s at a) 3000 rpm, b) 5000 rpm, c) 7000 rpm and d) 9000 rpm

As expected, Mastersizer analysis confirms that the particle size decreases with increasing shear speed (Figure 2.13). It was found that at 3000 rpm, the solid particles were unstable and started to aggregate. This was thought to be a result of the low shear speed, which was not high enough to emulsify the whole solution, consequently, an unstable emulsion was formed. Conversely, the optical microscopy image (Figure 2.14) displays particles below 10 µm. It is postulated that this is because the aggregates were larger, thus they had started to settle at the bottom of the vial, therefore, only the smaller particles were taken up in solution and analysed *via* microscopy. The particles formed at and above 5000 rpm form stable emulsions, however, in order to be comparable with previous microparticle projects performed by the industrial partner, Syngenta, the particles were aimed to be 10 µm in size. Therefore, at 5000 rpm the

particles were slightly too large and 9000 rpm too small, therefore, all of the particle formations were performed at 7000 rpm.

2.3.3 Particle Size Versus Stabiliser Concentration

After synthesis, the microparticles had a tendency to quickly settle whilst at 1% stabiliser. In fact, after just 15 minutes, the particles were highly unstable and had aggregated, resulting in the formation of large particles (> 1000 µm), as observed by light scattering analysis (Figure 2.15). Large clusters of particles were also observed *via* optical microscopy analysis, thus confirming particle aggregation (Figure 2.16).

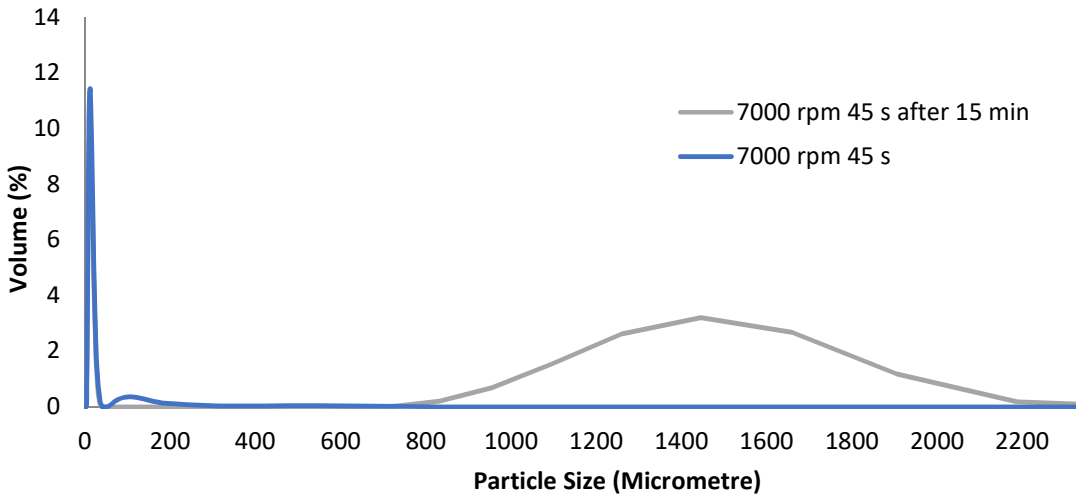

Figure 2.15: Mastersizer analysis showing change in size after 15 min Initial size: D[4, 3] = 10.5 µm, size after 15 min: D[4, 3] = 173 µm

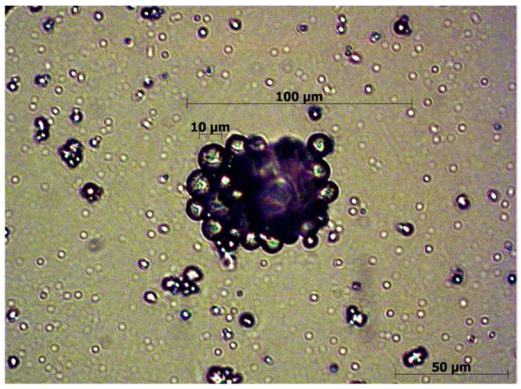

Figure 2.16: Optical microscopy images for microparticles after shear at 7000 rpm for 45 s left for 15 min

In order to accurately observe particle degradation and release, the particles are required to remain dispersed in solution, without aggregation. Therefore, to prevent the microparticles aggregating, varying stabiliser concentrations were investigated to try and stabilise the microparticle suspensions (Figure 2.17).

a)

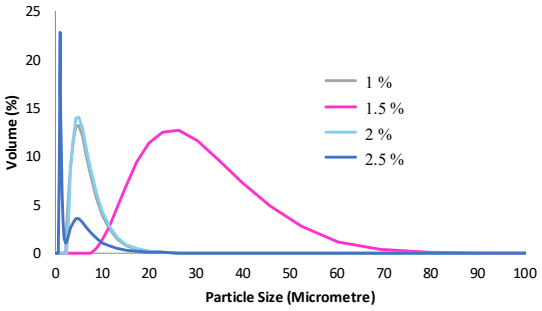

b)

[Stabiliser] (%)	Particle size (μm)	Dispersity
1	10	0.4
1.5	11	0.4
2	11	0.4
2.5	10	1.19

Figure 2.17: Mastersizer characterisation a) graphical analysis showing the change in particle size with varying [PVA] b) the change in volume weighted mean and particle size distribution with varying [PVA]

As expected, as the stabiliser concentration increased, the observed particle size distribution decreased. It was also found that at 1.5% PVA, the particles are less stable and have formed aggregates, evidenced by their larger dispersity within particle size. At a PVA concentration of 2%, the particles seemed to form microparticles with an average volume weighted mean of 11 μm and after subsequent analysis, it can be found that the particles are still stable and can be easily re-dispersed even after 36 h (Figure 2.18). Therefore, all subsequent analysis was performed using 2% PVA.

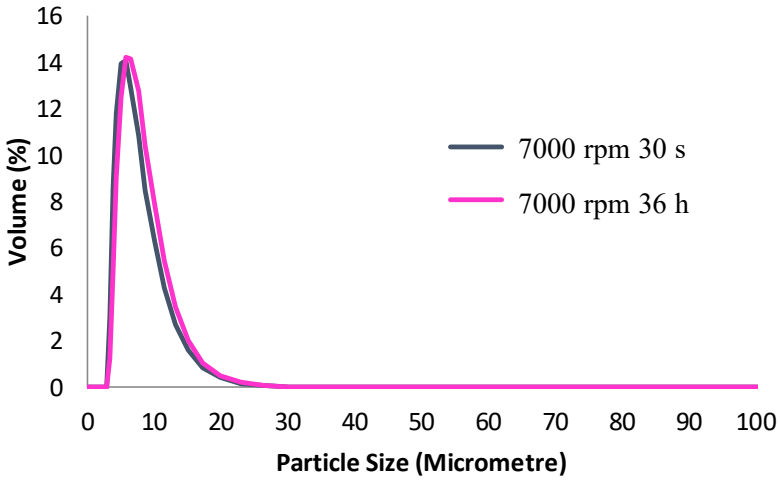

Figure 2.18: Mastersizer analysis showing PCL 25 microparticles initially and 36 h after emulsification at 7000 rpm for 30 s at 2% PVA

2.3.4 Temperature Effect on Particle Formation

After obtaining a stable emulsion, the solution was then transferred to a second flask with slow stirring to allow for complete evaporation of the organic solvent. As the solvent evaporates, the polymer starts to precipitate resulting in particle hardening. Therefore, the particle morphology and encapsulation behaviour is highly dependent on the volatility of the organic solvent and the rate of polymer precipitation.

The effect of temperature on particle size was investigated by varying the temperature during particle hardening. In order to do this, an emulsion using PCL 25 as the polymer was prepared and split into two separate batches. One batch was heated at 30 ˚C, whilst the other was kept at room temperature. Both solutions were left to stir overnight before characterising the particle size and morphology by light scattering and optical microscopy (Figure 2.19 and Figure 2.20 respectively).

a)

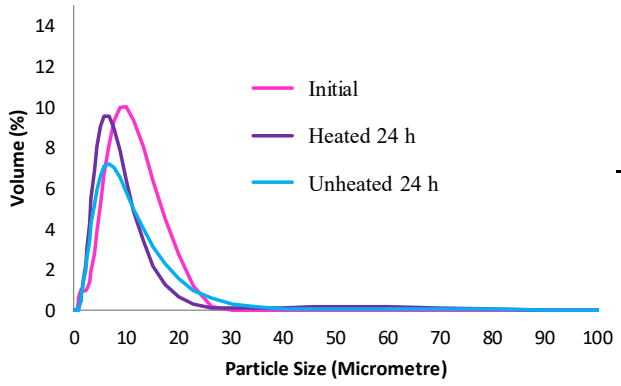

b)

Sample	Particle size (μm)	Dispersity
Initial	10	0.5
Heated 24 h	8	0.6
Unheated 24 h	59	9.0

Figure 2.19: Mastersizer characterisation a) graphical analysis showing the change in size distribution of particles whilst heated at 30 °C and unheated particles during particle hardening after 24 h a and b) table showing the change in volume weighted mean and particle size distribution

It was hypothesised that heating the particle solution would result in the dichloromethane evaporating at a quicker rate compared to the unheated particles, leading to decreased particle hardening time and thus larger particles. Light scattering analysis detailed that the heated microparticles shrink over time from 10 μm to 8 μm and increase in dispersity from 0.5 to 0.6 (Figure 2.19). This trend is as expected; the rapid solvent evaporation results in an increase in the rate of particle hardening, thus resulting in a broader particle size distribution. On the other hand, the unheated microparticles display an increase in volume weighted mean from 10 μm to 59 μm after 24 h. This is coupled with an increase in dispersity. Similarly to the heated particles, the unheated particles should also display a decrease in particle size during particle hardening, however, it was determined that the observed increase was a consequence of particle aggregation and broken particles. The broken particles can also be seen when characterising the suspension by optical microscopy (Figure 2.20) and confocal microscopy (Figure 2.21).

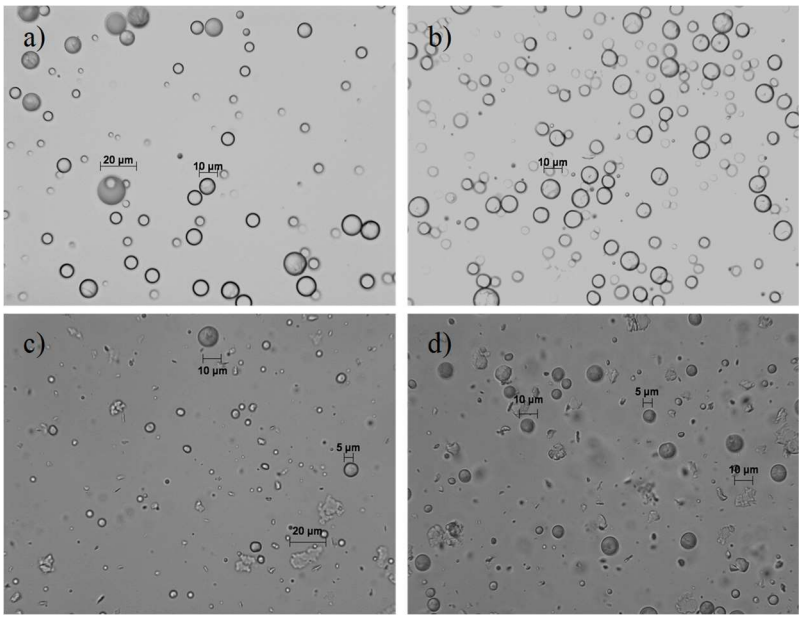

Figure 2.20: Optical microscopy images displaying the particle morphology of PCL 25 microparticles during particle hardening when heated for a) 2 h 30 and b) 24 h and unheated for c) 2 h 30 and d) 24 h

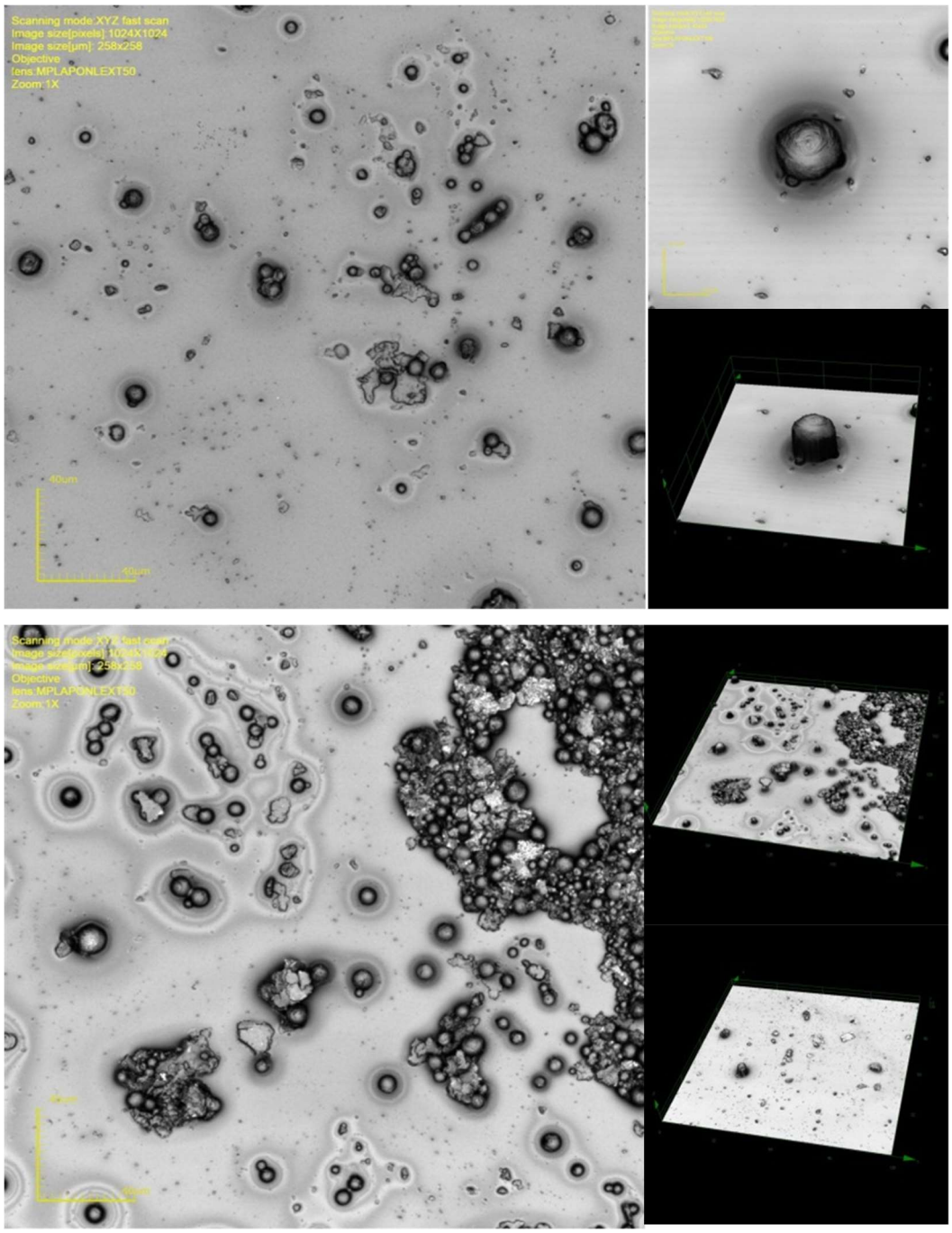

Figure 2.21: a) Confocal microscopy images for the heated PCL 25 after 24 h b) Confocal microscopy images for the unheated PCL 25 after 24 h

Before solvent evaporation, the particles are still soft and can be easily misshapen or broken. Whilst monitoring the effect of temperature on particle size, the solutions were stirred in round bottom flasks containing magnetic stirrer bars, however, it was postulated that the stirrer bars were causing the unhardened particles to break and fall apart before they could solidify, thus resulting in the formation of broken fragments

which could disrupt and affect the light scattering analysis. Therefore, for all subsequent particle hardening experiments, an overhead stirrer set on a low speed was used.

2.3.5 Molecular Weight Versus Particle Size

As the molecular weight and subsequently the length of the polymer chains increases, the molecules do not flow as easily in solution and therefore, the viscosity of the organic phase also increases. This increase in viscosity will therefore change the shear time required to achieve the desired 10 μm sized microparticles. Therefore, four emulsions of PCL particles were prepared using different molecular weight PCL. The subsequent particles were characterised by light scattering and optical microscopy (Figure 2.22 and Figure 2.23).

a)

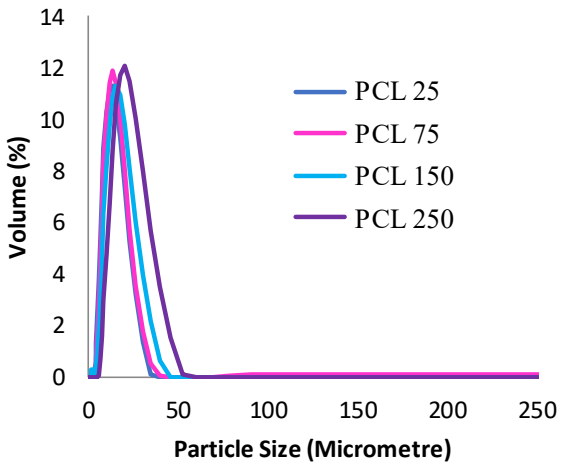

b)

PCL DP	Particle size (μm)	Dispersity
25	10	0.4
75	14	0.5
150	16	0.4
250	19	0.4

Figure 2.22: Mastersizer analysis of particles prepared by single oil-in-water emulsion using varying molecular weight PCL

As predicted, light scattering analysis revealed that as the molecular weight of the polymer increased, the particle size increased. The change in particle size with molecular weight was not as drastic as compared to when varying the shear time.

Furthermore, the change in particle size is not as evident *via* optical microscopy (Figure 2.23). However, for all molecular weights, no broken particles or aggregates were observed, thus suggesting that the emulsions were stable and had not been over-sheared.

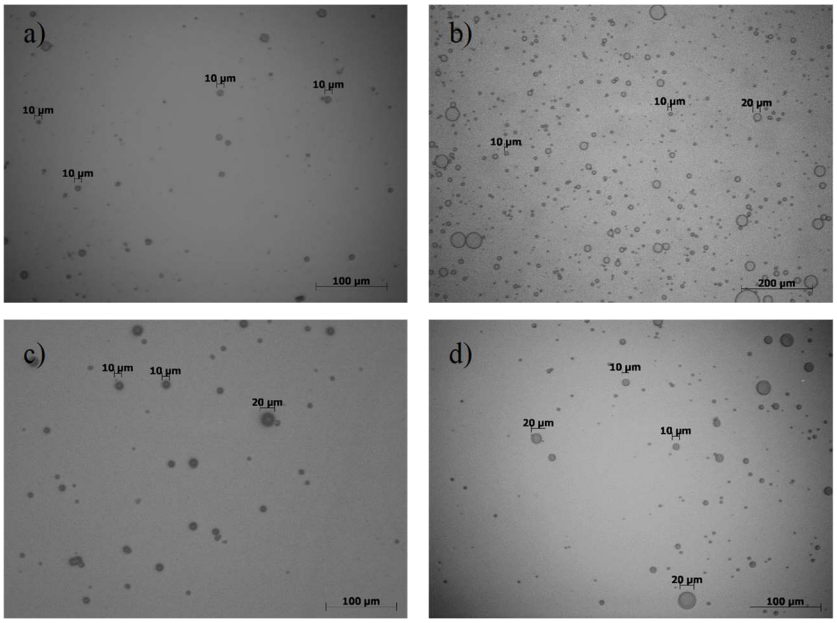

Figure 2.23: Optical microscopy images of a) PCL 25 b) PCL 75 c) PCL 100 and d) PCL 250

2.3.6 Varying Polymer

After the successful synthesis of varying molecular weight PCL microparticles, the same optimised emulsion conditions were investigated using PLLA, PDLLA and PHB. To accurately compare the resultant particle properties using the different polymeric systems, the emulsions were all prepared at the same concentration and conditions as for the optimised PCL 25 particles.

Table 2.6: Particle size of different polymeric emulsions determined by the volume weighted mean recorded *via* light scattering on the Mastersizer

Polymer DP[a]	Polymer Particle Size (μm)[b]			
	PLLA	PDLLA	PCL	PHB
25	12 ± 0.5	10 ± 0.3	10 ± 0.2	9 ± 0.2
75	15 ± 1.6	14 ± 0.6	14 ± 0.5	12 ± 1.2
100	15 ± 0.8	15 ± 0.5	16 ± 0.8	16 ± 0.6
250	19 ± 0.4	17 ± 0.7	19 ± 0.3	20 ± 1.6

[a]Determined by ^{1}H NMR spectroscopy, [b]Determined by volume weighted mean from light scattering analysis

All polymers display similar trends as previously seen with PCL, where the particle size increases as the molecular weight increases (Table 2.6). However, minimal change can be seen when varying between polymers. The particle morphology was determined *via* Scanning Electron Microscopy (SEM) (Figure 2.24).

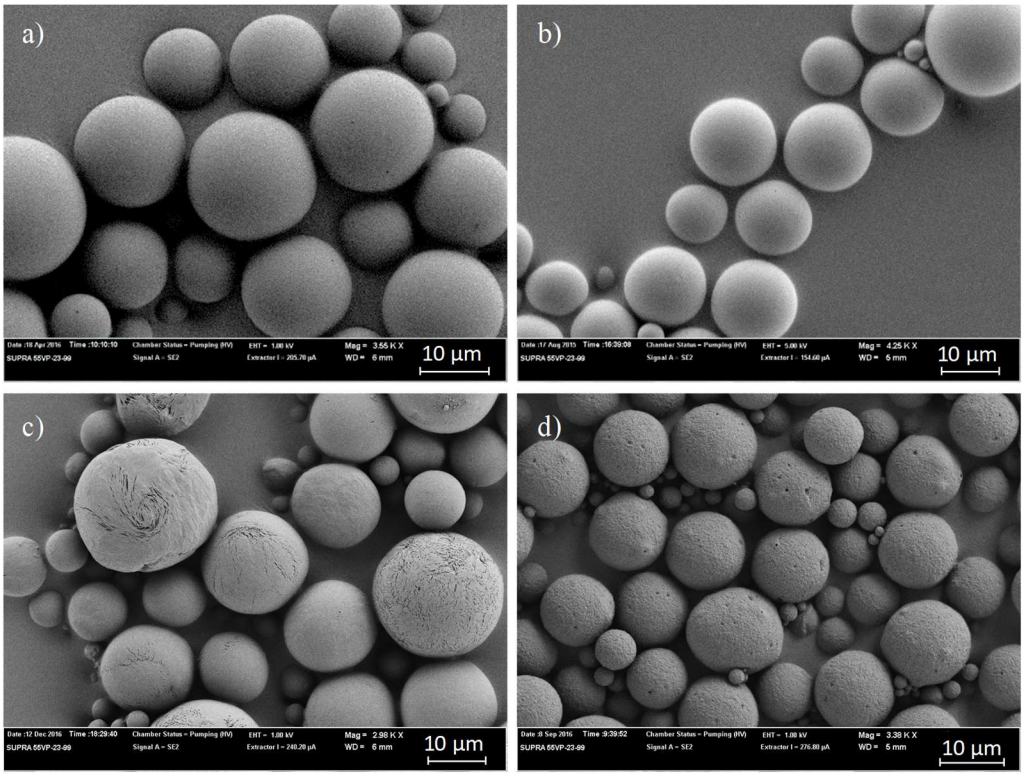

Figure 2.24: SEM analysis for a) PLLA 100 b) PDLLA 100, c) PCL 100 and d) PHB 100 polymeric particles

2.4 Conclusions

This chapter detailed the successful synthesis of biodegradable particles from polymers with a wide range of properties and molecular weights. Characterisation by ^{1}H NMR and SEC confirmed the successful ring opening polymerisation of PLLA, PDLLA and PCL using organocatalysts. The resulting polymers were proven to be well defined and exhibited low dispersity values and monomodal molecular weight distributions. Furthermore, the successful controlled polymerisation of PHB was reported for the first time using $Mg(BHT)_2(THF)_2$ as a catalyst. Investigation by ^{1}H NMR spectroscopy and SEC revealed that the molecular weight can be easily tuned whilst maintaining a monodisperse SEC trace, however, only a low conversion (ca. 40%) could be attained. This was postulated to be a consequence of crotonate formation during polymerisation. Therefore, it was hypothesised that the water released during crotonate formation reacted with the Mg catalyst thus reducing its catalytic capability. Reaction of the chain end with DPPCl allowed elucidation of the polymerisation mechanism *via* ^{31}P NMR spectroscopy. The DPPCl was found to react with an alkoxide chain end group producing a phosphate, which is characteristic of a coordination-insertion mechanism.

The well-defined polymers were utilised to synthesise 10 μm sized particles, prepared *via* a solvent evaporation technique. Characterisation by light scattering, optical microscopy and SEM detailed how the particle size was drastically altered by the shear time, shear speed and stabiliser concentration. Therefore, the particle size and stability were optimised by tuning the different variables, thus enabling the creation of a repeatable procedure for particle synthesis that can easily be applied to a wide variety of polymers and molecular weights.

These results illustrate the promising potential for degradable microparticles to be prepared from well-defined polymers with narrow molecular weight distributions, thus enabling further research into the tuneable time specific controlled degradation and release of agrochemicals.

2.5 References

1. R. Chandra and R. Rustgi, *Prog. Polym. Sci.*, 1998, **23**, 1273-1335.
2. A. K. Mohanty, M. Misra and G. Hinrichsen, *Macromol. Mater. Eng.*, 2000, **276-277**, 1-24.
3. D. Plackett, T. Løgstrup Andersen, W. Batsberg Pedersen and L. Nielsen, *Compos. Sci. Technol.*, 2003, **63**, 1287-1296.
4. L. S. Nair and C. T. Laurencin, *Prog. Polym. Sci.*, 2007, **32**, 762-798.
5. J. Rydz, W. Sikorska, M. Kyulavska and D. Christova, *Int. J. Mol. Sci.*, 2015, **16**, 564-596.
6. W. Sikorska, P. Dacko, M. Sobota, J. Rydz, M. Musioł and M. Kowalczuk, *Macromol. Symp.*, 2008, **272**, 132-135.
7. N. R. Washburn, C. G. Simon, A. Tona, H. M. Elgendy, A. Karim and E. J. Amis, *J. Biomed. Mater. Res.*, 2002, **60**, 20-29.
8. S. Karlsson and A.-C. Albertsson, *Polym. Eng. Sci.*, 1998, **38**, 1251-1253.
9. R. Grillo, A. d. E. S. Pereira, N. F. S. de Melo, R. M. Porto, L. O. Feitosa, P. S. Tonello, N. L. D. Filho, A. H. Rosa, R. Lima and L. F. Fraceto, *J. Hazard. Mater.*, 2011, **186**, 1645-1651.
10. N. Kamaly, B. Yameen, J. Wu and O. C. Farokhzad, *Chem. Rev.*, 2016, **116**, 2602-2663.
11. A. Roy, S. K. Singh, J. Bajpai and A. K. Bajpai, *Cent. Eur. J. Chem.*, 2014, **12**, 453-469.
12. S. Agarwal, *Polymer Science: A Comprehensive Reference*, Elsevier, Amsterdam, 2012.
13. G. Gallet, R. Lempiäinen and S. Karlsson, *Polym. Degrad. Stab.*, 2000, **71**, 147-151.
14. A. Noreen, K. M. Zia, M. Zuber, M. Ali and M. Mujahid, *Int. J. Biol. Macromol.*, 2016, **86**, 937-949.
15. S. K. Sahoo, A. K. Panda and V. Labhasetwar, *Biomacromolecules*, 2005, **6**, 1132-1139.
16. H. Pranamuda, Y. Tokiwa and H. Tanaka, *Appl. Environ. Microbiol.*, 1997, **63**, 1637-1640.
17. D. Rasselet, A. Ruellan, A. Guinault, G. Miquelard-Garnier, C. Sollogoub and B. Fayolle, *Eur. Polym. J.*, 2014, **50**, 109-116.

18. D.-M. Abou-Zeid, R.-J. Müller and W.-D. Deckwer, *J. Biotechnol.*, 2001, **86**, 113-126.
19. F. Faÿ, E. Renard, V. Langlois, I. Linossier and K. Vallée-Rehel, *Eur. Polym. J.*, 2007, **43**, 4800-4813.
20. C. Jérôme and P. Lecomte, *Adv. Drug Delivery Rev.*, 2008, **60**, 1056-1076.
21. S. M. Guillaume, E. Kirillov, Y. Sarazin and J.-F. Carpentier, *Chem. Eur. J.*, 2015, **21**, 7988-8003.
22. U. H. Choi, A. Mittal, T. L. Price, R. H. Colby and H. W. Gibson, *Macromol. Chem. Phys.*, 2016, **217**, 1270-1281.
23. J. Ling, X. Wang, L. You and Z. Shen, *J. Polym. Sci. Part A: Polym. Chem.*, 2016, **54**, 3012-3018.
24. H.-J. Fang, P.-S. Lai, J.-Y. Chen, S. C. N. Hsu, W.-D. Peng, S.-W. Ou, Y.-C. Lai, Y.-J. Chen, H. Chung, Y. Chen, T.-C. Huang, B.-S. Wu and H.-Y. Chen, *J. Polym. Sci. Part A: Polym. Chem.*, 2012, **50**, 2697-2704.
25. Y. Wang and M. Kunioka, *Macromol. Symp.*, 2005, **224**, 193-206.
26. A. Kumar, K. Garg and R. A. Gross, *Macromolecules*, 2001, **34**, 3527-3533.
27. C. G. Jaffredo, J.-F. Carpentier and S. M. Guillaume, *Macromolecules*, 2013, **46**, 6765-6776.
28. F. Nederberg, E. F. Connor, M. Möller, T. Glauser and J. L. Hedrick, *Angew. Chem. Int. Ed.*, 2001, **40**, 2712-2715.
29. K. S. Bisht, L. A. Henderson, R. A. Gross, D. L. Kaplan and G. Swift, *Macromolecules*, 1997, **30**, 2705-2711.
30. L. Zhang, X. Deng and Z. Huang, *Biotechnol. Lett.*, 1996, **18**, 1051-1054.
31. W.-J. Lin, D. R. Flanagan and R. J. Linhardt, *Polymer*, 1999, **40**, 1731-1735.
32. D. Wang, O. Molavi, M. E. C. Lutsiak, P. Elamanchili, G. S. Kwon and J. Samuel, *J. Pharm. Pharm. Sci.*, 2007, **10**, 217-230.
33. B. Han, X. Wang, X. Gao, J. Liu, F. Liang, X. Qu and Z. Yang, *J. Biomed. Mater. Res. Part B Appl. Biomater.*, 2011, **99B**, 120-126.
34. C. Berkland, K. Kim and D. W. Pack, *J. Controlled Release*, 2001, **73**, 59-74.
35. C. Berkland, E. Pollauf, D. W. Pack and K. Kim, *J. Controlled Release*, 2004, **96**, 101-111.
36. J. A. Champion, Y. K. Katare and S. Mitragotri, *J. Controlled Release*, 2007, **121**, 3-9.

37. V.-T. Tran, J.-P. Benoît and M.-C. Venier-Julienne, *Int. J. Pharm.*, 2011, **407**, 1-11.
38. J. Wang and S. P. Schwendeman, *J. Pharm. Sci.*, 1999, **88**, 1090-1099.
39. H. Rafati, A. G. A. Coombes, J. Adler, J. Holland and S. S. Davis, *J. Controlled Release*, 1997, **43**, 89-102.
40. Y. Capan, B. H. Woo, S. Gebrekidan, S. Ahmed and P. P. DeLuca, *J. Controlled Release*, 1999, **60**, 279-286.
41. J. M. Péan, M. C. Venier-Julienne, R. Filmon, M. Sergent, R. Phan-Tan-Luu and J. P. Benoit, *Int. J. Pharm.*, 1998, **166**, 105-115.
42. K. Makino, T. Mogi, N. Ohtake, M. Yoshida, S. Ando, T. Nakajima and H. Ohshima, *Colloids Surf. B Biointerfaces*, 2000, **19**, 173-179.
43. E. R. Kenawy, D. C. Sherrington and A. Akelah, *Eur. Polym. J.*, 1992, **28**, 841-862.
44. E. V. R. Campos, J. L. de Oliveira, L. F. Fraceto and B. Singh, *Agron. Sustain. Dev.*, 2015, **35**, 47-66.
45. M. W. Aktar, D. Sengupta and A. Chowdhury, *Interdisc. Toxicol.*, 2009, **2**, 1-12.
46. B. G. G. Lohmeijer, R. C. Pratt, F. Leibfarth, J. W. Logan, D. A. Long, A. P. Dove, F. Nederberg, J. Choi, C. Wade, R. M. Waymouth and J. L. Hedrick, *Macromolecules*, 2006, **39**, 8574-8583.
47. S. Csihony, D. A. Culkin, A. C. Sentman, A. P. Dove, R. M. Waymouth and J. L. Hedrick, *J. Am. Chem. Soc.*, 2005, **127**, 9079-9084.
48. M. J. Stanford and A. P. Dove, *Chem. Soc. Rev.*, 2010, **39**, 486-494.
49. P. Horeglad, A. Litwińska, G. Z. Żukowska, D. Kubicki, G. Szczepaniak, M. Dranka and J. Zachara, *Appl. Organomet. Chem.*, 2013, **27**, 328-336.
50. K. Makiguchi, T. Satoh and T. Kakuchi, *Macromolecules*, 2011, **44**, 1999-2005.
51. J. A. Wilson, S. A. Hopkins, P. M. Wright and A. P. Dove, *Polym. Chem.*, 2014, **5**, 2691-2694.
52. C. G. Jaffredo, J.-F. Carpentier and S. M. Guillaume, *Macromol. Rapid Commun.*, 2012, **33**, 1938-1944.
53. Z. Jedlinski, M. Kowalczuk and P. Kurcok, *Macromolecules*, 1991, **24**, 1218-1219.

3. Model Encapsulation and Release of a Fluorophore Using Biodegradable Microparticles

3.1 Introduction

Since the first reported use of an insecticide over 4,500 years ago, agrochemicals have revolutionised the agricultural industry.[1] Encapsulation of the agrochemical can serve to protect the active ingredient (AI) from harsh environmental conditions, reduce its loss through volatilisation and leaching and also act to reduce any associated toxicity of the encapsulated material.[2-4] By encapsulating the AI into the matrix of a biodegradable microparticle, this enables the controlled release of the agrochemical to the desired target as the particle degrades.[5] Therefore, the substance can be slowly and continuously released for up to several years.

There are four key mechanisms of biomaterial degradation; hydrolytic degradation, enzymatic degradation, oxidative degradation and physical degradation.[6] Polyesters are well known to be susceptible to hydrolytic degradation (Scheme 3.1).[7-10] Moreover, Untereker *et al*. have shown that the hydrolytic degradation of polyesters occurs *via* random scission of the hydrolysable ester bonds.[11] This in turn results in the formation of low molecular weight non-toxic species, which can be absorbed by microorganisms in the soil.[12-16] In particular, PLA has received a lot of attention as a consequence of its excellent biocompatibility and biodegradability.[16] Polymerisation of stereopure *L*-lactide enables the production of highly crystalline isotactic polymers.[17] Hydrolysis of the isotactic poly(*L*-lactide) results in the formation of lactic acid, which can be found naturally in the soil as a consequence of the presence of lactic acid producing bacteria.[18] The presence of lactic acid producing bacteria within soil has been shown to be highly advantageous as they can act to preserve vegetable products, to inhibit microorganisms responsible for spoilage and to treat cattle manures and sewage for odour abatement.[19]

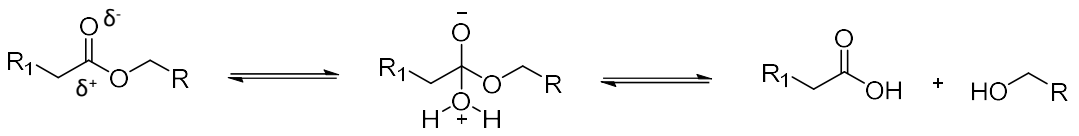

Scheme 3.1: Schematic representation of the hydrolysis of an ester bond.[6]

As a consequence of their biodegradable nature, polyesters have been shown to be the ideal materials for use as a microparticle matrix.[20, 21] PLGA particles prepared by oil-in-water solvent evaporation have been shown to display bulk degradation properties characteristic of degradation of the PLA polymer.[22] Furthermore, during particle degradation, diffusion of the degradation products is limited throughout the particle matrix.[23] Therefore, the increased quantity of degradation products creates pockets of decreased pH within the particle, thus leading to autocatalyzed degradation of the microparticle enabling a controlled release of the encapsulated substance.[24, 25] Ideally, the optimum release profile would display a constant release over time.[26] However, it is well reported that release profiles are more complex and often contain two main expulsion processes.[27]

1) Initial Burst: Where the contained AI is expelled from the particle surface.
2) Constant Release: This stage is dependent on both diffusion and degradation.

Particle synthesis *via* solvent evaporation requires the removal of a volatile organic solvent from an oil in water emulsion to form solid polymer particles. Consequently, as the solvent evaporates, the encapsulated AI diffuses to the particle edge, therefore, an initial burst release is particularly prominent in reports of particles prepared by solvent evaporation.[28] Currently, there are commercially available micro-encapsulated products that aim to achieve slow release effects used within the crop protection market, in particular Stomp Aqua (BASF), Samurai II CS Insecticide (J. Oliver Products) and Force (Syngenta).[29-32] However, only limited research has been done

into biodegradable particle degradation and release of an AI in environmental conditions.

In order to achieve a tuneable agrochemical release rate, a method for monitoring the the particle degradation and subsequent release was required. Consequently, to quantitatively monitor AI release, a model fluorescent dye was encapsulated. Furthermore, encapsulation of a hydrophobic dye allowed the change in fluorescence intensity to be monitored as the particles degraded and the fluorophore was released. To simulate a representative model for environmental degradation, specific focus in this Chapter is based on degradation and release from poly(*L*-lactide) (PLLA) in a variety of degradation media.

3.2 Encapsulation

Before encapsulation and release of an AI, it is crucial to determine information about the microparticle dye loading, degradation and release rate. Therefore, in order to quantify these parameters, a study was undertaken looking into the encapsulation of a fluorescent dye. Microparticles were synthesised according to the optimised single oil-in-water solvent evaporation technique detailed in Chapter 2, directly dissolving the dye with the polymer in dichloromethane.

3.2.1 Encapsulation of Rhodamine B

Rhodamine B (5 wt%) was easily dissolved with poly(*L*-lactide) DP 100 (PLLA 100) into the dichloromethane organic phase, before shearing for 30 s at 7000 rpm with an aqueous phase (containing Mowiol 488 (PVA) as a stabiliser). A sample of the Rhodamine B containing microparticle solution was taken and compared to a known concentration of Rhodamine B in water and the absorbance difference determined using UV/Vis spectroscopy, (Figure 3.1).

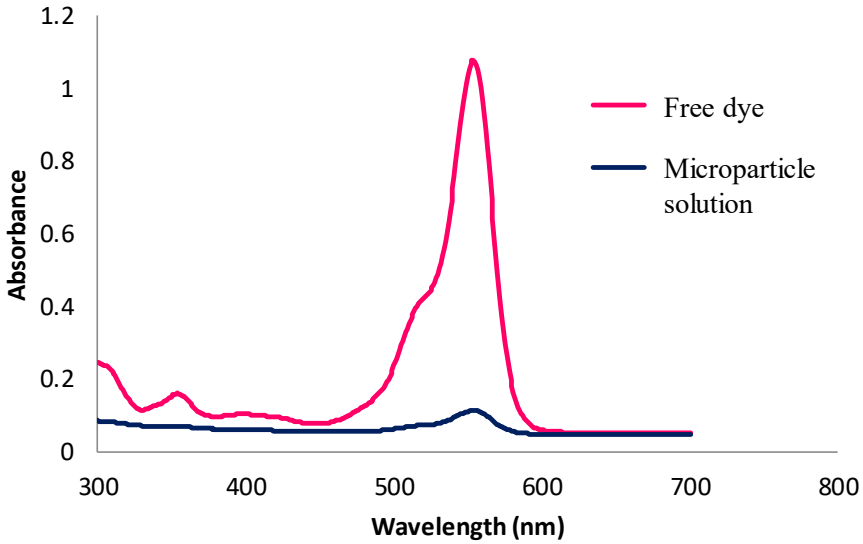

Figure 3.1: UV/Vis spectrum showing absorbance for free Rhodamine B and a sample of the solution after encapsulation into PLLA 100 microparticles

The initial encapsulation of Rhodamine B based on UV-Vis absorbance was determined to be 89.5%. After the promising initial results, a second experiment was performed to elucidate a direct calculation of the quantity of fluorescent proxy encapsulated in the particles. In order to do this, the microparticles were washed three times with deionised water to remove any excess dye before being fully dissolved in dichloromethane. However, subsequent UV-Vis spectroscopy characterisation revealed that the hydrophilic dye diffused out of the microparticles into the aqueous phase during particle washing. Therefore, it was proposed that the microparticles were unable to contain hydrophilic agrochemicals using the single oil-in-water emulsion technique.

3.2.2 Encapsulation of Nile Red

Nile red is a highly fluorescent hydrophobic dye that can be used as a lipophilic stain (Figure 3.2).[33] Therefore, it was predicted that the Nile red would either encapsulate in the particles or precipitate into the surrounding water, thus enabling its use as a suitable dye for a long-term stability study. The microparticles were prepared using the same single oil-in-water emulsion technique as previous, but with incorporation of Nile red (1 wt%) with PLLA 100 in the organic phase. The suspensions were stirred with overhead stirring overnight to enable evaporation of dichloromethane. The particle suspensions appeared pink and were characterised by optical microscopy (Figure 3.3).

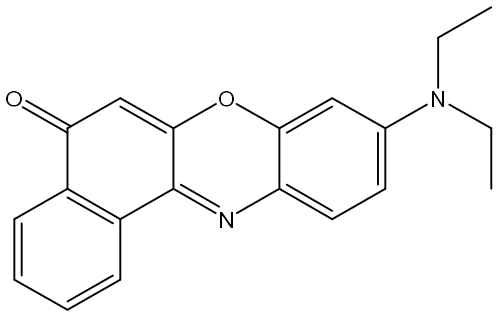

Figure 3.2: Chemical structure of Nile red

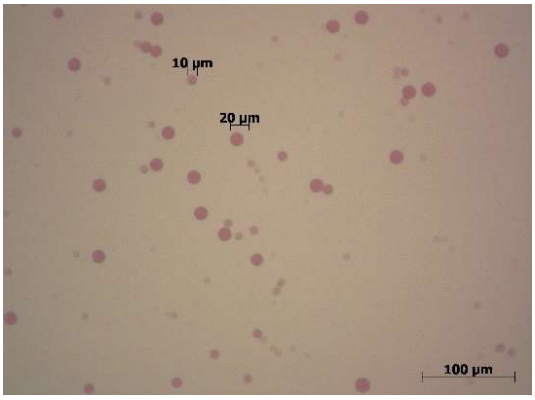

Figure 3.3: Optical microscope image of PLLA DP 100 microparticles with 1 wt% encapsulated Nile red

The particle size was characterised *via* light scattering analysis using a Malvern Mastersizer (Figure 3.4). Light scattering characterisation revealed that the particle size was not affected by the addition of Nile red in the organic phase, which suggested that the small molecular structure of the dye did not drastically affect the viscosity of the emulsion. However, a shoulder could be seen at increased particle size, suggesting the presence of larger particles in the solution. This was postulated to be a consequence of large crystals or clusters of free dye present in solution.

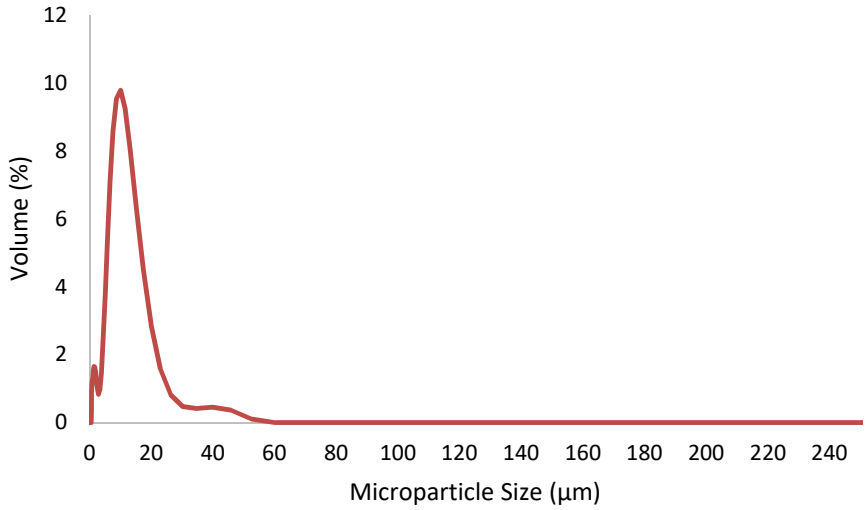

Figure 3.4: Light Scattering analysis of PLLA 100 microparticles containing Nile red (1 wt%)

In order to quantify the concentration of free dye in solution, the dye loading of Nile red within the PLLA microparticles was characterised using a fluorescence plate reader (Figure 3.5). The PLLA 100 particles were washed three times in DI water before being dissolved in dichloromethane. The subsequent fluorescence intensity was compared to the fluorescence intensity of a calibration of six known concentrations of Nile red in dichloromethane. Analysis of the fluorescence intensity determined a very high loading efficiency of 99% (Figure 3.5).

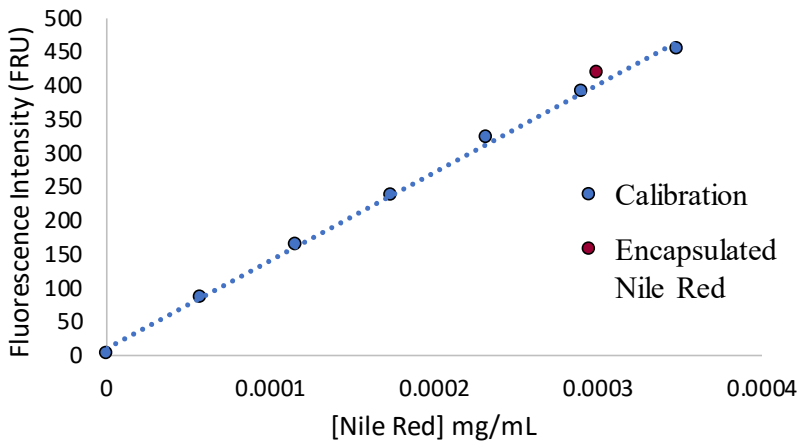

Figure 3.5: Fluorescence intensity of encapsulated Nile red compared to known standards of varying [Nile red]

3.2.2.1 Controlled Release of Nile Red

To determine the agrochemical release rate during particle degradation, a method for monitoring the agrochemical release was required. The hydrophobic nature of the dye prevented direct sampling of the fluorescence intensity of the aqueous solution over time. Therefore, an aliquot of the microparticle suspension was added to a 50:50 ethanol: water solution and the subsequent dye release monitored *via* fluorometry. This allowed for the extraction of the dye from the particles *via* diffusion of the dye into the ethanolic solution. It was hypothesised that a high fluorescence intensity would signify a fast, uncontrolled release from the particles, whereas successful encapsulation would provide a slow release over a longer period. As a reference, the change in fluorescence intensity of a sample of free dye was monitored over a period of five hours using a plate reader with filters at excitation 390 nm and emission 520 nm (Figure 3.6). Fluorescence characterisation revealed the free dye dissolved instantly into the ethanolic solution. To quantify the release of Nile red from PLLA 100 particles, an aliquot of particle solution was placed into a 50:50 water: ethanol solution. The subsequent release was monitored over 5 hours using a plate reader (Figure 3.6). Whilst monitoring the change in fluorescence intensity, it was observed that the particles displayed a very high burst release in respect to their calculated 99% dye loading efficiency (Figure 3.6). In fact, after just one day, 91% of the dye was released after 1 min in the 50:50 water: ethanol solution.

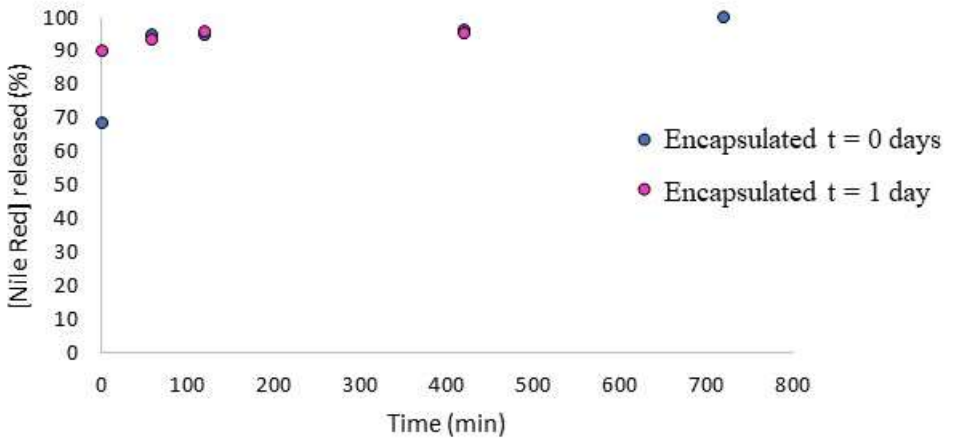

Figure 3.6: Release rate of Nile red from PLLA 100 particles into a 50% Water: EtOH solvent

Investigation into the particle morphology by TEM and SEM (Figure 3.7), revealed that crystals of the dye were visible on the particle surface. It was postulated that the large planar structure of Nile red induced phase separation of the dye from the bulk polymer, thus resulting in dye crystallisation.[34] Consequently, as the dye crystallised, the needle-like crystals perforated the particle wall, hence reducing the dye loading of the PLLA particle. After observing the phase separation between PLLA and Nile red, it could be deduced that the large crystals observed on the particle surface could also be the cause of the increased particle size observed *via* light scattering (Figure 3.4).

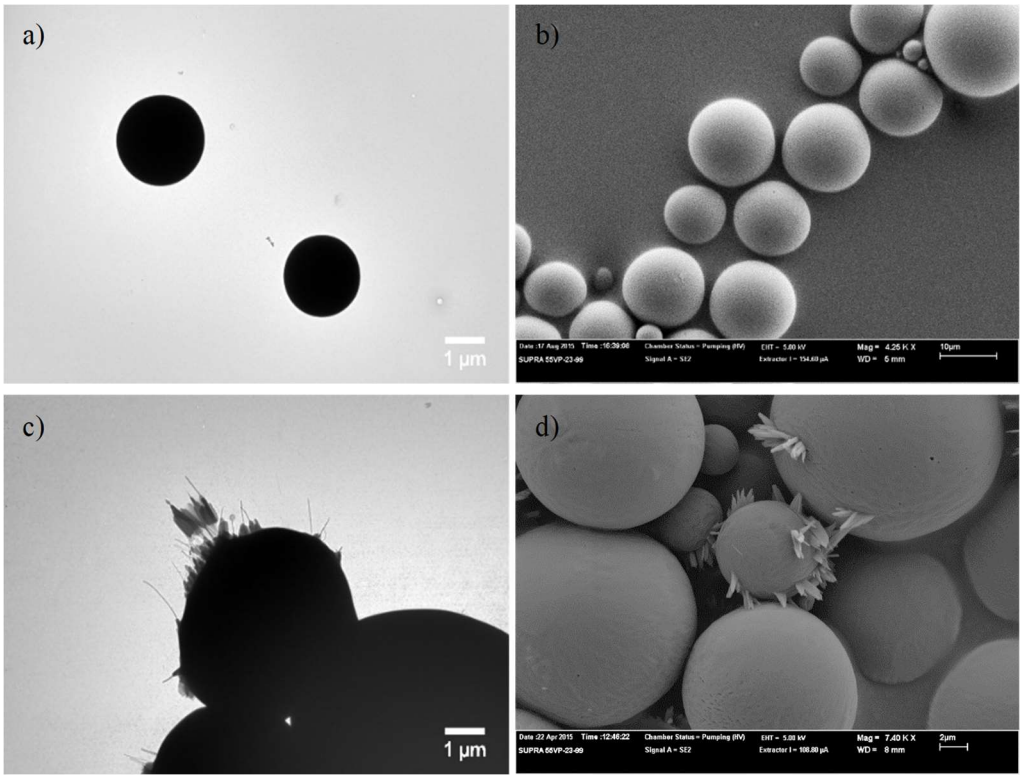

Figure 3.7: a) TEM and b) SEM analysis of particles without dye c) TEM and d) SEM analysis of particles with 1 wt% dye loading of Nile red

3.2.3 Encapsulation of Aminobromomaleimide

3-Bromo-4-(butylamino)-2,5-dihydro-1H-pyrrole-2,5-dione (ABM) is a highly fluorescent small molecule with a less planar structure compared to the structure of Nilered.[35] Therefore, it was reasoned that the smaller dye would be able to mix better within the microparticles without disrupting the particle morphology. The ABM was prepared using a method analogous to Awuah *et al*.[36] In brief, 2,3-dibromomaleimide, *n*-butylamine and sodium carbonate were stirred in tetrahydrofuran (THF) for 2.5 h, before removing the solvent *in vacuo*. The resultant yellow solid was purified *via* column chromatography with a 5:1 petroleum ether: ethyl acetate eluent.

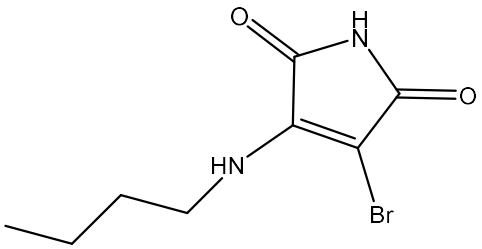

Figure 3.8: Chemical structure of Aminobromomaleimide

The particles were prepared using the optimised solvent evaporation technique as detailed for rhodamine B and Nile red encapsulation (Section 3.2.1 and 3.2.2 respectively), dissolving ABM (1 wt%) with PLLA 100 in the organic phase. The particles were left to harden overnight before washing with DI water and characterising *via* SEM (Figure 3.9). SEM characterisation revealed that in the presence of ABM (1 wt%), the microparticles still maintain their smooth surface and display no signs of dye crystallisation on the particle surface (Figure 3.9).

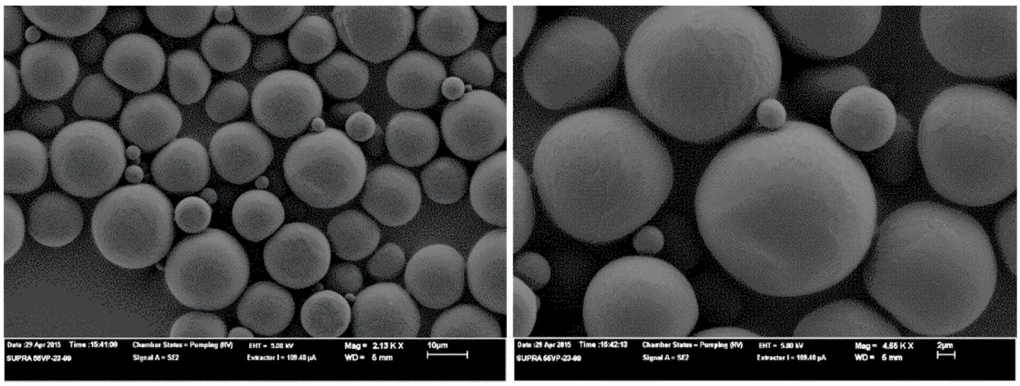

Figure 3.9: SEM images of PLLA microparticles containing 1 wt% aminobromomaleimide

3.2.3.1 Release of ABM from PLLA 100 Microparticles

Before monitoring the dye release into an ethanolic solution, the optimum excitation and emission wavelengths were determined using a 2D excitation-emission spectra. In more detail, the fluorescence intensity of ABM in 50% water/ ethanol was monitored between an emission range of 250 nm – 700 nm with the excitation wavelength

increasing from 205 nm to 450 nm in increments of 10 nm (Figure 3.10). The parallel diagonal lines across the contour plot (Figure 3.10) represent scattered light. The optimum excitation and emission wavelengths for the ABM in the 50% aqueous/ ethanol solvent system were determined to be around 375 nm and 520 nm respectively.

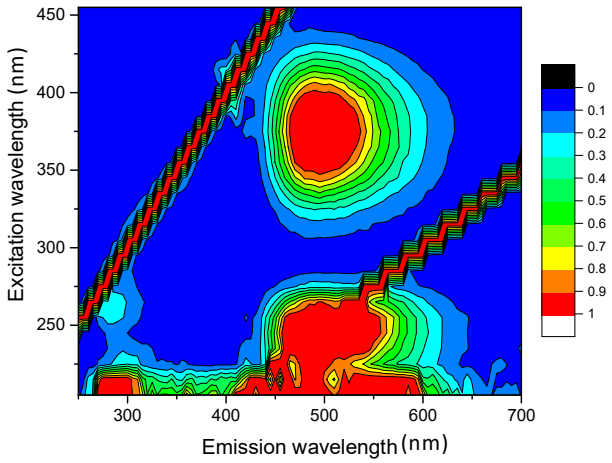

Figure 3.10: 2D excitation-emission spectra (with a 10 nm step) of the ABM in a 50% ethanol: water solution at 10 µM

3.2.3.2 Particle Swelling

Particle swelling has previously been observed during release systems, such as by Gasmi *et al*., when investigating the release of Ketoprofen from PLGA microparticles.[37] The microparticles prepared using a single oil-in-water emulsion technique have been reported to consist of a dense matrix structure.[38] Therefore, if the microparticles were to swell, the increased size of the particles would result in an increased permeability of the particle matrix. Consequently, the diffusion coefficient of the AI to the surrounding media would also increase, hence this could affect the AI release profile. Therefore, the change in particle size was monitored by light scattering (Figure 3.11) and optical microscopy (Figure 3.12) over 24 hours to determine the effect of the ethanolic solution on the particle size.

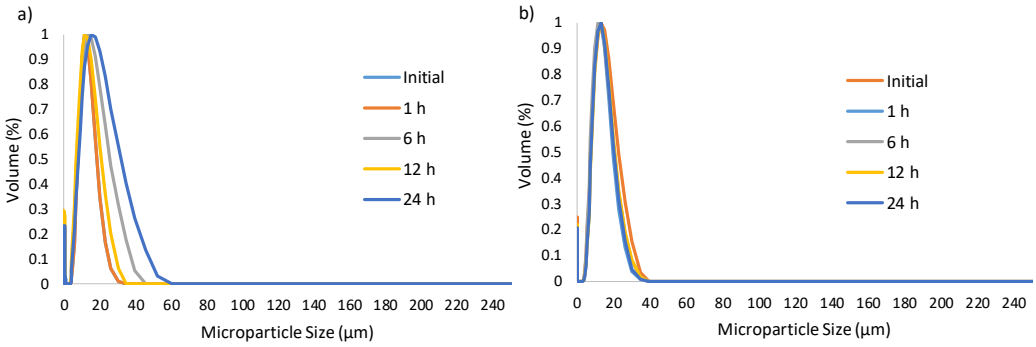

Figure 3.11: Light scattering analysis for swelling study of PLLA microparticles in a) a 50:50 water: ethanol solution and b) water

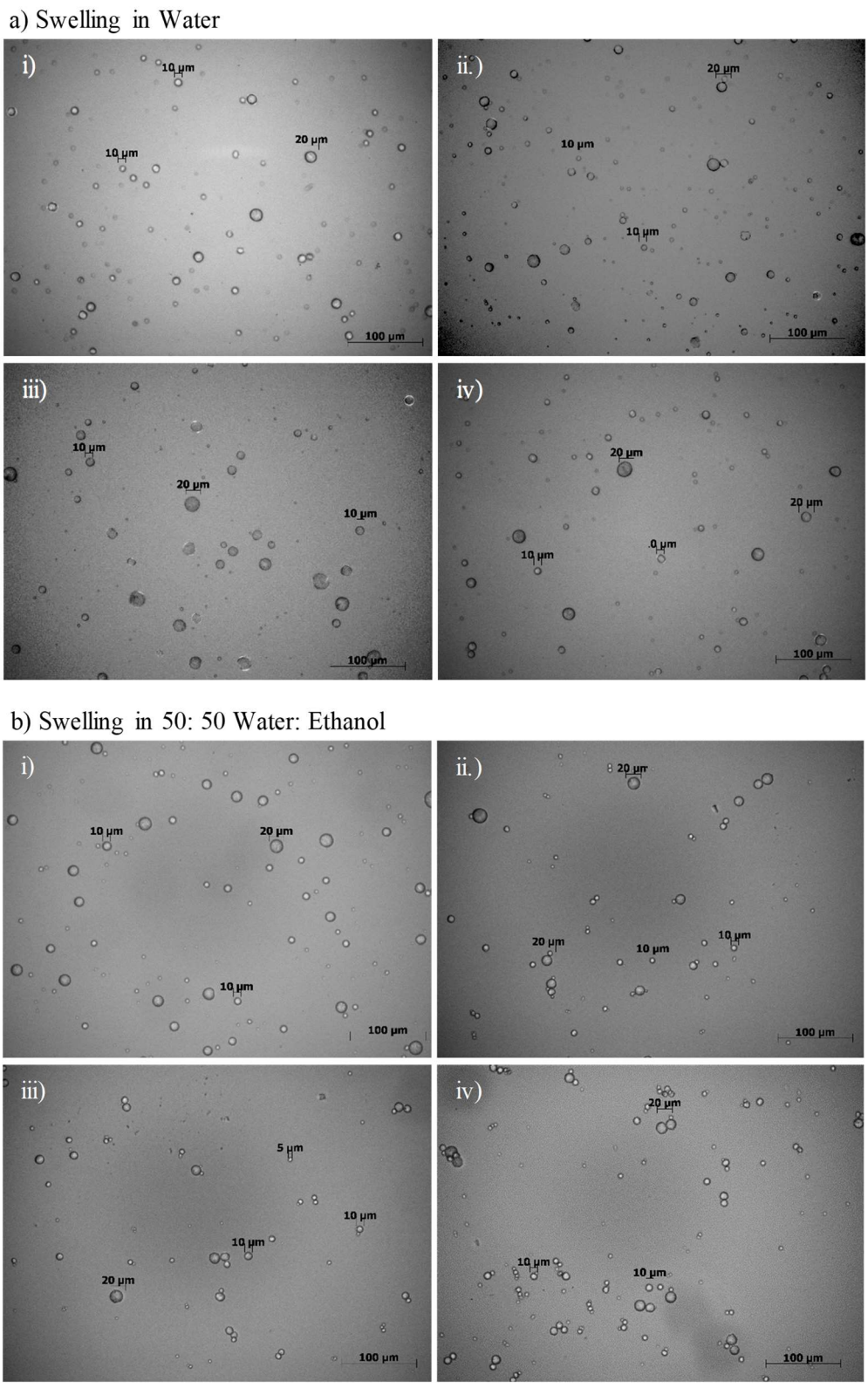

Figure 3.12: Optical microscopy characterisation of PLLA particles in a) water, b) A 50:50 water and ethanol solution i) Initial solution, ii) 6 h, iii) 12 h and iv) 24 h

Even after 24 hours, no change was observed with the particle size in water. Conversely, light scattering analysis of the particles in a 50% water: ethanol solution showed an increase in particle size over time (Figure 3.11). However, whilst observing the particles by optical microscopy, an increase in particle aggregation was observed, this was assumed to be the reason for the increase in particle size. PVA is slightly soluble in ethanol. Therefore, it was postulated that the addition of ethanol partially dissolved the stabilising PVA around the particles, thus resulting in particle destabilisation and aggregation.

3.2.3.3 ABM Dye Loading

To determine the ABM dye loading, PLLA 100 particles were prepared containing 1 wt% ABM. The subsequent particles were left to harden overnight and washed with DI water before being fully dissolved in dichloromethane. The fluorescence intensity of the particles was monitored between 5 washes and compared to a calibration of five known concentrations of ABM in dichloromethane using a fluorometer (Figure 3.13).

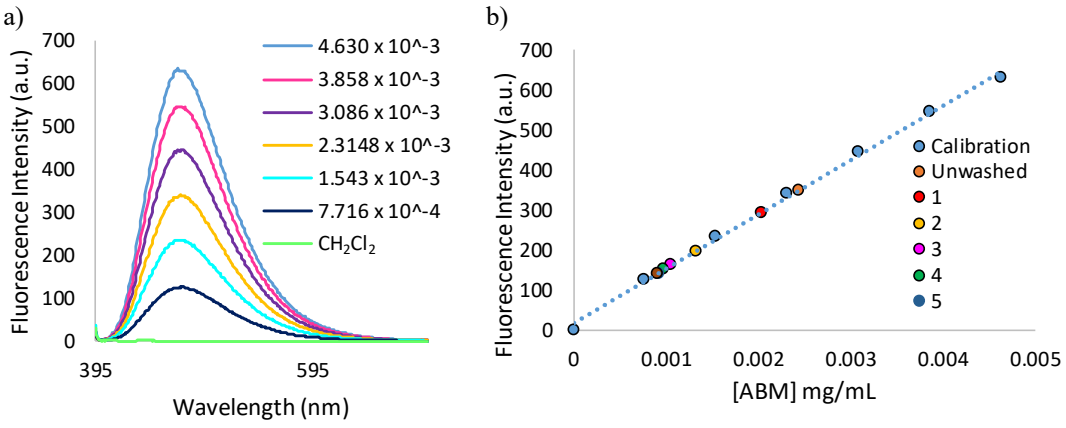

Figure 3.13: a) Plot showing the change in fluorescence intensity at each calibration concentration and b) Plot detailing how the fluorescence intensity changes between washes with deionised water

Fluorescence analysis revealed that initially the dye loading was 68%, however, after successive washes, the dye loading was reduced to 28%. This was postulated to be a

consequence of removal of excess unencapsulated dye collected on the particle surface. The variation in dye loading after three plus washes was only minimal, therefore, any further loss was postulated to be a consequence of sample loss between washes, thus deeming the actual dye loading as 28%.

3.3 Microparticle Degradation and Release

In order to be applicable within agriculture, microparticles ideally should be stable enough to be stored for up two years, but show signs of release under environmental conditions (*i.e*., soil, pH, enzymes, *etc*.). Multiple emulsion batches were prepared, washed and dried individually before combining the solid powder and re-immersing the particles into the desired solution. To prevent the particles from settling, the solutions were continuously rotated throughout the duration of the experiment. Aggregation during particle degradation could alter the particle release profile. Therefore, to prevent aggregation, a PVA stabiliser (Mowiol 488) was added to the system. However, before adding the stabiliser, an initial study was commenced to determine the effect of the stabiliser concentration on the particle degradation and release behaviour. No change was observed *via* SEM, SEC or dye release over a two-month period, therefore, the particles were prepared containing PVA (1 wt%) as stabiliser.

3.3.1 Varying Degradation Media

As a result of the diverse climate experienced around the world, soil composition can change considerably depending on the country and the time of year. Therefore, to obtain an accurate representation of particle degradation in a range of soil environments, the degradation and release of PLLA 100 microparticles was investigated in a variety of degradation media.

3.3.1.1 Aqueous Medium

Water is one of the key components in most soil compositions and often the chosen medium for storing the microparticle suspensions. Polyesters are known to degrade under hydrolytic conditions, consequently, an investigation was performed looking at the particles' stability in an aqueous environment. PLLA 100 microparticles

containing ABM (0.1 wt%) were synthesised, washed to remove excess dye and then re-suspended in deionised water (containing 1 wt% PVA stabiliser). Samples were taken once a week for the first 6 months and then fortnightly for the succeeding 6 months to monitor particle degradation *via* SEM and SEC (Figure 3.14 and Figure 3.15 respectively). No visual change of the particle morphology was observed *via* SEM throughout the 12-month period (Figure 3.14).

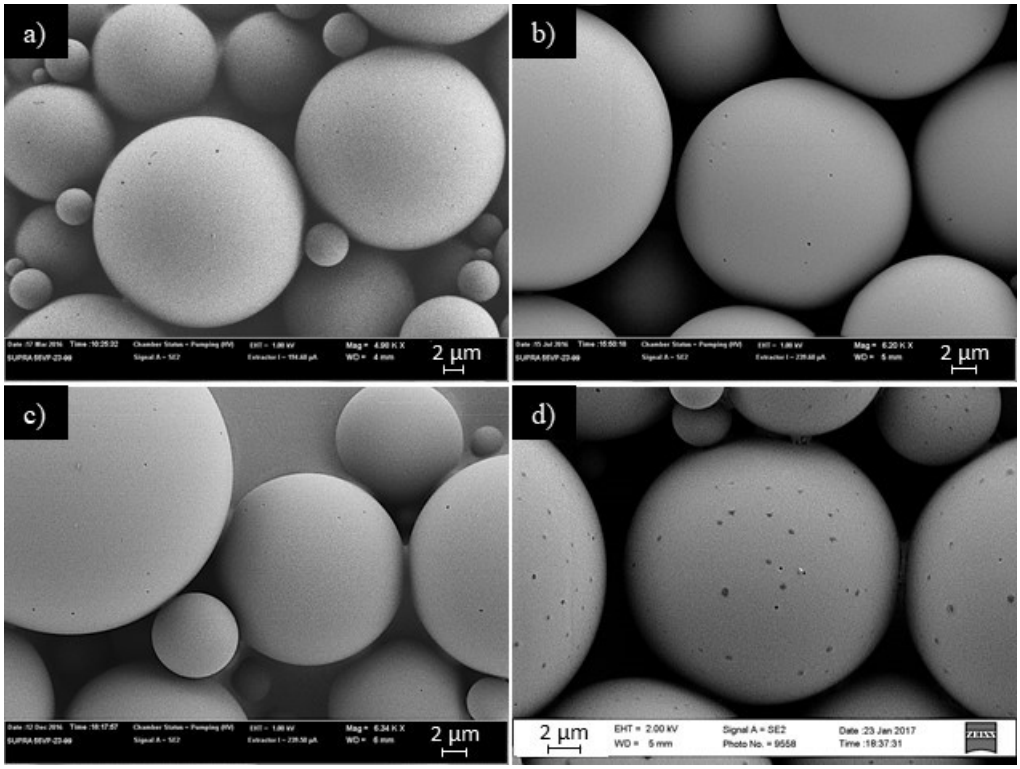

Figure 3.14: SEM characterisation of PLLA 100 microparticles after a) 0 months, b) 4 months, c) 8 months and d) 12 months in water

Characterisation of the particle degradation *via* SEC revealed the formation of lower molecular weight peaks after 7 months in an aqueous solution (Figure 3.15). During polyester hydrolysis, water can react with the carbonyl group of the ester, causing the polymer chain to fragment, thus resulting in the formation of lower molecular weight species. Therefore, the presence of low molecular weight peaks *via* SEC, suggests the onset of PLLA degradation. Conversely, the minimal variation in intensity of the main

polyester molecular weight SEC peak implied only negligible amounts of bulk degradation had occurred. The intensity of the observed low molecular weight peaks appeared to decrease and vary in molecular weight as time progressed. Previous investigation into the degradation of PLA and poly(glycolic acid) (PGA) by Hakkarainen *et al*., revealed that the amorphous regions within the semi-crystalline polymer degrade preferentially and is usually followed by a decrease in the observed degradation rate, which can be observed by the minimal presence of low molecular weight SEC peaks after 12 months (Figure 3.15).[39] Furthermore, research by Wang *et al*., demonstrated the high water solubility of the low molecular weight species generated during degradation.[40] To enable accurate SEC analysis of the microparticles, the PVA stabiliser was required to be removed, this was achieved by washing the particles three times with DI water. Therefore, it was hypothesised that the low molecular weight species were removed between washes, thus reducing observed intensity of the peaks.

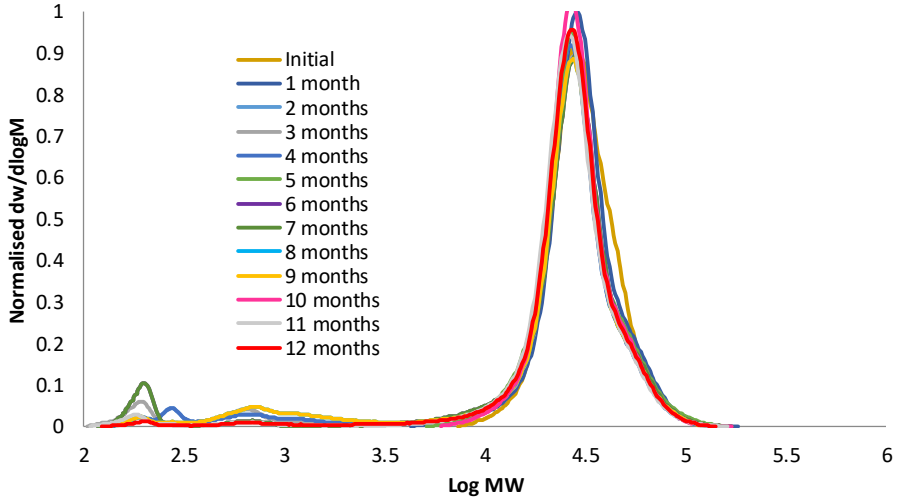

Figure 3.15: SEC characterisation of PLLA 100 particle degradation after 12 months in water

To elucidate the concentration of dye released throughout the 12-month degradation period, regular aliquots of the particle suspension were taken and added to a 50% ethanol/water solution, thus enabling the change in fluorescence intensity to be monitored using a plate reader. To calibrate the plate reader, six known concentrations of ABM were prepared that can be related to 120%, 100% 80%, 60%, 40% and 20% of the encapsulated ABM (0.1 wt%) in a 50% EtOH: H_2O solvent ratio. The fluorescence intensity was recorded using filters at excitation 390 nm and emission 520 nm. To test the efficiency of the 50% ethanol solution to fully dissolve the dye, a control experiment was performed comparing the time taken for free dye in solution to dissolve versus dye encapsulated into a PLLA 100 microparticle (Figure 3.16). The control experiment demonstrated that all of the free dye is quickly taken into solution (Figure 3.16).

Samples of the particle solution were taken regularly and the release into water/ethanol monitored over 12 months (Figure 3.16). The release of ABM into an ethanolic solution correlated well with the obtained degradation profile, where only a minimal change in fluorescence intensity (4%) was observed throughout the 12-month period (Figure 3.16). The minimal change in release observed throughout the 12 months displayed the high resistance of PLLA 100 to hydrolytic degradation under neutral aqueous conditions.

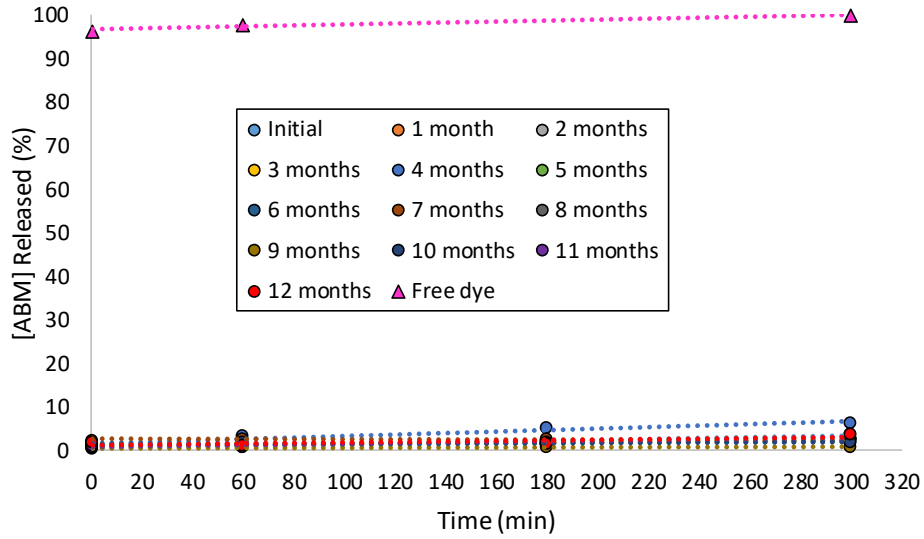

Figure 3.16: Plate reader characterisation detailing the observed change in fluorescence intensity over 5 h for free dye and dye encapsulated into PLLA 100 particles over 12 months

3.3.1.2 Enzymatic Medium

Microbes producing protease, lipase and esterase are abundant in the soil. However, microbe concentration fluctuates based on nutrient diffusion gradients, the soil composition and the immediate surroundings. To simulate a representative soil environment, the washed and dried particles were suspended in 1 mg/mL enzyme digestant (Cleanzyme). Cleanzyme contains a cocktail of enzymes similar to the enzymes found in soil, thus allowing a representative study of how the particles will degrade and release an encapsulated agrochemical in the soil.[41] The particle degradation was monitored *via* SEM and SEC (Figure 3.17 and Figure 3.19 respectively). After 4 months in Cleanzyme, several particles were observed to have a pitted appearance *via* SEM analysis, which intensified over the 12 months (Figure 3.17). The number of particles with visual pitting increased throughout the degradation study, however, even after 12 months in Cleanzyme, over 70% of the particles had maintained their original smooth particle morphology observed within the initial sample.

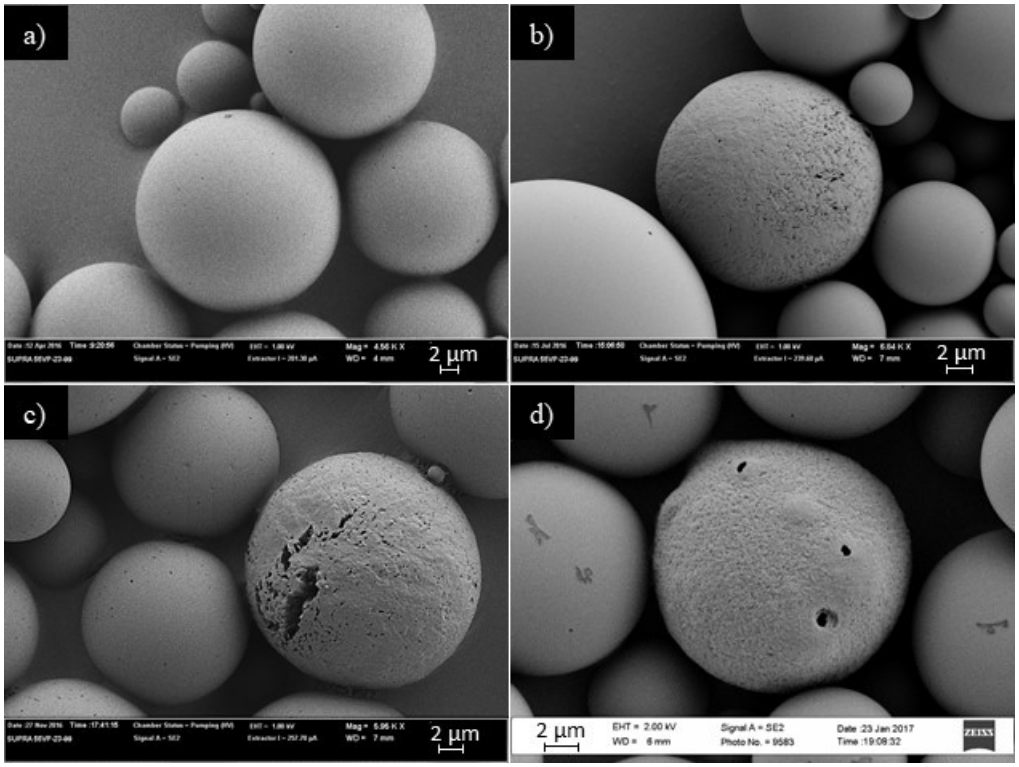

Figure 3.17: SEM characterisation of PLLA 100 microparticles after a) 0 months, b) 4 months, c) 8 months and d) 12 months in Cleanzyme

Interestingly, after 6 months degrading in Cleanzyme, clusters of smaller nanosized particles were evident *via* SEM (Figure 3.18). Hence, it was postulated that the presence of the smaller nanoparticles and the pitting observed on several particles throughout the sample, was a consequence of enzymatic hydrolysis of the PLLA polyester at the particle surface.

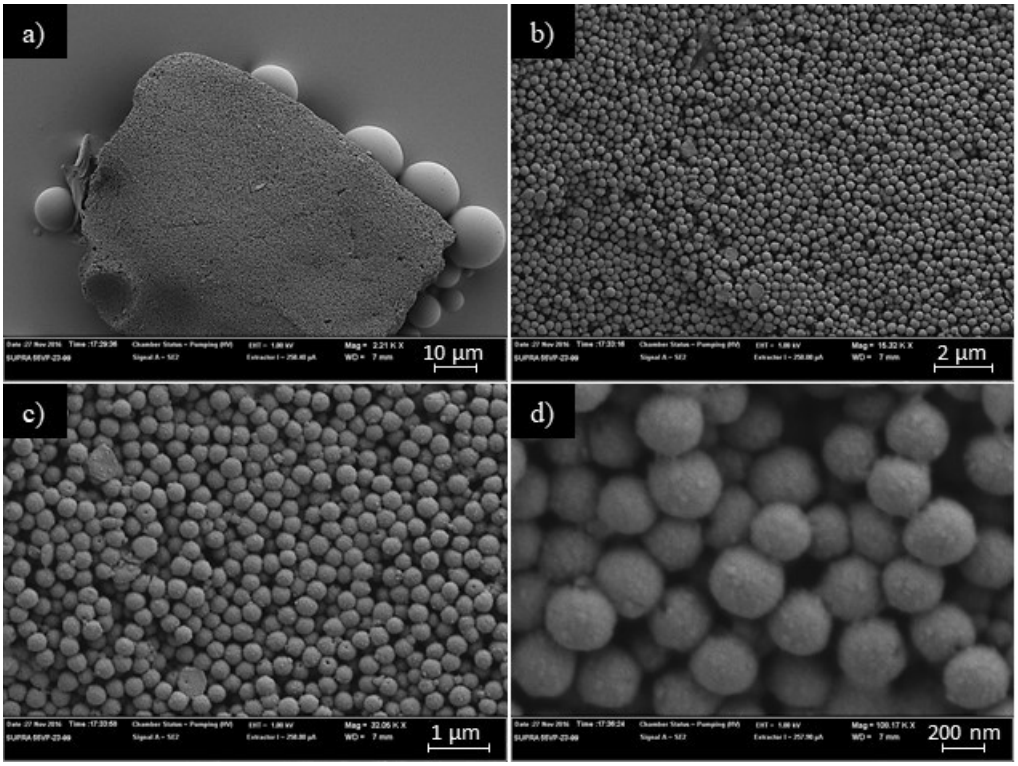

Figure 3.18: SEM characterisation of PLLA 100 microparticles after 6 months degrading in Cleanzyme with varied magnification a) 10 µm, b) 2 µm, c) 1 µm and d) 200 nm

Further characterisation of the particle degradation by SEC revealed the formation of low molecular weight peaks after 4 months of degradation in Cleanzyme (Figure 3.19). Formation of the lower molecular weight peaks was coupled with slight broadening and decrease in peak intensity of the main PLLA molecular weight SEC peak as the degradation time elapsed. Therefore, it was theorised that a combination of surface and bulk degradation was occurring.

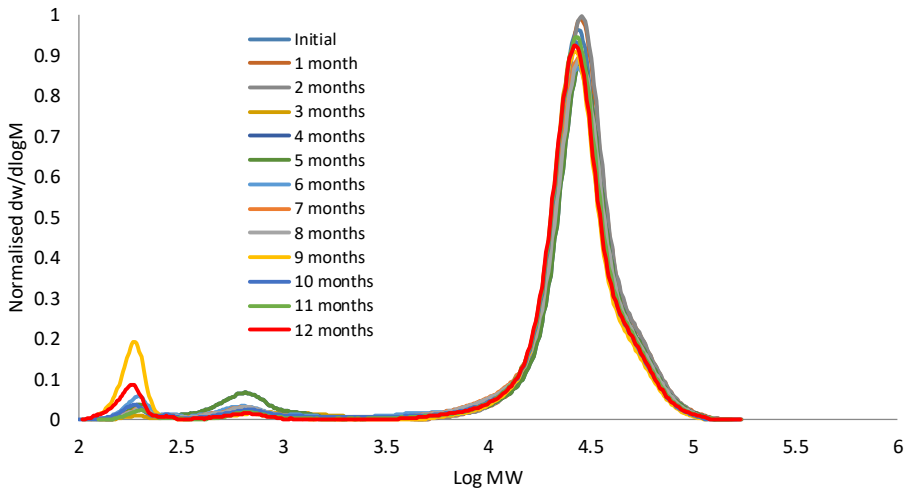

Figure 3.19: SEC characterisation of PLLA 100 particles after degradation in Cleanzyme for 12 months

Characterisation of the dye release into an ethanolic solution showed minimal release over the first 6 months, followed by a steady increase in both the burst and total [ABM] released (Figure 3.20). The minimal change in fluorescence intensity over the 5 hours further confirmed the occurrence of surface degradation. Moreover, dye released from near the particle surface will be instantly taken into the water/ ethanol solvent, whereas release of dye situated towards the particle centre would be limited by diffusion through the particle matrix, hence the observed slow release suggested the particle matrix was only partially degraded.

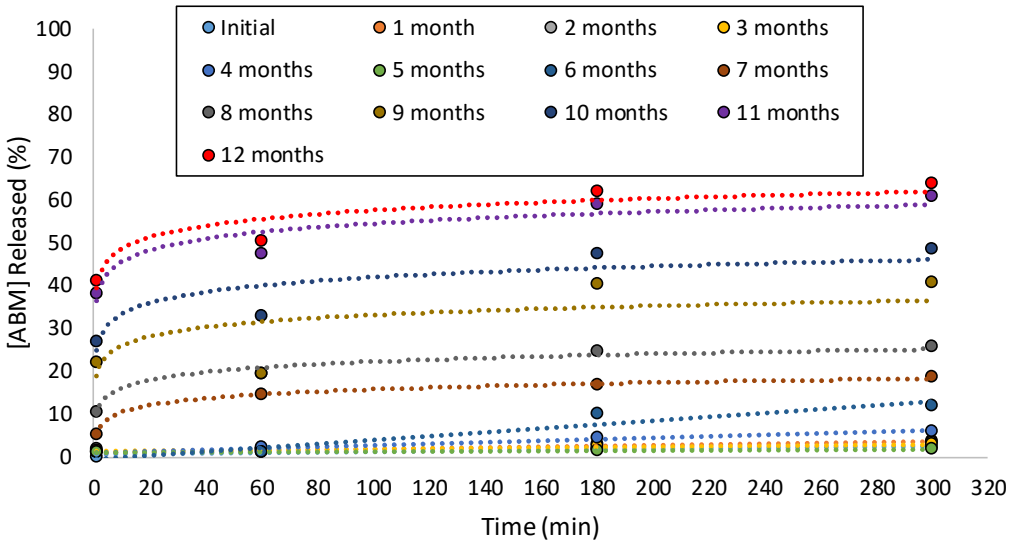

Figure 3.20: Plate reader characterisation detailing the observed change in fluorescence intensity over 5 h for PLLA 100 particles after degradation in Cleanzyme for 12 months

3.3.1.3 Varying pH

The pH of soil again can vary widely depending on the country and surrounding climatic conditions. Therefore, the degradation and release of PLLA 100 microparticles was investigated in acidic (pH 5), neutral (PBS) and basic (pH 10) media. Similarly to PLLA 100 degradation in water, only minimal change in particle degradation was observed with PLLA 100 particles under neutral degradation conditions (PBS pH 7.4), therefore only degradation in acidic and basic environments are discussed below, (for full characterisation of PLLA 100 particle degradation in PBS see Appendix (Chapter 10, Section 10.1.1)).

3.3.1.3.1 Acidic Media

The washed particles containing ABM (0.1 wt%) were suspended in a pre-prepared buffer solution of acetic acid and sodium acetate (pH 5). Characterisation of microparticle degradation *via* SEM over 12 months revealed that signs of degradation were visible after 6-8 months within an acidic environment (Figure 3.21). Moreover,

several particles appeared to have a wrinkled morphology after 6 months, with increasing evidence of degradation visible *via* SEM analysis after 12 months. However, similar to enzymatic degradation, over 70% of the particles maintained their original smooth particle morphology, thus suggesting only slight degradation was occurring throughout the sample.

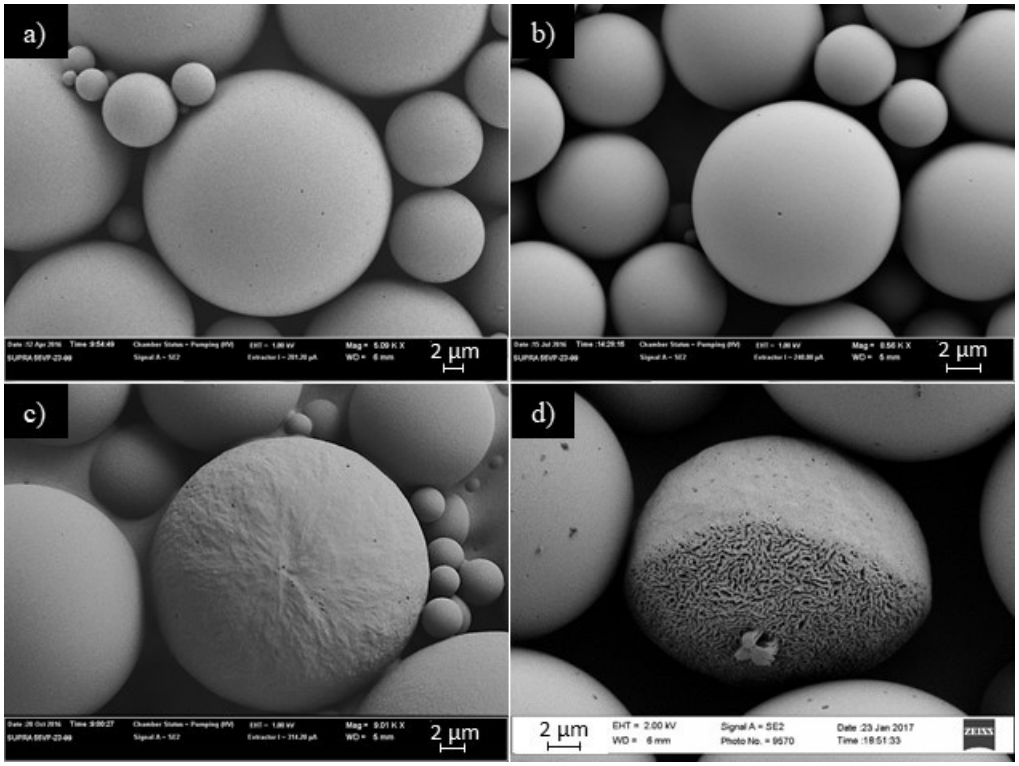

Figure 3.21: SEM characterisation of PLLA 100 microparticles after a) 0 months, b) 4 months, c) 8 months and d) 12 months at pH 5

Characterisation of the particle degradation by SEC confirmed the presence of bulk degradation by the appearance of lower molecular weight species after 6 months of degradation in an acidic environment (Figure 3.22). The formation of the lower molecular weight peaks was coupled with a decrease in intensity of the main PLLA SEC peak, thus confirming degradation of the main polyester chains. However, similarly to degradation in water, the small decrease in PLLA intensity implied that only slight degradation was occurring within the PLLA microparticles (Figure 3.22).

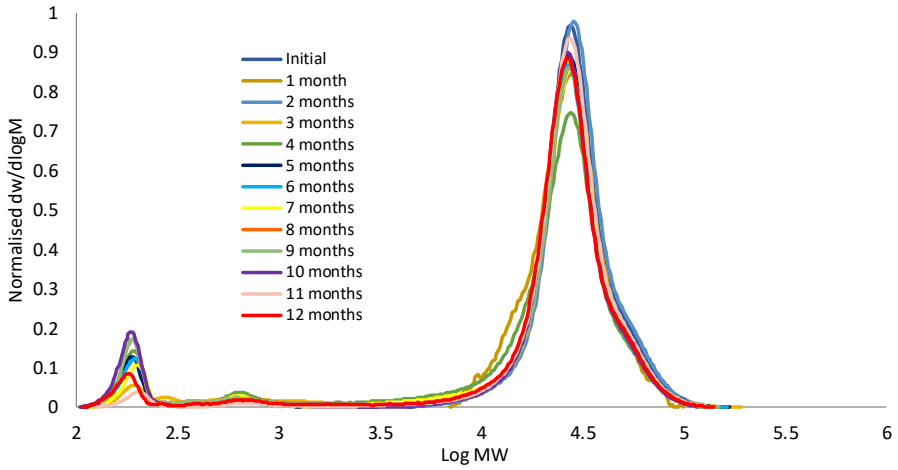

Figure 3.22: SEC characterisation of PLLA 100 particles after degradation for 12 months at pH 5

Characterisation of the release of ABM into a 50% water/ethanol solution and monitoring the change throughout the 12-month degradation period at pH 5 revealed a low release of only 10% after 12 months (Figure 3.23). The low release observed agreed with the slow particle degradation observed by SEM, SEC and mass loss. Indeed, the high resilience observed with PLLA particles in an acidic environment showcased the high potential for controlled agrochemical release from PLLA particles under environmental conditions.

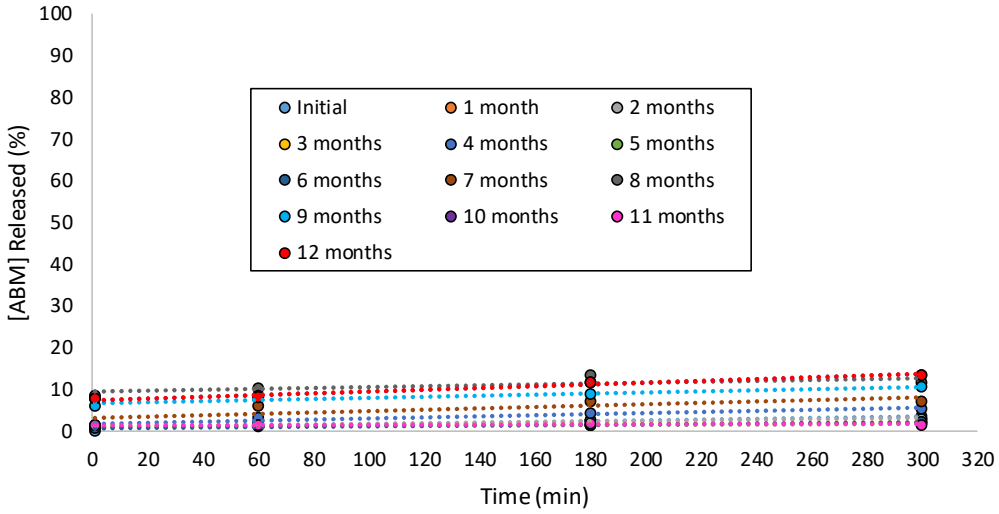

Figure 3.23: Plate reader characterisation detailing the observed change in fluorescence intensity for PLLA 100 particles after degradation at pH 5 for 12 months

3.3.1.3.2 Basic Media

To determine the degradation profile of PLLA 100 particles in a basic environment, a sample of the washed particles containing ABM (0.1 wt%) were suspended in a pre-prepared buffer solution of sodium carbonate and sodium hydrogen carbonate (pH 10). After one week in the degradation medium, samples were taken for characterisation of the particle degradation and release *via* SEC, SEM, mass loss and fluorometry. Whilst sampling, a clear visual colour change was evident, the degradation solution appeared colourless instead of the original expected yellow colour, characteristic of the encapsulated ABM. Furthermore, a clear decrease in fluorescence intensity was observed whilst monitoring the loss of *E* over time. Consequently, it was postulated that the dye was susceptible to hydrolysis in a basic environment. Subsequent characterisation of the fluorescence intensity of the dye in both aqueous and basic solutions confirmed dye hydrolysis by the observation of a dramatic reduction in fluorescence intensity after just one week (Figure 3.24). PLLA particles are known to undergo degradation under basic conditions, however, optimisation of encapsulation

and release of a different dye into PLLA 100 particles would be required to monitor the particle degradation and release in basic solution. Hence, no further experimentation into the particle degradation and release in a basic environment was undertaken.

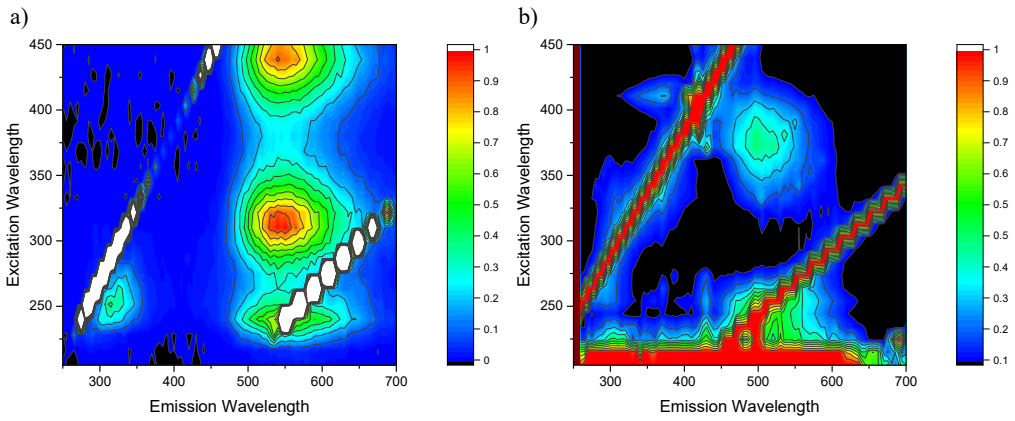

Figure 3.24: Fluorescence intensity of ABM after 1 month in a) water (pH 7) and b) basic solution (pH 10)

Several drugs and dyes have been reported to affect the particle degradation and release. Therefore, in order to determine if encapsulation of ABM does affect the particle degradation and release, a control degradation was performed by monitoring the degradation of PLLA 100 microparticles without dye in both an aqueous and enzymatic environment. The particles were monitored by SEM and SEC (Chapter 10, Section 10.1.2). Particles synthesised without ABM behaved similarly to PLLA 100 with encapsulated dye, therefore, further analysis over an extended time period would be required to determine the effect of ABM encapsulation on particle degradation.

3.4 Conclusions

In conclusion, the encapsulation and subsequent release of a model fluorescent dye *via* microparticle degradation was investigated. It was found that the optimised single oil-in-water emulsion technique detailed in Chapter 2 could be tailored to encapsulate hydrophobic dyes into a range of polyester microparticles. However, characterisation of the particle morphology and *E via* SEM and fluorometry revealed that the structure of the dye and dye loading can drastically affect the particle encapsulation and release. Indeed, the large, planar structure of Nile red resulted in the formation of crystals of the dye on the particle surface. On the other hand, the smaller, less planar ABM was found to encapsulate well into PLLA 100 with no observable dye crystallization evident *via* SEM analysis. Characterisation of PLLA 100 particle degradation and release *via* SEC, SEM, mass loss, ABM release and loss of *E* revealed the low susceptibility of PLLA 100 to hydrolysis within a variety of degradation media. The high resistance to hydrolysis observed by PLLA 100 particles demonstrates the great potential for the use of PLLA microparticles for controlled release of agrochemicals under environmental conditions.

3.5 References

1. V. V. Oberemok, K. V. Laikova, Y. I. Gninenko, A. S. Zaitsev, P. M. Nyadar and T. A. Adeyemi, *J. Plant Prot. Res.*, 2015, **55**, 221-226.
2. M. W. Aktar, D. Sengupta and A. Chowdhury, *Interdisc. Toxicol.*, 2009, **2**, 1-12.
3. B. Singh, D. K. Sharma and A. Gupta, *J. Hazard. Mater.*, 2009, **161**, 208-216.
4. D. Ali, N. S. Nagpure, S. Kumar, R. Kumar, B. Kushwaha and W. S. Lakra, *Food Chem. Toxicol.*, 2009, **47**, 650-656.
5. A. Roy, S. K. Singh, J. Bajpai and A. K. Bajpai, *Cent. Eur. J. Chem.*, 2014, **12**, 453-469.
6. R. P. Brannigan and A. P. Dove, *Biomater. Sci.*, 2017, **5**, 9-21.
7. M. D. Rowe, E. Eyiler and K. B. Walters, *Polym. Test.*, 2016, **52**, 192-199.
8. R. Chandra and R. Rustgi, *Prog. Polym. Sci.*, 1998, **23**, 1273-1335.
9. V. Speranza, A. De Meo and R. Pantani, *Polym. Degrad. Stab.*, 2014, **100**, 37-41.
10. H. Satoh, N. Yoshie and Y. Inoue, *Polymer*, 1994, **35**, 286-290.
11. S. Lyu and D. Untereker, *Int. J. Mol. Sci.*, 2009, **10**, 4033.
12. S. Agarwal, *Polymer Science: A Comprehensive Reference*, Elsevier, Amsterdam, 2012.
13. G. Gallet, R. Lempiäinen and S. Karlsson, *Polym. Degrad. Stab.*, 2000, **71**, 147-151.
14. A. Noreen, K. M. Zia, M. Zuber, M. Ali and M. Mujahid, *Int. J. Biol. Macromol.*, 2016, **86**, 937-949.
15. H. Pranamuda, Y. Tokiwa and H. Tanaka, *Appl. Environ. Microbiol.*, 1997, **63**, 1637-1640.

16. D. Rasselet, A. Ruellan, A. Guinault, G. Miquelard-Garnier, C. Sollogoub and B. Fayolle, *Eur. Polym. J.*, 2014, **50**, 109-116.

17. M. J. Stanford and A. P. Dove, *Chem. Soc. Rev.*, 2010, **39**, 486-494.

18. A. Torres, S. M. Li, S. Roussos and M. Vert, *J. Appl. Polym. Sci.*, 1996, **62**, 2295-2302.

19. N. K. N. Limanska, V. Biscola, T. Ivanytsia, A. Merlich, BDGM Franco, J. M. Chobert, V. Ivanytsia and T. Haertle, *J. Plant Pathol. Microb.*, 2015, **6**, 292-300.

20. N. Kamaly, B. Yameen, J. Wu and O. C. Farokhzad, *Chem. Rev.*, 2016, **116**, 2602-2663.

21. R. Grillo, A. d. E. S. Pereira, N. F. S. de Melo, R. M. Porto, L. O. Feitosa, P. S. Tonello, N. L. D. Filho, A. H. Rosa, R. Lima and L. F. Fraceto, *J. Hazard. Mater.*, 2011, **186**, 1645-1651.

22. H. K. Makadia and S. J. Siegel, *Polymers*, 2011, **3**, 1377.

23. A. Brunner, K. Mäder and A. Göpferich, *Pharm. Res.*, 1999, **16**, 847-853.

24. T. G. Park, W. Lu and G. Crotts, *J. Controlled Release*, 1995, **33**, 211-222.

25. B. S. Zolnik and D. J. Burgess, *J. Controlled Release*, 2007, **122**, 338-344.

26. D. H. Lewis and D. R. Cowsar, *Principles of Controlled Release Pesticides*, ACS Symp. Series, Washington, 1977, 1-16.

27. Y.-Y. Yang, T.-S. Chung, X.-L. Bai and W.-K. Chan, *Chem. Eng. Sci.*, 2000, **55**, 2223-2236.

28. J. L. Maia, M. H. A. Santana and M. I. Ré, *Braz. J. Chem. Eng.*, 2004, **21**, 01-12.

29. J. L. Ansiaux, F. Borgo, T. W. Cheung, J. Edmonds, T. E. Kunkel, G. L. Melchior, F. R. Miranda and G. D. Newberry, *Improved processes for the control of undesired vegetative growth in crops*, US 13, 813, 090, 2013.

30. J. Street and A. Jutsum, *Pesticidal mixtures giving synergistic pesticidal effects*, US 20110318272, 2013.

31. F. P. Silverman, J. Zhiguo, P. D. Petracek, D. F. Heiman and P. Warrior, *Herbicidal composition comprising a ps-ii inhibitor and sar inducer*, US 20040116293, 2004.

32. J. E. Van Koppenhagen, H. B. Scher, K. S. Lee, I. M. Shirley, P. Wade and R. Follows, *Base-triggered release microcapsules*, US 6544540, 2003.

33. P. Greenspan and S. D. Fowler, *J. Lipid Res.*, 1985, **26**, 781-789.

34. C. Wischke and S. P. Schwendeman, *Int. J. Pharm.*, 2008, **364**, 298-327.

35. A. B. Mabire, M. P. Robin, W.-D. Quan, H. Willcock, V. G. Stavros and R. K. O'Reilly, *Chem. Commun.*, 2015, **51**, 9733-9736.

36. E. Awuah and A. Capretta, *J. Org. Chem.*, 2011, **76**, 3122-3130.

37. H. Gasmi, F. Danede, J. Siepmann and F. Siepmann, *J. Controlled Release*, 2015, **213**, 120-127.

38. G. C. Bazzo, E. Lemos-Senna, M. C. Gonçalves and A. T. N. Pires, *J. Braz. Chem. Soc.*, 2008, **19**, 914-921.

39. M. Hakkarainen, A.-C. Albertsson and S. Karlsson, *Polym. Degrad. Stab.*, 1996, **52**, 283-291.

40. H. T. Wang, H. Palmer, R. J. Linhardt, D. R. Flanagan and E. Schmitt, *Biomaterials*, 1990, **11**, 679-685.

41. Janisource, Cleanzyme Enzyme Digestant, https://janisource.com/cleanzyme-enzyme-cleaner-spotter-odor-remover-1-gallon/, (accessed 13-06-17, 2017).

4. Controlled Fluorophore Release *via* Microparticle Degradation

4.1 Introduction

Since the pioneering work by Staudinger and Carothers, polymers have become an extremely important class of materials. Biodegradable polyesters have attracted a lot of attention as a consequence of their ability to undergo degradation under physiological and environmental conditions.[1] Polyesters, such as Poly(lactide) (PLA), poly(ε-caprolactone) (PCL) and Poly(3-hydroxybutryate) (PHB) are well known to be susceptible to hydrolytic degradation.[2-5] Untereker *et al*. have shown that the hydrolytic degradation of polyesters occurs *via* random scission of the hydrolysable ester bonds.[6] This in turn results in the formation of low molecular weight non-toxic species, which can be absorbed by microorganisms in the soil.[7-11]

In particular, PLA has received a lot of attention as a consequence of its tuneable stereochemistry.[11] The monomer of PLA, lactide, has two chiral centres, therefore, this can give rise to the production of three possible stereoisomers, *LL* (*L*-lactide), *DL* (*meso*-lactide) and *DD* (*D*-lactide) (Figure 4.1). Stereopure *L*-lactide and *D*-lactide produce isotactic polymers with highly crystalline structures.[12] Conversely, a 50:50 mixture of *L*-lactide and *D*-lactide produces a racemic mixture (*rac*-lactide) with an amorphous structure. Therefore, the isotactic and amorphous polymers display very different polymeric properties depending on their degree of crystallinity.[13] Indeed, poly(*rac*-lactide) has been shown to display a higher susceptibility to hydrolytic degradation as a consequence of its enhanced structural permeability.[14] Then again, both PLLA and PDLLA stereoisomers hydrolyse to produce the biocompatible non-toxic lactic acid. Lactic acid is commonly found in the soil. Furthermore, the presence of lactic acid within soil has been shown to be highly beneficial (*e.g.*, for the preservation of vegetable products *etc*.).[15, 16]

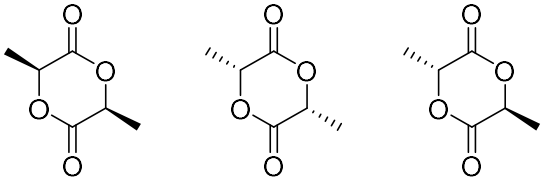

D-LA *L*-LA *Meso*-LA

Figure 4.1: Stereoisomers arising from the two chiral centres of Lactide

As a consequence of their biodegradable nature, polyesters have been shown to be the ideal materials for use as a microparticle matrix.[17, 18] As the particle breaks down, the encapsulated AI is released into the surrounding environment. Therefore, the rate of AI release is highly dependent on the polymer composition, the polymer molecular weight and the polymer crystallinity.[19-21] Each applied agrochemical has a specific application within plant health and protection. Therefore, the desired release period can vary widely depending on the type of response required from the agrochemical. Consequently, this Chapter investigates the degradation and release of a model fluorescent dye from a range of polyesters, with the aim to target the synthesis of a library of degradable microparticles with a range of polyester degradation profiles.

4.2 Results and Discussion

4.2.1 Microparticle Degradation and Release

4.2.1.1 Varying Molecular Weight

Polymer molecular weight is well-known to affect the particle degradation rate. After the promising stability observed with PLLA 100 in a variety of degradation media (Chapter 3, Section 3.3), it was interesting to observe the extent of control over the particle degradation offered by varying the polymer molecular weight. To achieve this, two separate particle studies were investigated, using PLLA with differing molecular weights; degree of polymerisation (DP) of 25 (PLLA 25) and DP 250 (PLLA 250). The particles were individually prepared with ABM (0.1 wt%) encapsulated using the optimised single oil-in-water solvent evaporation technique before being washed, dried and re-suspended into an enzymatic medium (1 mg/mL Cleanzyme) as detailed in Chapter 3 (Section 3.3.1.2). Cleanzyme consists of a cocktail of enzymes commonly found in the soil, thus enabling a comparable degradation study to particle degradation within a typical horticultural environment.[22] Microparticle degradation was monitored by scanning electron microscopy (SEM), size exclusion chromatography (SEC) and mass loss weekly for the first 6 months and then fortnightly for the succeeding months. Similarly to degradation of PLLA 100, no visible degradation was observed *via* SEM whilst monitoring PLLA 25 over 6 months and PLLA 250 over 8 months in Cleanzyme solution (Figure 4.2 and Figure 4.3 respectively). As a control, PLLA 25 and PLLA 250 particles were synthesised and their degradation and release monitored in water, however, minimal degradation and release was observed. For full characterisation of PLLA 25 and PLLA 250 particle degradation and release in water see Appendix (PLLA 25 (Chapter 10, Section 10.2.1), PLLA 250 (Chapter 10, Section 10.2.2)).

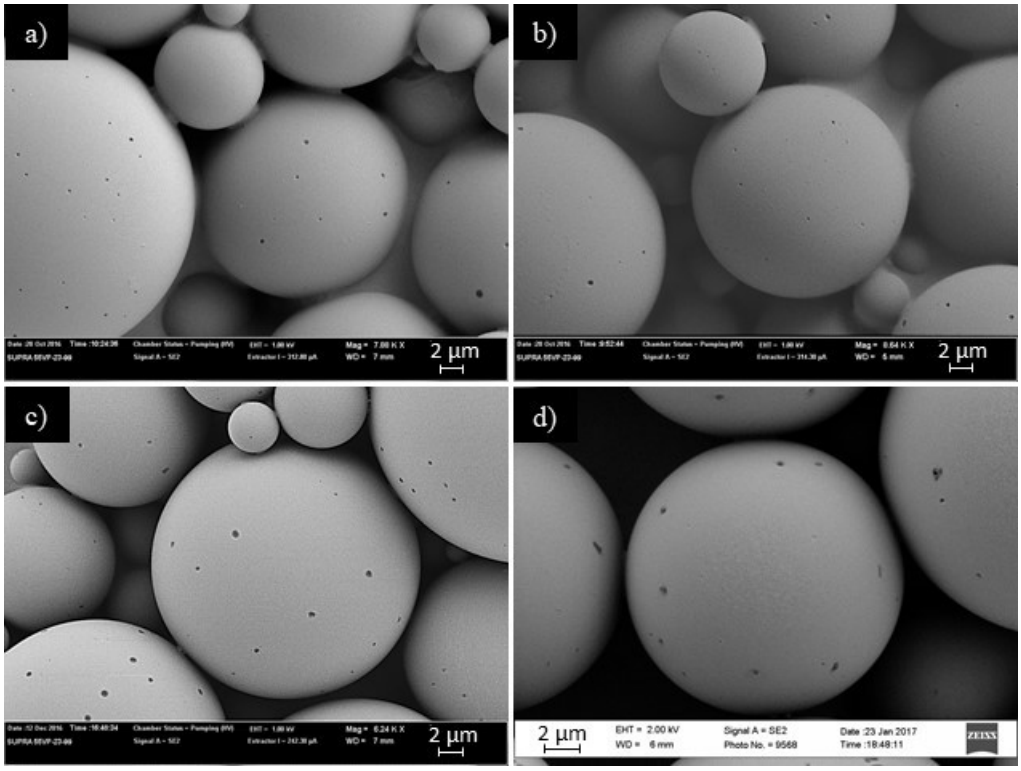

Figure 4.2: Characterisation of the change in particle morphology observed *via* SEM with PLLA 25 after a) 0 months, b) 2 months, c) 4 months and d) 6 months in Cleanzyme solution

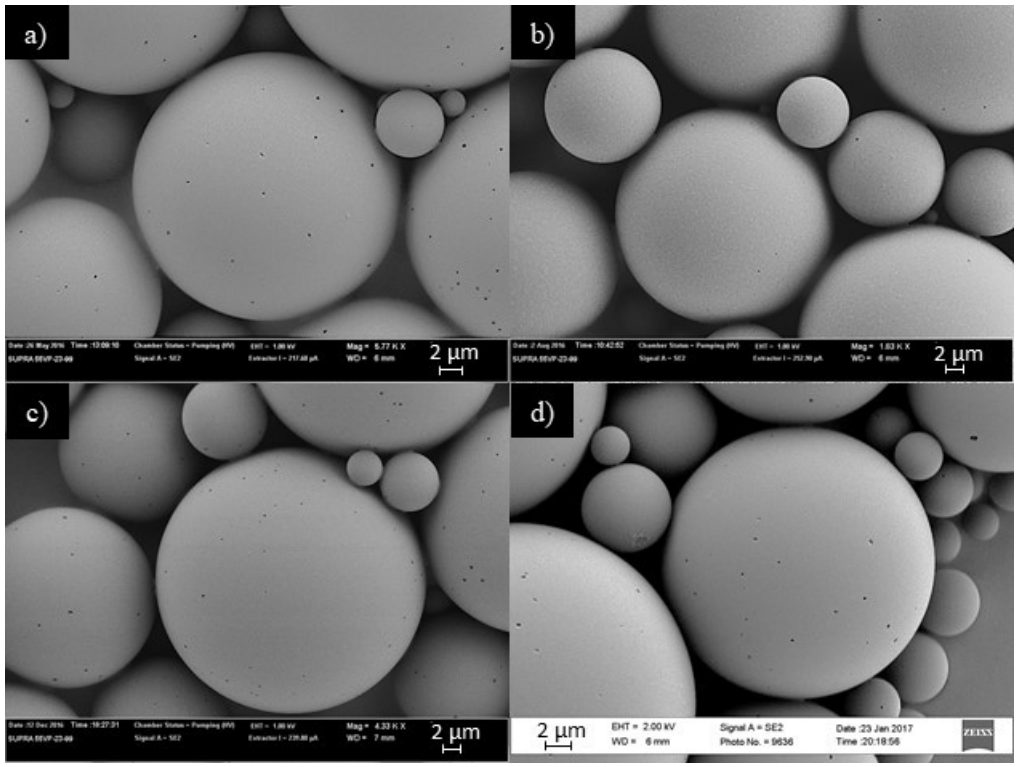

Figure 4.3: Characterisation of the change in particle morphology observed with PLLA 250 after a) 0 months, b) 3 months, c) 6 months and d) 8 months

Interestingly, SEC characterisation of both PLLA 25 and PLLA 250 displayed minimal signs of degradation after 6 months (Figure 4.4). In fact, only noticeable degradation of PLLA 250 was observed after 7 months in Cleanzyme, where a decrease in intensity was observed coupled with the formation of a lower molecular weight shoulder on the SEC chromatogram. The broad low molecular weight shoulder implied that a combination of both surface and bulk degradation was occurring, which is characteristic of enzymatic degradation.

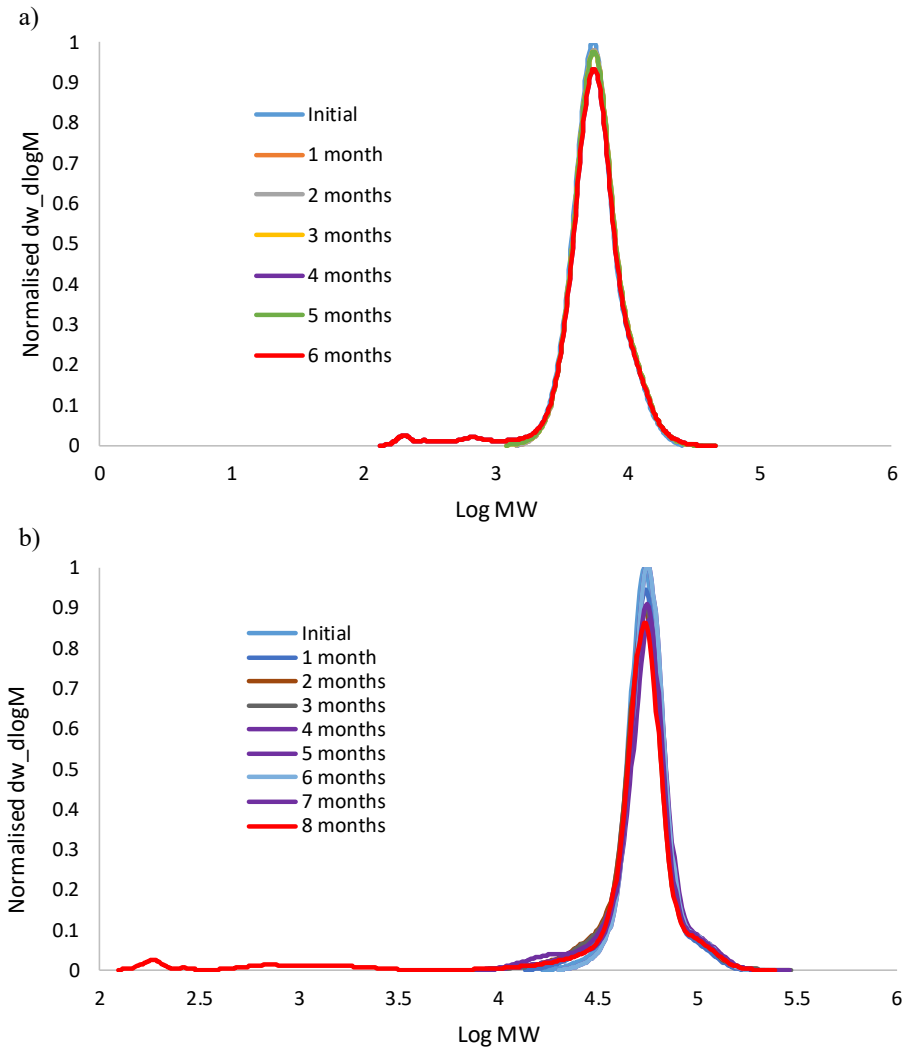

Figure 4.4: Characterisation of PLLA microparticle degradation in Cleanzyme solution *via* SEC a) PLLA 25, b) PLLA 250

To monitor the release of ABM during particle degradation, aliquots of the particle degradation were taken regularly, placed into a 50:50 water: ethanol solution and the subsequent change in fluorescence intensity monitored over 5 h using a fluorescence plate reader with excitation and emission filters of 390 nm and 520 nm respectively (Chapter 3, Section 3.2.3.1). The ABM release profile from PLLA 25 and PLLA 250 particles correlated well with the obtained degradation data, where only minimal change in fluorescence intensity was observed (Figure 4.5). Interestingly, after 4 months, PLLA 25 particles displayed a slight increase in total release after 5 h, which suggested the onset of particle degradation. However, continued monitoring of the particle degradation and release over a longer time-period would be required to confirm this.

Secondary to the release, the loss of dye loading (*E*) was also monitored during particle degradation. A sample of the particle solution was taken at regular intervals, washed and freeze-dried before completely solubilising in dichloromethane. Characterisation of the subsequent fluorescence intensity using a fluorometer enabled direct calculation of the [ABM] within the particle throughout degradation (Chapter 3, Section 3.2.3.3). Following from an initial loss of *E* observed with both degradation sets (Figure 4.4), only minimal change in *E* was observed with PLLA 250 particles throughout the 8 months. After 4 months PLLA 25 particles displayed a clear decrease in *E*. The reduced *E* implied that the particles have enhanced permeability, thus enabling increased dye loss between washings. The minimal signs of degradation and release observed with PLLA 25 and PLLA 250 particles implies the good resistance of PLLA to degradation under environmental conditions. However, future work is required to determine the full effect of molecular weight on particle degradation and release.

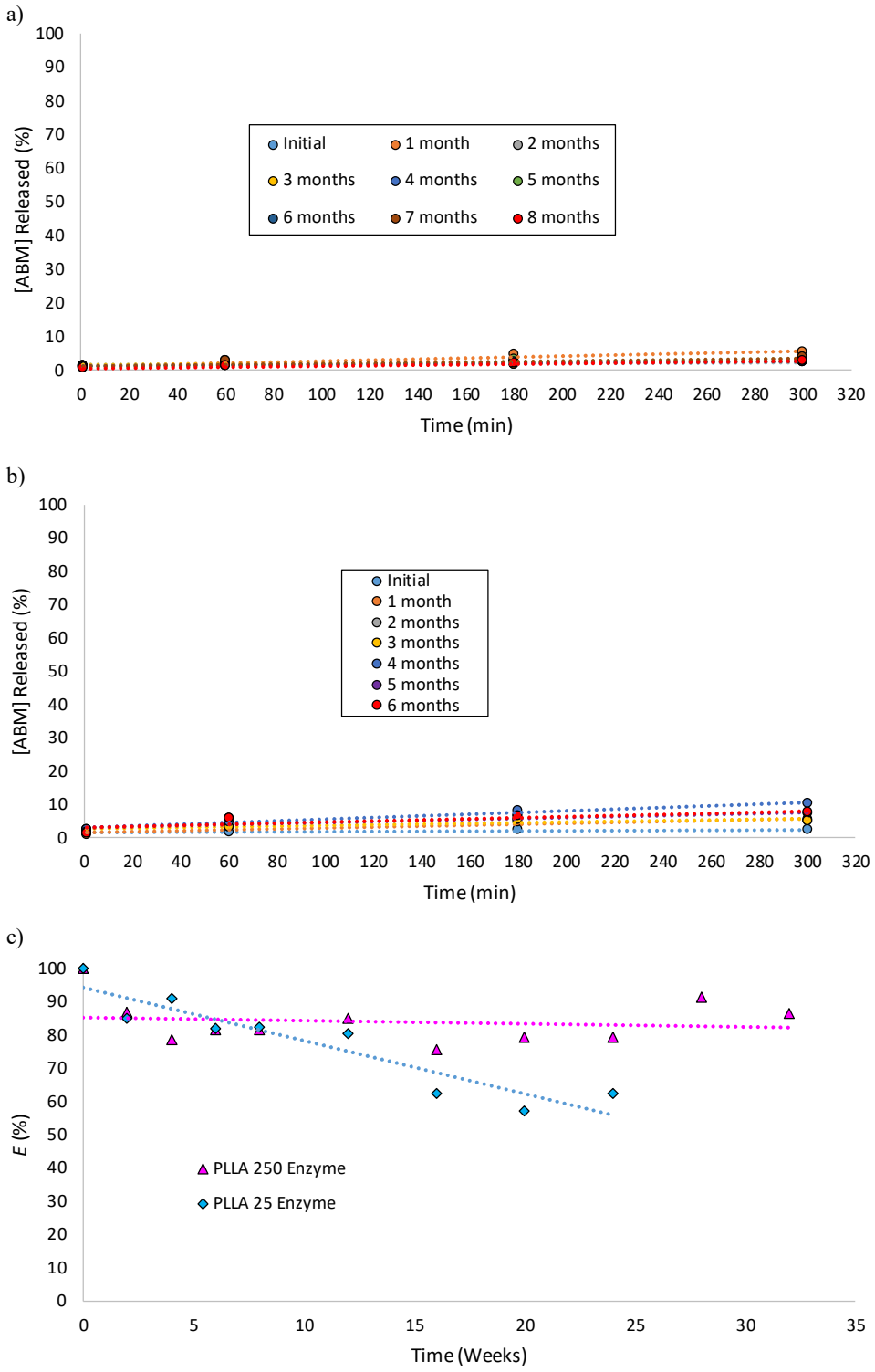

Figure 4.5: Release into water/ethanol observed with a) PLLA 250 and b) PLLA 25 and c) change in *E* with both PLLA 25 and PLLA 250 in Cleanzyme solution

4.2.1.2 Varying Polymer

The chirality, crystallinity and nature of the polymer can all drastically influence the particle degradation profile. Consequently, it was interesting to investigate the different particle degradation profiles observed with PDLLA, PCL and PHB under simulated environmental conditions. In order to be comparable, each polymer was synthesised with a DP of 100. Hence, even though the polymers have a different molecular weight, each chain would have 100 repeat units, hence the same number of degradable ester linkages on the polymer backbone.

4.2.1.2.1 Encapsulation of ABM into Varying Polymeric Microparticles

To determine the versatility of the ABM encapsulation, the dye loading into a different polymeric particle was investigated. PCL 100 particles containing ABM (1 wt%) were prepared using the optimised particle procedure. The particles were dried overnight before being washed three times with DI water and then fully dissolved in dichloromethane. The resultant fluorescence intensity was recorded using a fluorometer (Table 4.1).

Table 4.1: Table showing decrease in dye loading into PCL particles and the resultant dye content within the particles.

PCL Sample no.	[ABM] (wt%)[a]	Dye Loading (%)
1	1	15 ± 2.2
2	0.25	25 ± 0.7
3	0.1	73 ± 1.6
4	0.075	64 ± 0.9
5	0.05	75 ± 1.4
6	0.025	70 ± 2.0

[a]Calculated with respect to [PCL] in organic phase during particle synthesis, [b]Determined experimentally by comparing the fluorescence intensity of the dye inside the particles to a calibration of six known [ABM] in CH_2Cl_2

Analysis of the fluorescence intensity revealed that the PCL particles only had a very low dye loading of 15%. PCL has a high hydrophobicity and as a consequence of its linear backbone, the chains can tightly pack into extensive crystallites. As a consequence of the high crystallinity of the polymer, it was postulated that addition of the ABM can disrupt the crystallinity of the chains during particle synthesis, leading to the formation of large pores within the particle matrix. Furthermore, increased porosity of the particles would result in an increased particle permeability, and consequently a reduced dye loading. Therefore, it was hypothesised that a lower dye concentration would decrease the pore size within the particle, thus increasing the dye loading. Consequently, PCL 100 particles were prepared with decreasing concentrations of ABM. Characterisation *via* fluorometry revealed that the dye loading increased as the dye loading decreased. The change in particle crystallinity observed with decreasing dye concentration could also be observed *via* SEM (Figure 4.6).

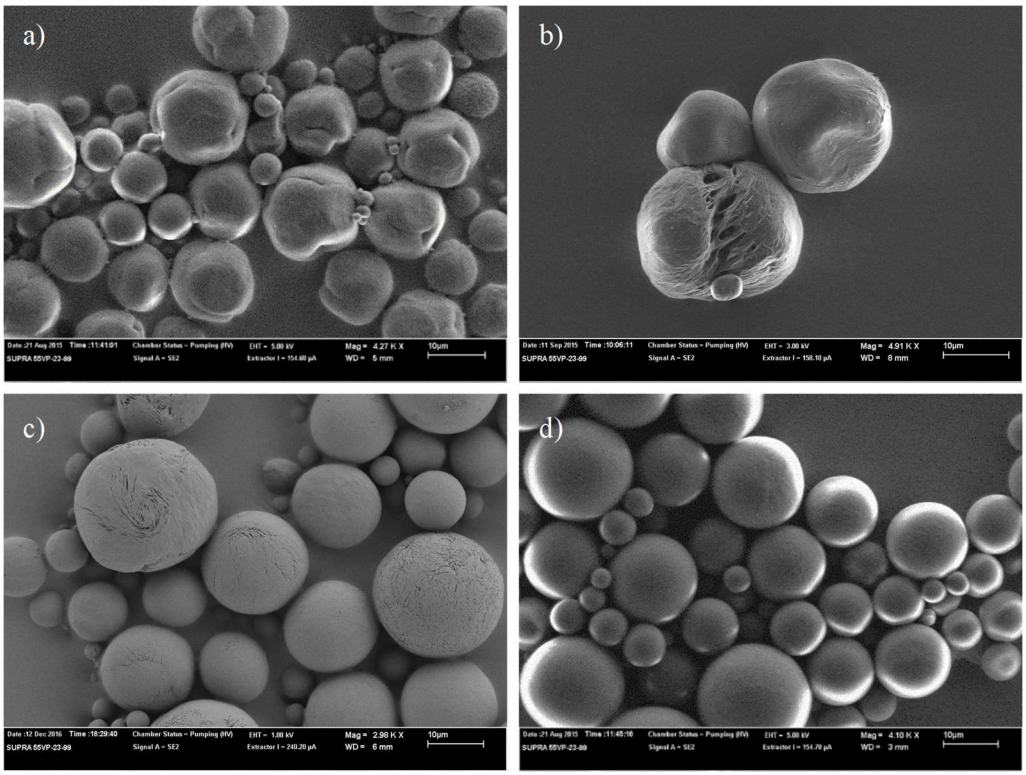

Figure 4.6: SEM analysis of PCL microparticles with a) 1 wt% ABM, b) 0.5 wt% ABM, c) 0.1 wt% ABM and d) No dye

SEM characterisation revealed that as the concentration of dye decreased, the particle morphology displayed an increase in homogeneity, with less evidence of particle disfigurement or surface roughness. Again, this was postulated to be a consequence of decreased disruption of the crystallinity of the PCL chains during particle synthesis.[23] The versatility of the ABM encapsulation with a decreased dye loading (0.1 wt%) was investigated further by monitoring the fluorescence intensity observed in particles with a range of polymeric matrices (PLLA, PDLLA and PHB) (Table 4.2).

Table 4.2: Encapsulation of dye loading of 0.1 wt% ABM into varying polymeric particles

Sample	Polymer	[ABM] (wt%)[a]	Dye Loading (%)[b]
1	PLLA 100	0.1	68 ± 1.4
2	PCL 100	0.1	73 ± 1.8
3	PDLLA 100	0.1	64 ± 1.6
4	PHB 100	0.1	54 ± 2.9

[a]Calculated with respect to [PCL] in organic phase during particle synthesis, [b]Determined experimentally by comparing the fluorescence intensity of the dye inside the particles to a calibration of six known [ABM] in CH_2Cl_2

Characterisation *via* fluorometry showed that each set of polymeric particles displayed a high dye loading, thus demonstrating the promising applicability of ABM encapsulation into a variety of different particles. As a consequence of the high dye loading observed with a lower dye loading and to maximise the change in fluorescence intensity observed during particle release, a dye loading of 0.1 wt% was applied for all subsequent particle characterisation.

4.2.1.2.2 Poly(D,L-Lactic Acid)

The symmetric nature of *L*-LA allows for the PLLA polymer chains to assemble into a highly ordered, densely packed structure. The close proximity of the polymer chains acts to increase the strength of the intermolecular bonds between chains, thus producing a highly crystalline polymer. On the other hand, PDLLA chains have varying chirality around the carbons containing the methyl side chain. Therefore, the polymer cannot pack as tightly, which reduces the strength of the intermolecular bonds between the polymer chains. Hence, PDLLA displays decreased crystallinity compared to PLLA. Consequently, the difference in chirality between the polymers will produce microparticles with distinctly different degradation and release profiles. PDLLA 100 was polymerised according to the method detailed in Chapter 2 and used in microparticle synthesis to encapsulate ABM (0.1 wt%) using the optimised single

oil-in-water technique (Chapter 3, Section 3.2.3). Multiple PDLLA 100 particle batches were synthesised and combined before being washed with water and freeze-dried. The subsequent dried particles were re-suspended in both Cleanzyme and water and the degradation monitored for 8 months, (for full characterisation of PDLLA 100 particle degradation in water, see Appendix (Chapter 10, Section 10.2.3)). Characterisation of the change in particle morphology *via* SEM over 8 months in Cleanzyme revealed no visible signs of degradation (Figure 4.7). Further characterisation of PDLLA 100 particle degradation in Cleanzyme by SEC revealed the formation of lower molecular weight peaks after 8 months (Figure 4.8). However, similarly to PLLA 100, only minimal degradation was observed over the 8-month period.

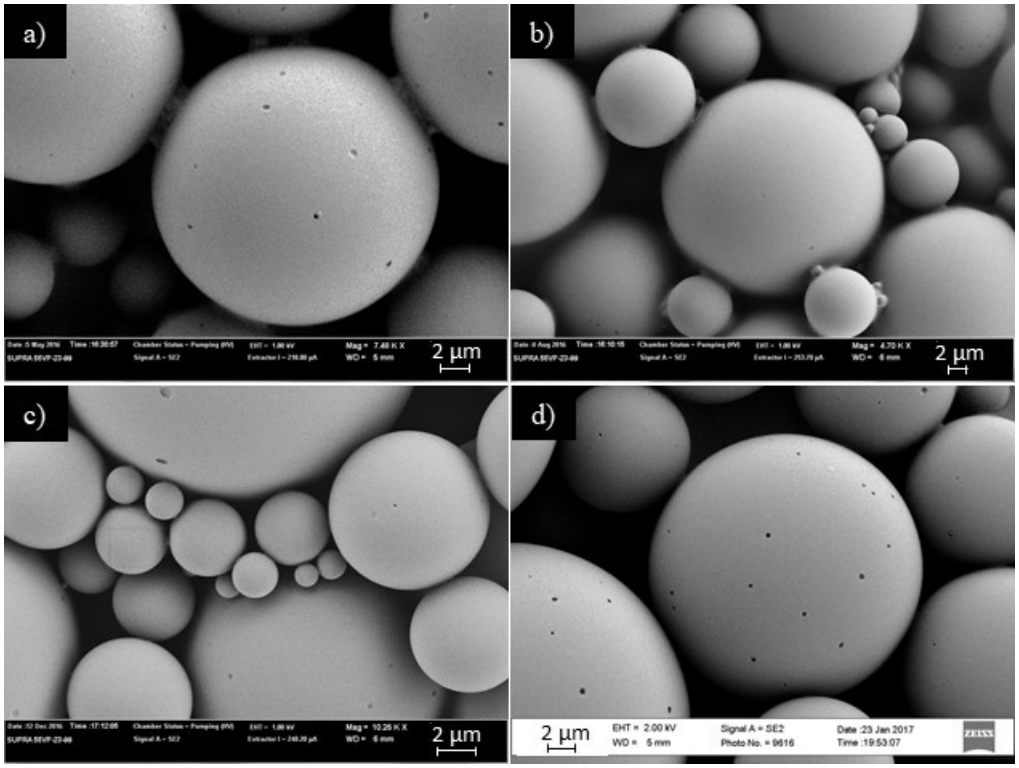

Figure 4.7: Characterisation of the change in particle morphology observed with PDLLA 100 in Cleanzyme solution *via* SEM after a) 0 months, b) 3 months, c) 6 months and d) 8 months

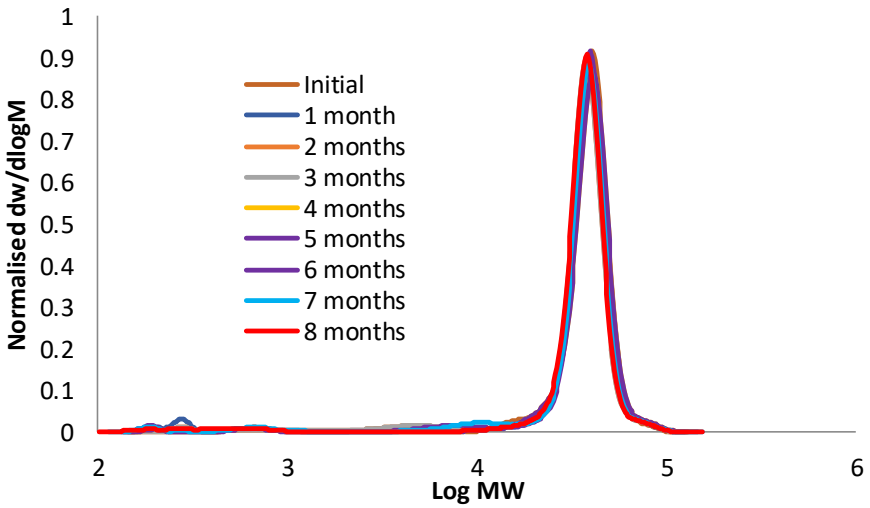

Figure 4.8: Characterisation of PDLLA 100 microparticle degradation in Cleanzyme solution *via* SEC over 8 months

PDLLA 100 particles displayed minimal signs of ABM release into the 50% water and ethanol solution throughout the 8 months degrading in Cleanzyme (Figure 4.9). Even with decreased crystallinity, PDLLA particles displayed similar degradation and release profiles to PLLA 100. Therefore, further monitoring of the particle degradation and release is required to elucidate the effect of polymer crystallinity on the particle degradation and release rate.

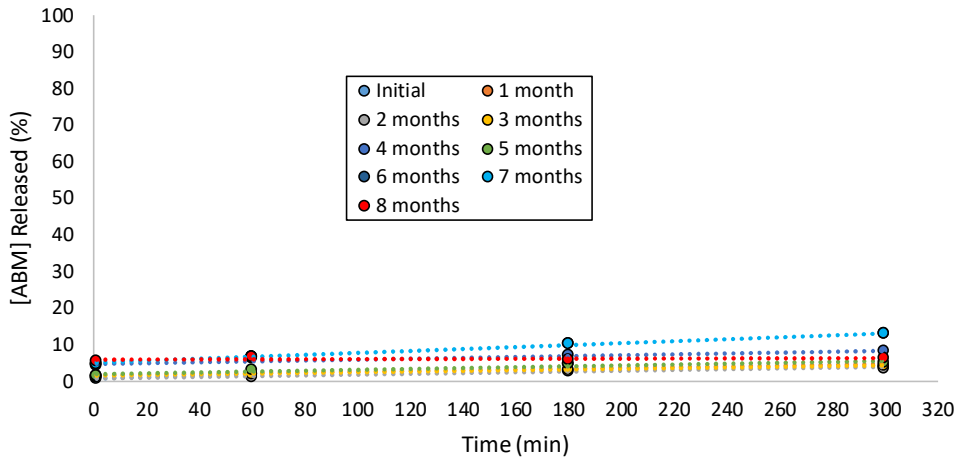

Figure 4.9: [ABM] released from PDLLA 100 particles observed by release study into water/ethanol over 8 months

4.2.1.2.3 Poly(ε-Caprolactone)

PCL has been widely studied as a consequence of its interesting mechanical properties and good biodegradability. The long aliphatic chain of PCL enables the production of strong intermolecular bonds between chains, thus resulting in the formation of a highly crystalline polymer with high hydrophobicity. Therefore, it was hypothesised that PCL would display increased stability towards microparticle degradation and release. PCL was polymerised using the method detailed in Chapter 2 (Section 2.2.1.3) and used as the particle matrix to encapsulate ABM (0.1 wt%) using an optimised single oil-in-water technique (Chapter 3, Section 3.2.3). The particles were washed and dried before being re-suspended in Cleanzyme and water, (for full characterisation of PCL 100 particle degradation in water, see Appendix (Chapter 10, Section 10.2.4)). SEM characterisation of PCL particles revealed an increased pitting formation on the particles during the 9-month degradation period (Figure 4.10).

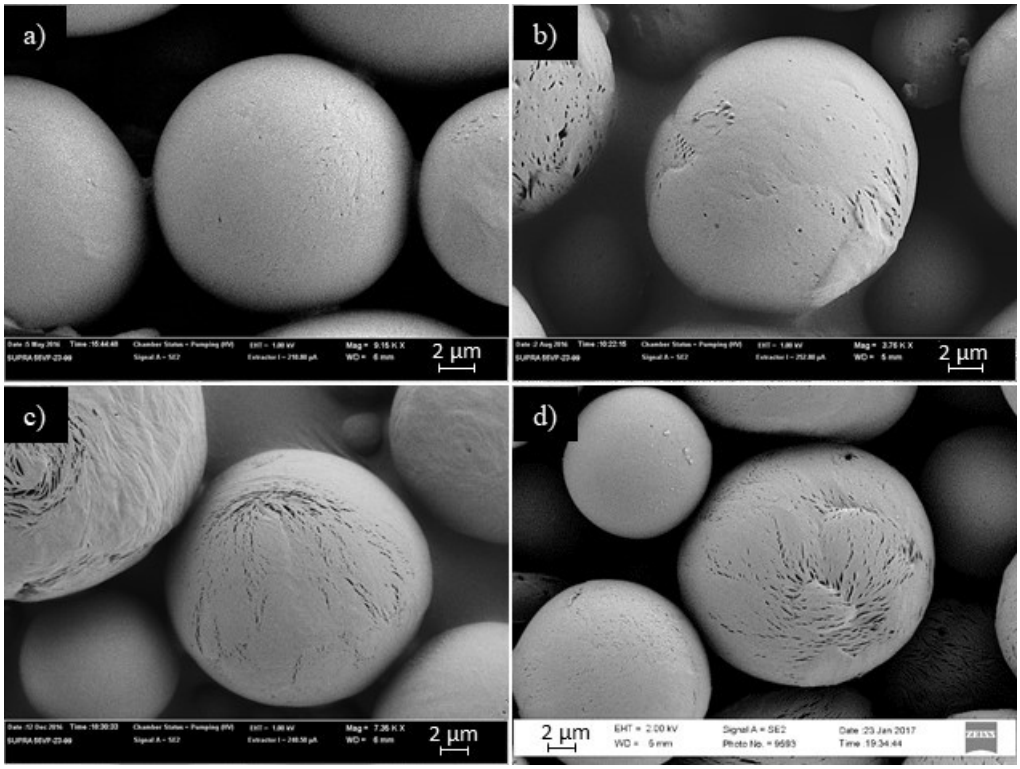

Figure 4.10: SEM characterisation of the change in particle morphology observed with PCL 100 in Cleanzyme solution after a) 0 months, b) 3 months, c) 6 months and d) 9 months

Further characterisation of the particle degradation by SEC showed signs of surface degradation after 6-months, signified by the distinctive broadening of the polymer SEC trace (Figure 4.11). Lower molecular weight peaks were observed after 7 months, which further confirmed the particle degradation. The presence of low molecular weight peaks implied that a combination of both bulk and surface degradation was occurring within the system. Furthermore, the difference between the SEC chromatograms between samples indicated that significant amounts of low molecular weight water-soluble oligomers were present and as such had been removed from the sample between particle washings. PCL 100 particles displayed minimal signs of ABM release into water and ethanol (Figure 4.12).

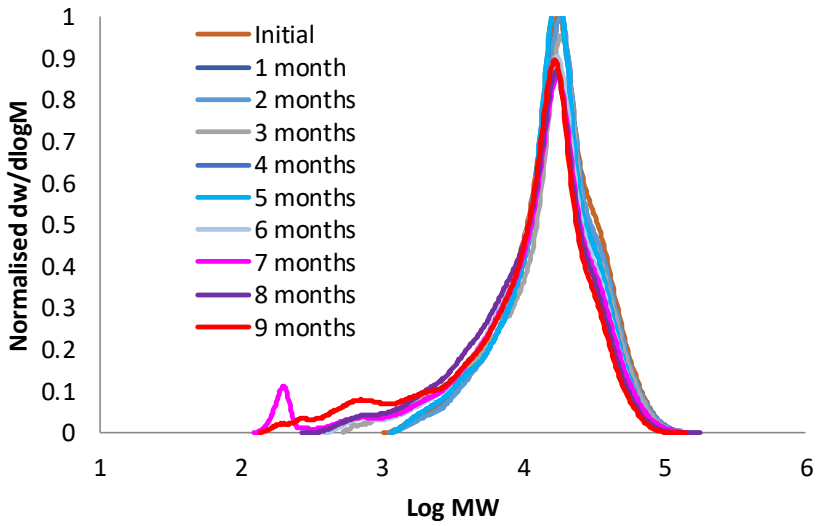

Figure 4.11: Characterisation of PCL 100 microparticle degradation in Cleanzyme solution *via* SEC over 9 months

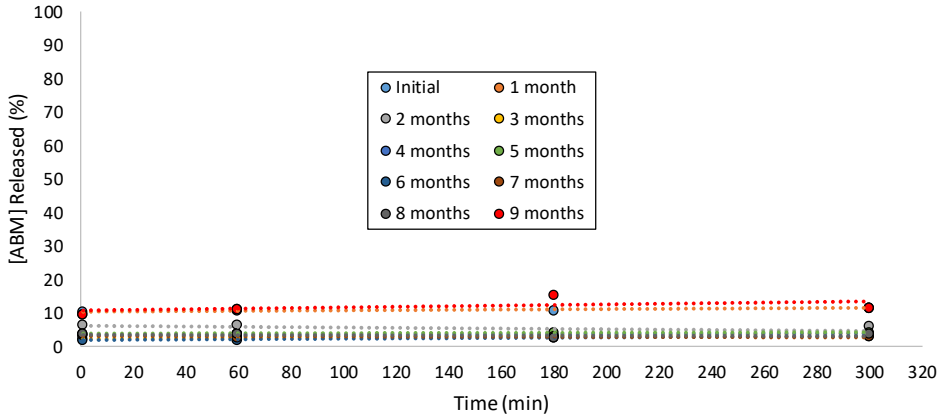

Figure 4.12: Particle release observed by release study into water/ethanol observed over 9 months

4.2.1.2.4 Poly(3-Hydroxybutyrate)

Poly(3-hydroxybutyrate) (PHB) is one of the most widely studied polyhydroxyalkanoates as a consequence of its good biodegradability and bio-derivation. PHB consists of a smaller length repeat unit compared to PLLA and PCL, hence the degradable ester linkages are closer together on the polymer backbone. It was hypothesised that the decreased chain length would enhance the pH change within

the particle matrix, thus enabling an increased degradation rate. PHB was polymerised to DP 100 (PHB 100) (Chapter 2, Section 2.2.1.4), before preparing multiple batches of PHB 100 particles with ABM (0.1 wt%) encapsulated. The particles were washed and dried before being re-suspended in water and enzymatic solution. Interestingly, after 5 months within aqueous solution, no visible degradation was evident *via* SEM analysis (Figure 4.13). Conversely, after 1 month in enzymatic solution, multiple broken particles were evident throughout the sample (Figure 4.14). Increasing particle degradation was observed throughout the 3 months, with nearly all particles appearing broken or degraded after 3 months.

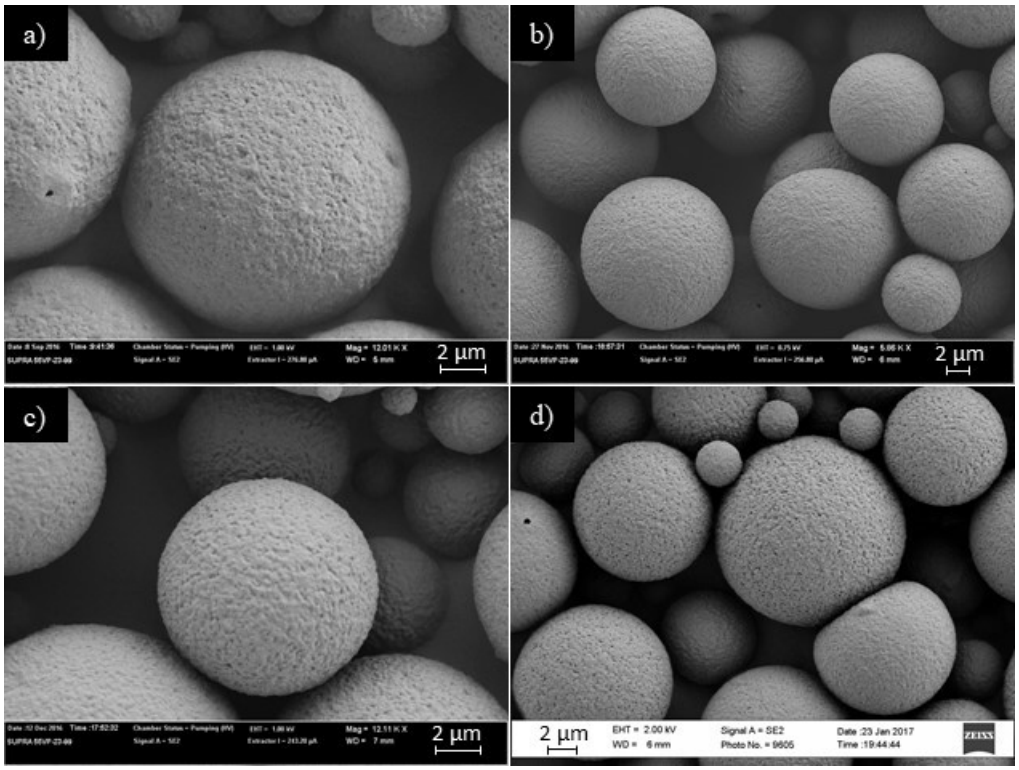

Figure 4.13: SEM analysis of PHB after a) 0 months, b) 2 months, c) 4 months and d) 5 months in water

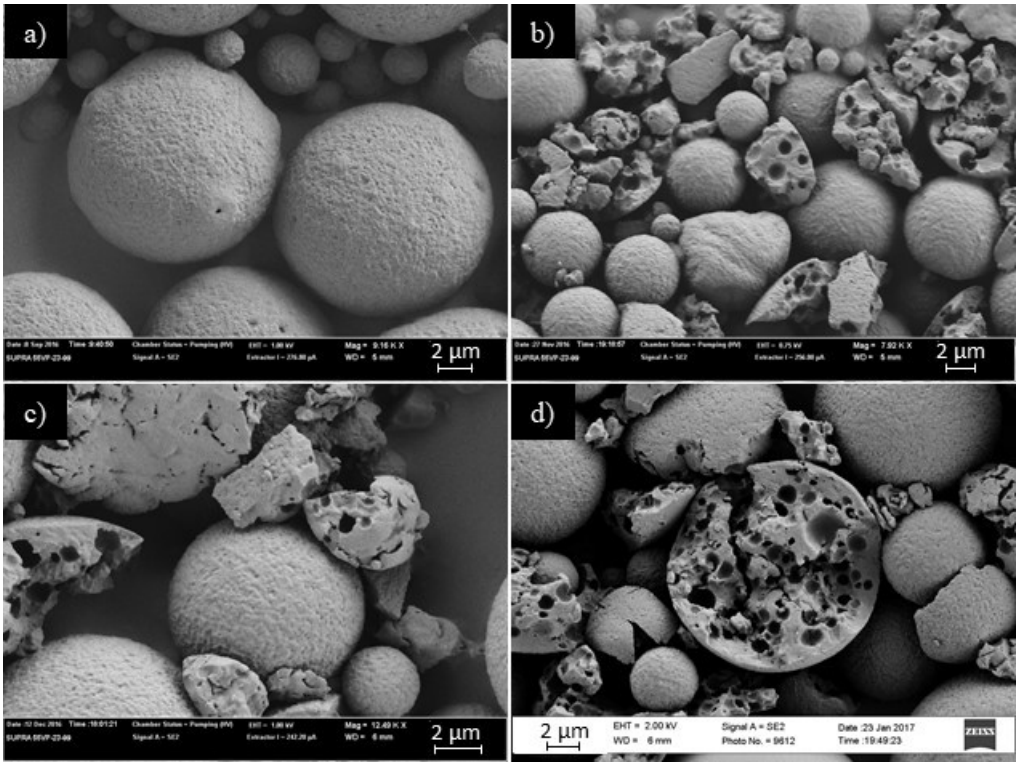

Figure 4.14: SEM analysis of PHB after a) Initial sample, b) 1 month, c) 2 months and d) 3 months in enzymatic solution

SEC Characterisation of PHB particle degradation in Cleanzyme and water correlated well with the degradation profiles observed by SEM analysis, where the onset of particle degradation was evident after 4 weeks in enzymatic solution (Figure 4.15). Indeed, broadening of the SEC peak as well as the formation of lower molecular weight peaks observed *via* SEC characterisation of PHB 100 in Cleanzyme implied that a combination of both surface and bulk degradation was acting to hydrolyse the PHB polyester chains. Conversely, only lower molecular weight peaks were evident *via* SEC characterisation of PHB 100 particles in water after 12 weeks, thus implying only bulk degradation had occurred.

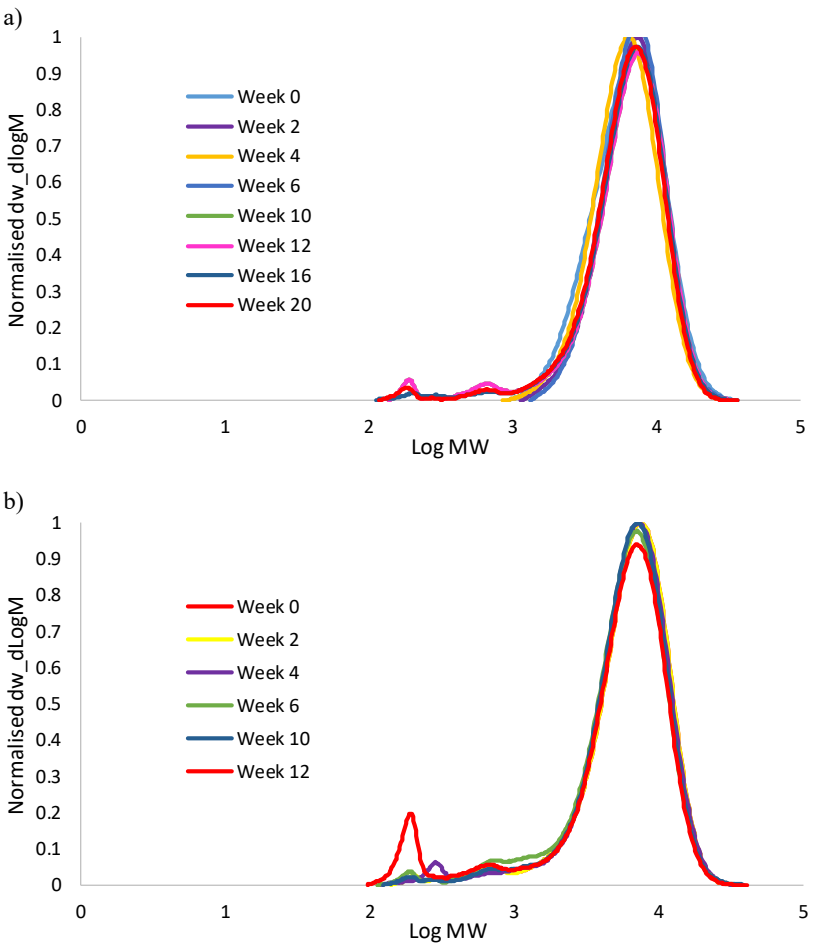

Figure 4.15: SEC characterisation of PHB in a) water and b) enzymatic solution

PHB 100 particles displayed only a low release of ABM into water and ethanol throughout the 20 weeks' aqueous degradation study (Figure 4.16 a). Conversely, PHB 100 particles in Cleanzyme displayed a large increase in burst release after 4 weeks, with full release of the encapsulated ABM after 12 weeks (Figure 4.16 b). The observed release agreed with the particle degradation profile determined *via* SEM and SEC, hence, the PHB 100 particles displayed a good control over ABM release as the particles degraded. Characterisation of the loss of *E* by fluorometry correlated well with the observed release for PHB 100 degradation in water (Figure 4.17). However, a full loss of *E* was observed after 10 weeks of PHB 100 particle degradation in Cleanzyme (Figure 4.17). This was postulated to be a consequence of the partially

degraded particles breaking during particle washing, thus resulting in full release from the broken particles.

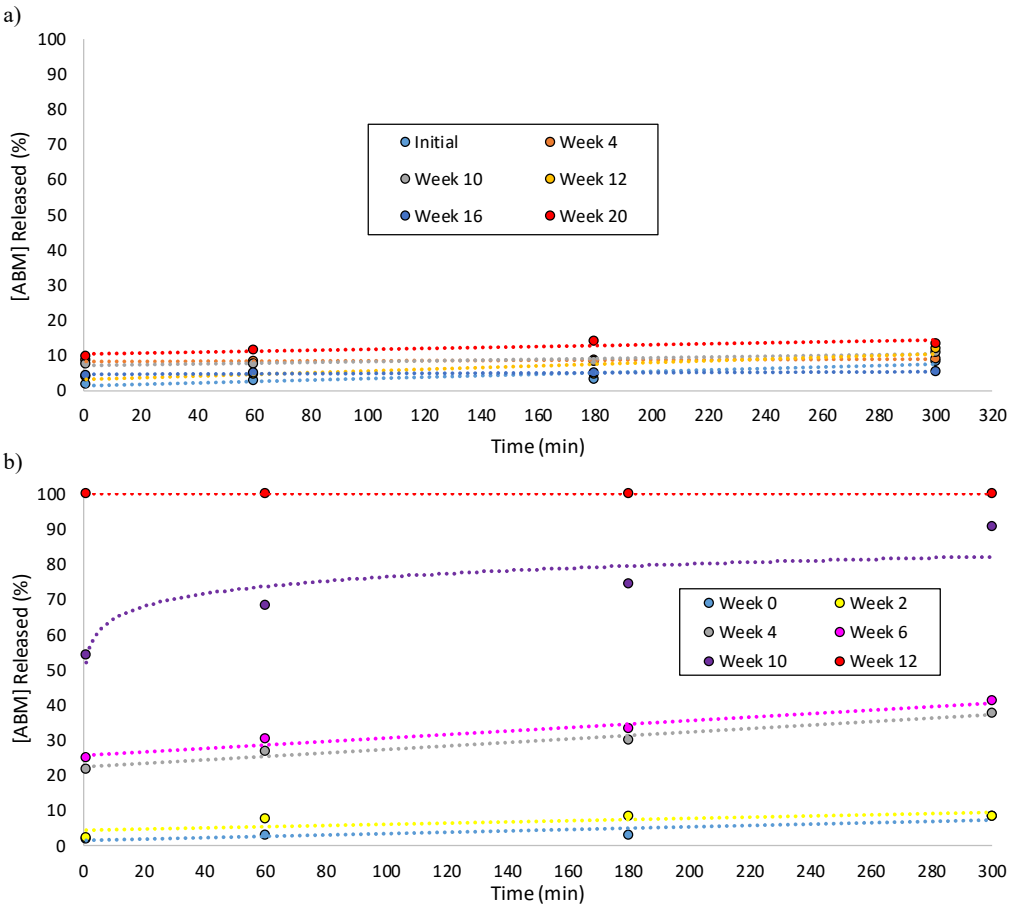

Figure 4.16: [ABM] released from PHB 100 particles observed by release study into water/ethanol in a) Water and b) Cleanzyme

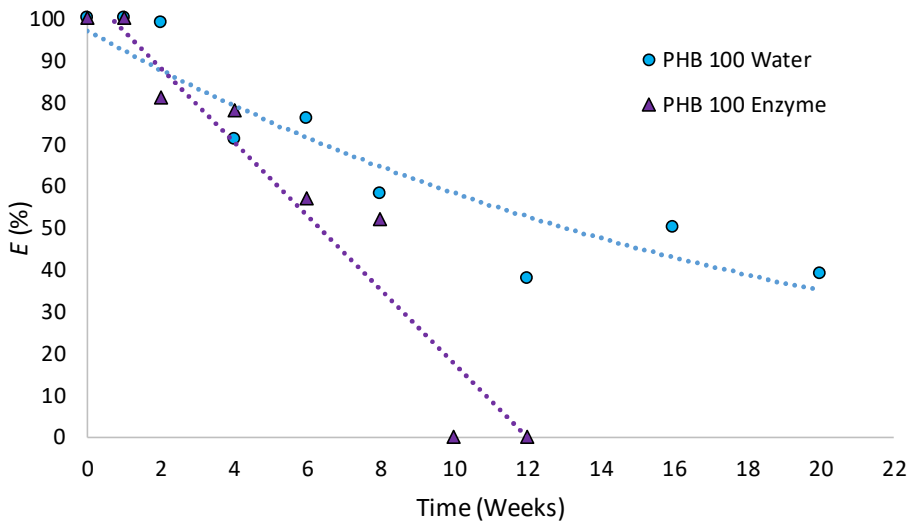

Figure 4.17: Change in *E* observed with ABM encapsulated into PHB 100 particles in water and Cleanzyme

4.3 Conclusions

In conclusion, the degradation of polyester microparticles in a simulated soil environment was investigated. Monitoring the particle degradation by SEC, SEM and mass loss revealed that PLLA, PDLLA and PCL display good stability towards hydrolysis in both an aqueous and enzymatic environment. Similarly, the release rate of ABM confirmed only minimal particle degradation had occurred. PHB was discovered to be less stable to enzymatic degradation under soil-like conditions, displaying full release of ABM and particle degradation after 12 weeks in Cleanzyme. Conversely, only minimal release was observed in aqueous solution. Further information regarding the particle degradation would be required to enable the production of a microparticle degradation library. However, the good control observed with PHB 100 displays the potential for polyester microparticles to be employed in a variety of controlled release applications within agriculture.

4.4 References

1. R. P. Brannigan and A. P. Dove, *Biomater. Sci.*, 2017, **5**, 9-21.
2. M. D. Rowe, E. Eyiler and K. B. Walters, *Polym. Test.*, 2016, **52**, 192-199.
3. R. Chandra and R. Rustgi, *Prog. Polym. Sci.*, 1998, **23**, 1273-1335.
4. V. Speranza, A. De Meo and R. Pantani, *Polym. Degrad. Stab.*, 2014, **100**, 37-41.
5. H. Satoh, N. Yoshie and Y. Inoue, *Polymer*, 1994, **35**, 286-290.
6. S. Lyu and D. Untereker, *Int. J. Mol. Sci.*, 2009, **10**, 4033-4065.
7. S. Agarwal, *Polymer Science: A Comprehensive Reference*, Elsevier, Amsterdam, 2012.
8. G. Gallet, R. Lempiäinen and S. Karlsson, *Polym. Degrad. Stab.*, 2000, **71**, 147-151.
9. A. Noreen, K. M. Zia, M. Zuber, M. Ali and M. Mujahid, *Int. J. Biol. Macromol.*, 2016, **86**, 937-949.
10. H. Pranamuda, Y. Tokiwa and H. Tanaka, *Appl. Environ. Microbiol.*, 1997, **63**, 1637-1640.
11. D. Rasselet, A. Ruellan, A. Guinault, G. Miquelard-Garnier, C. Sollogoub and B. Fayolle, *Eur. Polym. J.*, 2014, **50**, 109-116.
12. M. J. Stanford and A. P. Dove, *Chem. Soc. Rev.*, 2010, **39**, 486-494.
13. L. Xiao, B. Wang, G. Yang and M. Gauthier, *Poly(Lactic Acid)-Based Biomaterials: Synthesis, Modification and Applications*, INTECH, Croatia, 2012.
14. S. Li and S. McCarthy, *Biomaterials*, 1999, **20**, 35-44.
15. A. Torres, S. M. Li, S. Roussos and M. Vert, *J. Appl. Polym. Sci.*, 1996, **62**, 2295-2302.

16. N. K. N. Limanska, V. Biscola, T. Ivanytsia, A. Merlich, BDGM Franco, J. M. Chobert, V. Ivanytsia and T. Haertle, *J. Plant Pathol. Microb.*, 2015, **6**, 292-300.

17. N. Kamaly, B. Yameen, J. Wu and O. C. Farokhzad, *Chem. Rev.*, 2016, **116**, 2602-2663.

18. R. Grillo, A. d. E. S. Pereira, N. F. S. de Melo, R. M. Porto, L. O. Feitosa, P. S. Tonello, N. L. D. Filho, A. H. Rosa, R. Lima and L. F. Fraceto, *J. Hazard. Mater.*, 2011, **186**, 1645-1651.

19. J. Siepmann, N. Faisant, J. Akiki, J. Richard and J. P. Benoit, *J. Controlled Release*, 2004, **96**, 123-134.

20. R. Jeyanthi, B. C. Thanoo, R. C. Metha and P. P. Deluca, *J. Controlled Release*, 1996, **38**, 235-244.

21. J.-C. Jeong, J. Lee and K. Cho, *J. Controlled Release*, 2003, **92**, 249-258.

22. Janisource, Cleanzyme Enzyme Digestant, https://janisource.com/cleanzyme-enzyme-cleaner-spotter-odor-remover-1-gallon/, (accessed 13-06-17, 2017).

23. M. J. Kwon, J. H. Bae, J. J. Kim, K. Na and E. S. Lee, *Int. J. Pharm.*, 2007, **333**, 5-9.

5. Stimulus-Controlled Release of a Fluorescent Dye

5.1 Introduction

There is a continued need to reduce the amount of pesticide required to achieve safe and efficient crop growth.[1] One of the key areas that can help drive this is the use of more efficient pesticide formulations and 'smart'/responsive agrochemical delivery systems.[2-4] Encapsulating agrochemicals into biodegradable microparticles can allow for increased efficiency of the active ingredient (AI).[5-8] Moreover, Meyer *et al*., investigated the encapsulation of the insecticide imidacloprid into poly(lactic-*co*-glycolic acid) (PLGA) microparticles.[9] By encapsulating the pesticide, it was discovered that approximately 200 times less imidacloprid was required to achieve the same mortality of psyllids as the pesticide on its own without encapsulation. Hence, encapsulation can enable decreased toxicity of an active ingredient whilst still maintaining the required AI concentration necessary to achieve the desired drug efficiency.

Poly(malic acid) (PMA) is well known to be a hydrophilic, biodegradable and bioabsorbable polyester.[10, 11] PMA can be derived synthetically or by fermentation of specific microorganisms observed in natural or bacterial sources.[12] Synthetically, PMA is typically prepared *via* either polycondensation or ring-opening polymerisation (ROP) of the naturally occurring, non-toxic malic acid (MA).[13-17] MA consists of two carboxylic acids and an alcohol moiety, therefore, polycondensation can proceed *via* the formation of both α- and β-linkages (Scheme 5.1).

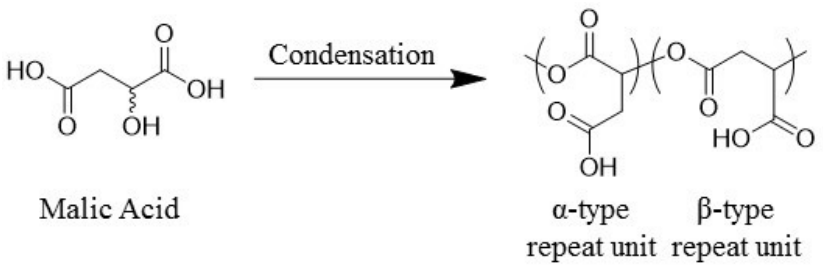

Scheme 5.1: Schematic representation of condensation of PMA *via* α-type and β-type repeat unit[13]

The properties and functionality of PMLA can be easily tailored *via* functionalisation of the pendent carboxyl group present in the malic acid monomer.[18-20] Moreover, functionalisation of the unreacted carboxyl group enables modulation of the polymer hydrophobicity, the stimuli sensitivity and also allows the introduction of bioactive ligands or drugs. Polyester microparticle degradation occurs *via* random hydrolytic scission of the cleavable ester bonds within the polymer backbone (Scheme 3.1).[21] During particle degradation, the encapsulated AI is released to the surrounding environment. Therefore, the rate of release is highly dependent on the type of polymer used, the polymer molecular weight and the polymer crystallinity.[22-24] Hence, the particle degradation and AI release can be tuned by variation of the material used for the particle matrix. Microparticles synthesised from blends of two biodegradable homopolymers present a promising alternative to controlling the particle degradability and the rate of drug release.[25-28] Blending at least two homopolymers enables combining the desirable properties of two or more polymers without the complexity and time required for copolymerisation.[29]

Stimuli-controlled release offers the advantages of the controlled release observed with degradable materials with the added benefit of control of the degradation onset *via* application of an external trigger. Stimuli-responsive polymers have been intensively studied as a consequence of their ability to change their chemical and/ or

physical properties upon exposure to an external stimulus.[30] Numerous stimuli have been explored (*e.g.* pH, thermoresponsive, CO_2 responsive *etc.*) and have found use within a wide range of applications such as medicinal, agricultural and architectural.[31-33] Recently, Summerlin *et al*., reported site-specific agrochemical delivery using pH-responsive poly(succinimide)-based nanoparticles.[34] The pH-responsive nanoparticles enabled the internal release of an AI as a consequence of the pH change observed within the phloem of the plant. Hence stimuli-controlled release enables excellent control over the AI release and thus offers great potential for use within agriculture.

In order to achieve the desired tuneable agrochemical release for a range of agricultural applications, biodegradable microparticles from blends of poly(*L*-lactide) (PLLA) and PMA were prepared and investigated in this Chapter. It was hypothesised that as the responsive PMA degraded, the acidic degradation products would accumulate within the particle matrix. This in turn would create pockets of lower internal pH within the particle matrix, thus resulting in the autocatalysed degradation of PLLA. Therefore, the AI release would be controlled by the initial concentration of the responsive polymer within the particle. Consequently, this Chapter presents the synthesis and characterisation of particle blends of PLLA with an acidic-responsive poly(ethyl malic acid) and a light-responsive poly(nitrobenzyl malic acid).

5.2 Results and Discussion

5.2.1 *Synthesis of pH-Responsive Polymer*

The pH of soil varies worldwide depending on the country, time of year and the surrounding conditions. It was hypothesised that particles prepared using blends of PMA and PLLA would show an enhanced degradation rate in an acidic environment. In order to maintain a controlled release and to allow for sufficient alteration of the pH within the particle matrix, diffusion through the particle ideally must be restricted. Therefore, the 'responsive' polymeric unit was desired to preferably be hydrophobic. PMA is well known to be a hydrophilic polymer, however, the hydrophobicity of PMA has been shown to be easily modified simply by the addition of a methyl unit to the malic acid chain end.[35]

5.2.1.1 Step-Growth Polymerisation of Methyl Malic acid

Methyl malic acid was synthesised according to the procedure by Miller *et al*., using a two-step one pot procedure (Scheme 5.2).[36] The successful methylation of MA was confirmed by the presence of the methyl resonance (δ = 3.8 ppm) by ^{1}H NMR spectroscopic analysis.

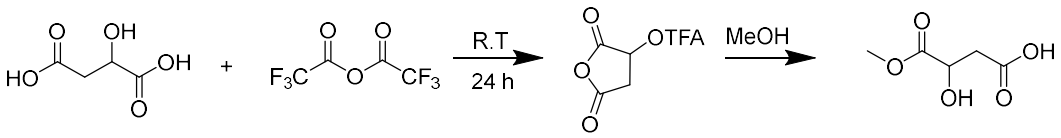

Scheme 5.2: Schematic representation of the synthesis of methyl malic acid

Polymerisation of methyl malic acid was performed *via* step-growth polymerisation. The monomer was stirred in bulk at 110 °C for three days under nitrogen. The successful polymerisation of methyl malic acid was confirmed by ^{1}H NMR spectroscopy (Figure 5.1), where a clear shift in the methine proton of the monomer (δ = 4.6 ppm) was observed with the formation of the characteristic peak of the

methine on the polymer backbone (δ = 5.6 ppm).[35] Integration of the aforementioned shifts enabled calculation of the monomer conversion (54%).

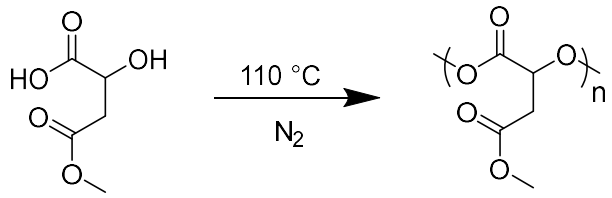

Scheme 5.3: Schematic representation of the synthesis of PMeMA

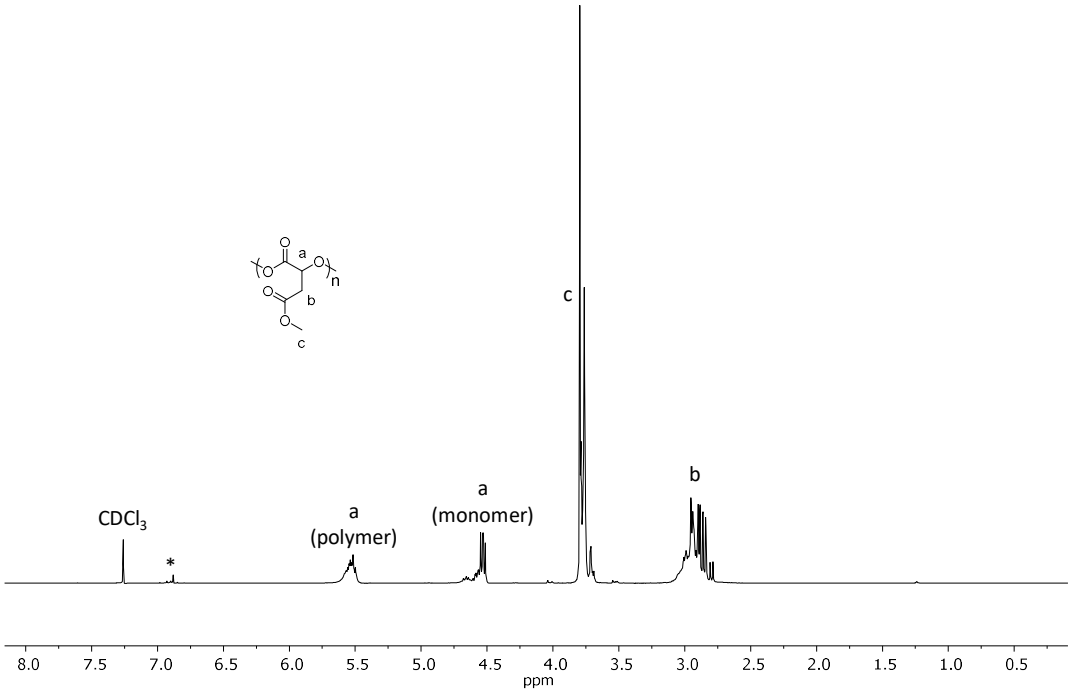

Figure 5.1: Crude ^{1}H NMR spectrum of PMeMA synthesised *via* step-growth polymerisation, * = olefinic hydrogen of fumaric acid, ($CDCl_3$, 300 MHz)

Initial investigations in the field of PMA polycondensation by Kajiyama *et al*., have highlighted the potential side reactions that can occur during polymerisation.[14] The polymerisation proceeds through the intermolecular dehydration of malic acid, however, it is a competitive reaction with the intramolecular dehydration of MA and depolymerisation. Consequently, this can lead to the undesirable formation of fumaric acid. The existence of fumaric acid within the synthesised PMeMA was confirmed by

the presence of an olefinic proton resonance in the ^{1}H NMR spectrum (δ = 6.8 ppm) (Figure 5.1). Additionally, the bimodal SEC chromatogram observed also implied the formation of the fumarate present as the low molecular weight peak (Figure 5.2).

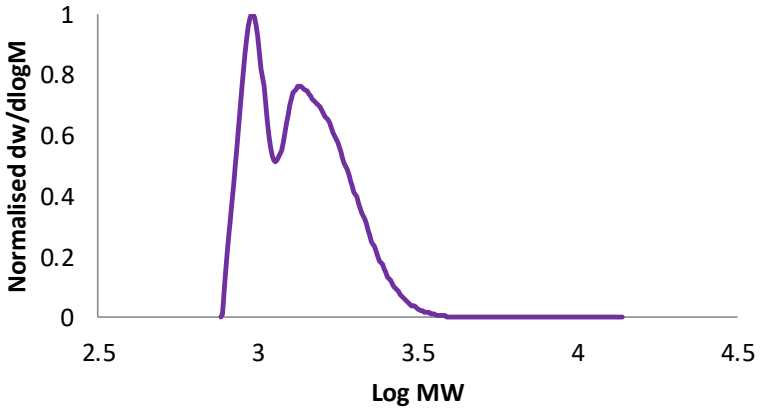

Figure 5.2: SEC characterisation of PMeMA synthesised *via* step growth polymerisation ($CHCl_3$, PS standard)

As the polymerisation progressed, an increasing quantity of translucent crystals were observed at the top of the reaction flask. Subsequent ^{1}H NMR spectroscopic analysis identified the crystals as unreacted MeMA monomer (Figure 5.3). Crystal formation was thought to be a consequence of the high reaction temperature and high volatility of MeMA, thus resulting in monomer sublimation. Furthermore, loss of monomer during polymerisation would act to shift the polymerisation equilibrium to favour side reactions, thus resulting in an increased concentration of fumaric acid in the final product. The high concentration of fumaric acid in the final polymer was confirmed by the high intensity of the low molecular weight peak observed *via* SEC characterisation (Figure 5.2).

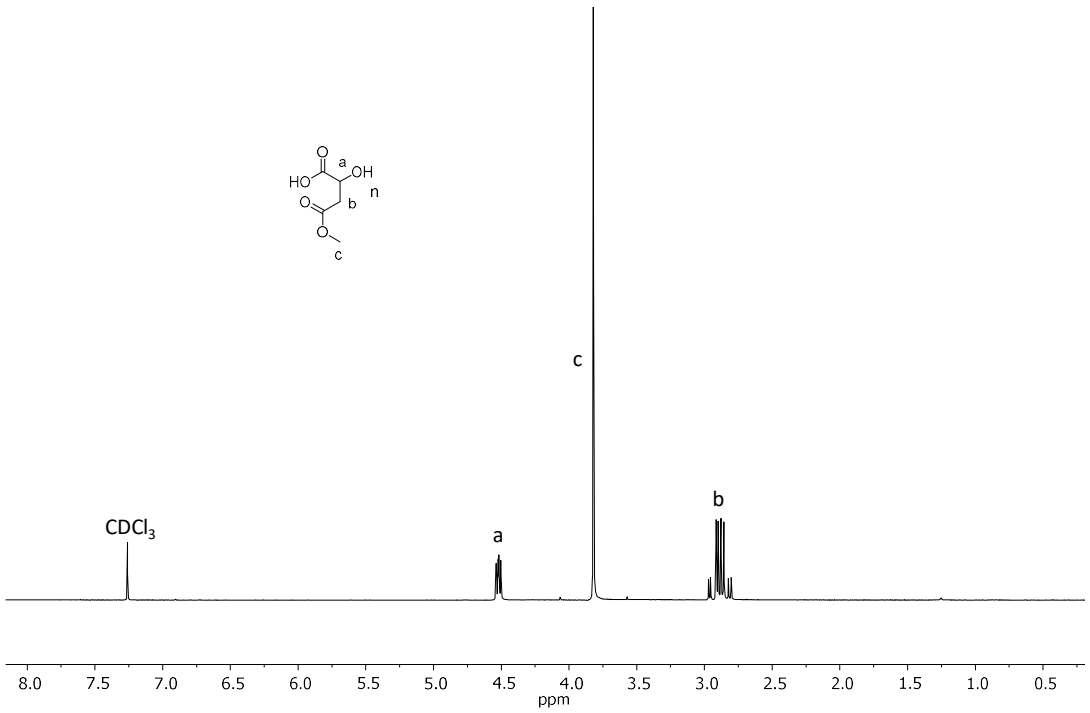

Figure 5.3: ^{1}H NMR spectrum of crystals formed during polymerisation of methyl malic acid ($CDCl_3$, 300 MHz)

5.2.1.2 Step growth Polymerisation of Ethyl Malic acid

As a consequence of the high fumarate formation and high volatility observed with MeMA, the polymerisation of a hydrophobic malic acid with increased stability was investigated. EtMA is less volatile than MeMA, consequently, it was hypothesised that EtMA would show increased resilience to side reactions, thus decreasing the concentration of fumaric acid in the final product. Ethyl malic acid was synthesised according to the procedure by Miller *et al.*, using the same two-step one pot procedure as for methyl malic acid (Scheme 5.4).[36]

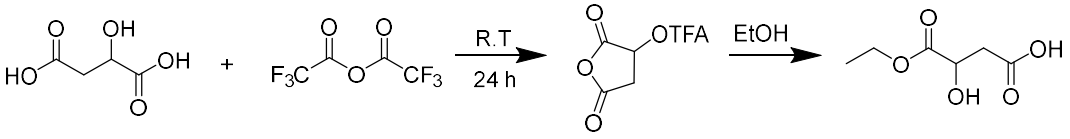

Scheme 5.4: Schematic representation of the synthesis of ethyl malic acid

Polymerisation of ethyl malic acid was performed *via* step-growth polymerisation in bulk at 110 °C (Scheme 5.5). The reaction was heated for three days under nitrogen. The successful polymerisation of ethyl malic acid was confirmed by ^{1}H NMR spectroscopy, where a clear shift and intensity decrease in the monomer methine proton (δ = 4.6 ppm) was observed with the formation of the characteristic shift for the methine on the polymer backbone (δ = 5.6 ppm).[37]

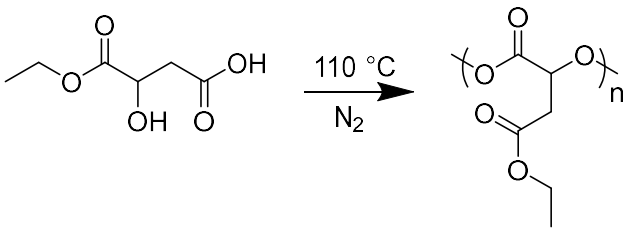

Scheme 5.5: Schematic representation of step-growth polymerisation of ethyl malic acid in bulk

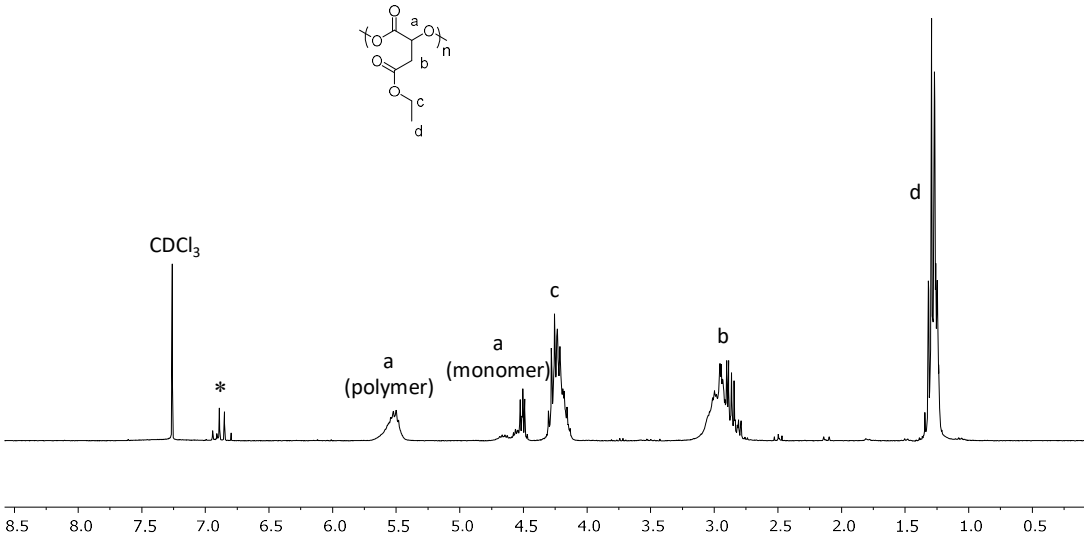

Figure 5.4: ^{1}H NMR spectrum of PEtMA synthesised *via* step growth polymerisation, * = olefinic hydrogen of fumaric acid, ($CDCl_3$, 300 MHz)

Evidence of fumaric acid was confirmed by the presence of the shift representative of the olefinic proton of the fumarate (δ = 6.8 ppm) in the ^{1}H NMR spectrum (Figure 5.4). Nevertheless, unlike MeMA polycondensation, crystal formation was not observed during polymerisation of EtMA. The final polymer was precipitated into petroleum ether before drying *in vacuo* and characterising by ^{1}H NMR spectroscopy and SEC (Figure 5.5). Furthermore, SEC analysis confirmed the predicted reduction in unwanted side reactions by the decreased intensity of the lower molecular weight fumarate peak present in the chromatogram (Figure 5.5).

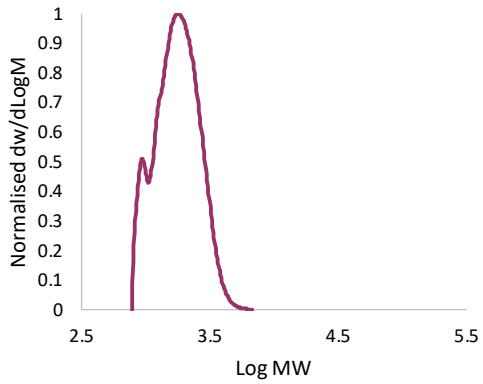

Figure 5.5: SEC characterisation of PEtMA synthesised *via* step-growth polymerisation, ($CHCl_3$, PS standard)

5.2.2 ***Synthesis of pH-Responsive Particles***

5.2.2.1 Poly(Ethyl Malic acid) Particle Synthesis

To determine the suitability and stability of PEtMA for use as the matrix of a microparticle, a reference batch of particles was prepared using optimised single oil-in-water solvent evaporation conditions (Chapter 2), using PEtMA as the particle matrix. As a general procedure, PEtMA was dissolved in dichloromethane before homogenising at 7000 rpm for 30 s with an aqueous solution (containing Mowiol 488 as a stabiliser (2 wt%)). The organic solvent was evaporated overnight before characterising the particle suspension *via* light scattering and scanning electron

microscopy (SEM) (Figure 5.6). Interestingly, even though the suspension appeared slightly cloudy, no particles could be detected by dynamic light scattering on a Malvern Mastersizer. Furthermore, only a low concentration of small particles (≤ 10 μm) were observed by microscopy. During particle synthesis, PEtMA was found to be only sparingly soluble in dichloromethane. Consequently, it was postulated that the low concentration of particles observed and the small particle size was a result of the low solubility of PEtMA in dichloromethane.

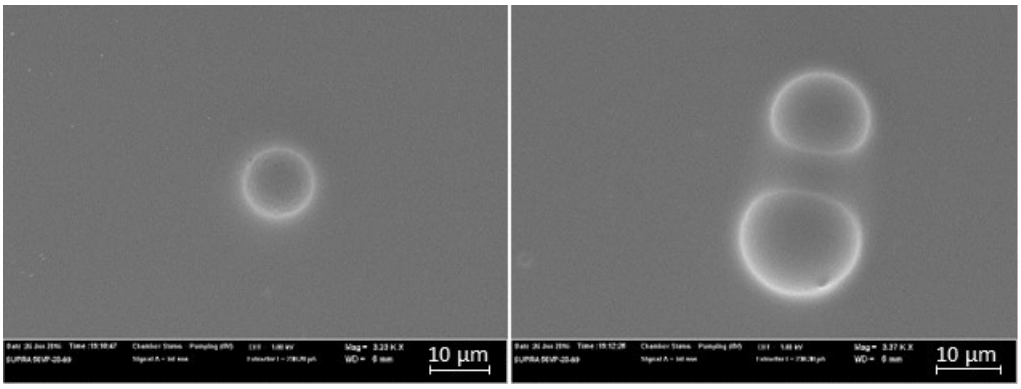

Figure 5.6: SEM analysis of PEtMA particles prepared *via* single oil-in-water solvent evaporation technique

With the aim of increasing the particle yield, the solubility of PEtMA was investigated in acetone. PEtMA was found to fully dissolve in acetone, therefore, the particle synthesis was repeated using acetone as the organic phase solvent. The solution was slowly stirred overnight to allow for evaporation of the acetone before characterising *via* light scattering and SEM (Figure 5.7).

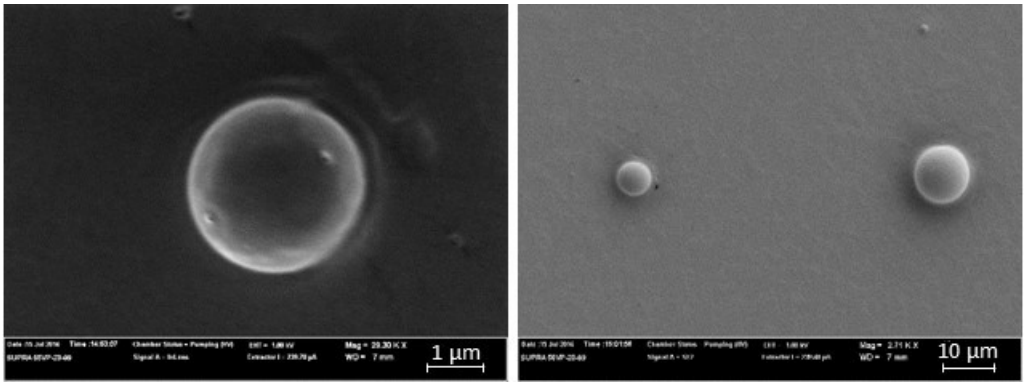

Figure 5.7: SEM characterisation of PEtMA particles using acetone as organic solvent

Again, SEM characterisation of the suspension revealed the formation of a low concentration of small particles (≤ 10 µm) (Figure 5.7). PEtMA fully dissolved in acetone, therefore, it was hypothesised that the observation of a decreased particle concentration and size was a consequence of the lower molecular weight of PEtMA compared to PLLA 100 (Table 2.1). Moreover, the lower polymer molecular weight would decrease the total viscosity of the system, which in turn would have the effect of reducing the particle size.

Particle size has been shown to affect the microparticle degradation and release profile.[38] Therefore, to ensure a comparable study between PEtMA and PLLA 100 particles, it was necessary to maintain a constant particle size between samples. Consequently, to increase the PEtMA particle size to 10 µm, multiple suspensions were prepared by systematically varying the initial concentration of PEtMA and the shear speed and time. However, even with an increased concentration of PEtMA and decreased shear speed and time, micron sized particles could not be detected *via* light scattering on the Mastersizer. Consequently, a sample of a particle suspension prepared with 15 s of shear at 5000 rpm, was characterised *via* dynamic light scattering on a Malvern Zetasizer Nano ZS instrument (DLS) (Figure 5.8).

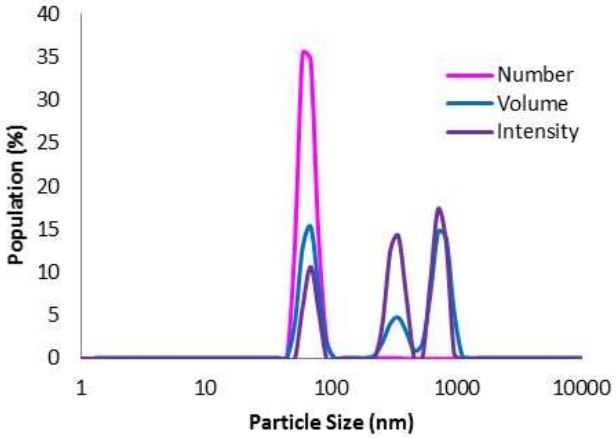

Figure 5.8: DLS characterisation of PEtMA (30 wt %) after 15 s of shear on a Silverson high shear mixer at 5000 rpm

Therefore, even at lower shear speed and time and increased concentration, DLS characterisation revealed the formation of nanoparticles. Therefore, it was hypothesised that PEtMA prepared by polycondensation would not be able to produce the required 10 μm sized particles *via* the optimised single oil-in-water conditions desired for use in this application.

5.2.2.2 Synthesis of Poly(Ethyl Malic Acid)/ Poly(L-Lactide) Particles

Even though microparticles with a PEtMA matrix were unattainable by solvent evaporation, it was hypothesised that PEtMA could still be used as an additive to enhance the microparticle degradation rate. Subsequently, PEtMA (25 wt%) was dissolved alongside PLLA 100 in dichloromethane. The resultant organic solution was homogenised with an aqueous solution for 30 s at 7000 rpm, before leaving the organic solvent to evaporate overnight. The resultant particle suspension was characterised *via* SEM (Figure 5.9).

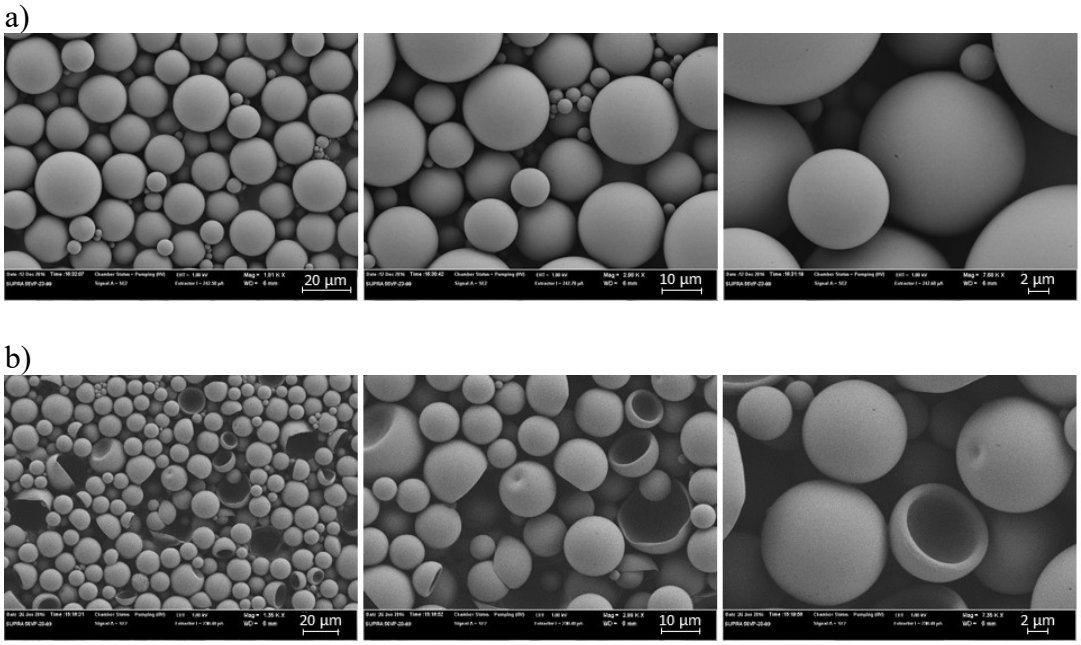

Figure 5.9: SEM images of a) PLLA 100 microparticles and b) PLLA 100 microparticles with PEtMA (25 wt%)

SEM analysis highlighted a drastic difference between the morphology of PLLA 100 microparticles compared to a particle blend of PLLA 100 with PEtMA (25 wt%) (Figure 5.9). The particles prepared from the homopolymer blend appeared to show decreased structural stability, displaying a mixture of dimpled, collapsed and broken particles (Figure 5.9 b). During particle synthesis, it was found that PEtMA was only sparingly soluble in dichloromethane. Therefore, it was postulated that during particle hardening, the PEtMA precipitated at a higher rate compared to PLLA, thus resulting in the deformation and collapse of the particles.

In order to investigate the miscibility of PEtMA and PLLA 100 further, a particle blend was prepared with a lower concentration of PEtMA (5 wt%). Again, PEtMA was observed to be only sparingly soluble in dichloromethane, however, after sonication and intense stirring, PEtMA fully dissolved alongside PLLA 100. The resultant organic solution was added to the aqueous phase and homogenised, before leaving the

solution to stir enabling evaporation of the organic solvent overnight. The resultant particle suspension was characterised *via* SEM (Figure 5.10).

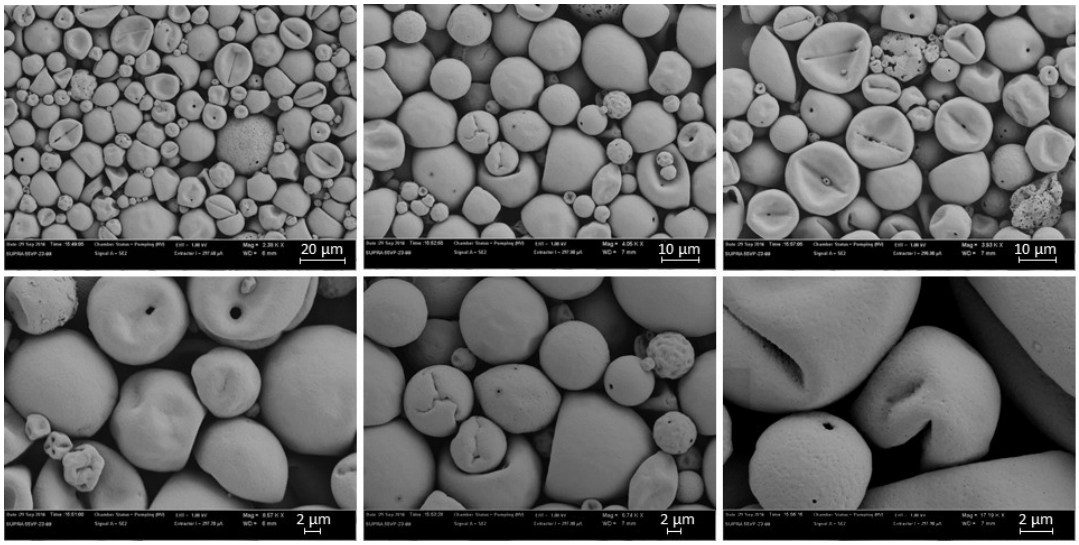

Figure 5.10: SEM characterisation of PLLA 100 microparticles with PEtMA (5 wt%) prepared *via* single oil-in-water solvent evaporation

Even with the decreased concentration of PEtMA, SEM characterisation showed that the particles still maintained a broken and collapsed structure when dichloromethane was used as organic solvent. Therefore, the solubility of PEtMA and PLLA was investigated in chloroform, acetone and tetrahydrofuran (THF). The most promising solvent appeared to be chloroform as at 5 wt% PEtMA, both polymers were soluble. Therefore, an emulsion was prepared with chloroform as the organic solvent. However, subsequent SEM analysis of the particle solution revealed again the formation of deformed, collapsed and broken particles (Figure 5.11).

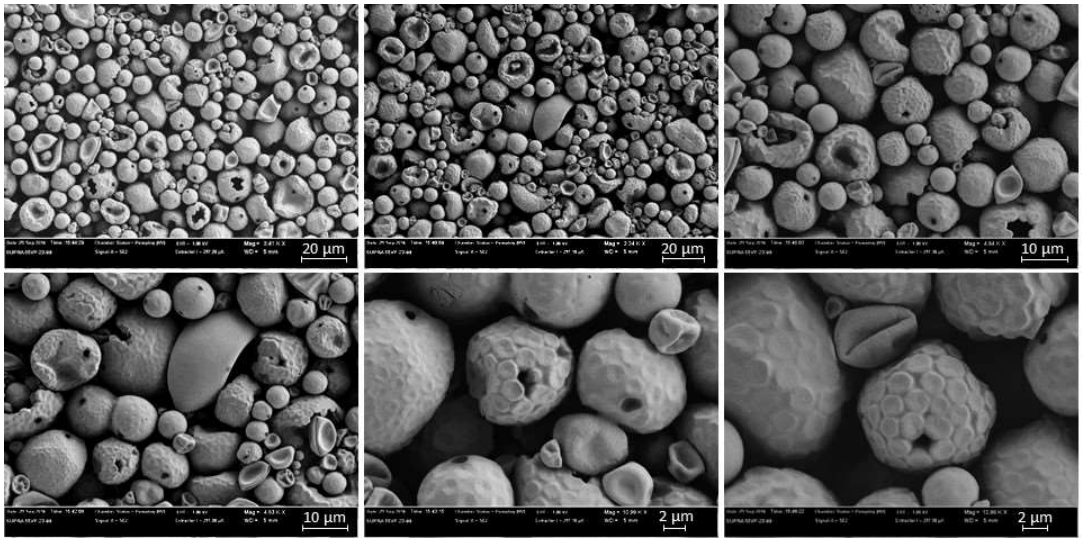

Figure 5.11: SEM characterisation of PLLA 100 microparticles with 5 wt% PEtMA prepared using single oil-in-water emulsion with $CHCl_3$ as organic solvent

The rough and broken particle morphology observed with the PLLA/PEtMA particle blends was postulated to be a consequence of phase separation between the two polymers. To further investigate the interaction between the two polymers, differential scanning calorimetry (DSC) was performed, thus enabling elucidation of the change in behaviour of the polymers physical mixture when subjected to heating scans (Figure 5.12). The DSC scans consisted of three heating and cooling cycles performed over a temperature range of -80 °C to 160 °C with a heating rate of 2 °C/ min. The first heating cycle has been shown to be affected by the thermal history of the polymer, therefore, the second heating cycle is reported as it provides a more reliable indication of the original polymeric properties.[39]

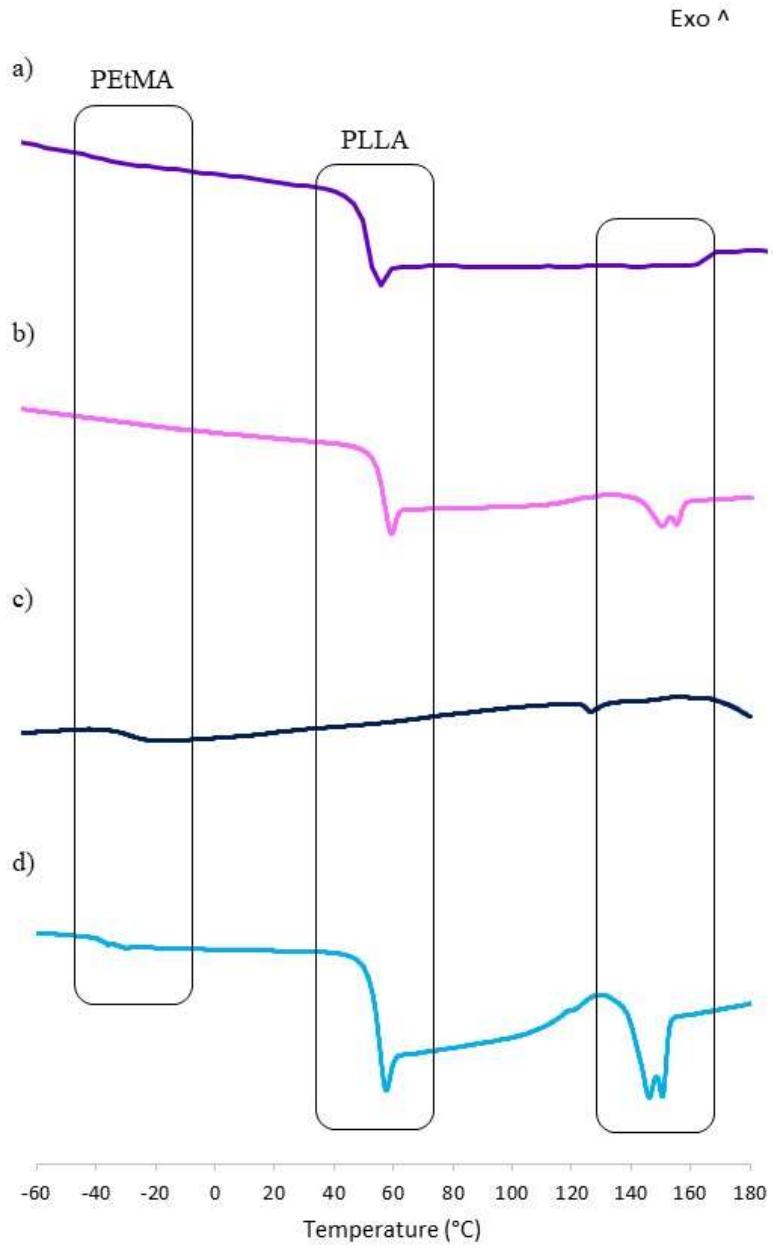

Figure 5.12: DSC thermograms of a) PLLA 100 polymer b) PLLA 100 particles c) PEtMA particles and d) Microparticle blend of PLLA 100 with PEtMA (25 wt%)

The DSC thermogram of the PLLA 100 homopolymer displayed an endothermic event at 55 °C, which corresponds to the glass transition temperature (T_g) of the polymer, in agreement with previous literature (Figure 5.12 a).[40] Whilst heating a polymer, the T_g denotes the temperature at which the polymer is converted from a rigid or glassy state

to a softer rubbery state, indicative of an increase in free volume. Additionally, the DSC thermogram of PLLA 100 microparticles displayed the equivalent T_g as for the homopolymer of PLLA 100 (55 °C), thus implying that the particle synthesis does not affect the mechanical properties of the polymer (Figure 5.12 b). Interestingly, the DSC thermogram of the PLLA 100 particles displayed a bimodal melt peak (150 °C). The bimodal melt peak was postulated to be a consequence of the particles collapsing under the increased heat, followed by the resultant polymer melting.

DSC characterisation of the homopolymer of PEtMA revealed a change in sample heat capacity, representative of a T_g at -25 °C (Figure 5.12 c). The PEtMA DSC thermogram also displayed an endothermic melt peak at 122 °C. Furthermore, evidence for the melt peak and the T_g's of both PLLA and PEtMA are present in the DSC thermogram of the particle blend of PLLA with PEtMA (25 wt%) (Figure 5.12 d). Jeong *et al*. have shown that if two polymers are fully miscible, then only one T_g will be evident in the resultant DSC thermogram.[41] Moreover, the T_g has been shown to be tuneable depending on the ratio of the two miscible polymers within the sample. The presence of two distinct T_g's within the particle blend confirmed that the polymers are phase separating. Therefore, it was assumed that homopolymer blends of PLLA and PEtMA would not be able to achieve the required miscibility desired to create stable microparticles capable of controlled release of an AI.

5.2.3 *Synthesis of Light Responsive Particles*

Light has been shown to be an excellent stimulus for triggering release of an encapsulated AI.[42, 43] In particular, *o*-nitrobenzyl esters are of specific interest as a consequence of the fast photolysis of the nitrobenzyl ester observed under UV light irradiation, thus breaking the ester linkage between the polymer and phototrigger.[44, 45] Following this concept, it was hypothesised that addition of poly(nitrobenzyl malic acid) (PNO_2BnMA) within a PLLA particle would enable degradation and release by exposure to UV light. Furthermore, the increased hydrophobicity provided by the addition of the benzyl ring to the malic acid moiety would increase the solubility of PNO_2BnMA in dichloromethane. Therefore, it was postulated that particle blends of PNO_2BnMA and PLLA would have an increased capability of forming stable microparticle suspensions.

5.2.3.1 Step-Growth Polymerisation of Poly(Nitrobenzyl Malic acid)

Nitrobenzyl malic acid was prepared with an analogous methodology to methyl malic acid and ethyl malic acid by ring opening from the trifluoroacetate of maleic anhydride with 2-nitrobenzyl alcohol before step-growth polymerisation in bulk at 110 °C. The mixture was heated for three days under nitrogen, before characterising the monomer conversion by ^{1}H NMR spectroscopy. The final polymer was precipitated three times into petroleum ether before drying *in vacuo* in order to be able to remove the excess of unreacted monomer. The successful polymerisation of PNO_2BnMA was confirmed by the presence of the methine resonance on the polymer backbone (δ = 5.5 ppm) and the α-methine resonance of the chain end (δ = 4.64 ppm) (Figure 5.13).

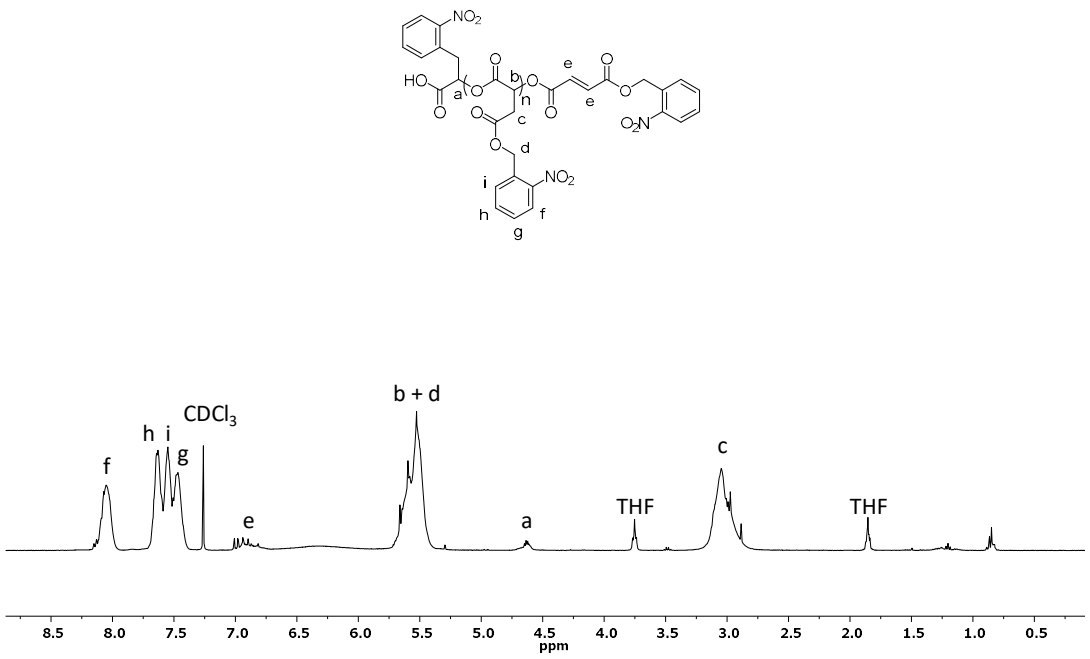

Figure 5.13: ^{1}H NMR spectrum of PNO_2BnMA synthesised *via* step growth polymerisation ($CDCl_3$, 300 MHz)

5.2.3.2 DIC Coupling of Poly(Nitrobenzyl Malic acid)

Step-growth polymerisation enabled a simple one pot approach to the synthesis of poly(nitrobenzyl malic acid). However, the high temperature associated with the bulk polymerisation is undesirable for large-scale industrial synthesis. Therefore, the polymerisation of NO_2BnMA was performed by *N*, *N*'-diisopropylcarbodiimide (DIC) coupling according to the method developed by Moore *et al*. at room temperature.[46] Nitrobenzyl malic acid was reacted with DIC and left to stir for 12 h at room temperature.

The polymer was characterised by ^{1}H NMR spectroscopy and SEC (Figure 5.14 and Figure 5.15 respectively). The successful polymerisation of PNO_2BnMA was confirmed by the presence of the methine resonance on the polymer backbone (δ = 5.5 ppm) (Figure 5.14).

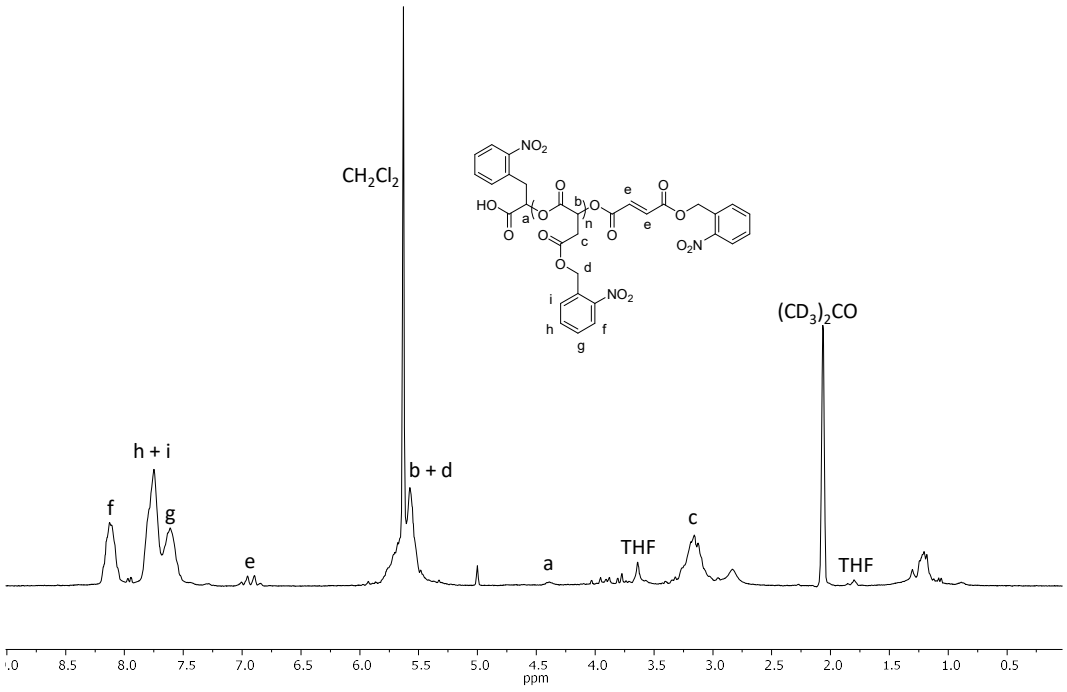

Figure 5.14: ^{1}H NMR spectrum of PNO_2BnMA synthesised *via* DIC coupling

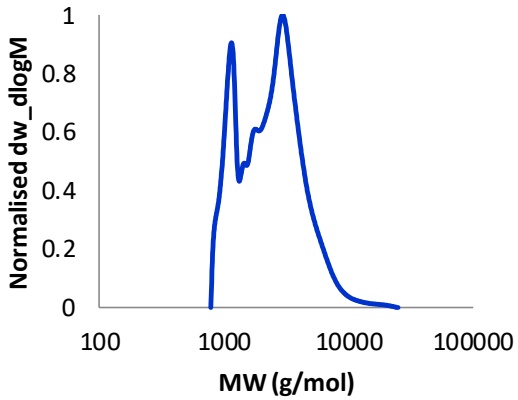

Figure 5.15: SEC chromatogram of PNO_2BnMA prepared *via* DIC coupling ($CHCl_3$, PS standards, 300 MHz)

5.2.3.3 Particle Synthesis Using Blends of Poly(L-Lactide) and Poly(Nitrobenzyl Malic Acid)

Particle blends of PNO_2BnMA (synthesised *via* polycondensation) and PLLA 100 were prepared analogous to blends of PEtMA and PLLA 100 (described in section 5.3.2.1), using optimised solvent evaporation conditions (Chapter 2). PNO_2BnMA dissolved easily alongside PLLA 100 in the dichloromethane organic phase. The organic solvent was evaporated from the emulsion overnight before characterising the particle size distribution *via* light scattering on the Mastersizer (Figure 5.16).

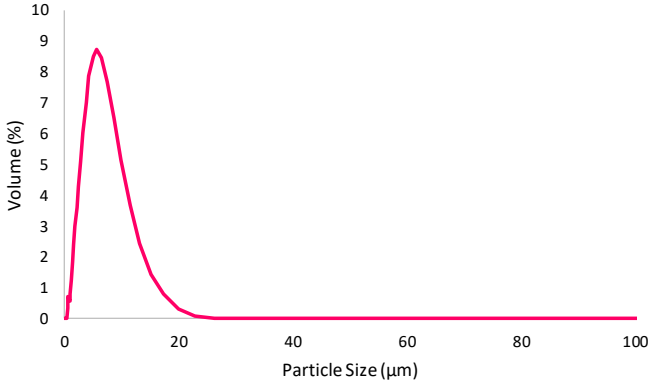

Figure 5.16: Light scattering analysis on a Malvern Mastersizer of a particle blend of PLLA 100 and PNO_2BnMA (50 wt%)

Mastersizer characterisation revealed the formation of a single particle size distribution with average particle size of 5 µm. The decreased particle size compared to 10 µm observed with PLLA 100 (Chapter 2) was postulated to be a consequence of the lower molecular weight of the PNO_2BnMA, which would act to decrease the viscosity of the emulsion. Further characterisation of the particles *via* SEM revealed that the PNO_2BnMA/PLLA particles have a spherical morphology with more defined shape and structure compared to particle blends of PEtMA/PLLA 100 (Figure 5.17). This was postulated to be a consequence of the increased solubility of PNO_2BnMA in dichloromethane and increased miscibility between PNO_2BnMA and PLLA 100.

Nevertheless, some of the particles displayed an uneven surface, thus implying phase separation between PNO_2BnMA and PLLA 100 (Figure 5.17).

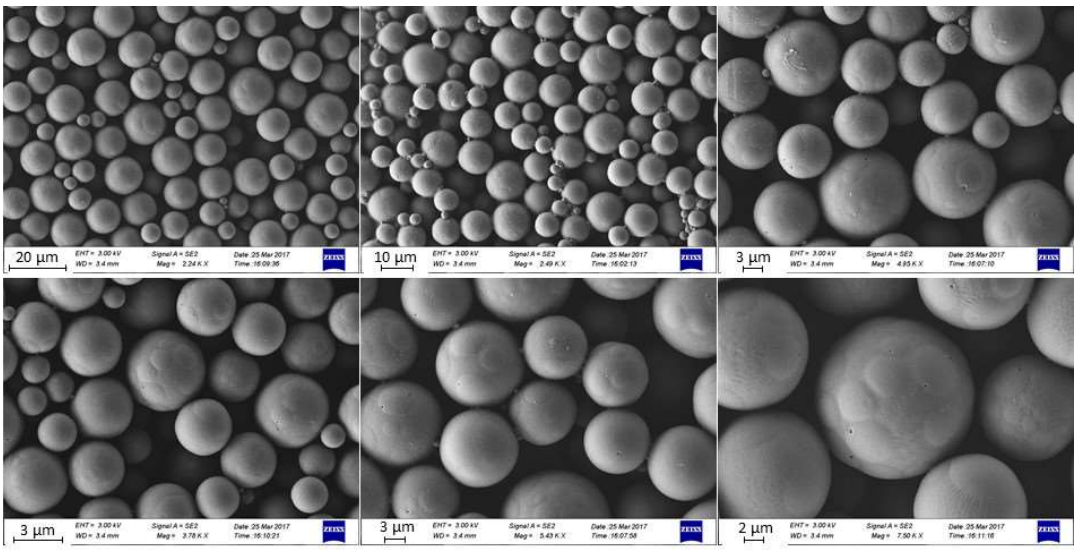

Figure 5.17: SEM characterisation of a particle blend of PLLA 100 and PNO_2BnMA (50 wt%)

To determine if the polymerisation procedure of PNO_2BnMA influenced the resultant particle morphology, particles of homopolymer blends of PLLA 100 and PNO_2BnMA synthesised at RT using DIC coupling (Section 5.2.3.2) were prepared and characterised *via* SEM. SEM characterisation revealed the formation of Janus and raspberry particle morphologies (Figure 5.18), thus confirming that the polymerisation method of PNO_2BnMA does not affect the resultant particle morphology. To investigate the effect of varying the ratio of PNO_2BnMA within the PLLA particles, particle blends were prepared at a lower incorporation of PNO_2BnMA (5 wt%). Characterisation of the resultant PLLA/PNO_2BnMA particle blend *via* SEM again revealed the presence of phase separation between PLLA and PNO_2BnMA (Figure 5.19).

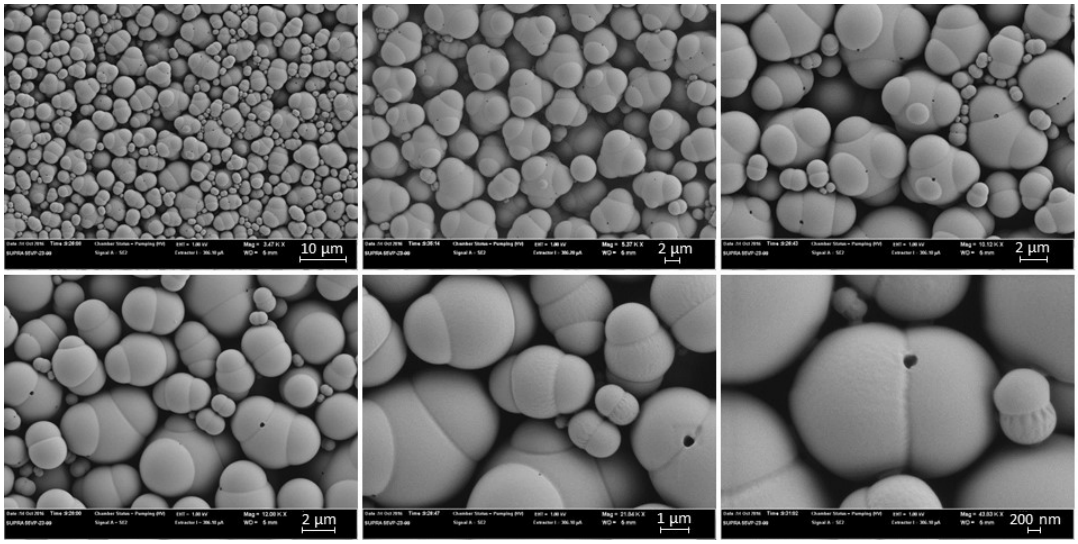

Figure 5.18: SEM characterisation of particle blends of PNO_2BnMA and PLLA 100 with 50 wt% PNO_2BnMA

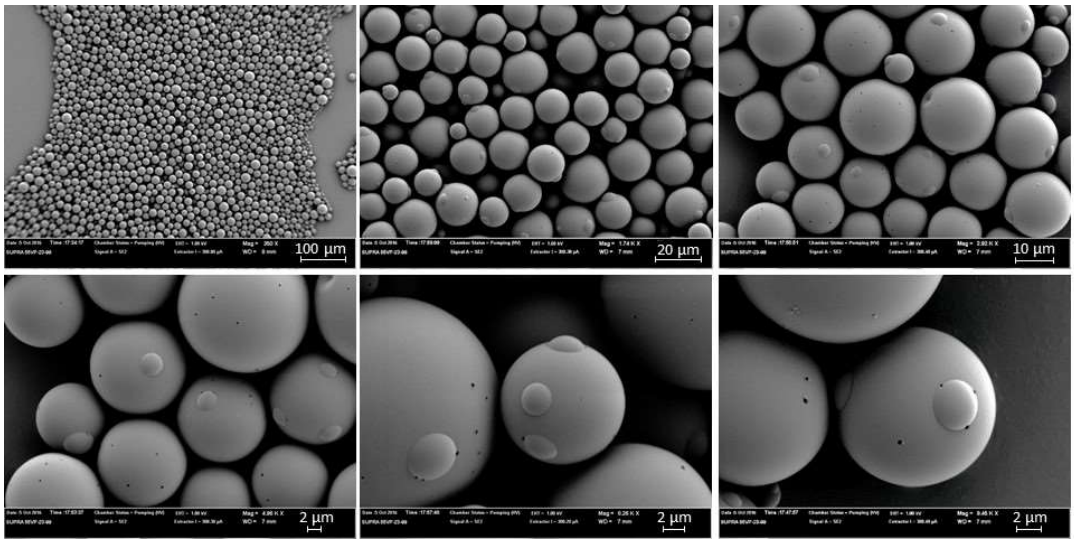

Figure 5.19: SEM characterisation of particle blends of PNO_2BnMA and PLLA 100 with 5 wt% PNO_2BnMA

In order to further explore the phase separation occurring between blends of PNO_2BnMA and PLLA, the homopolymers and blends were characterised by DSC (Figure 5.20). The separate DSC thermograms of the two homopolymers displayed single endothermic heat changes representative of the T_g of the respective polymers (PLLA (T_g = 55 °C), PNO_2BnMA (T_g = 14 °C)).

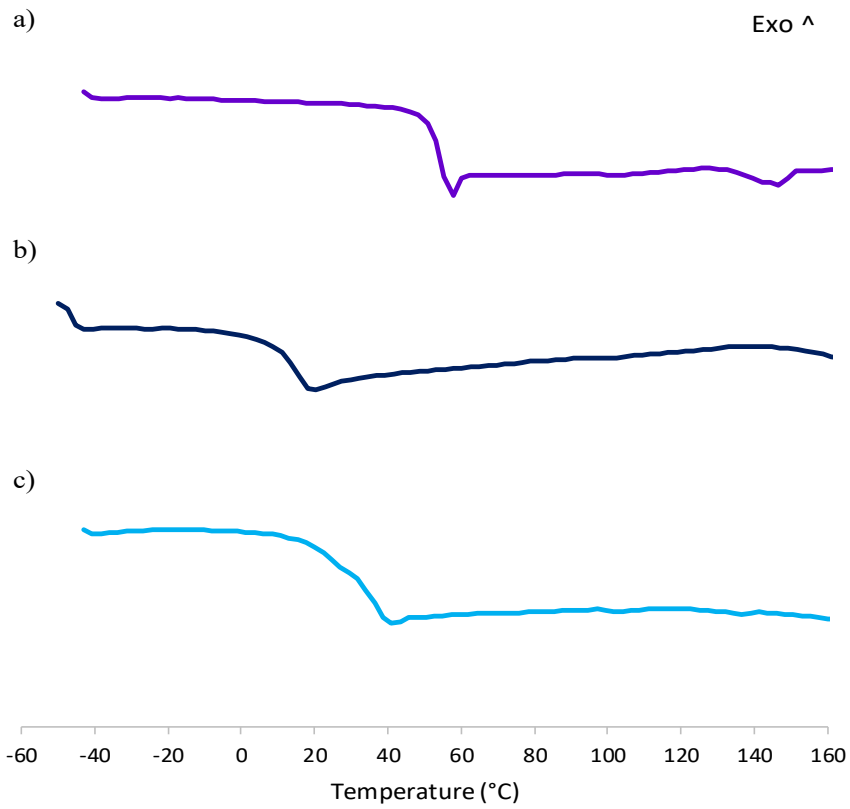

Figure 5.20: DSC thermograms displaying the second heating cycle of a) PLLA polymer b) PNO_2BnMA polymer c) a particle blend of PLLA 100 with 50 wt% PNO_2BnMA

Surprisingly, the DSC thermogram of a 50 wt% PNO_2BnMA/ PLLA polymer blend revealed the appearance of only one T_g (22 °C). Moreover, the T_g had shifted to a temperature in between the T_g of the respective homopolymers (PLLA 100 (T_g = 55 °C) and PNO_2BnMA (T_g = 14 °C)), thus implying that the two polymers are miscible. It was postulated that the PNO_2BnMA is susceptible to thermal history. Consequently, the three heat cycles were performed again on a fresh 50 wt% particle blend (Figure 5.21).

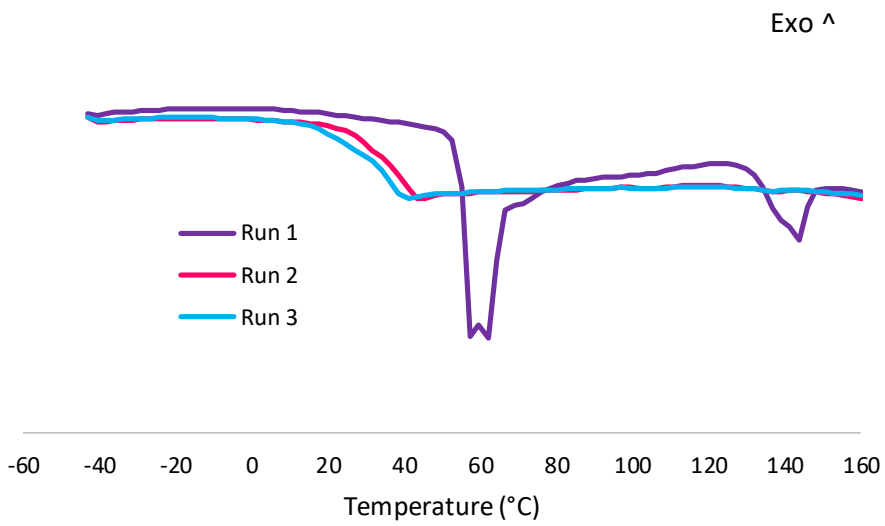

Figure 5.21: DSC thermograms displaying the three heat cycles for a particle blend of PLLA 100 and 50 wt% PNO_2BnMA

Interestingly, the first heating cycle observed in the DSC thermogram for the PLLA/PNO_2BnMA particle blend displayed a different profile compared to the second and third heating cycles (Figure 5.21). Moreover, the first heating cycle of the particle blend displayed a double melt peak at 60 °C, which was postulated to be a consequence of the particles collapsing under the increased heat followed by the resultant polymer melting. Moreover, the T_g observed in the second and third cycle of the particle blend was observed to be in between the characteristic homopolymer T_g's (T_g = 22 °C), which suggested that the polymers are miscible after being heated and cooled.

As a consequence of the interesting thermal properties observed with the particle blend, the particle formation was investigated further by subjecting a polymer blend (50 wt%) to 20 min of heat at 110 °C before using the blend for microparticle synthesis. The resultant particles were left to harden overnight before washing with DI water and characterising the particle morphology *via* SEM (Figure 5.22). SEM characterisation of the resultant particles revealed the formation of anisotropic

particles as previously observed with the unheated polymer blend, thus confirming that the phase separation still occurred after re-processing the polymers into microparticles.

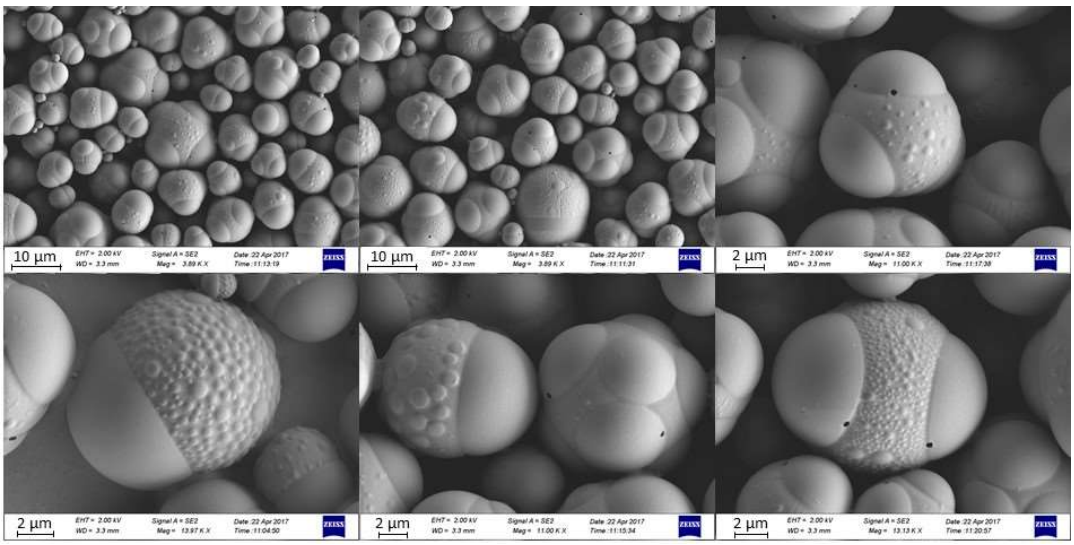

Figure 5.22: SEM characterisation of a 50 wt% particle blend using a preheated and cooled blend of PNO_2BnMA and PLLA 100

5.2.3.4 Degradation and Release from Particle Blends of Poly(L-Lactide) and Poly(Nitrobenzyl Malic acid) Synthesised via Polycondensation

Particle blends of PNO_2BnMA and PLLA 100 were investigated further by encapsulating 3-bromo-4-(butylamino)-2,5-dihydro-1H-pyrrole-2,5-dione (ABM). The particles were prepared using optimised single oil-in-water conditions, dissolving ABM (0.1 wt%) alongside PNO_2BnMA and PLLA 100 in the organic phase. Dichloromethane was evaporated overnight before washing the particles with deionised water to remove excess dye. Characterisation of the particles by fluorescence microscopy confirmed the successful encapsulation of the ABM into the PNO_2BnMA/ PLLA particles (Figure 5.23 b). Interestingly, further analysis of the subsequent particle morphology *via* SEM analysis revealed that in the presence of the ABM, the particles of PNO_2BnMA/ PLLA (50 wt%) blend do not display the

anisotropic morphology as observed without dye (Figure 5.23 and Figure 5.17 respectively). It was postulated that the small and mobile molecular structure of the dye enabled the ABM to act as a compatibiliser, exhibiting interfacial activities in the heterogeneous polymer blend.[47, 48] More specifically, the dye can interact with the two polymers *via* dispersive adhesion, thus reducing the surface tension, and improving the interfacial adhesion.

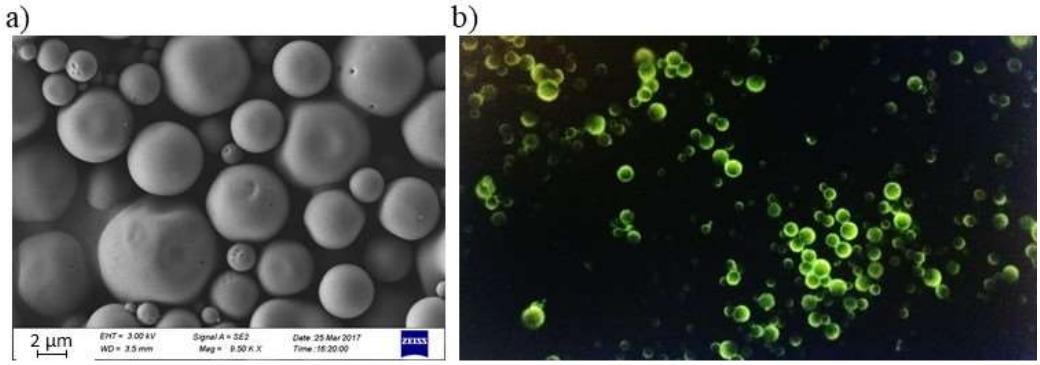

Figure 5.23: a) SEM characterisation and b) fluorescence microscopy of 50 wt% particle blend of PNO_2BnMA and PLLA 100 with encapsulated ABM (0.1 wt%)

The resultant particles were re-suspended in an aqueous solution (containing Mowiol 488 as stabiliser (1 wt%)), before exposing the particle solution to UV light (365 nm). Aliquots were taken every ten minutes and washed with DI water before characterisation by SEM and SEC. Excitingly, SEM analysis of the particles displayed distinct signs of particle degradation (Figure 5.24). Indeed, after just 10 minutes of exposure to UV light, an increased number of pores were evident in the particle morphology. Furthermore, as the UV exposure time increased, the particle porosity increased further, thus stimulating the collapse of the particles, illustrated by the increased number of broken particles and polymer strands evident by microscopy.

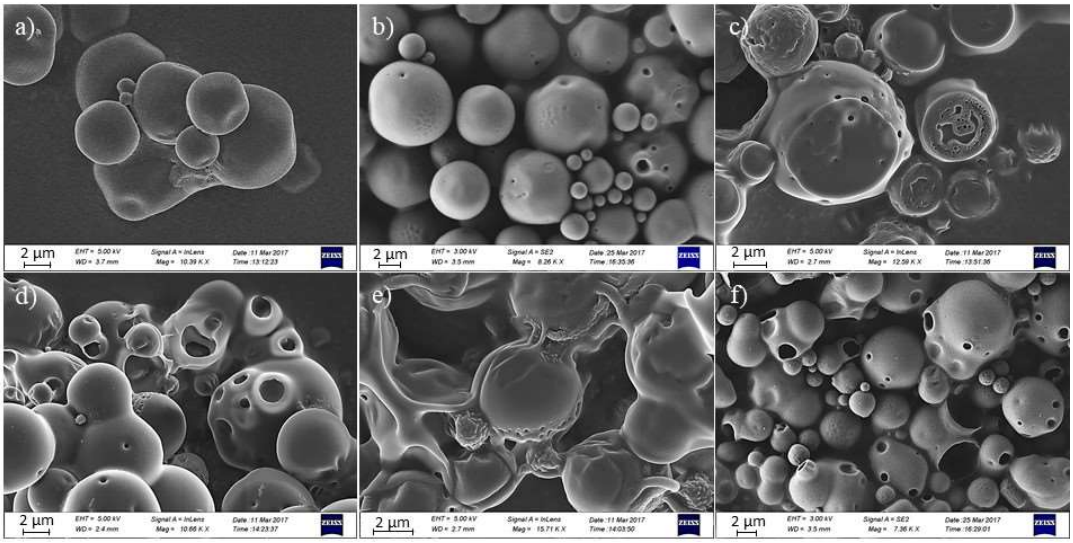

Figure 5.24: SEM characterisation of 50 wt% PNO_2BnMA/ PLLA particle blend after exposure to UV light for a) 0 min, b) 10 min, c) 20 min, d) 40 min, e) 50 min and f) 60 min

Particle degradation was also observed by SEC analysis, where a clear decrease in intensity of the PNO_2BnMA peak was observed over time in both the RI and UV (monitoring the loss of NO_2 group at λ = 265 nm) chromatograms (Figure 5.25). Interestingly, after 50 min of UV degradation, the intensity of the SEC response for PLLA decreased. This was postulated to be a consequence of the formation of acidic degradation products of PNO_2BnMA within the particle matrix, thus autocatalyzing the degradation of PLLA. This in turn would result in the formation of lower molecular weight PLLA species which could have been easily removed during particle washing, thus reducing the intensity of the SEC response.

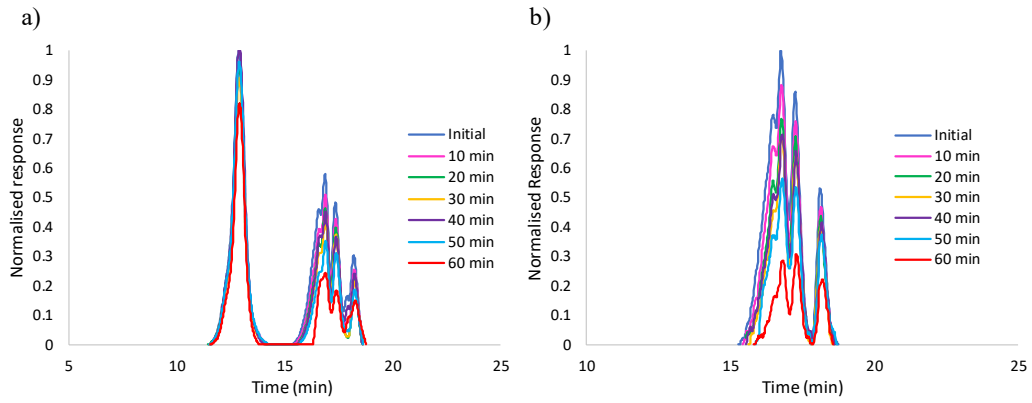

Figure 5.25: a) RI and b) UV (λ = 265 nm) SEC chromatograms displaying the degradation of a 50 wt% PNO_2BnMA/ PLLA particle blend during degradation under UV light (265 nm) ($CHCl_3$, PS standards).

Alongside particle degradation, the subsequent dye release was observed every ten minutes by monitoring the change in fluorescence intensity of the particles over a 5 h period into an ethanolic medium (optimised conditions detailed in Chapter 2) (Figure 5.26). A high initial burst release of 49% was observed followed by slower release, which is characteristic of dye diffusion through the particle. As the degradation time progressed, both the initial burst release (74%) and the total dye concentration released after 5 h (93%) increased, thus confirming that the dye is released as the particle degraded.

Alongside the particle release, the change in dye loading (E) was also monitored over time by comparing the fluorescence intensity of the encapsulated dye to the intensity of known concentrations of unencapsulated ABM using a fluorometer (Figure 5.26 b). In order to quantify the dye loading (E) of the particle blend, aliquots were again taken every ten minutes, washed to remove excess dye and freeze-dried before fully dissolving in dichloromethane. Similarly to the burst release observed by dye extraction into water/ethanol, a decrease in E was observed after ten minutes of particle exposure to UV light (28%). As the UV exposure time increased, the particles

showed a steady decrease in *E* with a sharp release after 60 min of UV exposure with only 4% remaining encapsulated within the particles.

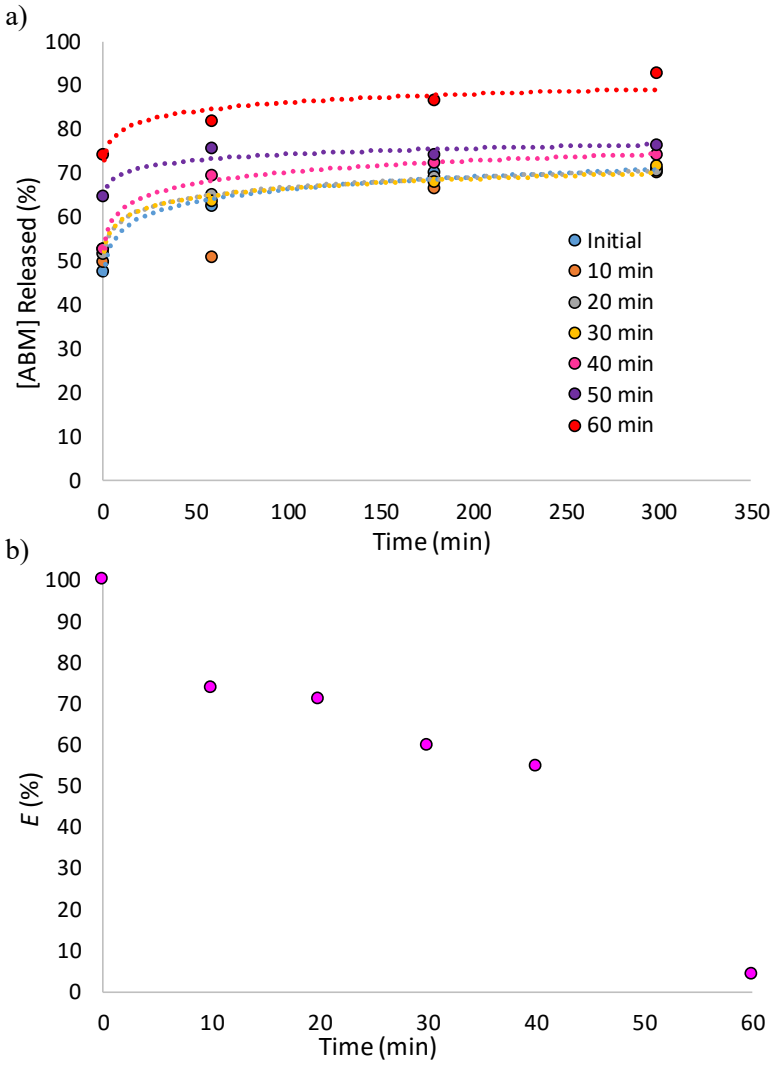

Figure 5.26: a) Release of ABM into water and ethanol and b) Change in *E* during UV degradation (λ = 265 nm), (control = sample after 1 h without UV-exposure)

The determined particle release and decrease in *E* correlated well with the obtained SEC and SEM degradation characterisation, revealing that ten minutes of exposure to UV light can trigger the onset of degradation. Moreover, near-complete dye release is attainable after 1 h exposure to UV light, thus confirming the promising potential for blends of PLLA and a responsive poly(malic acid) for controlled AI release.

5.3 Conclusions

In conclusion, the synthesis of novel particles from homopolymer blends of PLLA and PMA is reported and resulted in the enhanced degradation and release of a model fluorescent dye. Polycondensation of hydrophobic PMeMA resulted in crystal formation as a consequence of monomer sublimation at the high reaction temperature (110 °C). Therefore, side reactions, such as fumarate formation were favoured during polymerisation leading to a low yield of PMeMA. On the other hand, polycondensation of the less volatile EtMA resulted in a decreased concentration of fumarate in the final polymer compared to PMeMA, as confirmed by ^{1}H NMR spectroscopy and SEC.

Synthesis of PEtMA microparticles using an optimised single oil in water solvent evaporation technique revealed the formation of a low concentration of particles with a smaller particle size than expected compared to PLLA 100. Furthermore, even at a decreased shear speed, time and polymer concentration, only nanoparticles were attainable *via* optimised solvent evaporation conditions. Additionally, the incorporation of PEtMA within a PLLA particle was shown to yield broken and collapsed particles *via* SEM analysis. The irregular appearance of the PLLA particles with PEtMA (25 wt%) was postulated to be a consequence of the low solubility of PEtMA in dichloromethane and phase separation between PLLA and PEtMA.

Incorporation of a light-responsive malic acid moiety, in the form of PNO_2BnMA enabled the successful triggered degradation and release of the fluorescent proxy *via* the application of UV light. In fact, after only ten minutes the onset of degradation *via* SEC and SEM was visible. Furthermore, after 1 h of exposure to UV light, the microparticles were visibly broken as observed *via* microscopy and nearly all of the

dye had been released, with only 4 % remaining encapsulated within the particle sample.

Further investigation into the polymeric particle blends of PLLA and PNO_2BnMA revealed that PNO_2BnMA synthesised *via* RT DIC coupling showed enhanced phase separation compared to PNO_2BnMA *via* polycondensation at 110 °C. Therefore, it was postulated that PNO_2BnMA is affected by its thermal history. Interestingly, addition of the fluorescent ABM was found to act as a compatibilizer to aid miscibility between the PLLA and PNO_2BnMA. DSC characterisation of the homopolymer and particle blends revealed that after subjecting the blend to a heating and cooling cycle, the polymers are miscible. Moreover, utilising a pre-heated polymer blend of PLLA and PNO_2BnMA enabled the synthesis of spherical non-anisotropic microparticles, with evidence of phase separation visible *via* SEM.

This work details the great potential for use of stimuli responsive PLLA/PMA particle blends for controlled drug delivery and release. The degradation control afforded by incorporation of the UV sensitive PNO_2BnMA implies the high level of control achievable by tuning the ratio of PLLA and PNO_2BnMA within the particle matrix. Additionally, the easy functionalisation achievable with malic acid opens a wide range of possibilities for the addition of a variety of responsive units to target a broad range of properties and applications.

5.4 References

1. V. C. Baligar, N. K. Fageria and Z. L. He, *Commun. Soil Sci. Plant Anal.*, 2001, **32**, 921-950.
2. A. Pérez-de-Luque and D. Rubiales, *Pest Manage. Sci.*, 2009, **65**, 540-545.
3. S. F. Peteu, F. Oancea, O. A. Sicuia, F. Constantinescu and S. Dinu, *Polymers*, 2010, **2**, 229-251.
4. M. Chen, S. P. Jensen, M. R. Hill, G. Moore, Z. He and B. S. Sumerlin, *Chem. Commun.*, 2015, **51**, 9694-9697.
5. Z. Gerstl, A. Nasser and U. Mingelgrin, *J. Agric. Food Chem.*, 1998, **46**, 3797-3802.
6. M. W. Aktar, D. Sengupta and A. Chowdhury, *Interdisc. Toxicol.*, 2009, **2**, 1-12.
7. D. Ali, N. S. Nagpure, S. Kumar, R. Kumar, B. Kushwaha and W. S. Lakra, *Food Chem. Toxicol.*, 2009, **47**, 650-656.
8. B. Singh, D. K. Sharma and A. Gupta, *J. Hazard. Mater.*, 2009, **161**, 208-216.
9. W. L. Meyer, P. Gurman, L. L. Stelinski and N. M. Elman, *Green Chem.*, 2015, **17**, 4173-4177.
10. S. Cammas, M.-M. Béar, L. Moine, R. Escalup, G. Ponchel, K. Kataoka and P. Guérin, *Int. J. Biol. Macromol.*, 1999, **25**, 273-282.
11. S. Cammas, I. Renard, V. Langlois and P. Guéri, *Polymer*, 1996, **37**, 4215-4220.
12. N. Nagata, T. Nakahara, T. Tabuchi, R. Morita, J. R. Brewer and S. Fujishige, *Polym J*, 1993, **25**, 585-592.
13. S. L. King, V. X. Truong, C. Kirchhoefer, A. Pitto-Barry and A. P. Dove, *Green Materials*, 2014, **2**, 107-122.

14. T. Kajiyama, T. Taguchi, H. Kobayashi, K. Kataoka and J. Tanaka, *Polym. Degrad. Stab.*, 2003, **81**, 525-530.

15. T. Kajiyama, H. Kobayashi, T. Taguchi, K. Kataoka and J. Tanaka, *Biomacromolecules*, 2004, **5**, 169-174.

16. R. J. Pounder, D. J. Fox, I. A. Barker, M. J. Bennison and A. P. Dove, *Polym. Chem.*, 2011, **2**, 2204-2212.

17. T. Ouchi and A. Fujino, *Die Makromolekulare Chemie*, 1989, **190**, 1523-1530.

18. M.-A. Leboucher-Durand, V. Langlois and P. Guerin, *Polym. Bull.*, 1996, **36**, 35-41.

19. C. Braud, C. Bunel and M. Vert, *Polym. Bull.*, 1985, **13**, 293-299.

20. M. Vert, *Polym. Degrad. Stab.*, 1998, **59**, 169-175.

21. S. Lyu and D. Untereker, *Int. J. Mol. Sci.*, 2009, **10**, 4033-4065.

22. J. Siepmann, N. Faisant, J. Akiki, J. Richard and J. P. Benoit, *J. Controlled Release*, 2004, **96**, 123-134.

23. R. Jeyanthi, B. C. Thanoo, R. C. Metha and P. P. Deluca, *J. Controlled Release*, 1996, **38**, 235-244.

24. J.-C. Jeong, J. Lee and K. Cho, *J. Controlled Release*, 2003, **92**, 249-258.

25. U. Edlund and A.-C. Albertsson, *J. Polym. Sci. Part A: Polym. Chem.*, 2000, **38**, 786-796.

26. A. J. Domb, *J. Polym. Sci. Part A: Polym. Chem.*, 1993, **31**, 1973-1981.

27. S. E. M. Ibim, A. M. A. Ambrosio, M. S. Kwon, S. F. El-Amin, H. R. Allcock and C. T. Laurencin, *Biomaterials*, 1997, **18**, 1565-1569.

28. S. Freiberg and X. X. Zhu, *Int. J. Pharm.*, 2004, **282**, 1-18.

29. F.-L. Mi, Y.-M. Lin, Y.-B. Wu, S.-S. Shyu and Y.-H. Tsai, *Biomaterials*, 2002, **23**, 3257-3267.

30. D. Wang, M. D. Green, K. Chen, C. Daengngam and Y. Kotsuchibashi, *Int. J. Polym. Sci.*, 2016, **2016**, 1-2.

31. H. Yang, H. Zhu, M. M. R. M. Hendrix, N. J. H. G. M. Lousberg, G. de With, A. C. C. Esteves and J. H. Xin, *Adv. Mater.*, 2013, **25**, 1150-1154.

32. M. R. Aguilar and J. San Román, in *Smart Polymers and their Applications*, Woodhead Publishing, Cambridge, 2014, pp. 1-11.

33. A. Aghabegi Moghanjoughi, D. Khoshnevis and A. Zarrabi, *Drug Deliv. Transl. Res.*, 2016, **6**, 333-340.

34. M. R. Hill, E. J. MacKrell, C. P. Forsthoefel, S. P. Jensen, M. Chen, G. A. Moore, Z. L. He and B. S. Sumerlin, *Biomacromolecules*, 2015, **16**, 1276-1282.

35. C. E. Fernández, M. Mancera, E. Holler, J. J. Bou, J. A. Galbis and S. Muñoz-Guerra, *Macromol. Biosci.*, 2005, **5**, 172-176.

36. M. J. Miller, J. S. Bajwa, P. G. Mattingly and K. Peterson, *J. Org. Chem*, 1982, **47**, 4928-4933.

37. N. Ohtani, Y. Kimura and T. Kitao, *Kobunshi Ronbunshu*, 1987, **44**, 701-709.

38. D. Klose, F. Siepmann, K. Elkharraz, S. Krenzlin and J. Siepmann, *Int. J. Pharm.*, 2006, **314**, 198-206.

39. A. G. Hausberger and P. P. DeLuca, *J. Pharm. Biomed. Anal.*, 1995, **13**, 747-760.

40. C.-C. Chen, J.-Y. Chueh, H. Tseng, H.-M. Huang and S.-Y. Lee, *Biomaterials*, 2003, **24**, 1167-1173.

41. J. H. Jeong, D. W. Lim, D. K. Han and T. G. Park, *Colloids Surf. B*, 2000, **18**, 371-379.

42. K. Ding, L. Shi, L. Zhang, T. Zeng, Y. Yin and Y. Yi, *Polym. Chem.*, 2016, **7**, 899-904.

43. C. Lv, Z. Wang, P. Wang and X. Tang, *Int. J. Mol. Sci.*, 2012, **13**, 16387-16399.

44. X. Liu, J. He, Y. Niu, Y. Li, D. Hu, X. Xia, Y. Lu and W. Xu, *Polym. Adv. Technol.*, 2015, **26**, 449-456.

45. F. Yang, Z. Cao and G. Wang, *Polym. Chem.*, 2015, **6**, 7995-8002.

46. J. S. Moore and S. I. Stupp, *Macromolecules*, 1990, **23**, 65-70.

47. P. J. Marsac, T. Li and L. S. Taylor, *Pharm. Res.*, 2008, **26**, 139.

48. C. Koning, M. Van Duin, C. Pagnoulle and R. Jerome, *Prog. Polym. Sci.*, 1998, **23**, 707-757.

6. Synthesis of Degradable Microparticles *via* Radical Ring-Opening Polymerisation of Vinyl Acetate and a Cyclic Ketene Acetal

6.1 Introduction

In recent years, an increasing amount of research has been directed into expanding the range of properties attainable with poly(ε-caprolactone) (PCL) based material, with a specific emphasis based on incorporating functionality into the PCL backbone.[1-3] To this end, addition of functionality into PCL has been achieved through functionalisation of εCL, chain end modification and/ or copolymerisation of εCL with other functional monomers.[4-7] Nevertheless, even though each synthetic technique enabled introduction of functionality, each methodology presented limitations, including laborious syntheses, yield-lowering protection/deprotection steps during functional monomer synthesis, incompatibility between the functional group and desired reaction catalyst and polymerisation conditions, *etc*.[3, 6, 8-10] Therefore, incorporating functionality into PCL still remains synthetically challenging.

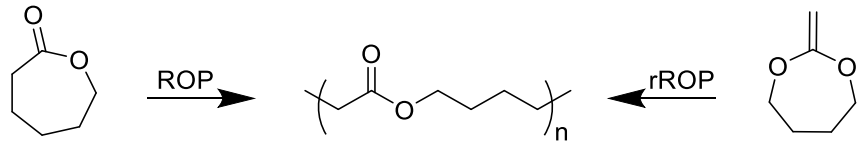

Scheme 6.1: Schematic representation of two different synthetic approaches to attain an equivalent aliphatic polyester

Radical ring-opening polymerisation (rROP) of cyclic ketene acetals (CKAs) has emerged as a promising, unconventional alternative to the synthesis of polyesters.[11] Since the first reported rROP of 3,9-dimethylene-1,5,7,11-tetraoxaspiro[5,5] undecane by Bailey *et al*., rROP of a wide range of CKAs has been investigated.[12-15] Of particular interest, free radical polymerisation of the seven-membered ketene acetal, 2-methylene-1,3-dioxepane (MDO), has been shown to undergo ring-opening to form an aliphatic polyester with a PCL-like structure (Scheme 6.1).[12] Additionally, rROP has been regarded as a highly advantageous synthetic route to produce

degradable polymers as a result of the easily scalable, industrially applicable radical polymerisation procedure.[16]

Investigation into the rROP mechanism of MDO by Bailey *et al*., revealed that the polymerisation proceeds by a process similar to conventional free radical polymerisation.[12] Hence, decomposition of the initiator results in the formation of a radical species, which can react with the double bond of the CKA (Scheme 6.2a). The resultant cyclic radical can then undergo isomerization by radical ring-opening polymerisation, to yield an initial primary radical (Scheme 6.2b). The primary radical can then react with a second CKA monomer, thus the reaction propagates and results in the growth of a polyester chain (Scheme 6.2c). Elucidation of the structural properties of PMDO by Gonsalves *et al*. highlighted that the resultant polyester consisted of a branched polymeric structure compared to the linear analogue obtained by ROP of εCL.[17] The branched structure was deemed to be a consequence of backbiting in the form of 1,4- and 1,7- hydrogen transfer reactions that have been shown to occur during polymerisation. Therefore, PMDO displays different mechanical properties (such as density, crystallinity and thermal properties) compared to PCL synthesised by ROP of εCL.[11]

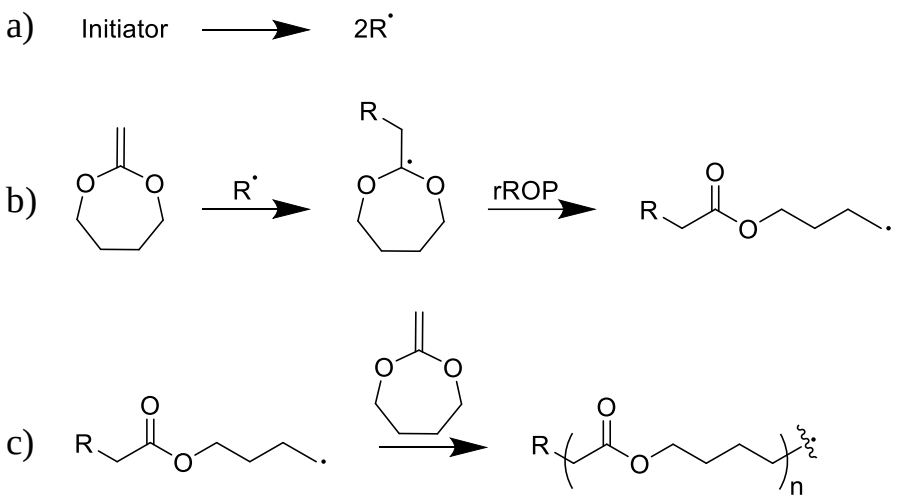

Scheme 6.2: Schematic representation of the mechanism for the rROP of MDO

Particular research interest has been focussed on copolymerising vinyl monomers with monomers containing ester units, thus enabling the incorporation of degradable ester repeat units within the conventionally non-degradable backbone of vinyl polymers.[11, 16] Indeed, a broad range of vinyl monomers have been studied and copolymerised with CKAs, such as vinyl acetate (VAc), 4-vinyl anisole, 2-hydroxyethyl methacrylate (HEMA) *etc*., to form copolymers with degradable properties.[13, 18, 19] However, several investigations into the copolymerisation of MDO with styrene (St) or methyl acrylate (MA) have resulted in the formation of a copolymer with a predominantly block-like microstructure.[20, 21] Consequently, the copolymer has a low incorporation of ester repeat units within the final polymer. The type of copolymer formed has been shown to be dependent on the monomers reactivity ratio *e.g.*, monomers with a similar reactivity ratio will form a random/alternative copolymer structure, whereas monomers with different reactivity ratios will be incorporated at different rates, thus leading to the formation of block-like polymers.[18, 19]

Copolymerisation of VAc and MDO has been reported to successfully form degradable polymers with a random monomer distribution.[18, 19, 22] Hedir *et al*. reported

that the final copolymer composition can successfully be tuned depending on the initial monomer feed of MDO:VAc.[22] Further investigation by Hedir *et al*., into the copolymerisation of MDO and vinyl bromobutanoate (VBr), revealed that the degradation rate of the copolymer is highly dependent on the copolymer composition. Therefore, as a consequence of the random copolymer composition observed with both P(MDO-*co*-VBr) and P(MDO-*co*-VAc), it was hypothesised that the degradation profile of P(MDO-*co*-VAc) can be targeted by varying the initial MDO:VAc monomer ratio. The potential ability to tune the degradation rate coupled with the industrially relevant rROP copolymer synthesis implies that P(MDO-*co*-VAc) would be the ideal material for use as a microparticle matrix to encapsulate a wide range of compounds applicable for a range of industrial applications (*e.g.*, pharmaceutical, agricultural, *etc*.). Encapsulation of an active ingredient (AI) can help to reduce any associated toxicity of the chemical and also act to protect the AI from loss, leaching and degradation occurring under various environmental conditions.[23-25] Consequently, controlled release from biodegradable particles promises an efficient alternative to conventional agrochemical delivery.[26]

Inspired by the work by Hedir *et al*., this Chapter discusses the introduction of tuneable degradability into PVAc microparticles by incorporating MDO degradable ester linkages into the polymer backbone through copolymerisation of VAc and MDO. Encapsulation of 3-bromo-4-(butylamino)-2,5-dihydro-1H-pyrrole-2, 5-dione (ABM) into the P(MDO-*co*-VAc) particles is also investigated and compared to encapsulation into PVAc particles. Furthermore, the attained random copolymer and ease of functionality previously reported with vinyl polymers highlight the range of possibilities achievable through the synthesis of microparticles from degradable vinyl polymers through copolymerisation with CKAs.

6.2 Results and Discussion

6.2.1 Free Radical Polymerisation of Vinyl Acetate

Vinyl acetate was polymerised by free radical polymerisation using the method reported by Albertsson *et al*., (Scheme 6.3).[18] As a general example, vinyl acetate was polymerised in bulk at 60 °C under an atmosphere of nitrogen, using 2, 2-azobisisobutyronitrile (AIBN) as radical initiator. The polymerisation was heated for 2 h before characterising the monomer conversion by monitoring the loss of the ethylene resonance (δ = 4.55 ppm) and appearance of the methine resonance characteristic of the polymer backbone (δ = 4.8 ppm) *via* ^{1}H NMR spectroscopy. The white polymer was precipitated three times into petroleum ether to remove excess monomer, before drying *in vacuo*. ^{1}H NMR spectroscopy revealed the characteristic resonances for PVAc, in good agreement with previous literature (Figure 6.1). The polymer was further characterised *via* SEC analysis, which revealed an M_n of 19,000 g/mol and a broad dispersity ($Đ_M$) of 5.2 characteristic of uncontrolled free radical polymerisation (Figure 6.2).

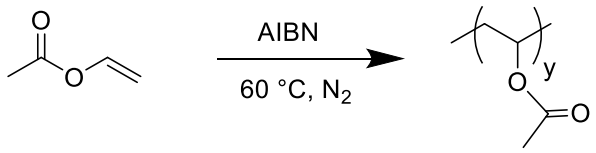

Scheme 6.3: Schematic representation of free radical polymerisation of PVAc using AIBN as initiator

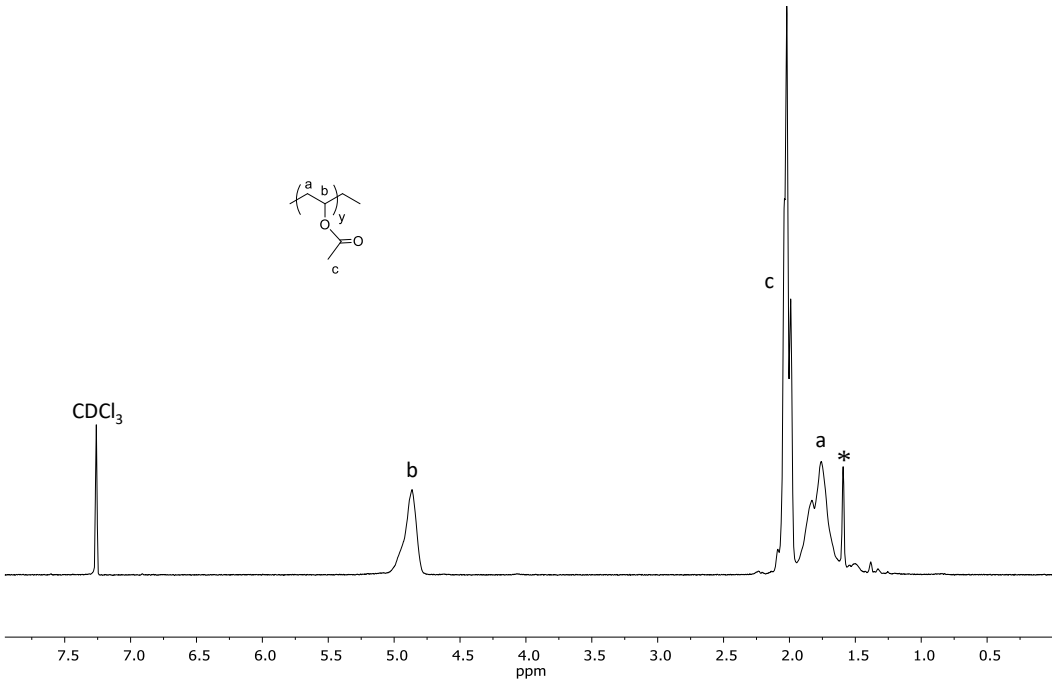

Figure 6.1: ^{1}H NMR spectrum of PVAc synthesised *via* free radical polymerisation, *=Water residue ($CDCl_3$, 300 MHz)

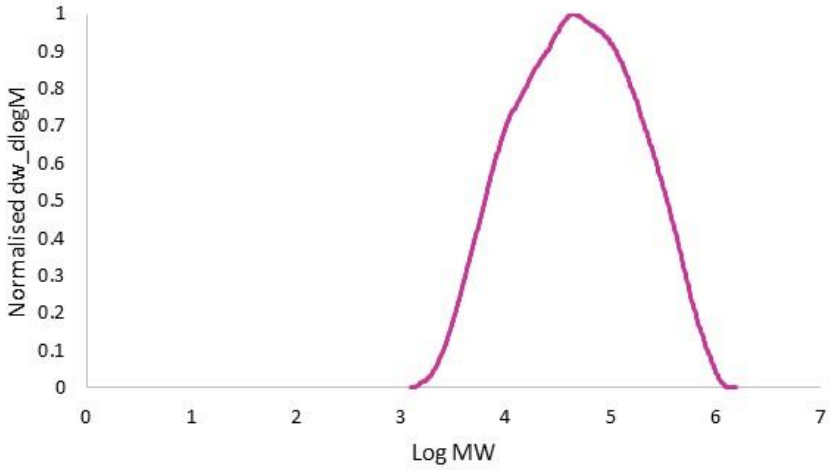

Figure 6.2: SEC chromatogram of PVAc synthesised *via* free radical polymerisation ($CHCl_3$, PS standards).

6.2.2 Microparticle Synthesis Using Poly(Vinyl Acetate)

Microparticles from PVAc were synthesised using the single oil-in-water solvent evaporation technique optimised for PLLA in Chapter 2. As a general procedure, PVAc was dissolved in dichloromethane, before emulsifying the organic phase with an aqueous phase (containing Mowiol 488 (2 wt%) as stabiliser). Dichloromethane was evaporated overnight, thus enabling particle hardening, before characterising the suspension *via* light scattering and optical microscopy (Figure 6.3 a) and b) respectively).

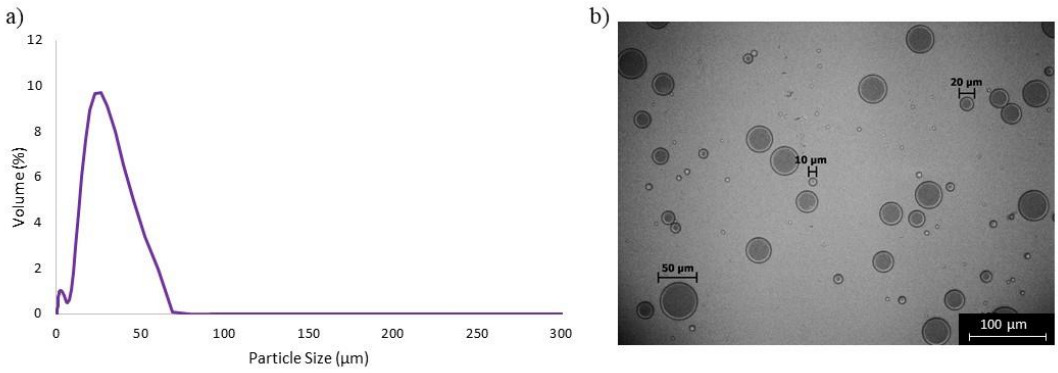

Figure 6.3: Characterisation of PVAc particle suspension *via* light scattering and optical microscopy

Characterisation of the PVAc particle suspension by light scattering revealed the formation of an increased volume weighted mean particle size of 22 µm and a broader particle size distribution compared to PLLA and PCL (Chapter 2, Section 2.3.5). Nevertheless, the absence of particle aggregation observed by optical microscopy implied that the increased particle size was a consequence of the increased molecular weight of PVAc compared to previously synthesised polyester particles (Chapter 2). Therefore, it was assumed that the particle size could easily be tuned by increasing the shear speed and shear time. The PVAc particles were characterised further by analysing the particle morphology *via* Scanning Electron Microscopy (SEM). To

achieve this, a sample of the particle suspension was washed with deionised water, before being dried onto a carbon tab fitted to an aluminium SEM stub. The sample was gold coated before SEM analysis, which revealed that the PVAc particles display a smooth, spherical morphology (Figure 6.4).

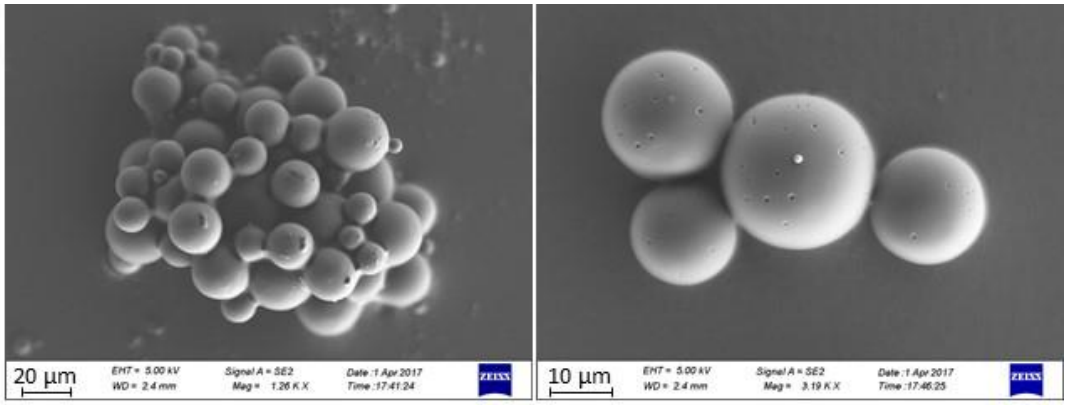

Figure 6.4: SEM characterisation of PVAc microparticles synthesised *via* single oil-in-water solvent evaporation technique.

Interestingly, during particle washing, the particles tended to aggregate and required increased sonication to maintain a non-aggregated state. Indeed, after three wash cycles the particles mainly appeared in an aggregated state (Figure 6.5). Burt *et al*., also observed aggregation between washes of ethylene-VAc particles.[27] This was reasoned to be a consequence of the increase in interfacial tension observed with removing the mowiol 488 stabiliser.

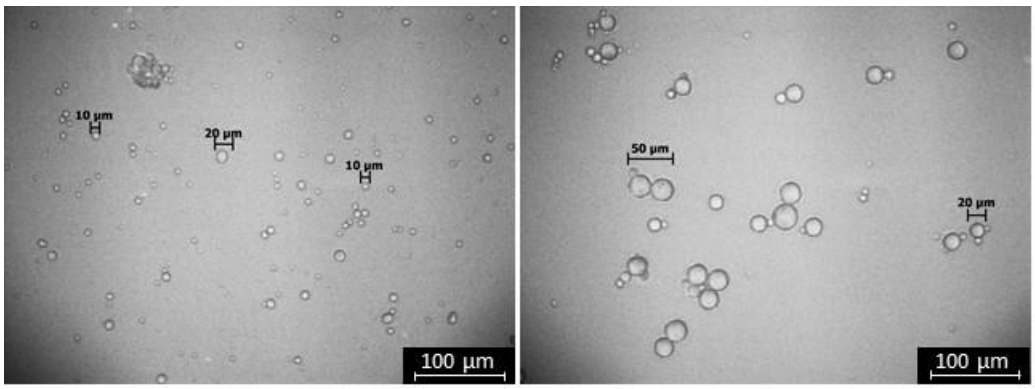

Figure 6.5: Optical microscopy analysis of PVAc particles after washing three times in deionised water

The synthesis of PVAc particles was investigated further by encapsulating 3-bromo-4-(butylamino)-2,5-dihydro-1H-pyrrole-2,5-dione (ABM) using the optimised encapsulation procedure detailed in Chapter 3, section 3.2.3. In general, ABM (0.1 wt%) and PVAc were dissolved in dichloromethane, before emulsifying with an aqueous solution (containing Mowiol 488 as stabiliser (2 wt%)) for 30 s at 7000 rpm. The dichloromethane was evaporated overnight thus enabling particle hardening. To quantify the dye loading (*E*) of the PVAc particles, a known concentration of particles was washed with DI water to remove excess dye and stabiliser, before removing water by freeze-drying the sample overnight. The resultant dried particles were dissolved in dichloromethane. The *E* was characterised using a fluorometer by comparing the fluorescence intensity of the sample against the fluorescence intensity of six known concentrations of free ABM in dichloromethane. The particles displayed a good *E* of 34%, thus confirming successful encapsulation of ABM into PVAc particles.

After the successful determination of the *E* of ABM within PVAc microparticles, it was interesting to determine if addition of the dye affects the particle morphology. To facilitate this, a sample of the washed particle suspension in water was placed onto a carbon tab on an aluminium stub and allowed to air dry overnight. The sample was

coated with gold before characterising the particle morphology *via* SEM (Figure 6.6). SEM characterisation confirmed that the particles maintained a smooth, spherical morphology. Furthermore, no evidence of dye crystallisation was visible throughout the sample.

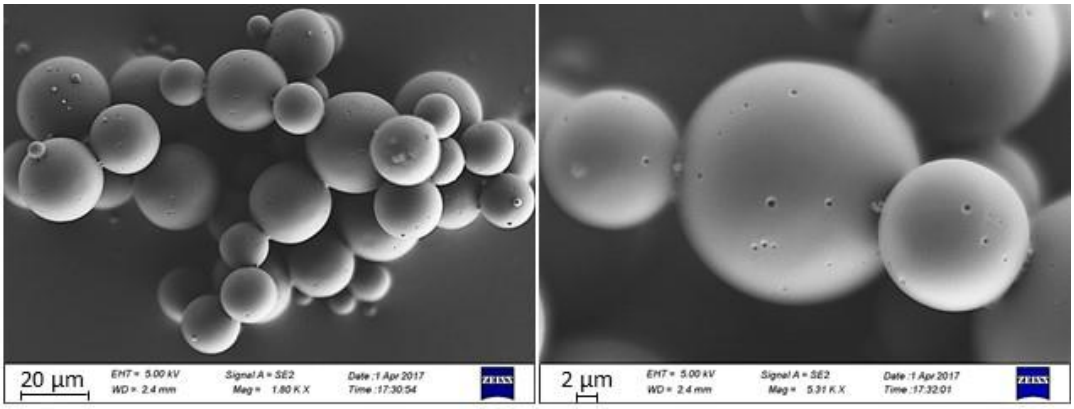

Figure 6.6: SEM analysis of PVAc microparticles with encapsulated ABM (0.1 wt%) prepared *via* a single oil-in-water solvent evaporation technique

To determine the release rate of ABM from PVAc microparticles, an aliquot of the PVAc suspension was placed in a 50:50 solution of ethanol/ water, thus enabling rapid extraction of both unencapsulated dye and dye from the particle surface followed by a slower release rate of encapsulated dye, extracted from the particle matrix by diffusion. The change in fluorescence intensity was monitored over 5 h and compared to the fluorescence intensity of six known concentrations of free ABM using a plate reader. Characterisation of the change in fluorescence intensity unveiled that PVAc microparticles exhibited full release after just 1 min in the ethanolic medium (Figure 6.7). Further investigation into the complete dye release exposed that the PVAc microparticles were soluble in the 50:50 ethanol and water release medium. Therefore, future work is required to determine a more appropriate solvent system for determining dye release rate from PVAc microparticles.

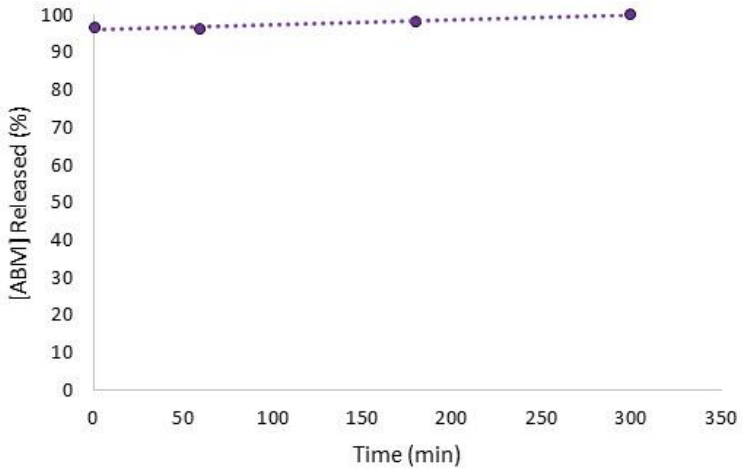

Figure 6.7: Characterisation of the full release of ABM from PVAc particles contained within an ethanolic release medium by monitoring the change in fluorescence intensity on a plate reader

6.2.3 Free Radical Copolymerisation of P(MDO-co-VAc)

Copolymerisation of PVAc and MDO with a 50% monomer feed was achieved by free radical polymerisation in line with the report by Albertsson *et al*., (Scheme 6.4).[18] As a general procedure, VAc and MDO were copolymerised in bulk at 60 °C for 4 h under an atmosphere of nitrogen, using 2, 2-azobisisobutyronitrile (AIBN) as radical initiator. After quenching the polymerisation in an ice bath, the copolymer was precipitated three times into hexane to remove excess monomer, before drying *in vacuo*. The successful copolymerisation of MDO and VAc was confirmed by ^{1}H NMR spectroscopic analysis (Figure 6.8).

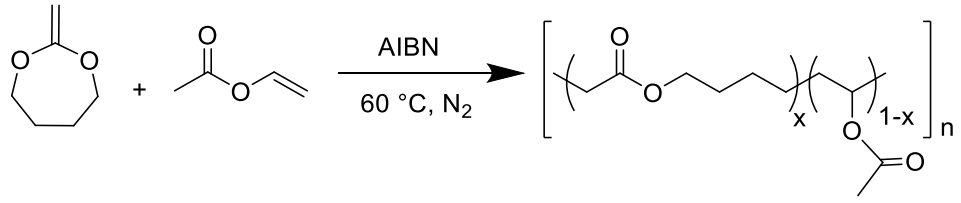

Scheme 6.4: Schematic representation of free radical copolymerisation of MDO and VAc using AIBN as initiator.

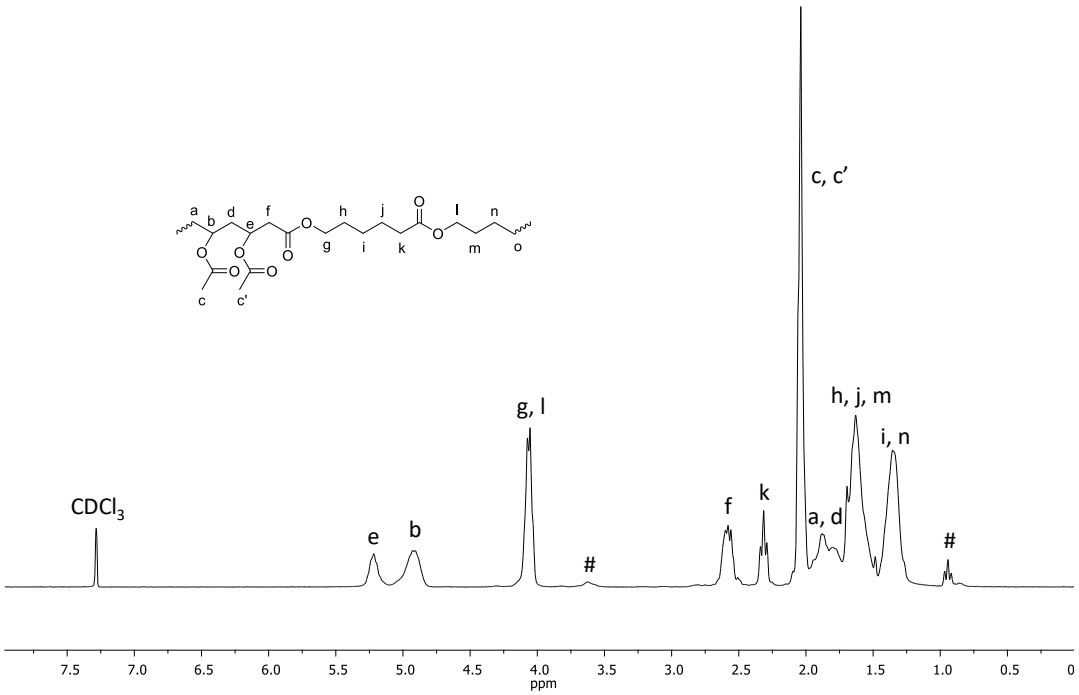

Figure 6.8: ^{1}H NMR spectrum of P(MDO-*co*-VAc) (41:59) synthesised *via* free radical polymerisation, (# signals of the side reactions of 1,4- and 1,7- hydrogen transfer ($CDCl_3$, 300 MHz)

^{1}H NMR spectroscopic analysis enabled calculation of the individual monomer incorporation of VAc and MDO in the final copolymer (Figure 6.8). Indeed, comparison of the integrals of the methine protons from VAc and the methylene protons of MDO from the polymer backbone at δ = 4.80 - 5.20 and 4.00 ppm respectively revealed the mole fraction of each monomer within the final copolymer (41% MDO and 59% VAc). Further examination of the ^{1}H NMR spectrum of P(MDO-*co*-VAc) revealed the presence of resonances at δ = 0.90 ppm and 3.68 ppm, characteristic for the presence of side branches within the copolymer (Scheme 6.5). During rROP, the growing primary radical is highly reactive and unstable. Therefore, to increase the radical stability, the growing polymer chain can undergo intramolecular 1,4- and 1,7- hydrogen transfer reactions, resulting in branch points along the polymer backbone. An estimation of the percentage of side chains within the copolymer (15%) was determined by comparing the integral of the side chain branch resonances

(δ = 0.90 ppm and δ = 3.68 ppm), with the methylene resonance close to the MDO carbonyl group on the polymer backbone (δ = 4.00 ppm). The polymer was further characterised *via* SEC, which revealed a high M_n (31,300 g/mol) and a broad dispersity ($Đ_M$) 8.98 which is synonymous with free radical polymerisation and the introduction of MDO into the copolymer (Figure 6.9).

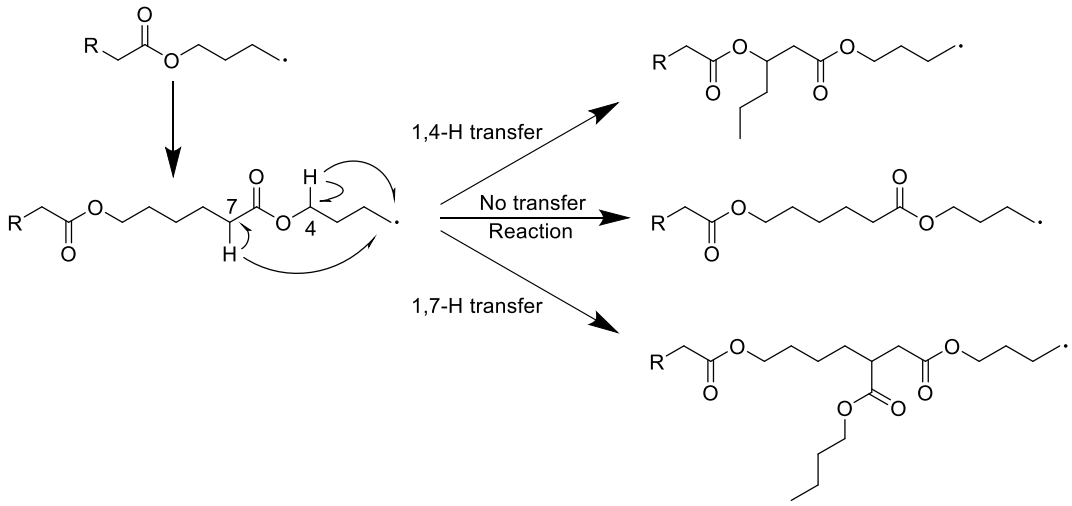

Scheme 6.5: Schematic illustration detailing the possible side reactions occurring during rROP with MDO *via* 1,4- and 1,7-hydrogen transfer

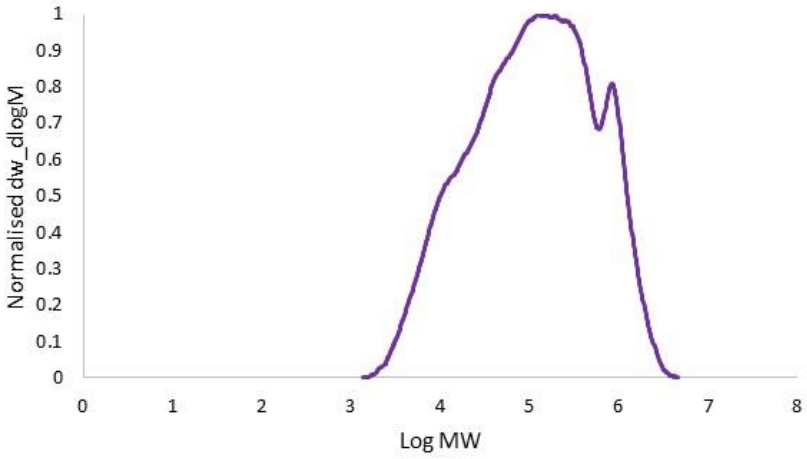

Figure 6.9: SEC chromatogram of P(MDO-*co*-VAc) (41:59) synthesised *via* free radical polymerisation ($CHCl_3$, PS standards)

6.2.4 Microparticle Synthesis Using P(MDO-co-VAc)

Microparticles of P(MDO-*co*-VAc) were synthesised using optimised single oil-in-water solvent evaporation conditions detailed in Chapter 2. Subsequently, P(MDO-*co*-VAc) (41:59) was dissolved in dichloromethane before emulsifying with an aqueous solution (containing 2 wt% Mowiol 488 as stabiliser). The dichloromethane was evaporated overnight allowing the particles to harden. The resultant solution appeared to be a white cloudy suspension, with no evidence of sedimentation within the reaction flask. Characterisation of the particle suspension by light scattering displayed a broad particle size distribution with a volume weighted mean of 25 μm (Figure 6.10 a)). Further characterisation of the particle suspension by optical microscopy revealed that similarly to PVAc particles, no evidence for particle aggregation was observed (Figure 6.10 b)). Hence, it was expected that the large particle size was a result of the increased molecular weight of the copolymer compared to the ring opened polymers analysed in previous chapters. Therefore, it was assumed that the particle size could easily be tuned by increasing the shear speed and shear time.

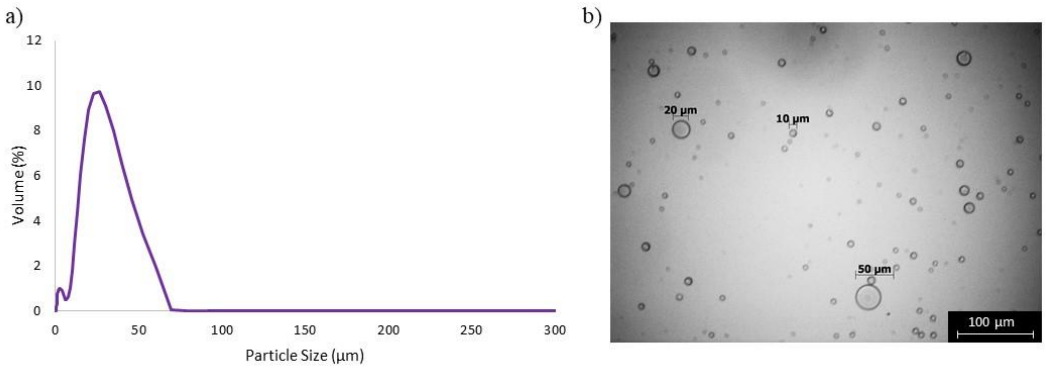

Figure 6.10: Characterisation of P(MDO-*co*-VAc) (41:59) particle suspension *via* a) light scattering and b) optical microscopy

P(MDO-*co*-VAc) particle synthesis was investigated further by encapsulating ABM using the same optimised encapsulation conditions as for PVAc particle encapsulation. In order to characterise the encapsulation of ABM into P(MDO-*co*-VAc) microparticles, the *E* was calculated. To do this, the particles were washed three times in DI water (to remove excess dye and stabiliser) and freeze dried overnight before dissolving the sample in dichloromethane. Similar to the synthesised PVAc microparticles, slight aggregation was observed during particle washing (Figure 6.11). The *E* of the P(MDO-*co*-VAc) particles was characterised by comparing the fluorescence intensity of the washed particles to the fluorescence intensity of known concentrations of ABM in dichloromethane. The P(MDO-*co*-VAc) particles displayed a good *E* of 42%, similar to the *E* calculated for PVAc particles (34%), thus implying the incorporation of MDO into the polymeric particles does not affect the particles ability to encapsulate AI's.

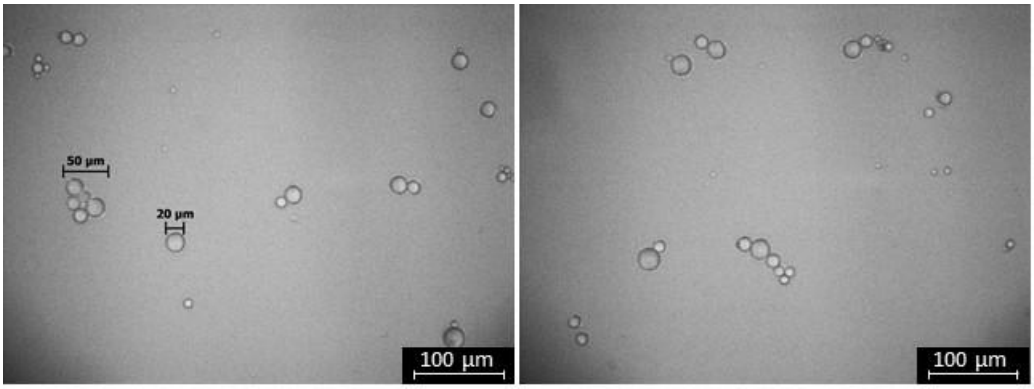

Figure 6.11: Optical microscopy of P(MDO-*co*-VAc) (41:59) particles after three washes with DI water

After the promising encapsulation properties observed with P(MDO-*co*-VAc) particles, it was interesting to determine if the addition of MDO within the polymeric matrix affects the particle morphology. SEM characterisation of the P(MDO-*co*-VAc) particles both with and without dye revealed the presence of flattened, circular discs,

which appeared as a film-like deposit on the carbon tab instead of the spherical morphology expected based on previously imaged PVAc particles (Figure 6.12). Hence, the observed flat morphology of P(MDO-*co*-VAc) particles suggested that the particles had collapsed during the required drying and high vacuum sample preparation. Albertsson *et al*. have demonstrated that the random incorporation of MDO (T_g = -60 °C) into the polymeric backbone of PVAc (T_g = 30 °C) decreases the T_g of the resultant copolymer.[18] Indeed, the T_g has been shown to be readily tuneable based on the composition of MDO:VAc in the final copolymer.[18] It was hypothesised that the decreased T_g of the 41:59 MDO:VAc copolymer (T_g = -45 °C) decreased the structural stability of the particle, hence as water was removed, the intrinsically swollen particle collapsed, thus, resulting in the appearance of flattened and collapsed structures, as observed *via* SEM.[28]

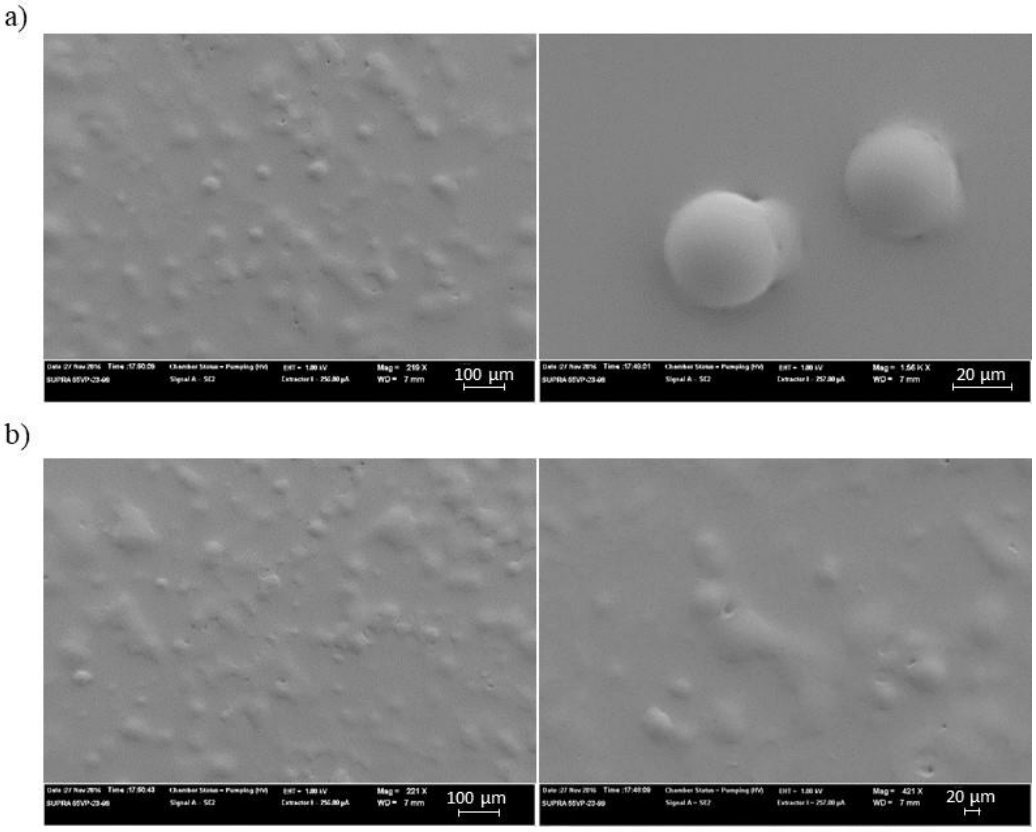

Figure 6.12: SEM characterisation of P(MDO-*co*-VAc) (41:59) microparticles a) without dye and b) with dye

To further investigate the particle collapse observed with P(MDO-*co*-VAc) particles, a sample of the particle suspension was monitored *via* optical microscopy before and after drying on a glass slide for 1 h (Figure 6.13). Interestingly, particle aggregation and coalescence was evident after air-drying for one hour (Figure 6.13 b)). To further elucidate the particle morphology change, the particle suspension was also monitored during particle drying by optical microscopy (Figure 6.14). Interestingly, as the water evaporated, the larger particles appeared to elongate, this was postulated to be a consequence of particle collapse during drying. However, full particle collapse was not visible by optical microscopy on either study. Therefore, it was postulated that application of vacuum during SEM analysis removed final traces of water present in the sample, thus further destabilising the particles and resulting in complete particle

collapse. Consequently, it would be interesting to study PVAc particles with a lower incorporation of MDO, to determine if a balance between good degradability and stability is attainable at lower MDO ratios. Furthermore, the ease of copolymerisation between vinyl polymers and CKAs by rROP in addition to the ease of functionality previously reported with vinyl polymers implies the broad potential future scope for this project, such as variable degradability, incorporation of functionality into the particle and production of stimulus-responsive particles.

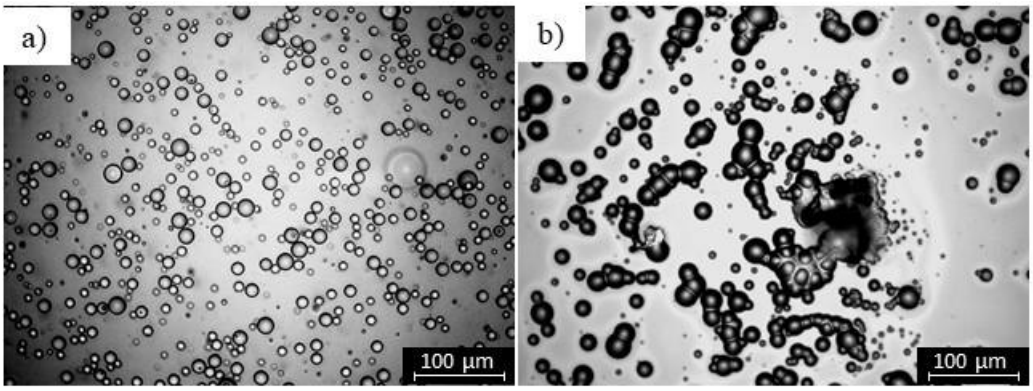

Figure 6.13: Optical microscopy analysis of P(MDO-*co*-VAc) (41:59) particles a) before drying b) after air-drying for 1 h

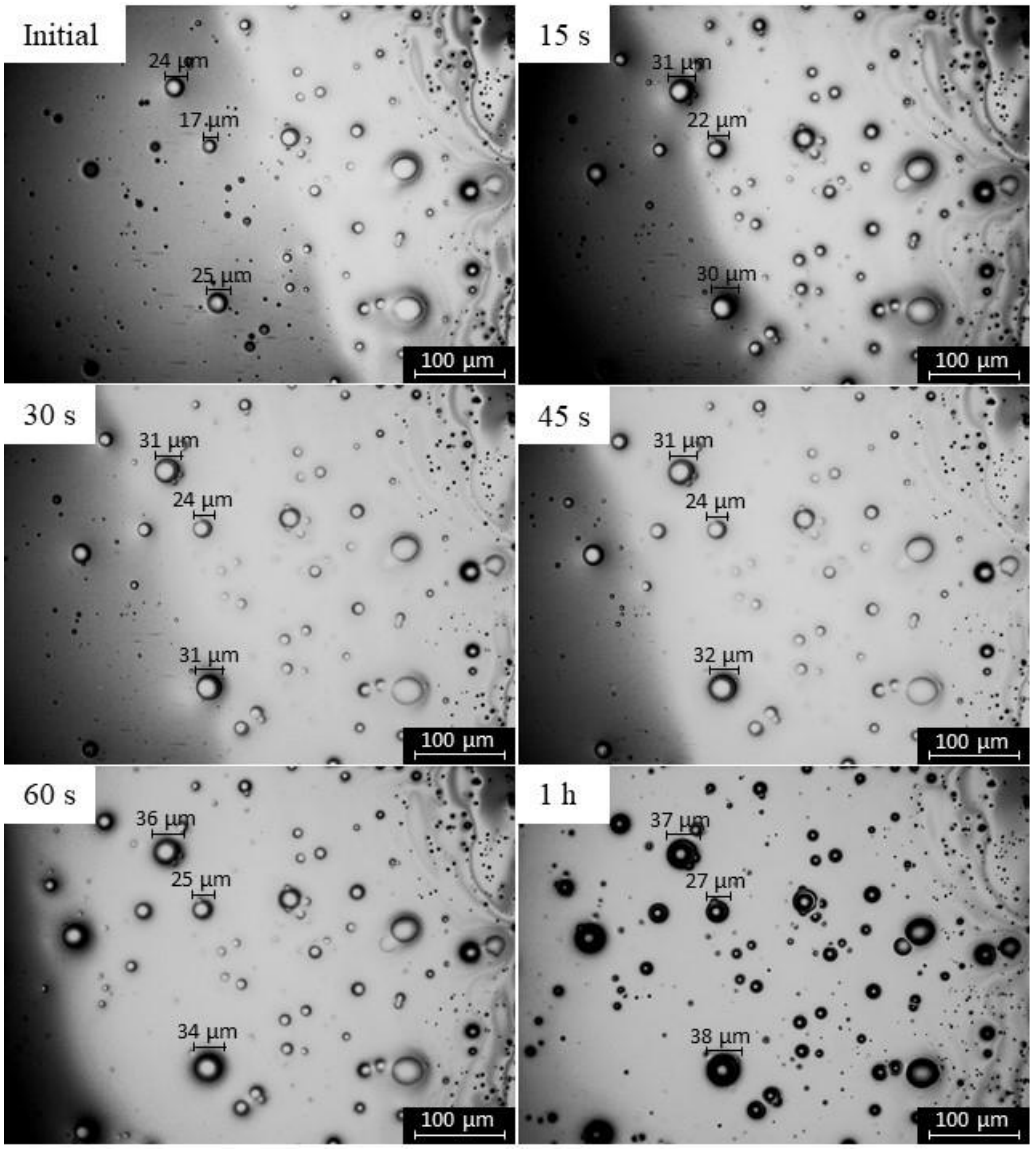

Figure 6.14: Optical microscopy analysis of P(MDO-*co*-VAc) (41:59) particles during drying

In order to elucidate information regarding the ABM release rate from P(MDO-*co*-VAc) particles, an aliquot of the particle suspension was placed into a 50:50 water: ethanol solution and the change in fluorescence intensity monitored over 5 h. Interestingly, conversely to PVAc microparticles, the P(MDO-*co*-VAc) particles were insoluble and displayed minimal signs of release after five hours within the release medium (Figure 6.15).

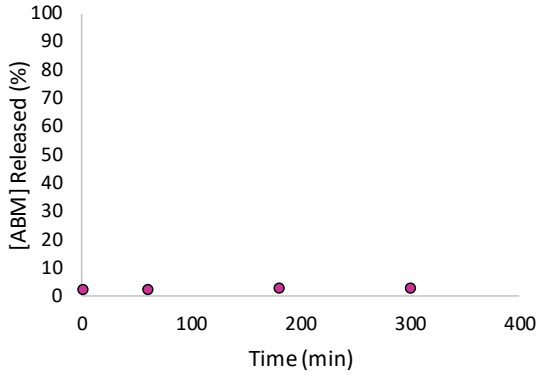

Figure 6.15: Characterisation of the change in fluorescence intensity observed with P(MDO-*co*-VAc) (50:50) particles in a 50:50 water: ethanol solution over five hours using a plate reader

6.3 Conclusions

In conclusion, the successful incorporation of enhanced degradability into PVAc microparticles was achieved by utilising a copolymer of VAc and MDO, prepared by rROP, as the particle matrix. Characterisation by light scattering and optical microscopy revealed that both PVAc and P(MDO-*co*-VAc) particles could be successfully attained using an optimised single oil-in-water solvent evaporation technique. Furthermore, both sets of polymeric particles displayed a broader particle size distribution compared to the polyesters synthesised *via* ROP in Chapter 2. Nevertheless, the absence of observed aggregates and sediment implied that the particle size could easily be tailored by varying the particle shear speed and time.

Investigation into the encapsulation of a fluorescent dye revealed that both PVAc and P(MDO-*co*-VAc) particles were able to successfully encapsulate ABM and displayed good *E*'s of 34% and 42% respectively, as confirmed by fluorometry. Whilst monitoring dye release into a 50% water: ethanol medium, negligible release was observed with P(MDO-*co*-VAc) particles over a 5 h period. Conversely, full, immediate dye release was observed with PVAc particles, as a consequence of the high solubility of PVAc within the ethanolic release medium. Therefore, future work would be required to find the suitable conditions for dye release from PVAc particles. Further characterisation of PVAc particles by SEM revealed that the particles exhibited a smooth, spherical morphology with or without dye. On the other hand, only collapsed particle morphologies were evident *via* SEM characterisation of P(MDO-*co*-VAc) particles. It was hypothesised that the low glass transition temperature (T_g) of 2-methylene-1,3-dioxepane (MDO) decreased the stability of the particles and as such, the particles collapsed upon drying. It was postulated that a lower concentration of MDO within the microparticle would enable the production of stable

microparticles. The attained random copolymer and ease of functionality previously reported with vinyl polymers highlight the range of possibilities available through the synthesis of microparticles from vinyl polymers and CKAs.

6.4 References

1. S. Cajot, P. Lecomte, C. Jerome and R. Riva, *Polym. Chem.*, 2013, **4**, 1025-1037.
2. R. Riva, S. Schmeits, F. Stoffelbach, C. Jerome, R. Jerome and P. Lecomte, *Chem. Commun.*, 2005, **42**, 5334-5336.
3. A. L. Korich, A. R. Walker, C. Hincke, C. Stevens and P. M. Iovine, *J. Polym. Sci. Part A: Polym. Chem.*, 2010, **48**, 5767-5774.
4. M. Liu, N. Vladimirov and J. M. J. Fréchet, *Macromolecules*, 1999, **32**, 6881-6884.
5. C. Vaida, M. Takwa, M. Martinelle, K. Hult, H. Keul and M. Möller, *Macromol. Symp.*, 2008, **272**, 28-38.
6. G. Carrot, J. G. Hilborn, M. Trollsås and J. L. Hedrick, *Macromolecules*, 1999, **32**, 5264-5269.
7. A. G. O. de Freitas, S. G. Trindade, P. I. R. Muraro, V. Schmidt, A. J. Satti, M. A. Villar, A. E. Ciolino and C. Giacomelli, *Macromol. Chem. Phys.*, 2013, **214**, 2336-2344.
8. C. K. Williams, *Chem. Soc. Rev.*, 2007, **36**, 1573-1580.
9. J. M. Campos, M. R. Ribeiro, M. F. Ribeiro, A. Deffieux and F. Peruch, *Eur. Polym. J.*, 2013, **49**, 4025-4034.
10. S. Hvilsted, *Polym. Int.*, 2012, **61**, 485-494.
11. S. Agarwal, *Polym. Chem.*, 2010, **1**, 953-964.
12. W. J. Bailey, Z. Ni and S.-R. Wu, *J. Polym. Sci. Polym. Chem. Ed.*, 1982, **20**, 3021-3030.
13. W. J. Bailey, Z. Ni and S. R. Wu, *Macromolecules*, 1982, **15**, 711-714.
14. W. J. Bailey, S.-R. Wu and Z. Ni, *Makromol. Chem. Rapid Comm.*, 1982, **183**, 1913-1920.
15. T. Yokozawa, R. Hayashi and T. Endo, *J. Polym. Sci. Part A: Polym. Chem.*, 1990, **28**, 3739-3746.
16. V. Delplace and J. Nicolas, *Nat Chem*, 2015, **7**, 771-784.
17. S. Jin and K. E. Gonsalves, *Macromolecules*, 1997, **30**, 3104-3106.
18. J. Undin, T. Illanes, A. Finne-Wistrand and A.-C. Albertsson, *Polym. Chem.*, 2012, **3**, 1260-1266.
19. S. Agarwal, R. Kumar, T. Kissel and R. Reul, *Polym. J*, 2009, **41**, 650-660.

20. L. F. Sun, R. X. Zhuo and Z. L. Liu, *J. Polym. Sci. Part A: Polym. Chem.*, 2003, **41**, 2898-2904.
21. W. J. Bailey, T. Endo, B. Gapud, Y.-N. Lin, Z. Ni, C.-Y. Pan, S. E. Shaffer, S.-R. Wu, N. Yamazaki and K. Yonezawa, *J. Macromol. Sci. Part A Chem.*, 1984, **21**, 979-995.
22. G. G. Hedir, C. A. Bell, N. S. Ieong, E. Chapman, I. R. Collins, R. K. O'Reilly and A. P. Dove, *Macromolecules*, 2014, **47**, 2847-2852.
23. M. W. Aktar, D. Sengupta and A. Chowdhury, *Interdisc. Toxicol.*, 2009, **2**, 1-12.
24. B. Singh, D. K. Sharma and A. Gupta, *J. Hazard. Mater.*, 2009, **161**, 208-216.
25. D. Ali, N. S. Nagpure, S. Kumar, R. Kumar, B. Kushwaha and W. S. Lakra, *Food Chem. Toxicol.*, 2009, **47**, 650-656.
26. A. Roy, S. K. Singh, J. Bajpai and A. K. Bajpai, *Cent. Eur. J. Chem.*, 2014, **12**, 453-469.
27. H. M. Burt, J. K. Jackson, S. K. Bains, R. T. Liggins, A. M. C. Oktaba, A. L. Arsenault and W. L. Hunter, *Cancer Lett.*, 1995, **88**, 73-79.
28. K. K. Lai, R. Renneberg and W. C. Mak, *Green Chem.*, 2016, **18**, 1715-1723.

7. Microparticles, Films and Polymerisation-Induced Self-Assembly with Poly(ω-Pentadecalactone) and its Copolymers

7.1 Introduction

Ring-opening polymerisation (ROP) of cyclic lactones has opened a pathway to a wide range of polyesters with a diverse scope of mechanical and thermal properties (*e.g.*, crystallinity, glass transition temperature, degradation rate, *etc.*).[1] Currently, most research has been focussed on the polymerisation of small ring lactones (4-, 6- and 7-membered rings), such as poly(lactic acid) (PLA) or poly(ε-caprolactone (εCL)).[2-4] The high ring strain observed with the smaller ring lactones has enabled the successful synthesis of high molecular weight polyesters with rapid propagation kinetics, using a wide range of initiators and catalysts. Conversely, macrolactones have been less widely studied as a consequence of the decreased ring strain observed with larger ring monomers. Hence, traditional reaction methods have been shown to only yield low molecular weight polymers with slow kinetic propagation rates.[5] Since the pioneering work by Kobayashi *et al*., in 1995 investigating enzymatic ROP of 12-, 13- and 16-membered lactones, there has been an increase in research into polymerisation of macrolactones, as a consequence of the promising properties offered by the larger rings, (such as high molecular weight polymers and high tensile strength).[6-10]

ω-Pentadecalactone (PDL) is a 16-membered lactone naturally found in fragrant fruits, animal musk and angelica root oil (Figure 7.1).[11] When polymerised, the resultant poly(ω-pentadecalactone) (PPDL) consists of a long, 15- carbon alkyl repeat unit. Hence, polymerisation of PDL is an efficient synthetic route to the production of high molecular weight polymers. PPDL displays high crystallinity as a consequence of its long aliphatic backbone.[12] Moreover, the high crystallinity observed with PPDL, has been shown to exhibit high mechanical and tensile strength properties comparable to that of low density polyethylene (LDPE) (Figure 7.1 b) and c)).[13-15]

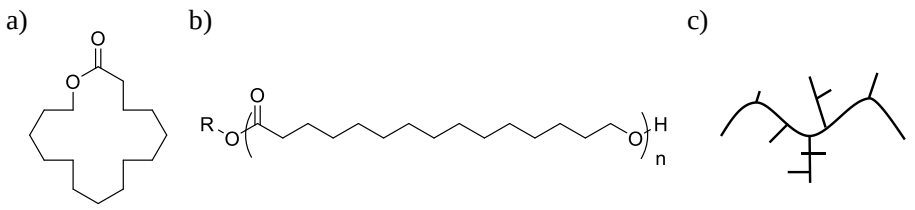

Figure 7.1: Chemical structure of a) PDL, b) PPDL and c) LDPE

Polyesters are well known for undergoing hydrolysis *via* hydrolytic scission of the ester linkage within the polymer backbone.[16-19] The long aliphatic backbones observed with macrolactones promises the possibility of increased stability towards hydrolytic degradation.[20] Indeed, the high crystallinity and high hydrophobicity observed with PPDL contribute to the low susceptibility of PPDL to hydrolytic degradation. In fact, PPDL has only been shown to degrade enzymatically or under high temperature (425 °C).[6] On the other hand, PPDL has been shown to exhibit signs of degradation in compost, thus rendering it an extremely interesting polymer for agrochemical applications.[21]

PDL has been copolymerised with a range of smaller degradable ring lactones in attempts to enhance the biodegradability profile.[22, 23] The copolymerisation of PDL and εCL has been studied using several catalyst systems. Investigation into the copolymerisation kinetics revealed that either εCL or PDL was consumed preferentially before the growth of the second monomer, depending on the applied catalyst. However, in each case, transesterification side reactions occurred, thus resulting in the synthesis of random copolymers.[24-26] Furthermore, Ceccorulli *et al.* revealed that copolymers of PDL and εCL displayed cocrystallinity, thus the melting temperature (T_m) and crystallisation temperature (T_c) were linearly dependent on the initial molar ratio of the monomer feed (PDL: εCL).[27] The significant influence observed on the copolymer properties when varying the initial monomer ratio

highlights the promising potential of copolymers of PPDL and smaller ring degradable lactones, to yield tuneable, degradable copolymers.

This chapter demonstrates the promising potential of PPDL and its copolymers to yield a range of highly advantageous biodegradable morphologies, (microparticles, thin films and cylindrical micelles). PPDL was applied in a single oil-in-water solvent evaporation technique to achieve highly crystalline microparticles. Furthermore, the random copolymers formed through copolymerisation of PDL and εCL were used to prepare biodegradable thin films. The high crystallinity associated with PPDL was exploited to achieve worm-like micelles *via* a hybrid method of polymerisation-induced crystallization-driven self-assembly (PICDSA) during copolymerisation with ε-decalactone (εDL). The interesting properties possessed by PPDL, imply the highly beneficial achievements attainable by incorporating PPDL into microparticles, films and cylindrical micelles, each capable of achieving the controlled release of an agrochemical.

7.2 Results and Discussion

7.2.1 Poly(ω-Pentadecalactone) Microparticles

7.2.1.1 Ring-Opening Polymerisation of Poly(ω-Pentadecalactone)

The ROP of PDL was performed in line with the previous report from Wilson *et al*., using benzyl alcohol as an initiator and $Mg(BHT)_2(THF)_2$ as a catalyst (Scheme 7.1).[28] $Mg(BHT)_2(THF)_2$ was synthesised according to the method described by Ittel *et al*..[29] In order to enable comparable results to microparticle degradation in Chapter 4, PPDL was polymerised to a degree of polymerisation (DP) of 100 (PPDL 100). The reaction was polymerised at 80 °C for 16 h before characterising the conversion by ^{1}H NMR spectroscopy *via* the ratio of the integrations of the α-methylene shift of PDL (δ = 4.15 ppm) compared to PPDL (δ = 4.05 ppm), in agreement with previous literature.[30] The resultant polymer was purified by precipitation into methanol before being dried *in vacuo*. Characterisation of the white polymer by ^{1}H NMR spectroscopy enabled the calculation of the DP through the integration of the benzyl methylene resonance (δ = 5.11 ppm) to the α-methylene resonance of PPDL (δ = 4.05 ppm) (Figure 7.2).

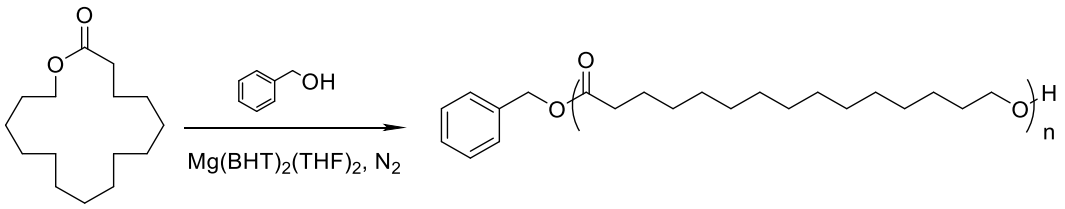

Scheme 7.1: Schematic representation of ROP PDL using $Mg(BHT)_2(THF)_2$ as a catalyst at 1 M PDL in toluene

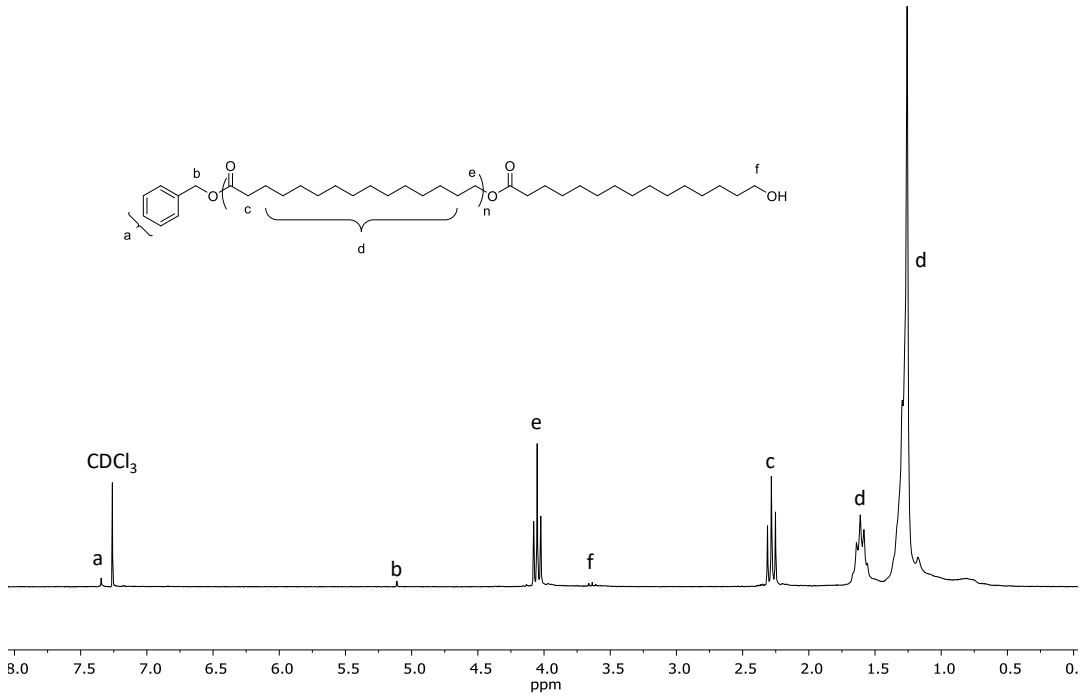

Figure 7.2: ^{1}H NMR spectrum of PPDL 100 ($CDCl_3$, 300 MHz, 298 K)

Further characterisation of the polymer by size exclusion chromatography (SEC) revealed a dispersity ($Đ_M$) of 2.18, with evidence of a lower molecular weight shoulder visible on the SEC chromatogram (Figure 7.3). The broad $Đ_M$ and low molecular weight shoulder were attested to transesterification side reactions occurring synchronously with polymerisation during ROP. Consequently, through back-biting, the active chain end can react with the ester linkage on the polymer backbone, thus resulting in a shortened chain and a cyclic species, leading to a broad dispersity.

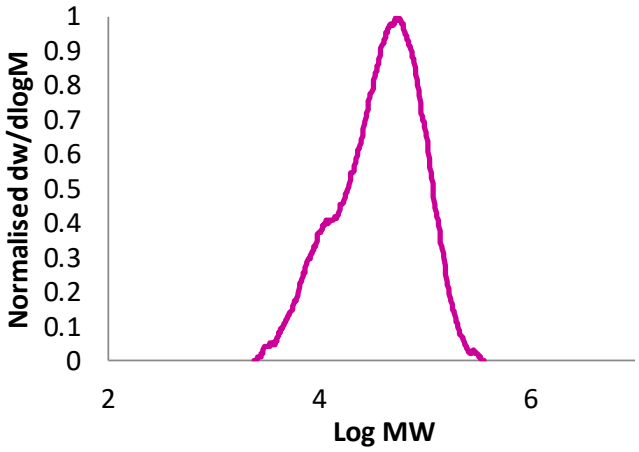

Figure 7.3: SEC characterisation of PPDL 100 ($CHCl_3$, PS standards)

7.2.1.2 Synthesis of PPDL Microparticles

Microparticles from PPDL 100 were prepared using the optimised single oil-in-water solvent evaporation conditions from Chapter 2. In brief, PPDL 100 was dissolved in dichloromethane before homogenising at 7000 rpm for 30 s with an aqueous solution (containing Mowiol 488 (2 wt%) as a stabiliser). The organic solvent was evaporated overnight before characterising the particle suspension *via* light scattering (Figure 7.4).

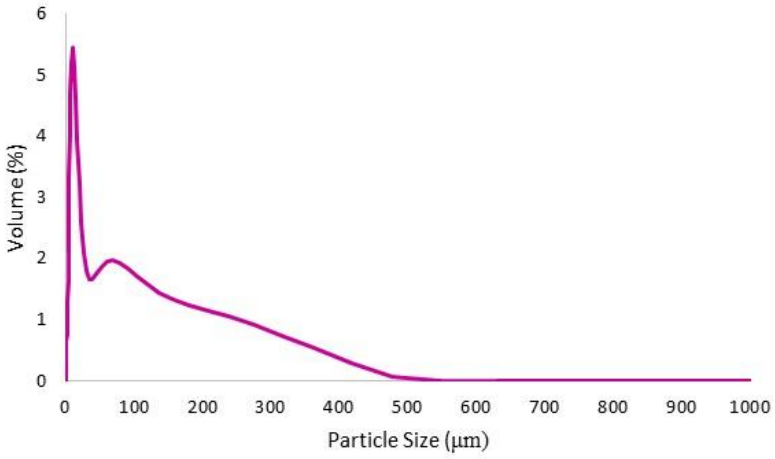

Figure 7.4: Light scattering characterisation of PPDL microparticles prepared *via* single oil-in-water solvent evaporation

Light scattering of the particle suspension revealed an average volume weighted mean particle size of 10 μm, however, larger aggregates were evident in the solution, ranging up to 500 μm in size. During particle synthesis, PPDL 100 was only just soluble in dichloromethane, consequently, sediment was also observed at the base of the emulsion. Characterisation of the particle morphology by scanning electron microscopy (SEM) revealed the formation of perforated crystalline particles (Figure 7.5). The long aliphatic backbone of PPDL enables the polymer chains to assemble into a highly ordered, densely packed structure. Hence, during particle formation, the long chain length of the polymer could prevent tight packing between the PPDL chains, thus reducing the strength of the intermolecular bonds between the polymer chains. Furthermore, the low solubility of PPDL 100 in dichloromethane would result in the polymer precipitating before the dichloromethane can fully evaporate. Therefore, it was postulated that the low solubility and long crystalline chain of the polymer would result in the formation of highly porous particles as confirmed *via* SEM analysis (Figure 7.5).

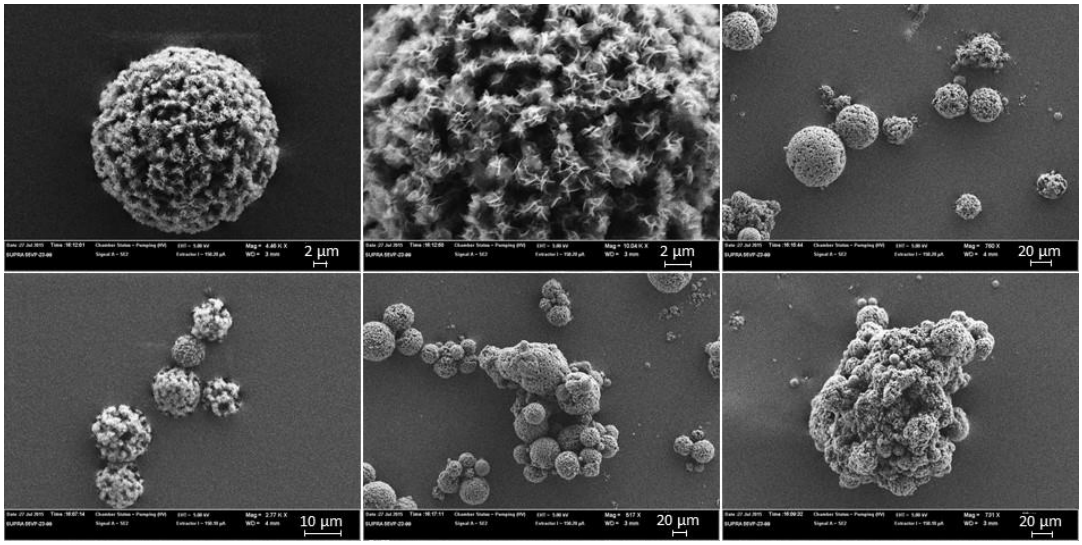

Figure 7.5: SEM characterisation of PPDL microparticles using CH_2Cl_2 as organic phase

As a consequence of the low solubility of PPDL 100 in dichloromethane, various organic solvents were investigated with the aim to decrease the concentration of sedimentation formed during particle synthesis. The most promising solvent appeared to be chloroform. PPDL 100 dissolved easily into chloroform, however, a similar level of sedimentation was observed at the base of the reaction flask as noted with particle synthesis using dichloromethane. The particles were characterised *via* SEM (Figure 7.6), which confirmed the successful synthesis of PPDL 100 microparticles with a smooth surface morphology. However, SEM analysis of the sediment confirmed the presence of broken and deformed particles. It was postulated that the increased solubility of PPDL 100 in chloroform compared to dichloromethane enabled the formation of microparticles with increased surface smoothness. However, the long chain length of the polymer still resulted in the formation of large pores within the microparticle, thus decreasing the particle stability. Consequently, the particles would be more susceptible to breaking or falling apart.

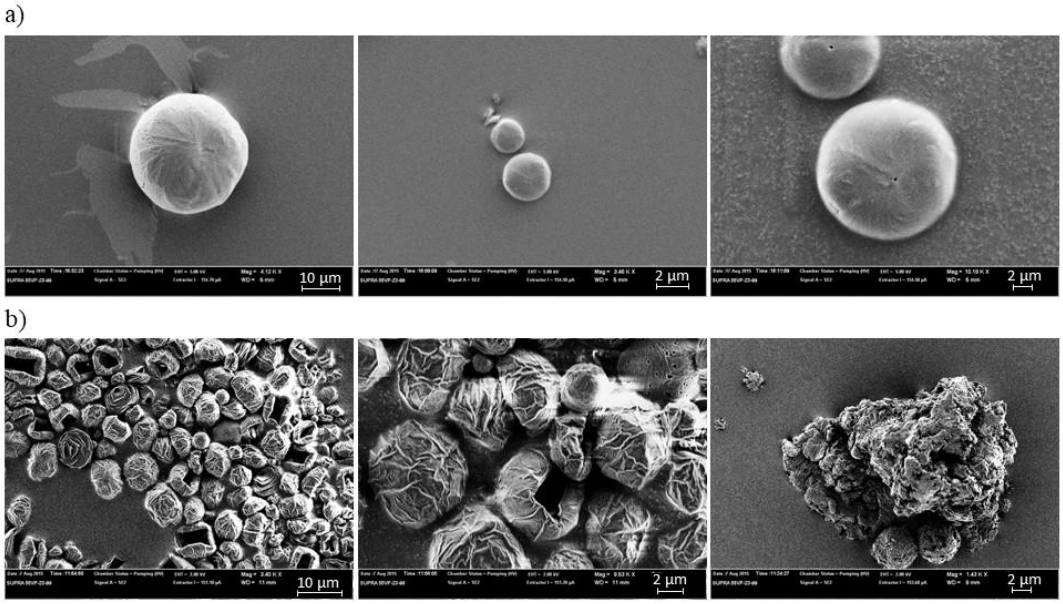

Figure 7.6: SEM characterisation of a) PPDL microparticle suspension and b) sediment arising with $CHCl_3$ as organic solvent

The synthesis of PPDL 100 microparticles was investigated further by encapsulating 3-bromo-4-(butylamino)-2,5-dihydro-1H-pyrrole-2,5-dione (ABM). The particles were prepared using the optimised single oil-in-water conditions. ABM (0.1 wt%) was dissolved in conjunction with PPDL 100 into chloroform, before emulsifying with an aqueous solution (containing Mowiol 488 (2 wt%) as stabiliser). Chloroform was evaporated overnight before washing the particles with deionised water and freeze drying. The washed and dried sample was dissolved in dichloromethane, to enable an accurate determination of the percentage of encapsulated dye. The particle dye loading (*E*) was determined by comparing the fluorescence intensity of the encapsulated dye against the intensity of six known concentrations of unencapsulated ABM using a fluorometer. However, the resultant particles synthesised with both dichloromethane and chloroform as the organic phase displayed low *E* ($\geq$ 12%). The observed low *E* was postulated to be a consequence of the broken particle morphology and large pore size. As a consequence of the low *E* observed with PPDL microparticles, it would be interesting to investigate particles synthesised from homopolymer blends or copolymers of PPDL and a smaller ring lactone, such as poly(3-hydroxybutyrate) (PHB), PLA or a responsive polymer.

7.2.2 Synthesis of Thin Films from Poly(ω-Pentadecalactone), Poly(ε-Caprolactone) and their Copolymers

7.2.2.1 Copolymerisation of Poly(ω-Pentadecalactone) and Poly(ε-Caprolactone)

Polymeric films have been proven to be ideal structural materials for controlling AI release.[31-33] The one-pot copolymerisation of PDL with εCL has been shown to yield random copolymers, resulting from transesterification side reactions.[24-26] Therefore, the thin film degradation rate can be controlled by tuning the copolymer composition of PPDL and PCL. Copolymers of P(PDL-*co*-εCL) were synthesised by one-pot ROP using an equimolar ratio of benzyl alcohol initiator and $Mg(BHT)_2(THF)_2$ catalyst, with a total monomer concentration of 2 M in toluene at 80 °C, in line with the procedure by Wilson *et al*. (Scheme 7.2).[24]

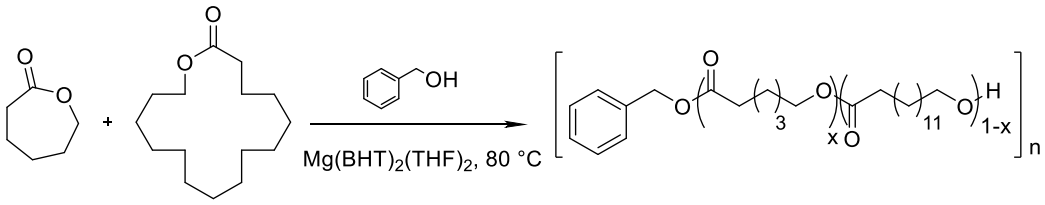

Scheme 7.2: Schematic representation of copolymerisation of PDL and εCL

To be consistent with previous degradation chapters, an overall DP of 100 was targeted. The incorporation of each monomer within the final copolymer was systematically varied by modifying the initial ratio of PDL: εCL. The monomers were polymerised for the desired time before characterising the monomer conversion by ^{1}H NMR spectroscopy (Table 7.1). The individual α-methylene shifts for both PPDL and PCL appeared at δ = 4.05 ppm, therefore, the calculation of individual monomer conversion could not be achieved by ^{1}H NMR spectroscopy. Conversely, the overall monomer conversion was calculated by integration of the polymer α-methylene shift (δ = 4.05 ppm) compared to the monomer α-methylene shift (δ = 4.06 ppm). The

polymerisation was quenched by addition of acidified methanol before precipitating the copolymers into methanol to remove any excess monomer. The polymers were dried *in vacuo* before characterisation by ^{1}H NMR spectroscopy, quantitative ^{13}C NMR spectroscopy and SEC (Figure 7.7 and Table 7.1). To enable a comparative study, homopolymers of PPDL and PCL were polymerised to DP 100 using previously discussed methods (Section 7.2.1 and Section 2.2.1.3 respectively).

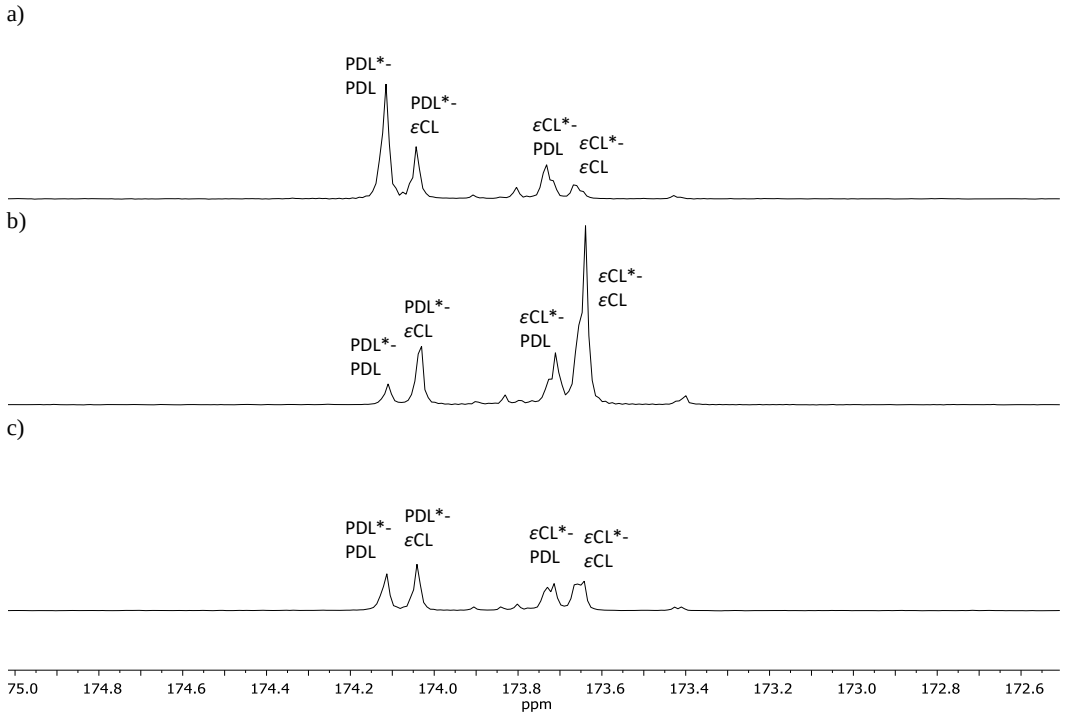

Figure 7.7: Quantitative ^{13}C NMR spectroscopic analysis of P(PDL-*co*-εCL) copolymers with (PDL: εCL) monomer composition a) 75:25 b) 25:75 and c) 50:50 (700 MHz, $CDCl_3$, 298 K)

Table 7.1: Copolymerisation of PDL and εCL targeting DP 100 with varying monomer ratio's

[PDL]: [PCL]	*p* (%)	$M_{n\ theory}$ (kDa)[a,b]	$M_{n\ NMR}$ (kDa)[a]	$M_{n\ SEC}$ (kDa)[c]	$Đ_{M\ SEC}$[c]	Diads[d]			
						PDL*-PDL	PDL*-εCL	εCL*-PDL	εCL*-εCL
100:0	97	23,400	27,000	24,500	2.18	- (1.00)	- (0.00)	- (0.00)	- (0.00)
75:25	96	20,200	20,200	16,600	2.18	0.03 (0.04)	0.17 (0.16)	0.15 (0.16)	0.65 (0.64)
50:50	94	16,800	15,700	14,700	1.83	0.23 (0.23)	0.25 (0.25)	0.25 (0.25)	0.27 (0.27)
25:75	98	14,400	17,000	7,600	1.42	0.47 (0.49)	0.23 (0.21)	0.20 (0.21)	0.10 (0.09)
0:100	95	11,000	16,000	15,300	1.08	- (0.00)	- (0.00)	- (0.00)	- (1.00)

[a]Determined by ^{1}H NMR spectroscopy, [b]Calculated from ([εCL and/or PDL]$_0$/[BA] × *p* × (molecular weight of εCL and/or PDL) + (molecular weight of BA), [c]Determined by SEC analysis in $CHCl_3$ against PS standards, [d]Derived from quantitative ^{13}C NMR spectroscopy, where * denotes the analysed carbonyl, numbers in parentheses show theoretical values based on the composition calculated using the equation P(A*-B)=fa×fb

Synthesis of random copolymers was confirmed by the presence of four carbonyl diad resonances within the quantitative ^{13}C NMR spectra for the three copolymer compositions, which corresponded to PDL*-PDL, PDL*-εCL, εCL*-PDL and εCL*-εCL (where * is the observed carbonyl). Furthermore, the intensities of the diad resonances fit well with the expected intensities for the corresponding desired ratio of PDL: εCL within the final copolymer. SEC characterisation revealed the formation of narrow, monomodal traces during polymerisation of εCL, however, as PDL was introduced into the copolymer, the $Đ_M$ increased and evidence for low molecular weight species were present in the SEC chromatograms. The increased $Đ_M$ and low molecular weight species present in the copolymers were a result of transesterification side reactions and unavoidable cyclic species arising during the polymerisation of strainless macrolactones.

7.2.2.2 PPDL Film Formation

7.2.2.2.1 Solvent Casting

Initially, the formation of PPDL 100 films *via* solvent casting was investigated. In order to achieve this, three different concentrations of PPDL 100 in chloroform (2 wt%, 5 wt% and 10 wt%) were prepared. Several drops of the respective solution were distributed evenly onto a glass slide, before leaving the chloroform to evaporate overnight. However, at all concentrations, the PPDL appeared to have detached from the glass slide (Figure 7.8 a). This was postulated to be a consequence of the rapid evaporation rate of the chloroform. Therefore, to decrease the chloroform evaporation rate, PPDL (10 wt%) was evenly distributed onto a glass slide and placed within a tall PTFE cup. The chloroform was evaporated overnight before characterising the film height by interferometry (Figure 7.8 b).

a) b)

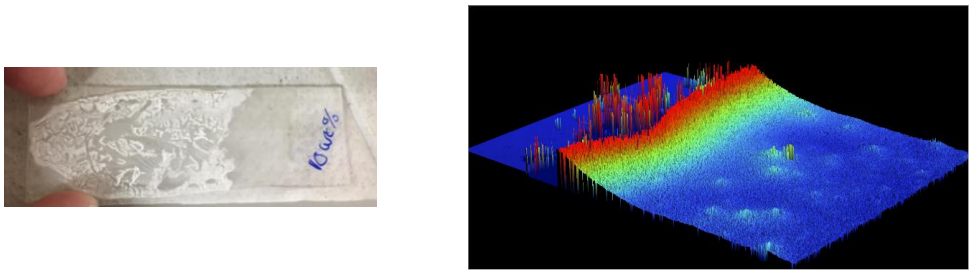

Figure 7.8: Solvent casting of PPDL 100 (10 wt%) films onto a) a glass slide on the bench b) interferometry characterisation of solvent casting onto a glass slide in a PTFE cup

Interferometry analysis of a PPDL 100 (10 wt%) film after solvent casting onto a glass slide within a PTFE cup revealed the formation of a 4 μm thick film with a rough surface. The rough surface was also evident for PPDL at 2 wt% and 5 wt% in chloroform and was attributed to an uneven layering of the PPDL 100 during chloroform evaporation. It was evident that to achieve reproducible PPDL film synthesis with comparable film thickness, a more controlled technique was required.

7.2.2.2.2 Spin Coating

Spin coating enables evaporation of the organic solvent during high speed rotation of the sample. Consequently, the combination of the resulting centripetal force and surface tension of the solution results in the formation of evenly coated films.[34] Therefore, the three concentrations of PPDL in chloroform (2 wt%, 5 wt% and 10 wt%) were applied onto a glass slide before spin coating for 1 min at 2000 rpm. The subsequent films were characterised *via* interferometry (Figure 7.9).

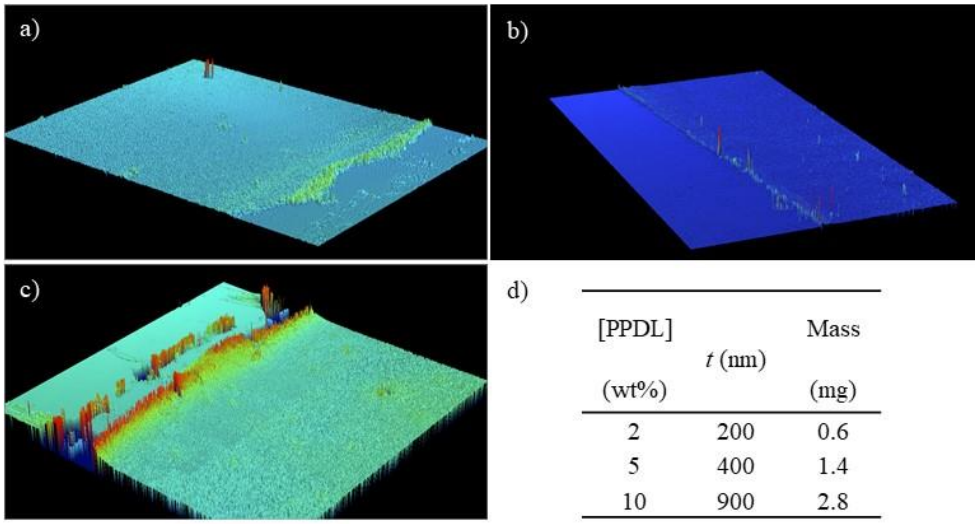

[PPDL] (wt%)	*t* (nm)	Mass (mg)
2	200	0.6
5	400	1.4
10	900	2.8

Figure 7.9: Interferometry analysis of PPDL 100 films after spin coating for 1 min at 2000 rpm with an initial [PPDL] in chloroform of a) 2 wt%, b) 5 wt% and c) 10 wt% d) resultant mass and film height at the three concentrations

Spin coating at a concentration of both 2 wt% and 5 wt% PPDL 100 in chloroform, yielded an even, uniform film, however, slight peeling was observed with the higher concentration of 10 wt% PPDL 100 in chloroform. Characterisation of the synthesised film mass revealed that only films synthesised at 5 wt% and above yielded films with a high enough mass to be characterizable *via* SEC. Therefore, all further film synthesis was performed at a concentration of 5 wt% polymer in chloroform.

7.2.2.3 Thin Film Degradation

As a consequence of the diverse soil composition experienced worldwide, the degradation profile of the films was monitored in three degradation media: neutral, enzymatic (10 mg/mL) and basic (pH 10). Protease, lipase and esterase are well known to be synthesised by microbes within the soil. The concentration of each enzyme can change rapidly depending on diffusion, the soil composition and the immediate plant surroundings. Therefore, to enable a comparable study to direct degradation in soil, the films were immersed in a solution of Cleanzyme, which contains a cocktail of enzymes commonly found in the soil.

Multiple films were synthesised for each copolymer composition by spin coating for 1 min at 2000 rpm at a polymer concentration of 5 wt% in chloroform. To characterise the films by SEC, the films were extracted from the slides by dissolving in chloroform, allowed to dry-down into a vial and then re-dissolved into the chloroform SEC solvent. Subsequent SEC characterisation of the films revealed both the original polymer and film had the same SEC chromatogram, with identical M_n and $Đ_M$. Therefore, film synthesis does not affect the properties of the polymer. Initial samples of the films were characterised by SEC and interferometry, thus enabling comparison of both the total mass loss and film height loss during degradation (Table 7.2).

Table 7.2: Film thickness and mass of films synthesised by spin coating from PPDL, PCL and their respective copolymers at 5 wt% [polymer] in chloroform

[PPDL]:[PCL]	[a]*t (nm)*	$M_{n\ SEC}$ (g/mol)[b]	$Đ_{M\ SEC}$[b]
100:0	400	24,500	2.18
75:25	500	16,600	2.18
50:50	800	14,700	1.83
25:75	400	7,600	1.42
0:100	300	15,300	1.08

[a]Film thickness determined by interferometry analysis [b]Determined by SEC characterisation in $CHCl_3$ against PS standards

After synthesis, the films were immersed directly into the desired degradation media. However, after one week of degradation, the films had detached from the glass slides, therefore, the degradation study could not be continued (Figure 7.10). This was postulated to be a consequence of the high hydrophobicity of the polymer compared to the glass slide. Consequently, for future progress, it was hypothesised that films could be spin coated onto either silanised glass (thus increasing the hydrophobicity of the glass) or on to a different substrate, such as silicon.

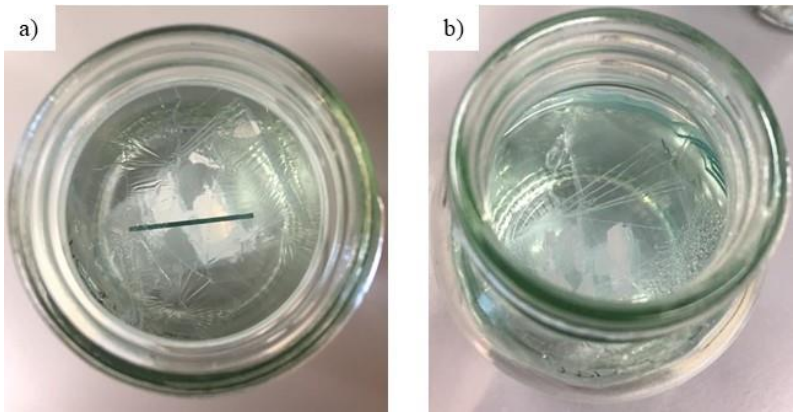

Figure 7.10: Visual observation of detached films after one week in a) aqueous and b) basic (pH(10)) degradation media *Imagery of detached films in enzymatic medium was unattainable as a consequence of the milky white colouration of cleanzyme. The films were observable floating on the top of the solution, however, the thin films split and fell apart when removed from the jar.

7.2.3 Polymerisation-Induced Self-Assembly of Poly(ω-Pentadecalactone-co-ε-Decalactone)

Self-assembly of block copolymers is generally achieved *via* post-polymerisation techniques, such as solvent switch and direct dissolution. These robust techniques enable the production of a wide array of structures, *e.g.*, spheres, cylinders, vesicles, *etc*.[35-38] The attained morphology can be controlled by the degree of repulsion, the initial molar monomer ratio and the selectivity of the solvent, which can all influence the packing parameter of the copolymer (Figure 7.11).[36] The resultant self-assembled structures have been shown to have high industrial relevance and have been applied for a range of applications *e.g.*, coatings, elastomers and drug delivery.[39-41] However, large scale synthesis of nanostructures *via* post-polymerisation self-assembly is currently challenging and most resultant nanostructures are in highly dilute concentration.[42, 43]

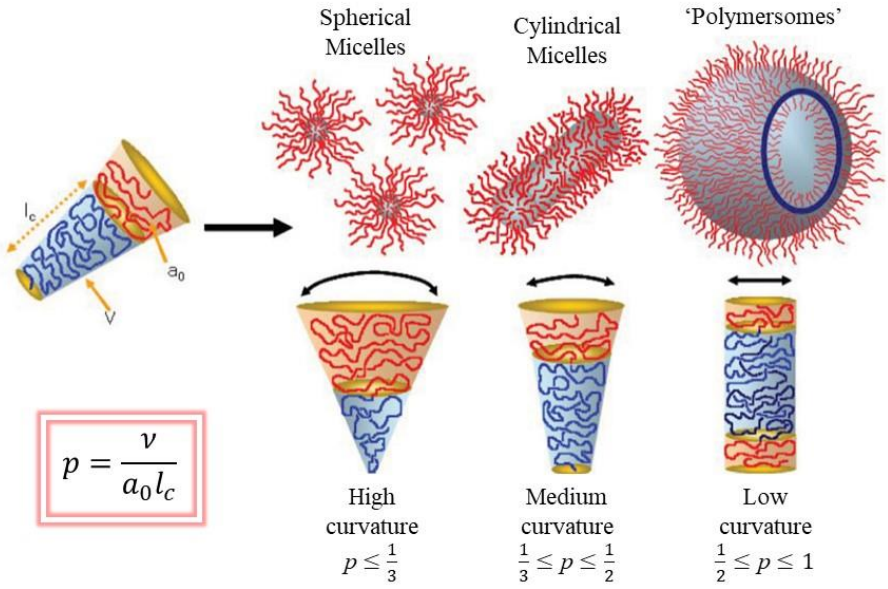

Figure 7.11: Schematic representation of the self-assembled morphologies available in a block-selective solvent where p = dimensionless packing parameter, v = volume of the hydrophilic chains, a_0 = contact area of the hydrophobic head group and l_c = length of the hydrophobic tail[36]

In recent years, polymerisation-induced self-assembly (PISA) has arisen and promises to solve the associated problems with post-polymerisation self-assembly.[44, 45] To achieve self-assembled structures using PISA, the block copolymers are prepared in a selective solvent, chosen so that the first block is completely soluble, yet the second block is insoluble.[46] Therefore, the polymer remains in solution during polymerisation of the first block, but as the second block is added to the chain, the insolubility of the growing second block results in polymer self-assembly. Currently, the majority of research has utilised reversible-addition-fragmentation chain transfer (RAFT) methodologies with vinyl monomers, therefore, PISA using ROP of polyesters opens the possibility to achieve a wide array of structures with interesting and diverse degradable properties.[47]

The unique structural properties associated with cylindrical or worm-like micelles have been shown to improve the mechanical properties of epoxy resins, be useful as templates for electronic materials and have enhanced drug delivery capability (as a consequence of their long circulation time and altered cell internalisation pathways when compared to spherical micelles).[48-51] Nevertheless, only a narrow composition window is available when using the hydrophobic effect as the main driving force for assembly.[36] Therefore, obtaining pure cylindrical morphologies has been proven to be challenging. Conversely, crystallization-driven self-assembly (CDSA) of block copolymers combines the hydrophobic effect with the high crystallinity of the hydrophobic block, thus providing a powerful and effective methodology for the selective synthesis of cylindrical micelles.[52-54]

7.2.3.1 ROP of P(PDL-co-εDL)

Polymerisation induced self-assembly (PISA) enables the production of hierarchical structures, such as micelles, cylinders and vesicles, *etc*., in a one-pot polymerisation

system.[43] It was postulated that the high crystallinity observed with PPDL would enable crystallisation driven self-assembly (CDSA) when copolymerised into a block copolymer. Therefore, it was interesting to investigate the one pot block copolymer synthesis of poly(ω-pentadecalactone-*co*-ε-decalactone) (P(PDL-*co*-eDL). The copolymerisation of PPDL and PeDL was performed targeting a 1:4 monomer ratio (respectively) using the method reported by Wilson *et al*., (Scheme 7.3).[55]

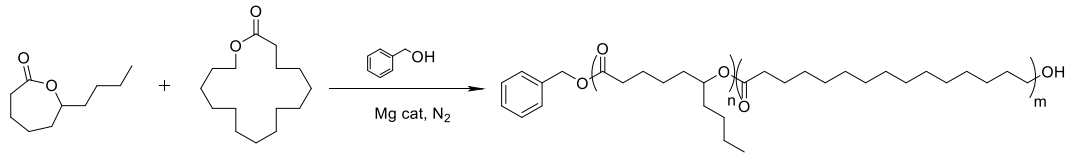

Scheme 7.3: Schematic representation of ROP of εDL and PDL

The successful copolymerisation of P(PDL-*co*-εDL) was confirmed by monitoring the decrease in the monomer α-methylene shifts of PPDL and PDL (δ = 4.11 ppm and δ = 4.22 ppm respectively) coupled with the formation of the polymer α-methylene shifts of PDL and PPDL (δ = 4.86 ppm and 4.05 ppm respectively). After polymerisation for 12 h, the polymerisation was quenched by addition of acidified methanol before precipitation into cold methanol. The resultant white powder was dried *in vacuo* before characterisation by ^{1}H NMR spectroscopy (Figure 7.12).

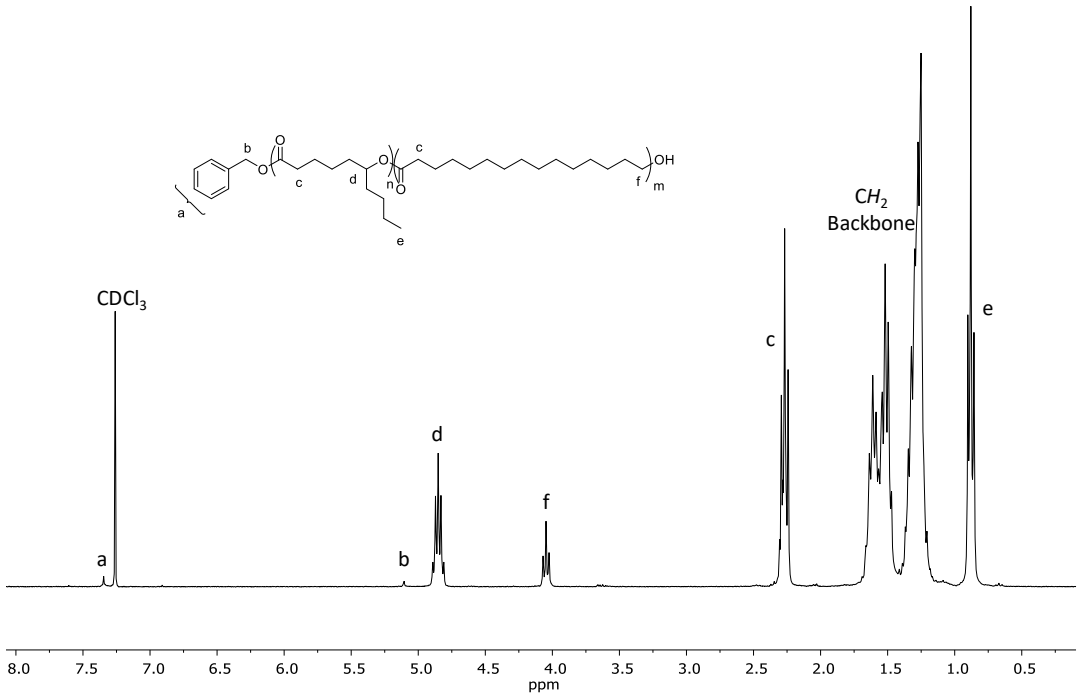

Figure 7.12: ^{1}H NMR spectrum of P(PDL-*co*-PDL) ($CDCl_3$, 300 MHz, 298 K)

Characterisation by ^{1}H NMR spectroscopy enabled calculation of the DP of each polymer by end group analysis. Moreover, comparison of the integrals of the benzyl methylene resonance of the chain end (δ = 5.11 ppm) to the α-methylene resonance of PPDL (δ = 4.05 ppm) and PDL (δ = 4.86 ppm), revealed a DP of 40 and 160 for PPDL and PDL respectively (Figure 7.12). The copolymer was further characterised *via* SEC, which again confirmed the presence of low molecular weight cyclic species characteristic of the polymerisation of macromonomers (Figure 7.13).

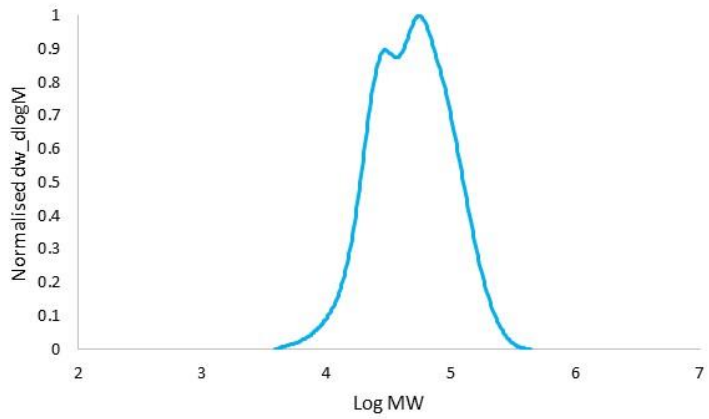

Figure 7.13: SEC chromatogram of P(PDL-*co*-DL) ($CHCl_3$, PS standards)

Fernández *et al*., reported that during copolymerisation εDL is consumed at a faster rate compared to PDL as a consequence of the different reactivity of the co-monomers.[23] Therefore, εDL is fully polymerised before PDL is incorporated into the chain, thus leading to the formation of block-like rather than random copolymers. To confirm the structure of the synthesised P(PDL-*co*-DL), the polymer was further characterised *via* quantitative ^{13}C NMR spectroscopy (Figure 7.14). The resultant ^{13}C NMR spectrum revealed the formation of the characteristic block copolymer shifts at δ = 174.1 ppm and 173.4 ppm representative of carbonyl diad resonances of PDL*-PDL and εDL*-εDL respectively. However, the appearance of a third, low intensity, carbonyl resonance at δ = 173.8 ppm, representative of PDL*-εDL implied that even though the polymers have a block-like structure, there is some graduation where a PDL unit neighbours an εDL unit within the copolymer. The relative ratios observed by integration of the carbonyl diad resonances revealed that the PPDL to PDL is approximately 1:4 and thus agrees with the initial monomer feed ratio.

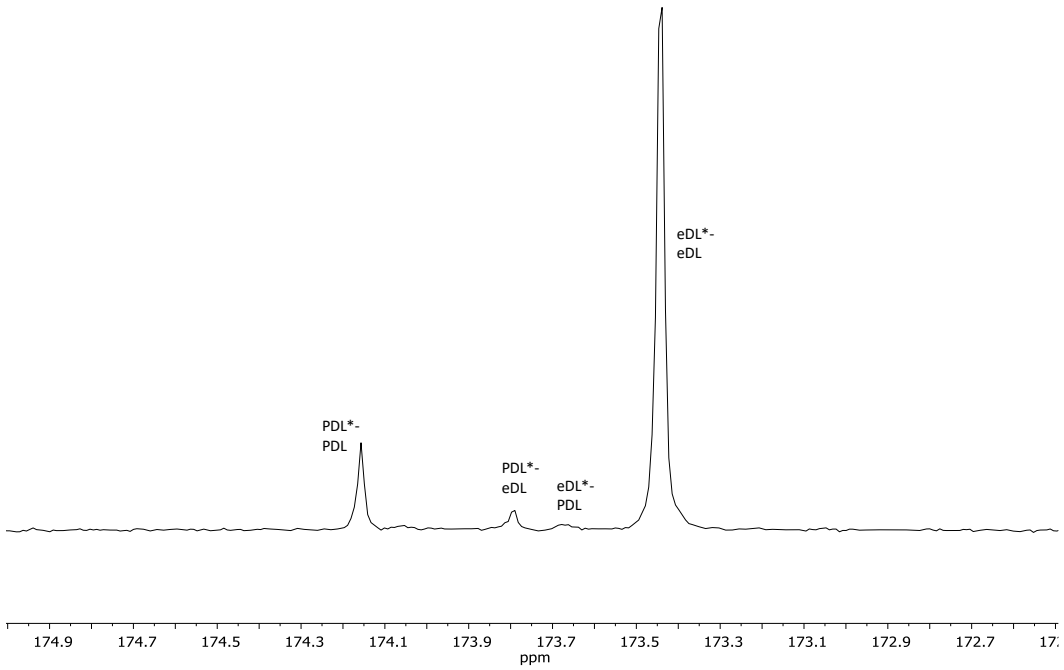

Figure 7.14: Quantitative ^{13}C NMR spectrum of P(PDL-*co*-DL), (125 MHz, $CDCl_3$, 298 K)

7.2.3.2 Homopolymerisation of ε-Decalactone and ω-Pentadecalactone

To successfully achieve PISA, the first block synthesised remains soluble within the chosen reaction solvent during polymerisation, however, the second block is insoluble in the reaction medium, thus destabilising the copolymer and driving self-assembly. Therefore, to elucidate the optimum solvent for PISA of P(PDL-*co*-DL), the solubility of PDL and PPDL in the desired reaction solvent was required. Therefore, εDL was polymerised to DP 160 using the same polymerisation conditions as detailed for homopolymerisation of PPDL (Section 7.2.1.1) (Scheme 7.4). In brief, εDL was polymerised to DP 160 using an equimolar ratio of benzyl alcohol initiator and $Mg(BHT)_2(THF)_2$ catalyst, with a total monomer concentration of 2 M in toluene. The reaction was polymerised at 80 °C for 12 h before characterising the conversion by ^1H NMR spectroscopy. The reaction was quenched by addition of acidified methanol, before precipitation into methanol and drying *in vacuo*. The successful synthesis of

PDL was confirmed by ^{1}H NMR spectroscopy and SEC (Figure 7.15 and Figure 7.16 respectively). Comparison of the integration of the PDL methine on the polymer backbone (δ = 4.86 ppm) and the methylene of the benzyl end group (δ = 5.11 ppm) enabled calculation of the polymer DP, in good agreement with previous literature (Figure 7.15).[56]

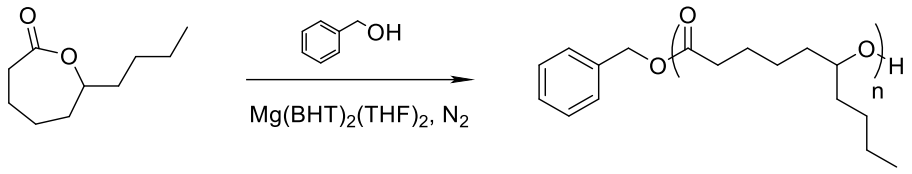

Scheme 7.4: Schematic representation of ROP of εDL using $Mg(BHT)_2(THF)_2$ as catalyst

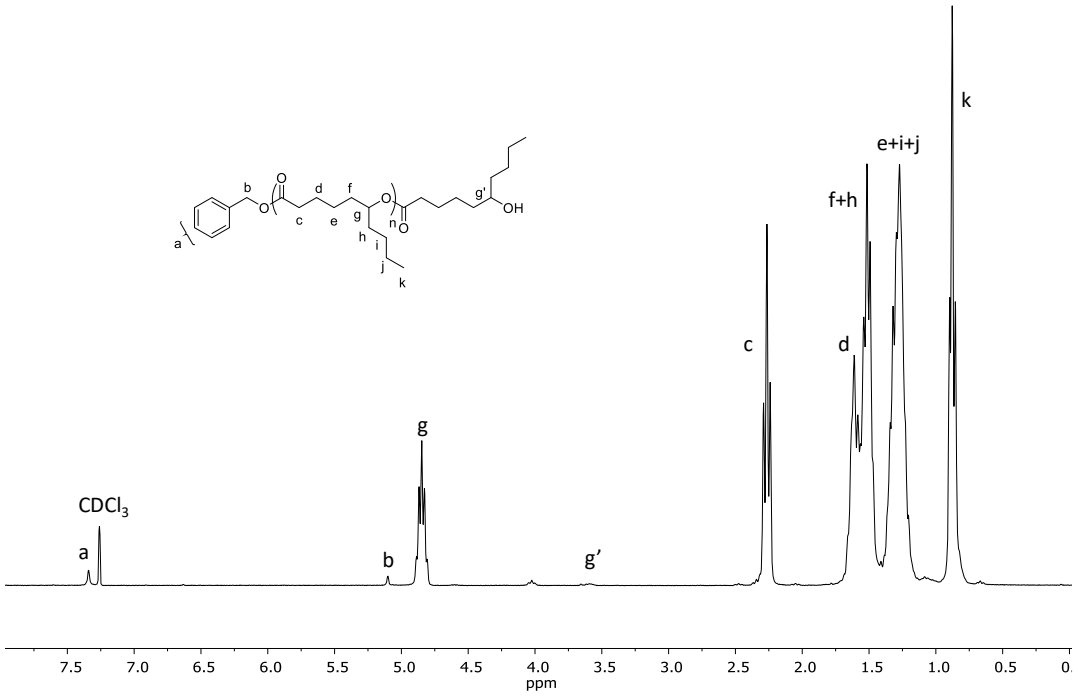

Figure 7.15: ^{1}H NMR spectrum of PDL DP 160 ($CDCl_3$, 30 MHz, 298 K)

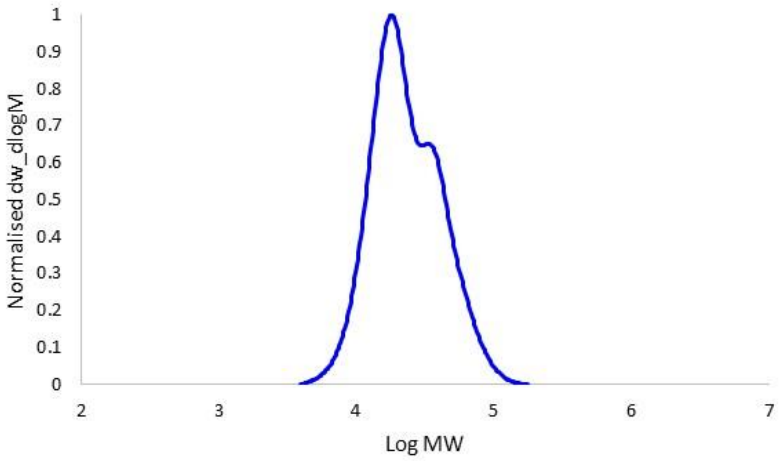

Figure 7.16: SEC chromatogram of PDL DP 160 ($CHCl_3$, PS standards)

To enable comparable solubility to the PPDL block of the 1: 4 PDL: εDL ratio of the polymerised P(PDL-*co*-εDL), PPDL was polymerised to DP 40 using the method detailed in Section 7.2.1.1. The polymerisation was heated at 80 °C for 4 h, before quenching the polymerisation by addition of acidified methanol. The resultant polymer was precipitated into methanol and dried overnight *in vacuo*, before being characterised *via* ^{1}H NMR spectroscopy and SEC (Table 7.3).

Table 7.3: Characterisation of homopolymerisation of PDL DP 160, PPDL DP 40 and copolymerisation of P(PDL-*co*-DL) DP 200 (ratio 1:4 respectively) using $Mg(BHT)_2(THF)_2$ as catalyst and benzyl alcohol (BA) initiator

Polymer	Target [M]/[I]	Time (h)	$M_{n\ theory}$ (g mol^{-1})[a,b]	$M_{n\ NMR}$ (g mol^{-1})[a]	$M_{n\ SEC}$ (g mol^{-1})[c]	$Đ_{M\ SEC}$[c]	Actual [M]/[I]
PPDL 40	40	4	8,800	8,700	9,800	2.20	36
PDL 160	160	12	26,800	27,000	19,500	1.39	158
P(PDL-*co*-DL)	200	12	33,400	35,400	35,800	1.68	191

[a]Determined by ^{1}H NMR spectroscopy, [b]Calculated from ([Monomer]$_0$/[BA] × conv. × (M.W of monomer) + (molecular weight of BA), [c]Determined by SEC analysis in $CHCl_3$ against PS standards

7.2.3.3 Solubility Study

To successfully achieve self-assembly *via* PISA, the solubility of both segments of the copolymer in the polymerisation solvent is highly important. Therefore, it was reasoned that the optimum solvent must adhere to three main solubility criteria:

1) PDL must be fully soluble
2) PPDL should be insoluble at room temperature, but soluble at an elevated temperature
3) P(PDL-*co*-DL) should be soluble at high temperatures and remain in solution when cooled back to room temperature

To determine the optimum conditions for PISA of P(PDL-*co*-DL), the solubility of PDL, PPDL and P(PDL-*co*-DL) was investigated in an initial visual analysis in a variety of solvents (Table 7.4). Furthermore, the polymers were immersed in the different solvents at room temperature, 80 °C and 110 °C and the cloudiness of the solution monitored over time. A copolymer ratio of PDL: DL of 1: 4 was targeted as in a normal self-assembly, this would enable the production of spheres, however, in CDSA, cylindrical structures should be evident. Ethyl benzene and butyl benzene appeared to be the most promising solvents. Moreover, both solvents were able to fully solubilise PDL at room temperature and elevated temperature and only solubilise PPDL at higher temperatures. Furthermore, both solvents were found to solubilise P(PDL-*co*-DL) at 80 °C and 110 °C and interestingly, the copolymer remained in solution even after the solution was cooled.

Table 7.4: Solubility of PPDL, PDL and P(PDL-*co*-DL) ratio of 1:4 at 50 mg/mL in a variety of solvents

Solvent	Polymer								
	PPDL			PDL			PPDL-*co*-PDL		
	RT	80 °C	110 °C	RT	80 °C	110 °C	RT	80 °C	110 °C
Hexane	x	x	x	-	-	-	x	x	x
Octane	x	✓*	✓*	-	-	-	-	-	-
Decane	x	✓	✓	✓	✓	✓	x	✓	✓
Butanol	x	✓*	✓	✓	✓	✓	x	✓	✓
Octanol	x	✓	✓	✓	✓	✓	x	✓	✓
Toluene	✓	✓	✓	✓	✓	✓	✓	✓	✓
Ethyl Benzene	x	✓	✓	✓	✓	✓	✓*	✓	✓
Butyl Benzene	x	✓	✓	✓	✓	✓	✓*	✓	✓
Propylene Carbonate	x	x	✓	✓*	✓	✓	-	-	-

x = insoluble, ✓* = partially soluble and ✓ = soluble

7.2.3.4 Self-Assembly of Poly(ω-Pentadecalactone-co-ε-Decalactone)

After the promising solubility observed visually of P(PDL-*co*-DL) in both ethyl benzene and butyl benzene, it was interesting to determine if after cooling the solution, the copolymer had formed a self-assembled structure or fully dissolved in the solvent. To further elucidate the potential copolymeric transformation, a solution of the P(PDL-*co*-DL) in ethyl benzene (50 mg/mL) was prepared and heated to 80 °C for one hour, before leaving the solution to cool to room temperature overnight. The initial 50 mg/mL solution and a diluted solution of 1 mg/mL were characterised *via* dynamic light scattering (Figure 7.17).

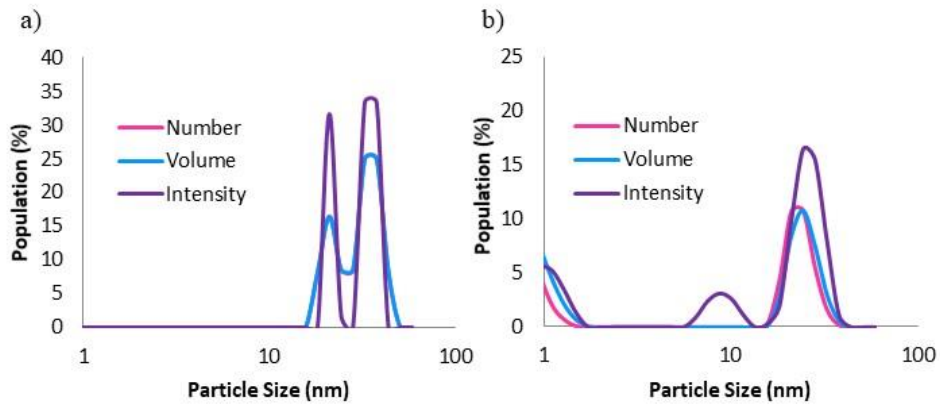

Figure 7.17: DLS characterisation of P(PDL-*co*-DL) self-assembly in ethylbenzene a) 50 mg/mL and b) 1 mg/mL

Interestingly, light scattering characterisation of the initial 50 mg/mL copolymeric solution in ethylbenzene revealed the formation of two distinct particle size distributions (Figure 7.17a)). It was postulated that the concentration of particles in solution was too high for accurate characterisation and was resulting in interparticle interactions, thus interfering with the characterisation. Therefore, the solution was diluted to a lower concentration of 1 mg/mL (Figure 7.17b). Nevertheless, even at a lower concentration, multiple distributions were evident by light scattering analysis. DLS functions on the assumption that the particles are spherical. Therefore, it was postulated that the multiple distributions evident by dynamic light scattering (DLS) could be a consequence of self-assembled cylindrical morphologies. To further investigate the self-assembly behaviour of P(PDL-*co*-DL) in ethyl benzene, the solution was characterised *via* transmission electron microscopy (TEM) (Figure 7.18a). To do this, a drop of the initial solution was placed on a carbon lacey film with 300 mesh copper grid and dried overnight before staining with uranyl acetate. To prevent sample aggregation or over-crowding on the TEM grid, a diluted sample was also characterised *via* TEM (10 mg/mL) (Figure 7.18b). At both concentrations,

cylindrical micelles could be observed, thus implying the polymer had undergone CDSA after cooling to room temperature.

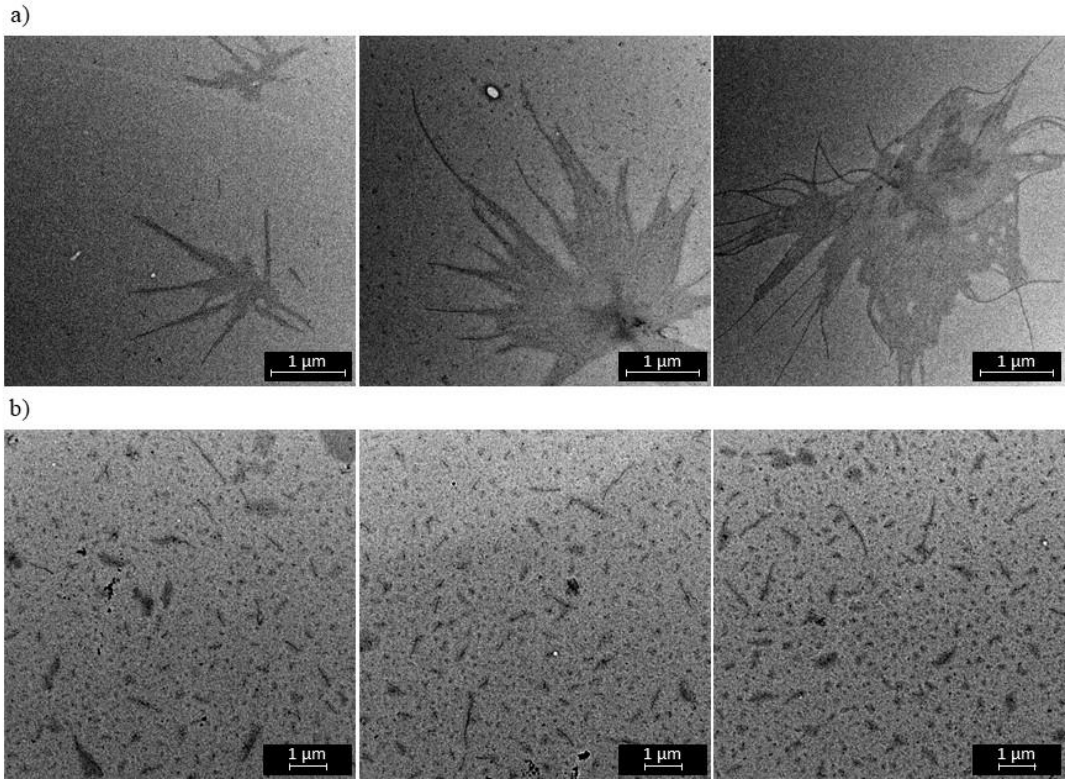

Figure 7.18: TEM characterisation of self-assembled structures of PPDL-*co*-PeDL self-assembly in ethylbenzene at a) 50 mg/mL and b) 10 mg/mL

7.2.3.5 Attempt at PISA of Poly(ω-Pentadecalactone-co-ε-Decalactone)

To further examine the self-assembly behaviour observed with P(PDL-*co*-DL), a one-pot copolymerisation was performed at 2 M in ethyl benzene. The copolymerisation was heated at 80 °C for 12 h, before leaving to cool to room temperature overnight. Interestingly, after twelve hours of heating, the copolymer had a gel-like consistency when heated and after cooling. Derry *et al*., recently reported critical gel temperature associated with the formation of worm-like micelles assembled during PISA in hexane with poly(lauryl methacrylate)-poly(benzyl methacrylate).[39] A sample of the polymerisation solution was diluted in ethyl benzene before characterisation *via* TEM. However, no self-assembled structures were evident *via* TEM analysis.

7.3 Conclusions

In conclusion, this Chapter detailed the wide variety of advantageous morphologies attainable from PPDL and its copolymers. When applied in a single oil-in-water solvent evaporation technique, PPDL yielded highly crystalline spherical microparticles as observed *via* SEM. However, large aggregates were observed forming during particle hardening, thus resulting in the formation of sediment at the base of the reaction flask. Investigation into the encapsulation of a fluorescent ABM within a PPDL microparticle resulted in a low *E* (12%), presumably as a consequence of the low solubility and high crystallinity of PPDL. However, the interesting particle structure and polymeric properties afforded with PPDL highlight the great potential offered by PPDL microparticles potentially achievable through copolymerisation or blending of PPDL with a smaller ring lactone or responsive polymer.

Copolymerisation of PDL with εCL yielded random copolymers, whose composition could be accurately tuned by varying the initial molar monomer ratio, as confirmed by quantitative ^{13}C NMR spectroscopy. Investigation into the synthesis of films from PPDL 100 revealed that spin coating at 2000 rpm for 1 min enabled the formation of thin, evenly distributed films with no evidence of peeling at concentrations of 2 wt% and 5 wt%. Expanding the investigation to different P(PDL-*co*-CL) compositions enabled the production of thin films with characterizable profiles by SEC and interferometry when prepared at 5 wt% polymer in chloroform. However, after one week in aqueous, enzymatic and basic degradation media, all film compositions had detached from the glass slides. This was postulated to be a consequence of the difference in hydrophobicity of the glass slide compared to the PPDL and PCL films. Nevertheless, the ease of film synthesis and characterisation suggest the potential for

PPDL film degradation to be achievable by using a different substrate, such as silanised glass or silicon.

One pot copolymerisation of PPDL and PDL with $Mg(BHT)_2(THF)_2$ as catalyst yielded block-like copolymers, as confirmed by quantitative ^{13}C NMR spectroscopy. Investigation into the solubility of P(PDL-*co*-DL) revealed that ethyl benzene and butyl benzene were able to solubilise P(PDL-*co*-DL) at elevated temperature, but not at room temperature. However, it was observed that after heating, the copolymer remained in solution even when cooled to room temperature. Characterisation of the resultant solution by TEM revealed the presence of worm-like micelles. Furthermore, the morphology of the copolymer was characterised directly after polymerisation in ethyl benzene *via* TEM, however, no self-assembled structures were observable, therefore, future work optimising the PICDSA conditions would be required. Nevertheless, the high versatility achieved through copolymerisation of PPDL highlights the wide array of potential enhancements attainable to the agricultural industry *via* application of PPDL and its copolymers.

7.4 References

1. C. Jérôme and P. Lecomte, *Adv. Drug Delivery Rev.*, 2008, **60**, 1056-1076.
2. B. J. O'Keefe, M. A. Hillmyer and W. B. Tolman, *J. Chem. Soc., Dalton Trans.*, 2001, **15**, 2215-2224.
3. A. P. Dove, *Chem. Commun.*, 2008, **48**, 6446-6470.
4. A.-C. Albertsson and I. K. Varma, *Biomacromolecules*, 2003, **4**, 1466-1486.
5. R. Nomura, A. Ueno and T. Endo, *Macromolecules*, 1994, **27**, 620-621.
6. M. Letizia Focarete, M. Scandola, A. Kumar and R. A. Gross, *J. Polym. Sci. B Polym. Phys.*, 2001, **39**, 1721-1729.
7. Z. Jiang, H. Azim, R. A. Gross, M. L. Focarete and M. Scandola, *Biomacromolecules*, 2007, **8**, 2262-2269.
8. M. de Geus, I. van der Meulen, B. Goderis, K. van Hecke, M. Dorschu, H. van der Werff, C. E. Koning and A. Heise, *Polym. Chem.*, 2010, **1**, 525-533.
9. N. Simpson, M. Takwa, K. Hult, M. Johansson, M. Martinelle and E. Malmström, *Macromolecules*, 2008, **41**, 3613-3619.
10. U. Hiroshi, T. Kazuhiro and K. Shiro, *Bull. Chem. Soc. Jpn.*, 1995, **68**, 56-61.
11. D. McGinty, C. S. Letizia and A. M. Api, *Food Chem. Toxicol.*, 2011, **49, Supplement 2**, S193-S201.
12. J. Cai, B. S. Hsiao and R. A. Gross, *Polym. Int.*, 2009, **58**, 944-953.
13. J. Cai, C. Liu, M. Cai, J. Zhu, F. Zuo, B. S. Hsiao and R. A. Gross, *Polymer*, 2010, **51**, 1088-1099.
14. M. Gazzano, V. Malta, M. L. Focarete, M. Scandola and R. A. Gross, *J. Polym. Sci. B Polym. Phys.*, 2003, **41**, 1009-1013.
15. P. Skoglund and Å. Fransson, *Polymer*, 1998, **39**, 1899-1906.
16. S. Lyu and D. Untereker, *Int. J. Mol. Sci.*, 2009, **10**, 4033-4065.
17. M. D. Rowe, E. Eyiler and K. B. Walters, *Polym. Test.*, 2016, **52**, 192-199.
18. R. P. Brannigan and A. P. Dove, *Biomater. Sci.*, 2017, **5**, 9-21.
19. V. Speranza, A. De Meo and R. Pantani, *Polym. Degrad. Stab.*, 2014, **100**, 37-41.
20. M. Bouyahyi and R. Duchateau, *Macromolecules*, 2014, **47**, 517-524.
21. Y. Nakayama, N. Watanabe, K. Kusaba, K. Sasaki, Z. Cai, T. Shiono and C. Tsutsumi, *J. Appl. Polym. Sci.*, 2011, **121**, 2098-2103.

22. J. Liu, Z. Jiang, S. Zhang, C. Liu, R. A. Gross, T. R. Kyriakides and W. M. Saltzman, *Biomaterials*, 2011, **32**, 6646-6654.
23. J. Fernández, A. Etxeberria, A. L. Varga and J.-R. Sarasua, *Polymer*, 2015, **81**, 12-22.
24. J. A. Wilson, S. A. Hopkins, P. M. Wright and A. P. Dove, *Macromolecules*, 2015, **48**, 950-958.
25. A. Kumar, B. Kalra, A. Dekhterman and R. A. Gross, *Macromolecules*, 2000, **33**, 6303-6309.
26. M. Bouyahyi, M. P. F. Pepels, A. Heise and R. Duchateau, *Macromolecules*, 2012, **45**, 3356-3366.
27. G. Ceccorulli, M. Scandola, A. Kumar, B. Kalra and R. A. Gross, *Biomacromolecules*, 2005, **6**, 902-907.
28. J. A. Wilson, S. A. Hopkins, P. M. Wright and A. P. Dove, *Polym. Chem.*, 2014, **5**, 2691-2694.
29. J. Calabrese, M. A. Cushing and S. D. Ittel, *Inorg. Chem.*, 1988, **27**, 867-870.
30. M. Eriksson, L. Fogelström, K. Hult, E. Malmström, M. Johansson, S. Trey and M. Martinelle, *Biomacromolecules*, 2009, **10**, 3108-3113.
31. M. Jamshidian, E. A. Tehrany and S. Desobry, *Food Bioprocess Tech.*, 2013, **6**, 1450-1463.
32. E. Can, G. Udenir, A. I. Kanneci, G. Kose and S. Bucak, *AAPS PharmSciTech*, 2011, **12**, 1442-1453.
33. Y. Gao, G. P. Zago, Z. Jia and M. J. Serpe, *ACS Appl. Mater. Interfaces*, 2013, **5**, 9803-9808.
34. K. Norrman, A. Ghanbari-Siahkali and N. B. Larsen, *Annu. Rep. Prog. Chem., Sect. C: Phys. Chem.*, 2005, **101**, 174-201.
35. G. Riess, *Prog. Polym. Sci.*, 2003, **28**, 1107-1170.
36. A. Blanazs, S. P. Armes and A. J. Ryan, *Macromol. Rapid Commun.*, 2009, **30**, 267-277.
37. C. Limouzin-Morel, F. Dutertre, W. Moussa, C. Gaillard, I. Iliopoulos, D. Bendejacq, T. Nicolai and C. Chassenieux, *Soft Matter*, 2013, **9**, 8931-8937.
38. D. E. Discher and A. Eisenberg, *Science*, 2002, **297**, 967-973.
39. M. J. Derry, L. A. Fielding and S. P. Armes, *Polym. Chem.*, 2015, **6**, 3054-3062.
40. J. Y. Cheng, A. M. Mayes and C. A. Ross, *Nat. Mater.*, 2004, **3**, 823-828.

41. Z. Nie, A. Petukhova and E. Kumacheva, *Nat Nano*, 2010, **5**, 15-25.
42. R. C. Hayward and D. J. Pochan, *Macromolecules*, 2010, **43**, 3577-3584.
43. A. Blanazs, J. Madsen, G. Battaglia, A. J. Ryan and S. P. Armes, *J. Am. Chem. Soc.*, 2011, **133**, 16581-16587.
44. N. J. Warren and S. P. Armes, *J. Am. Chem. Soc.*, 2014, **136**, 10174-10185.
45. L. D. Blackman, K. E. B. Doncom, M. I. Gibson and R. K. O'Reilly, *Polym. Chem.*, 2017, **8**, 2860-2871.
46. M. J. Derry, L. A. Fielding and S. P. Armes, *Prog. Polym. Sci.*, 2016, **52**, 1-18.
47. S. L. Canning, G. N. Smith and S. P. Armes, *Macromolecules*, 2016, **49**, 1985-2001.
48. J. Liu, Z. J. Thompson, H.-J. Sue, F. S. Bates, M. A. Hillmyer, M. Dettloff, G. Jacob, N. Verghese and H. Pham, *Macromolecules*, 2010, **43**, 7238-7243.
49. X.-S. Wang, H. Wang, N. Coombs, M. A. Winnik and I. Manners, *J. Am. Chem. Soc.*, 2005, **127**, 8924-8925.
50. Y. Geng, P. Dalhaimer, S. Cai, R. Tsai, M. Tewari, T. Minko and D. E. Discher, *Nat Nano*, 2007, **2**, 249-255.
51. K. Zhang, R. Rossin, A. Hagooly, Z. Chen, M. J. Welch and K. L. Wooley, *J. Polym. Sci. A Polym. Chem.*, 2008, **46**, 7578-7583.
52. L. Sun, N. Petzetakis, A. Pitto-Barry, T. L. Schiller, N. Kirby, D. J. Keddie, B. J. Boyd, R. K. O'Reilly and A. P. Dove, *Macromolecules*, 2013, **46**, 9074-9082.
53. A. Pitto-Barry, N. Kirby, A. P. Dove and R. K. O'Reilly, *Polym. Chem.*, 2014, **5**, 1427-1436.
54. J. A. Massey, K. Temple, L. Cao, Y. Rharbi, J. Raez, M. A. Winnik and I. Manners, *J. Am. Chem. Soc.*, 2000, **122**, 11577-11584.
55. J. A. Wilson, S. A. Hopkins, P. M. Wright and A. P. Dove, *Biomacromolecules*, 2015, **16**, 3191-3200.
56. J.-O. Lin, W. Chen, Z. Shen and J. Ling, *Macromolecules*, 2013, **46**, 7769-7776.

8. Conclusions and Future Work

8.1 Conclusions

In conclusion, the synthesis and characterisation of biodegradable microparticles for the controlled release of an active ingredient (AI) has been shown to be an excellent platform for the production of enhanced agricultural formulations. In the first approach, a range of lactones were polymerised to yield well-defined polyesters with tuneable molecular weights. Magnesium 2,6-di-tert-butyl-4-methylphenoxide ($Mg(BHT)_2(THF)_2$) was found to be an efficient catalyst for the ring-opening polymerisation of poly(3-hydroxybutyrate) (PHB). However, high monomer conversion was unattainable using the polymerisation system as a consequence of monomer deprotonation during initiation. Microparticle formation using the synthesised polyesters was demonstrated using a versatile single oil-in-water solvent evaporation technique. Characterisation of the particles *via* light scattering and microscopy revealed the high influence of formulation variables on the resultant particle size and stability. Optimisation of the emulsification parameters enabled the creation of a repeatable procedure for microparticle synthesis that was demonstrated to be easily applicable to a wide variety of polymers and molecular weights.

The optimised single oil-in-water technique was further expanded and was discovered to be highly versatile for the encapsulation of hydrophobic dyes. However, characterisation of the particle morphology and dye loading *via* scanning electron microscopy (SEM) and fluorometry revealed that the structure of the dye and its compatibility with the polymeric particle can drastically alter the particle encapsulation and release rate. The degradation and release profiles of the different polyester microparticles was investigated under simulated environmental conditions, which showcased the high resistance to hydrolysis of poly(*L*-lactide) (PLLA), poly(*D*,*L*-lactide) (PDLLA) and poly(ε-caprolactone) (PCL) in a range of degradation

media. PHB was discovered to be less stable under enzymatic degradation conditions, exhibiting complete dye release and particle collapse after 12 weeks.

The synthesis and characterisation of novel microparticles prepared from homopolymer blends of PLLA and poly(malic acid) (PMA) was reported. The miscibility of the polymer blends was discovered to highly influence the resultant microparticle morphology. Visible phase separation between PLLA and poly(nitrobenzyl malic acid) (PNO_2BnMA) resulted in the formation of janus-type raspberry microparticles. Conversely, addition of 3-bromo-4-(butylamino)-2,5-dihydro-1H-pyrrole-2,5-dione (ABM) aided polymer miscibility and enabled the formation of spherical microparticles as observed *via* SEM analysis. The successful triggered degradation and release of ABM from PLLA/PNO_2BnMA particles was demonstrated, with near complete release observed after exposure of the particles to UV-light for 1 h.

The versatility of the optimised solvent evaporation technique was further demonstrated *via* the synthesis of novel particles using a random copolymer of poly(2-methylene-1,3-dioxepane-*co*-vinyl acetate) (P(MDO-*co*-VAc)) prepared by free radical-ring opening polymerisation (rROP). The P(MDO-*co*-VAc) particles were shown to display a smooth particle morphology and were able to successfully encapsulate ABM. However, the low glass transition temperature (T_g) of 2-methylene-1, 3-dioxepane (MDO) decreased the stability of the particles and as such, the particles collapsed upon drying.

The optimised particle synthesis was also applied to the ring-opened macrolactone poly(ω-pentadecalactone) (PPDL), however, only low yields and low dye loading were achieved. Therefore, this approach was deemed unsuitable for the preparation of

PPDL microparticles. Copolymers of PPDL and PCL were prepared by one-pot ROP using $Mg(BHT)_2(THF)_2$ and thin films successfully synthesised *via* spin-coating the copolymers onto glass slides. The P(PDL-*co*-PCL) films could be readily characterised *via* interferometry and size exclusion chromatography (SEC). However, as a consequence of the high hydrophobicity of the polymers, the films detached from the glass slides after one week in the respective degradation media. A preliminary investigation into the potential for Polymerisation-induced self-assembly (PISA) of PPDL and poly(ε-decalactone) (PDL) was investigated, with the promising formation of cylindrical micelles observed *via* transmission electron microscopy (TEM) *via* self-assembly in ethyl benzene.

8.2 Future Work

Having established and optimised techniques for particle synthesis, encapsulation of ABM and degradation and release procedures, there are many future opportunities attainable based on the work detailed in this thesis. For instance, continuation of the microparticle degradation and release studies detailed in Chapter 3 and 4 would enable the production of a degradation library with full, comparable information regarding particle stability and effect of polymer type, molecular weight and crystallinity on the particle degradation and release profiles. Furthermore, the observed triggered degradation and release attained by incorporation of the UV sensitive PNO_2BnMA within a PLLA particle implies the great potential for tuneable degradation and release controlled by varying the ratio of PLLA and PNO_2BnMA within the particle matrix. Additionally, the easy functionalisation achievable with malic acid opens a wide range of possibilities for the incorporation of numerous responsive units within the microparticles to target a broad range of properties and applications (*e.g.*, pH responsive or enzymatic responsive for triggered release as the particle lands on the

soil). With a similar aim, it would also be interesting to study the change in particle degradation and release rate observed with varying the MDO and VAc copolymer composition. Furthermore, the ease of functionality previously reported with vinyl polymers has the potential to provide an alternative pathway for the incorporation of functionality into the microparticles and for the synthesis of stimulus-responsive particles.

Although the PPDL microparticles could only be attained in low yields, incorporation of a second polymer or copolymerisation of PDL with PLA, PHB or a responsive polymer could potentially act to increase the solubility of PPDL in the organic solvent. Therefore, this could also act to increase the stability of the resultant microparticles enabling their use for the controlled release of an AI under environmental conditions. The versatile film synthesis and characterisation technique developed in Chapter 7 could easily be adapted to prevent film detachment during degradation *via* spin coating the films onto a different substrate (*e.g.*, silanised glass or silicon). Further development of the procedure could be investigated for the encapsulation of an AI, thus enabling investigation into the degradation and release profile observed with PPDL films.

9. Experimental

9.1 Materials

L-Lactide (*L*LA) (Purac) and *D*,*L*-lactide (*D*,*L*LA) (Purac) were recrystallized once from dichloromethane and twice from toluene before standing over 3 Å molecular sieves for 3 days followed by a final toluene recrystallisation. Benzyl alcohol (BnOH) (Sigma-Aldrich), ε-decalactone (εDL) (Sigma-Aldrich), ε-caprolactone (εCL) (Acros), β-butyrolactone (βBL) (Sigma-Aldrich) and 1,8-diazabicyclo[5.4.0]undec-7-ene (DBU) (Sigma-Aldrich) were distilled twice from calcium hydride (CaH_2) (Sigma-Aldrich) prior to use. Diphenylphosphate (DPP) (Apollo Scientific Ltd.) was dried over phosphorous pentoxide in a vacuum desiccator for 4 days prior to use. ω-Pentadecalactone (PDL) (Sigma-Aldrich) was dissolved in toluene (75 wt%) and dried overnight on 3 Å molecular sieves. Vinyl acetate (VAc) (Sigma-Aldrich) was de-inhibited before use by passing through a basic alumina plug. 2,2-Azobis(2-methyl propionitrile) (AIBN) (Sigma-Aldrich) was re-crystallized from methanol prior to use. Magnesium 2,6-di-tert-butyl-4-methylphenoxide ($Mg(BHT)_2(THF)_2$) was synthesised according to the method by Ittel *et al.*[1] 3-Bromo-4-(butylamino)-2,5-dihydro-1H-pyrrole-2,5-dione (ABM) was synthesised using the previously reported method by Mabire *et al.*[2] 2-Methylene-1,3-dioxepane (MDO) was synthesized using the previously described method by Bailey *et al.*[3] Mowiol 4-88 (M_w = 31,000 g/mol, Sigma-Aldrich), nile red (99%, Acros) and Cleanzyme (JANI SOURCE) were used as received. Deuterated-chloroform (Apollo Scientific Ltd.) and deuterated-benzene (Apollo Scientific Ltd.) were dried over 3 Å molecular sieves and distilled under vacuum before use. All other solvents and reagents were purchased from either Sigma-Aldrich or Fisher Scientific and used as received.

9.2 Instrumental Methods

Proton (^{1}H) nuclear magnetic resonance (NMR) spectra were obtained on a Bruker DPX 300 and 400 spectrometer (300 MHz and 400 MHz) at 293 K. Carbon (^{13}C) NMR spectra were recorded using a Brucker DPX 400 spectrometer and Bruker DRX 500 spectrometer (400 MHz and 500 MHz) at 293 K or Bruker AV-II-700 spectrometer. Phosphorous (^{31}P) NMR spectra were obtained on a Bruker DPX spectrometer. All chemical shifts were reported as δ in parts per million (ppm) and referenced to the residual solvent signal ($CDCl_3$; δ = 7.26 ppm and 77.16 ppm for ^{1}H and ^{13}C NMR spectra respectively). Size exclusion chromatography (SEC) was used to determine the dispersities ($Đ_M$) and molecular weights of synthesised polymers. SEC was conducted in chloroform ($CHCl_3$) using a Varian PL-GPC 50 system equipped with 2 x PLgel 5 μm MIXED-D columns in series, a UV detector and a differential refractive index (RI) detector at a flow rate 1.0 mL min^{-1}. The system was calibrated against a Varian Polymer Laboratories Easi-Vial poly(styrene) (PS) standard and analysed by the software package Cirrus v3.3. Particle size distributions and mean diameters were determined using a Malvern Mastersizer at 293 K (Mastersizer S, Malvern Instruments Limited, U.K.). Particle size analysis of microspheres was performed using an optical microscope and a confocal microscope with a MPLAPONLEXT50 lens. Images were captured and processed by Image Pro Plus software. Scanning Electron Microscopy samples were air-dried onto an aluminium stub fitted with a carbon tab before being gold coated using a Quorum sputter coater. Particle morphology was determined using a Zeiss SUPRA 55VP FEGSEM fitted with EDX X-ray analysis system and an EBSD camera or a Zeiss GeminiSEM 500 fitted with SDD-EDX and STEM detectors. Transmission electron microscopy (TEM) samples were prepared on graphene-oxide (GO) TEM grid and imaged without staining or carbon lacey film with 300 mesh

copper grid with uranyl acetate staining. TEM analysis was performed using a JEOL 2000 FX electron microscope operating at 200 kV accelerating voltage. Fluorescence wavelength scans were recorded using an Agilent Cary Eclipse Fluorescence spectrophotometer. Release studies were performed using the FLUOstar OPTIMA plate reader with 96 F-bottom Greiner black well plates at excitation 390 nm and emission 520 nm unless otherwise stated. DLS analyses were carried out using a Malvern Zetasizer Nano ZS instrument operating at 25 °C with a Mw He-Ne 633 nm laser module. Measurements were made at an angle of 173° (back scattering) and results were analysed using Malvern DTS 6.32 software. Film height and profilometry data was obtained using a Bruker Contour GT-X Optical Profiler and subsequently analysed using the software package Vision 64. Vertical Scanning Interferometry (VSI) was employed utilising either green or white light, a $5x$ objective lens, a $1x$ multiplier, $3x$ scanning speed and a 1% threshold value, the resultant data was reconstructed and visualized in the Gwyddion 2.47 software. Differential scanning calorimetry (DSC) was obtained using a Mettler Toledo DSC1 star system. Heating and cooling cycles were run in triplicate in series under a nitrogen atmosphere in a 40 μL aluminium crucible.

9.3 Experimental Procedures

9.3.1 General Experimental Procedures for Chapter 2

9.3.1.1 General Ring-Opening Polymerisation Procedure for Lactide

Using a modified version of the previously reported procedure, in a typical lactide ring-opening polymerisation, *L*-lactide (1 g, 6.938 mmol, 25 equiv) was dissolved in dichloromethane (10 mL, 0.7 M) before adding benzyl alcohol (28.7 μL, 0.278 mmol, 1 equiv.), followed by DBU (10.4 μL, 6.938 x 10^{-5} mol, 1 mol%).[4] The polymerisation reaction mixture was then stirred for the appropriate reaction time. An aliquot of the

crude polymerisation reaction was characterised by ^{1}H NMR spectroscopy to determine the monomer conversion (98%). The polymer was purified *via* precipitating the crude polymer twice into pet ether and once into methanol. The final polymer was then characterised by ^{1}H NMR (300 MHz; $CDCl_3$): δ 7.33 ppm (m, 5H, $C_6H_5CH_2$), 5.18 (q, 1H, OCOC*H*(CH_3)OCO), 1.56 (d, 3H, OCOCH(C*H*$_3$)OCO, $^{3}J_{H\text{-}H}$ = 2.9 Hz) and SEC ($CHCl_3$): M_n = 4,900 g/mol, $Đ_M$ = 1.17.

Poly(*D*,*L*-Lactide):

Monomer conversion by ^{1}H NMR spectroscopy = 94%, ^{1}H NMR (300 MHz; $CDCl_3$): δ 7.38-7.29 (m, 5H, $C_6H_5CH_2$), 5.25-5.11 (m, 1H, OCOC*H*(CH_3)OCO), 1.60-1.51 (m, 3H, OCOCH(C*H*$_3$)OCO) and SEC ($CHCl_3$) M_n = 3,800 g/mol, $Đ_M$ = 1.17.

9.3.1.2 General Procedure for Ring Opening Polymerisation of ε-Caprolactone

Synthesised in-line with the previously reported procedure, ε-caprolactone (1 g, 8.320 mmol, 25 equiv.) was dissolved in toluene (10 mL, 1 M) before adding BnOH (34.5 μL, 0.333 mmol, 1 equiv.), followed by DPP (83.3 mg, 0.333 mmol, 1 equiv.).[5] The polymerisation was stirred for the appropriate reaction time. Before quenching the polymerisation, a portion of the polymerisation mixture was separated and used to determine the conversion based on the ^{1}H NMR measurement (97%). The polymerisation was quenched through the addition of Amberlyst 21, before precipitating the crude polymer three times into hexane. The final polymer was then characterised by ^{1}H NMR (300 MHz; $CDCl_3$): δ 7.37-7.29 (m, 5H, $C_6H_5CH_2$), 5.11 (s, 2H, $C_6H_5CH_2$), 4.05 (t, 2H, $OCOCH_2CH_2CH_2CH_2CH_2CO$, $^{3}J_{H\text{-}H}$ = 7.9 Hz), 3.64 (t, 2H, C*H*$_2$OH, $^{3}J_{H\text{-}H}$ =7.7 Hz), 2.30 (t, 2H, OCOC*H*$_2$$CH_2CH_2CH_2CH_2CO$, $^{3}J_{H\text{-}H}$ = 9 Hz), 1.73-1.28(m, 4H, $OCOCH_2CH_2CH_2CH_2CH_2CO$), 2H, $OCOCH_2CH_2CH_2CH_2CH_2CO$) and SEC ($CHCl_3$): M_n = 4,700 g/mol, $Đ_M$ = 1.06.

9.3.1.3 General Procedure for Ring Opening Polymerisation of β-Butyrolactone

BnOH (3.8 μL, 3.485 x 10^{-5} mol, 1 equiv.) and $Mg(BHT)_2(THF)_2$ (21.2 mg, 3.485 x 10^{-5} mol, 1 equiv.) were added to an ampoule containing β-butyrolactone (284 μL, 3.485 mmol, 100 equiv.) in toluene (1.742 mL, 2 M) and left to stir at 80 ˚C overnight. A crude sample was taken for determination of the monomer conversion by ^{1}H NMR spectroscopy (40%) before quenching the polymerisation with acidified methanol. The polymer was precipitated three times into hexane before drying *in vacuo*. ^{1}H NMR (300 MHz; $CDCl_3$): δ 7.35 (m, 5H, end group, $C_6H_5CH_2$), 5.25 (m, 1H, backbone, $CH(CH_3)O$), 5.12 (s, 2H, chain end, $C_6H_5CH_2$), 2.57-2.43 (m, 2H, backbone, $COCH_2$), 1.29 (m, 3H, backbone, CH_3), SEC ($CHCl_3$): M_n = 4,800 g/mol, $Đ_M$ = 1.15.

9.3.1.4 General Procedure for Microparticle Synthesis

A typical procedure for the synthesis of microparticles is as follows: The organic phase (2 g, 10 wt%) was prepared by dissolving PCL 25 (0.25 g, 2.190 mmol, 12.5 wt%) in dichloromethane (1.75 g, 0.0206 mol, 87.5 wt%). This was added to the aqueous phase (18 g, 90 wt%) which consisted of mowiol 4-88 (2.67 g, (15 wt % aqueous solution), 1.212 x 10^{-5} mol, 2 wt%) in water (15.33 g, 0.852 mol). The two solutions were emulsified using a Silverson high shear mixer at 7000 rpm for 30 s. The solution was then transferred to a larger beaker and left with low shear overhead stirring to harden overnight. The particles were characterised *via* light scattering and optical microscopy (Table 9.1).

Table 9.1: Particle size of different polymeric emulsions determined by the volume weighted mean recorded *via* light scattering

Polymer DP[a]	Polymer Particle Size (μm)[b]		
	PLLA	PDLLA	PCL
25	12	10	10
75	15	14	14
100	15	15	16
250	19	17	19

[a]Determined by ^{1}H NMR spectroscopy, [b]Determined by volume weighted mean from light scattering analysis

9.3.1.5 General Procedure for Encapsulation of a Fluorescent Dye

Rhodamine B (0.0125 g, 2.609 x 10^{-5}, 5 wt%) was dissolved in the organic phase (2 g, 10 wt%) with PLLA (0.238 g, 1.653 mmol) and emulsified with the aqueous phase (18 g, 90 wt%) as detailed in section 9.3.14. An aliquot of the microparticle solution was taken (500 μL, 6.944 x 10^{-4} g/mL) and compared by UV/Vis spectroscopy to a solution of Rhodamine B in water (6.944 x 10^{-4} g/mL). The absorption maxima of the rhodamine B microparticle containing solution was taken away from the absorption maxima at λ_{max} = 554 nm of the Rhodamine B solution to determine the amount of fluorescent dye encapsulated (89.5%). The particles were washed three times with deionised water before freeze-drying the sample followed by dissolving the powder in dichloromethane to determine the encapsulated content within the microparticles.

9.3.2 General Experimental Procedures for Chapter 3

9.3.2.1 Typical Procedure for Microparticle Swelling Study

Polymer and particles were prepared using the method described above. The dried particles (0.125 g) were dispersed in either deionised (DI) water (10 mL) or a 50:50 water: ethanol (10 mL) solution. Samples were taken at regular time intervals and the change in particle size and morphology monitored *via* light scattering and optical microscopy.

9.3.2.2 General Procedure for Microparticle Degradation and Release Studies

The polymer and particles were synthesised according to the previously described procedures. The dried particles were suspended in the desired degradation medium (8.289 mg/mL) before being stored with rotation on a Stuart rotator at room temperature (RT) in the dark. After predetermined times, samples (300 µL) were collected and washed three times with deionised water before freeze-drying for particle characterisation *via* SEM, SEC ($CHCl_3$) and fluorescence monitoring of the dye loading (*E*). Further aliquots (200 µL) of the particle degradation medium were added to a solution of 50:50 EtOH: H_2O (1.8 mL). The change in fluorescence intensity was monitored over 5 h, regular samples of the release medium, were collected, filtered through a 0.22 µm polyethersulphone filter and the resultant fluorescence intensity measured on the plate reader at excitation 390 nm and emission 520 nm (unless otherwise stated). The fluorescence intensity was compared to six known concentrations of ABM to determine the percentage ABM released from the particles.

9.3.3 Experimental Procedures for Chapter 5

9.3.3.1 General procedure for functionalisation of malic acid

Malic acid was functionalised using a modified version of the previously reported procedure by Miller *et al*.[6] In general, for the synthesis of methyl malic acid, malic acid (5 g, 37.3 mmol) was cooled over ice, before slowly adding trifluoroacetic anhydride (12.5 mL, 88.6 mmol). After stirring for 3 h at 0 °C, volatiles were removed under reduced pressure before adding an excess of methanol (50 mL, excess). The reaction was left to proceed for a further 12 h at RT before removing excess methanol *in vacuo*. The reaction mixture was diluted with EtOAc (300 ml) and extracted with Na2CO3 (10 %, 3 x 200 ml). The aqueous phase was acidified to pH 7 using 1 M HCl

and excess EtOH was extracted using EtOAc (4 x 100 ml) before recollecting the aqueous phase, acidifying further to pH 2/3 and extracting the pure monoester with more EtOAc (5 x 200 ml). The solution was dried using MgSO4 before having solvent removed via rotary evaporation to leave a white solid. Yield: g, 32%, ^{1}H NMR (300 MHz; $CDCl_3$): δ 4.52 (t, 1H, $CO_2HCH(CH_2CO_2CH_3)OH$, $^{3}J_{H\text{-}H}$ = 5.4 Hz), 3.84 (s, 3H, $CH_2CO_2CH_3$), 2.98-2.76 (m, 2H, $CH_2CO_2CH_3$), ^{13}C NMR (400 MHz; $CDCl_3$): δ 173.01, 76.32, 56.79, 51.82, 39.70.

Ethyl malic acid:

Yield: 18.9 g, 54%, ^{1}H NMR (300 MHz; $(CD_3)_2CO$): δ 4.49 (t, 1H, $CO_2HCH(CH_2CO_2CH_2CH_3)OH$, $^{3}J_{H\text{-}H}$ = 6 Hz), 4.21-4.13 (m, 2H, $CH_2CO_2CH_2CH_3$), 2.82-2.64 (m, 2H, $CH_2CO_2CH_2CH_3$), 1.24 (t, 3H, $CH_2CO_2CH_2CH_3$, $^{3}J_{H\text{-}H}$ = 7.1 Hz), ^{13}C NMR (400 MHz; $(CD_3)_2CO$): δ 205.47, 172.85, 171.05, 67.50, 60.68, 38.54, 13.52.

Nitrobenzyl malic acid:

Yield: 5.05 g, 50%, ^{1}H NMR (300 MHz; $(CD_3)_2CO$): δ 8.15-8.13 (m, 1H, aromatic, $C_4H_3CHCNO_2CCH_2O$), 7.81-7.76 (m, 1H, aromatic, $C_4H_3CHCNO_2CCH_2O$), 7.61-7.66 (m, 1H, aromatic, $C_4H_3CHCNO_2CCH_2O$), 5.58 (m 2H, $C_6H_4NO_2CH_2O$), 4.68-4.65 (dd, 1H, $CO_2HCH(CH_2)OH$, $^{3}J_{H\text{-}H}$ = 4.8 Hz), 2.91-2.74 (m, 2H, $CO_2HCH(OH)CH_2$), ^{13}C NMR (400 MHz; $(CD_3)_2CO$): δ 205.35, 172.48, 170.98, 147.34, 133.91, 129.25, 124.77, 67.60, 63.06, 38.43.

9.3.3.2 Typical step growth polymerisation of functionalised malic acid

For a general step growth polymerisation of functionalised malic acid for example for the synthesis of poly(methyl malic acid); methyl malic acid (2 g, 15.1 mmol) was heated and stirred at 110 °C for three days under nitrogen. An aliquot of the

polymerisation was analysed *via* ^{1}H NMR spectroscopy to determine the monomer conversion (47%). ^{1}H NMR (300 MHz; $CDCl_3$): δ 7.00–6.73 (m, 1H, C*H*, fumaric acid), 5.66-5.45 (m, 1H, $CO_2HCH(CH_2CO_2CH_3)OH$), 3.80 (s, 3H, $CH_2CO_2CH_3$), 3.09-2.82 (m, 2H, $CH_2CO_2CH_3$), SEC (DMF): M_n 1,300 g/mol, $Đ_M$ 1.40.

Poly(Ethyl Malic Acid):

^{1}H NMR (400 MHz, $(CD_3)_2CO$) δ 7.00–6.73 (m, 1H, C*H*, fumaric acid), 5.80–5.32 (m, 1H, $OCOCH(CH_2CO_2CH_2CH_3)O$), 4.28–4.15 (m, 2H, $OCOCH_2CH_3$), 3.37–2.58 (m, 2H, $CH_2OCOCH2CH3$), 1.27 (t, 3H, $OCOCH_2CH_3$, $^{3}J_{H\text{-}H}$ = 7.3 Hz), SEC (DMF): M_n 1,600 g/mol, $Đ_M$ 1.16.

Poly(Nitrobenzyl Malic Acid):

^{1}H NMR (300 MHz; $CDCl_3$): δ 8.17–8.07 (m, 1H, aromatic, $C_4H_3CHCNO_2CCH_2O$), 7.75–7.36 (m, 3H, aromatic, $C_4H_3CHCNO_2CCH_2O$), 7.03–6.77 (m, 1H, $OCOCHCHOCO$, 1H, $OCOCHCHOCO$), 5.85–5.41 (m, 1H, $CO_2HCH(CH_2OCOBnNO_2)O$, 2H, $OCOCH_2C_6H_4NO_2$), 4.65 (s, 1H, $CO_2HCH(CH_2OCOBnNO_2)O$, chain end), 3.35–2.79 (m, 2H, $CHCH_2OCOBnNO_2$), SEC ($CHCl_3$): M_n 4,700 g/mol, $Đ_M$ 1.06.

9.3.3.3 Typical DIC coupling of nitrobenzyl malic acid

Nitrobenzyl malic acid (162 mg, 1 mmol) was dissolved in $CHCl_3$ (1 mL) before adding DPTS (64.7 mg, 0.2 mmol) with stirring. The reaction was cooled in an acetone/ dry ice bath before adding DIC (189.3 mg, 1.5 mmol) dropwise over 1 min. The reaction was left with stirring at RT for 5 h before precipitating the polymer into cold hexane/methanol (10:1, v/v). The polymeric solution was passed through a silica plug before removing the solvent *in vacuo*. ^{1}H NMR (300 MHz; $(CD_3)_2CO$): δ 8.24–8.10 (m, 1H, aromatic, $C_4H_3CHCNO_2CCH_2O$), 7.88–7.51 (m, 3H, aromatic,

$C_4H_3CHCNO_2CCH_2O$), 7.03–6.77 (m, 1H, OCOC*H*CHOCO, 1H, OCOCHC*H*OCO), 5.83–5.42 (m, 1H, $CO_2HCH(CH_2OCOBnNO_2)O$, 2H, $OCOCH_2C_6H_4NO_2$), 4.40 (s, 1H, $CO_2HCH(CH_2OCOBnNO_2)O$, chain end), 3.32–3.01 (m, 2H, $CHCH_2OCOBnNO_2$), SEC ($CHCl_3$): M_n = 1,900 g/mol, $Đ_M$ 1.40.

9.3.3.4 General procedure for microparticle synthesis using homopolymer blends

Similar to the particle procedure detailed in Section 9.3.1.4, the organic phase (2 g, 10 wt%) was prepared by dissolving PLLA 100, the malic acid based polymer with or without ABM in dichloromethane (1.75 g, 20.6 mmol, 87.5 wt%). This was added to the aqueous phase which consisted of mowiol 4-88 (2.67 g, (15wt % aqueous solution), 1.212 x 10^{-5} mol, 2 wt%) in water (15.33 g, 0.852 mol). The two solutions were emulsified using a Silverson high shear mixer at 7000 rpm for 30 s. The solution was then transferred to a larger beaker and left with low shear overhead stirring to harden overnight. The particles were characterised *via* light scattering and optical microscopy.

9.3.3.5 General procedure for UV-triggered microparticle degradation

Microparticles were prepared using the optimised single oil-in-water technique detailed in Section 9.3.1.5. The particles were washed three times with DI water and freeze-dried before being re-suspended in DI water (8.289 mg/mL). The particles were exposed to UV light (365 nm) for 1 h, with aliquots sampled every 10 min. Particle characterisation was determined *via* SEM, SEC ($CHCl_3$), mass loss, release on a plate reader (excitation: 390 nm, emission: 520 nm) and change in *E* on a fluorometer (excitation: 360 nm, emission: 365-700 nm).

9.3.4 Experimental Procedures for Chapter 6

9.3.4.1 Typical procedure for the radical-ring-opening polymerisation of vinyl acetate

VAc was polymerised according to the previously reported procedure by Albertsson *et al*.[7] In an inert environment, VAc (2 g, 0.0232 mol) and AIBN (0.19 g, 1.157 mmol, 5 mol%) were stirred for 2 h at 60 °C in an ampoule. The polymerisation was quenched by placing the ampoule into an ice bath. A sample of the polymerisation was characterised by ^{1}H NMR spectroscopy to determine the conversion (40%). The polymer was dissolved in chloroform and precipitated three times into cold hexane to remove excess monomer, before drying the white polymer *in vacuo* overnight. ^{1}H NMR (300 MHz; $CDCl_3$): δ 5.06-4.77 (m, 1H, $CH_2CH(CO_2CH_3)$), 2.01 (s, 3H, $CH_2CH(CO_2CH_3)$), 1.76 (m, 2H, $CH_2CH(CO_2CH_3)$), SEC ($CHCl_3$): M_n = 19,000 g/mol, $Đ_M$ = 5.2.

9.3.4.2 Typical procedure for the radical ring-opening copolymerisation of MDO and vinyl acetate

A 50:50 MDO:VAc was synthesised in line with the previously reported procedure by Albertsson *et al*.[7] In an inert environment, MDO (1.32 g, 0.0116 mol), VAc (1 g, 0.0116 mol) and AIBN (0.095 g, 5.785 x 10^{-4} mol, 5 mol%) were stirred for 4 h at 60 °C in an ampoule. The polymerisation was quenched by placing the ampoule into an ice bath. A sample of the polymerisation was characterised by ^{1}H NMR spectroscopy to determine the conversion (72%). The polymer was dissolved in chloroform and precipitated three times into cold hexane to remove excess monomer, before drying the white polymer *in vacuo* overnight. Characterised by ^{1}H NMR spectroscopy and SEC. ^{1}H NMR (300 MHz; $CDCl_3$): δ 5.20-4.85 (m, 1H, CH_2CHOCO), 4.06-4.02 (m, 4H, OCH_2CH_2), 3.62 (s, 3H, CH_3CCOCH), 2.60-2.58 (m, 2H, $CHCH_2COOCH_2CH_2$),

2.33-2.29 (m, 2H, $CH_2CH_2COOCH_2CH_2$), 2.09-1.97 (m, 3H, $CHOOCCH_3$), 1.95-1.45 (m, 2H, $CH_2CHOCOCH_2$), 1.45-1.10 (m, 2H, $CH_2CH_2CH_2CH_3$, 2H, $CH_2CH_2CH_2CH_3$, 2H, $CH_2COOCH_2CH_2CH_2$), 1.46-1.24 (m, 2H, $COOCH_2CH_2CH_2$, 2H, $COOCH_2CH_2CH_2$), 0.90 (t, 3H, $CH_2CH_2CH_2CH_3$), Copolymer composition by ^{1}H NMR spectroscopy: VAc = 40%, MDO = 60%, SEC ($CHCl_3$): M_n = 31,300 g/mol, $Đ_M$ = 8.98.

9.3.5 Experimental Procedures for Chapter 7

9.3.5.1 General ring-opening polymerisation procedure using $Mg(BHT)_2(THF)_2$

PDL and eDL were polymerised according to the reported procedure by Wilson *et al.*[8] For the polymerisation of PDL; BnOH (4.76 μL, $1.248x10^{-5}$ mol, 1 equiv.) and $Mg(BHT)_2(THF)_2$ (7.58 mg, $1.248x10^{-5}$ mol, 1 equiv.) were added to an ampoule containing PDL (0.3 g, 1.248 mmol, 100 equiv.) in toluene (1.248 mL, 1 M) and left to stir at 80 ˚C overnight. A crude sample was taken for determination of the monomer conversion by ^{1}H NMR spectroscopy (97%) before quenching the polymerisation with acidified methanol. The polymer was precipitated three times into methanol and dried *in vacuo*. ^{1}H NMR (300 MHz; $CDCl_3$): δ 7.35-7.34 (m, 5H, aromatic $C_6H_5CH_2$), 5.11 (s, 2H, $COOCH_2C_6H_5$), 4.05 (t, 2H, CH_2CH_2COO, $^3J_{H-H}$ = 6.8 Hz), 3.63 (t, 2H, CH_2CH_2OH, $^3J_{H-H}$ = 8.4 Hz), 2.30-2.26 (t, 2H, $OCOCH_2CH_2$, $^3J_{H-H}$ = 7.5 Hz), 1.65-1.25 (m, 24H, CH_2 backbone), SEC ($CHCl_3$): M_n = 24,500 g/mol, $Đ_M$ = 2.18.

ε-Decalactone:

^{1}H NMR (300 MHz; $CDCl_3$): δ 7.32-7.35 (m, 5H, aromatic $C_6H_5CH_2$), 5.10 (s, 2H, $COOCH_2C_6H_5$), 4.84-4.81 (m, 1H, $CH_2CH(C_4H_9)OCO$), 2.26 (t, 2H, $OCOCH_2CH_2$, $^3J_{H-H}$ = 7.5 Hz), 1.61-1.27 (m, 12H, CH_2, backbone), 0.88 (t, 3H, CH_3, backbone, $^3J_{H-H}$ = 4.2 Hz), SEC ($CHCl_3$): M_n = 19,500 g/mol, $Đ_M$ = 1.39.

9.3.5.2 Typical procedure for the copolymerisation of ω-pentadecalctone and a lactone

All copolymerisation's were performed using standard glovebox and Schlenk-line techniques using the previously reported procedure by Wilson *et al*.[9] In a typical procedure for copolymerisation of PDL and ε-CL, BnOH (8.6 μL, 8.294 x 10^{-5} mol, 1 equiv.), $Mg(BHT)_2(THF)_2$ (10 mg, 16.5 μmol, 1 equiv.), ε-CL (460 μL, 4.147 mmol, 50 equiv.) and PDL (1 g, 4.147 mmol, 50 equiv.) were added to a sealed ampoule, before heating at 80 °C for a defined time period. The reaction was quenched with the addition of acidified methanol (5 % HCl). The polymer was taken up in chloroform and precipitated three times into excess methanol until no further monomer residue was observed. ^{1}H NMR (300 MHz, $CDCl_3$, ppm): δ 7.37-7.35 (m, 5H, aromatic $C_6H_5CH_2$), 5.11 (s, 2H, $COOCH_2C_6H_5$), 4.06 (t, 2H, CH_2OCOCH_2 PCL, 2H, CH_2OCOCH_2 PPDL $^3J_{H\text{-}H}$ = 4.2 Hz), 2.31-2.28 (m, 2H, CH_2OCO), 1.67-1.25 (m, 2H, CH_2, backbone), ^{13}C NMR (700 MHz, $CDCl_3$): δ 174.14 (PDL*-PDL, $OCOCH_2$), 174.08 (PDL*-εCL, $OCOCH_2$), 173.74 (εCL*-PDL, $OCOCH_2$), 173.65 (εCL*-εCL, $OCOCH_2$), Total monomer conversion determined by ^{1}H NMR spectroscopy = 94%, SEC ($CHCl_3$): M_n = 14,700 g/mol, $Đ_M$ = 1.83.

ω-pentadecalctone and ε-decalactone:

^{1}H NMR (300 MHz, $CDCl_3$, ppm): δ 7.38-7.35 (m, 5H, aromatic $C_6H_5CH_2$), 5.12 (s, 2H, $COOCH_2C_6H_5$), 4.90-4.85 (m, 1H, $CH_2CH(C_4H_9)OCO$), 4.07 (t, 2H, CH_2CH_2OH, $^3J_{H\text{-}H}$ = 4.5 Hz), 2.29 (t, 2H, $OCOCH_2CH_2$, $^3J_{H\text{-}H}$ = 4.5 Hz), 1.64-1.24 (m, 2H, CH_2, backbone), 0.90 (t, 3H, CH_3, backbone, $^3J_{H\text{-}H}$ = 2.8 Hz), SEC ($CHCl_3$): M_n = 35,800 g/mol, $Đ_M$ = 1.67.

9.3.5.3 Typical procedure for film synthesis via solvent casting

As a general procedure for film synthesis *via* solvent casting, PPDL (0.2 g, 1.664 x 10^{-4} mol, 2 wt%) was dissolved in chloroform (2 mL). The subsequent solution was distributed evenly onto a glass slide and placed at the base of a PTFE cup before leaving overnight to dry. Film height was characterised *via* Interferometry = 4 μm.

9.3.5.4 Typical procedure for film synthesis via spin coating

As a general procedure for film synthesis *via* spin coating, PPDL (0.2 g, 1.664 x 10^{-4} mol, 2 wt%) was dissolved in chloroform (2 mL). Several drops of the polymeric solution were dropped onto a glass slide before spin coating for 1 min at 2000 rpm. The films were characterised *via* SEC ($CHCl_3$): M_n 24.500 g/mol, $Đ_M$ 2.18 and Interferometry = 200 nm.

9.3.5.5 General procedure for film degradation

In a typical film degradation, the glass slides containing the spin coated-films were immersed in a pre-prepared solution of DI water, Cleanzyme[10] or a basic buffer solution of sodium carbonate and sodium hydrogen carbonate (pH 10).

9.3.5.6 Typical polymerisation-induced self-assembly procedure for poly(ω-pentadecalactone-co-ε-decalactone)

In a polymerisation procedure, analogous to block copolymerisation detailed in Section *9.3.5.2*, the polymerisation solution was cooled to room temperature overnight before characterising the polymeric structures *via* TEM and DLS.

9.4 References

1. J. Calabrese, M. A. Cushing and S. D. Ittel, *Inorg. Chem.*, 1988, **27**, 867-870.
2. A. B. Mabire, M. P. Robin, W.-D. Quan, H. Willcock, V. G. Stavros and R. K. O'Reilly, *Chem. Commun.*, 2015, **51**, 9733-9736.
3. W. J. Bailey, Z. Ni and S.-R. Wu, *J. Polym. Sci. Polym. Chem. Ed.*, 1982, **20**, 3021-3030.
4. B. G. G. Lohmeijer, R. C. Pratt, F. Leibfarth, J. W. Logan, D. A. Long, A. P. Dove, F. Nederberg, J. Choi, C. Wade, R. M. Waymouth and J. L. Hedrick, *Macromolecules*, 2006, **39**, 8574-8583.
5. K. Makiguchi, T. Satoh and T. Kakuchi, *Macromolecules*, 2011, **44**, 1999-2005.
6. M. J. Miller, J. S. Bajwa, P. G. Mattingly and K. Peterson, *J. Org. Chem*, 1982, **47**, 4928-4933.
7. J. Undin, T. Illanes, A. Finne-Wistrand and A.-C. Albertsson, *Polym. Chem.*, 2012, **3**, 1260-1266.
8. J. A. Wilson, S. A. Hopkins, P. M. Wright and A. P. Dove, *Polym. Chem.*, 2014, **5**, 2691-2694.
9. J. A. Wilson, S. A. Hopkins, P. M. Wright and A. P. Dove, *Macromolecules*, 2015, **48**, 950-958.
10. Janisource, Cleanzyme Enzyme Digestant, https://janisource.com/cleanzyme-enzyme-cleaner-spotter-odor-remover-1-gallon/, (accessed 13-06-17, 2017).

10. Appendix

10.1 Complementary Data for Chapter 3

10.1.1 PLLA 100 Particle Degradation and Release in PBS

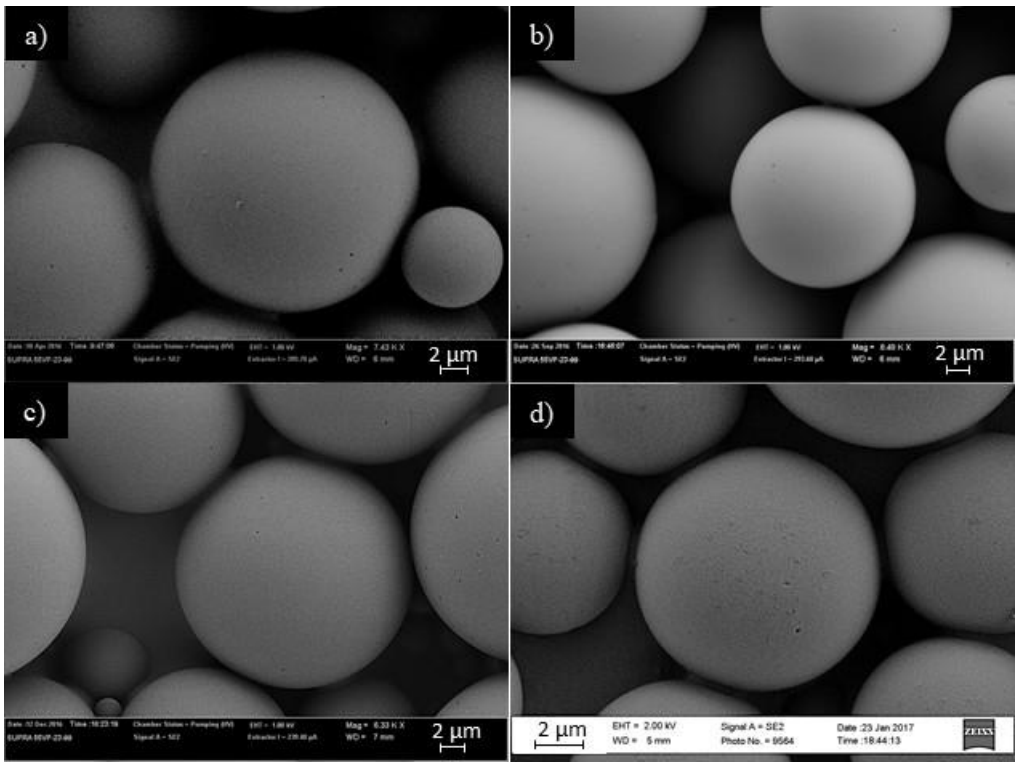

Figure 10.1: SEM characterisation of PLLA 100 particles after degradation in PBS for 12 months

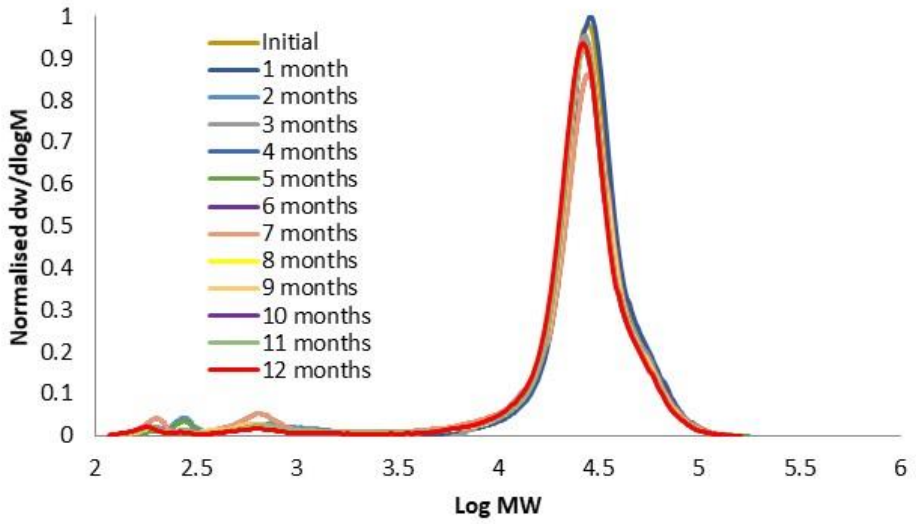

Figure 10.2: SEC characterisation of PLLA 100 particles after degradation in PBS for 12 months

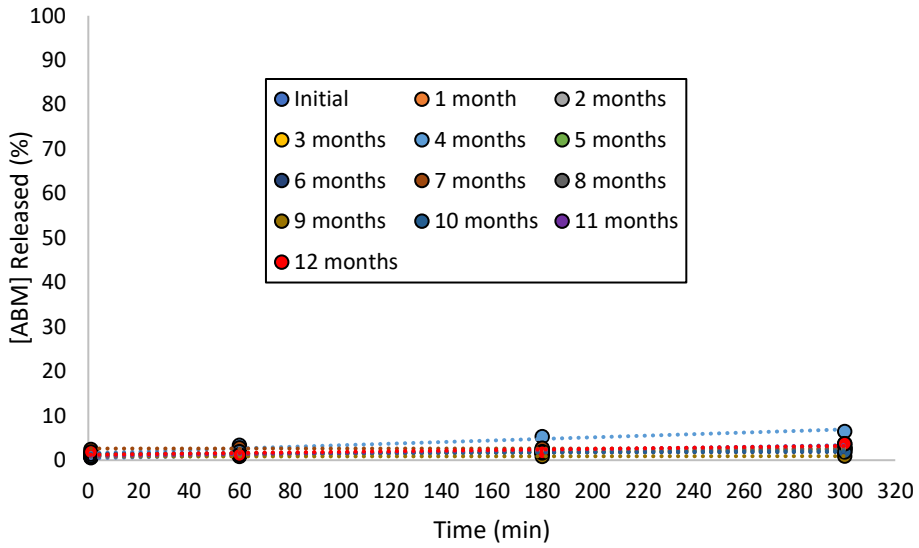

Figure 10.3: Observed [ABM] released from PLLA 100 particles after degradation in PBS for 12 months

10.1.2 Empty PLLA 100 Particle Degradation

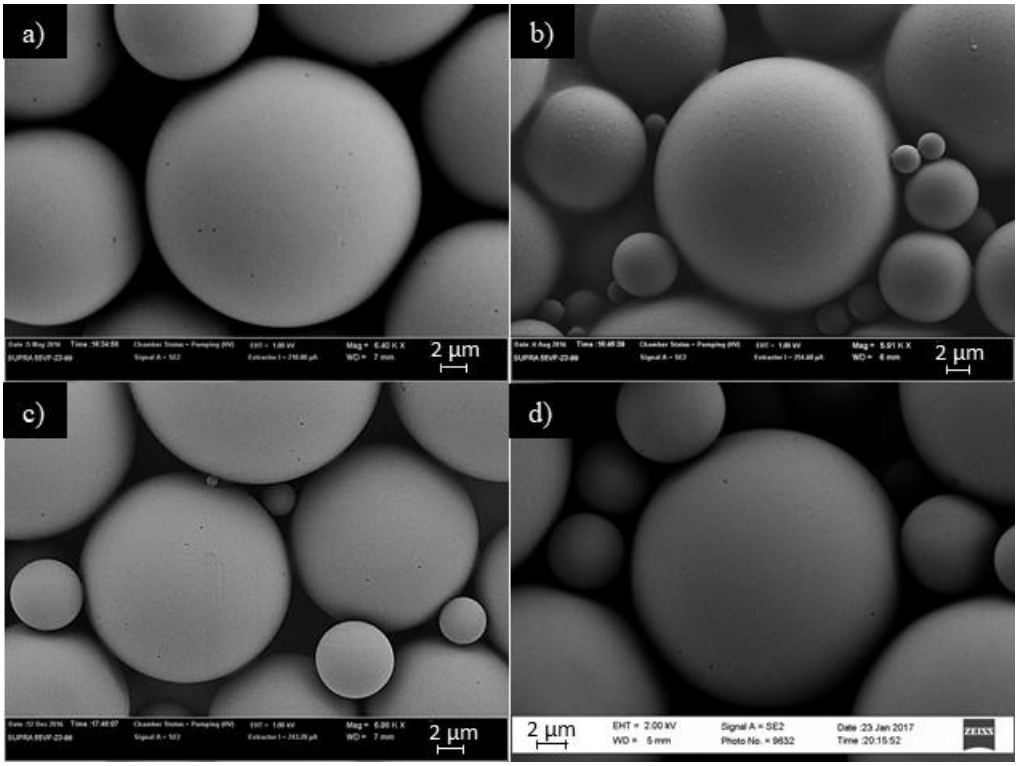

Figure 10.4: SEM characterisation of PLLA 100 particles without dye after degradation in water for a) 0 months, b) 3 months, c) 6 months and d) 8 months

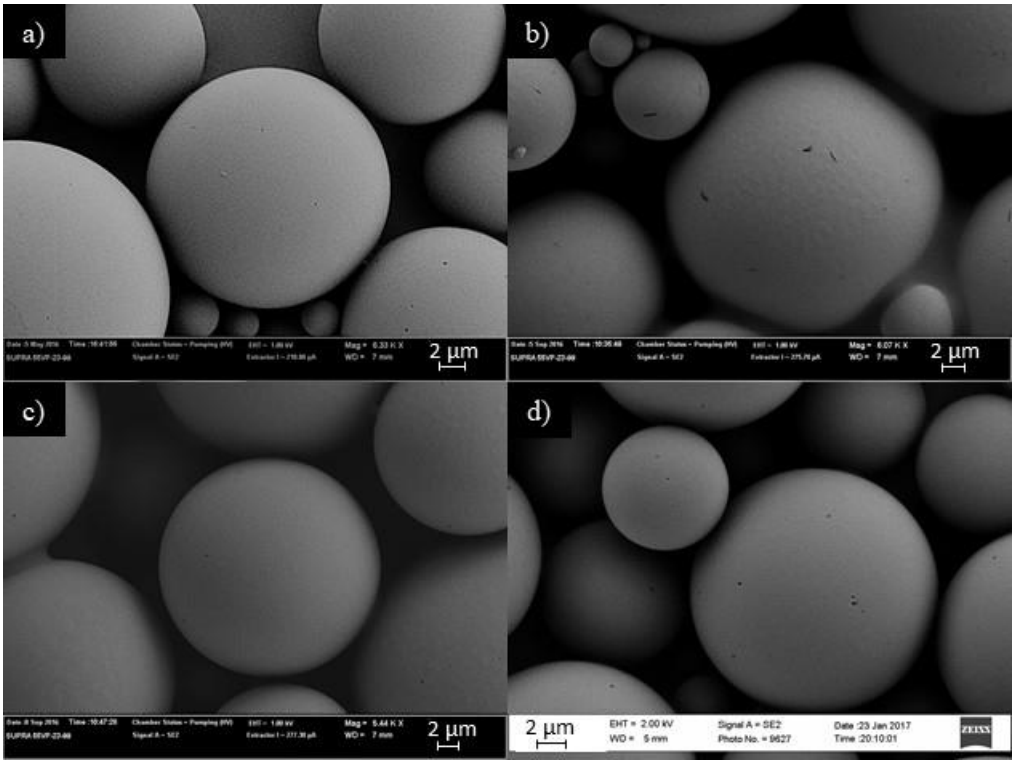

Figure 10.5: SEM characterisation of PLLA 100 particles without dye after degradation in Cleanzyme for a) 0 months, b) 3 months, c) 6 months and d) 8 months

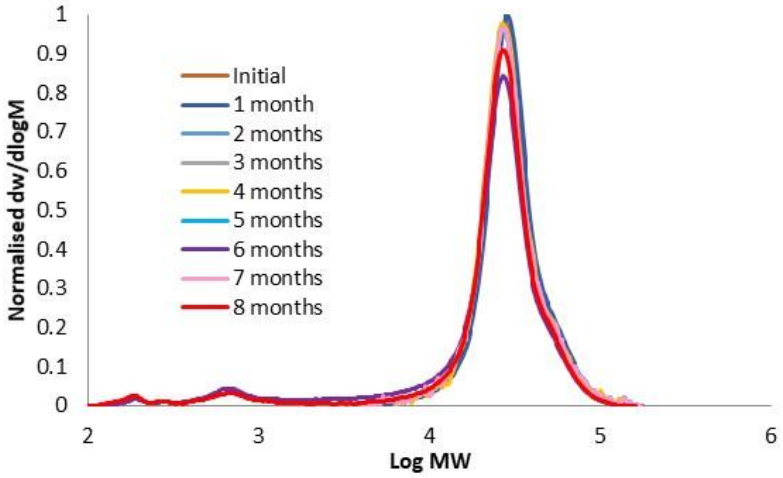

Figure 10.6: SEC characterisation of PLLA 100 particles without dye after degradation in water for 12 months

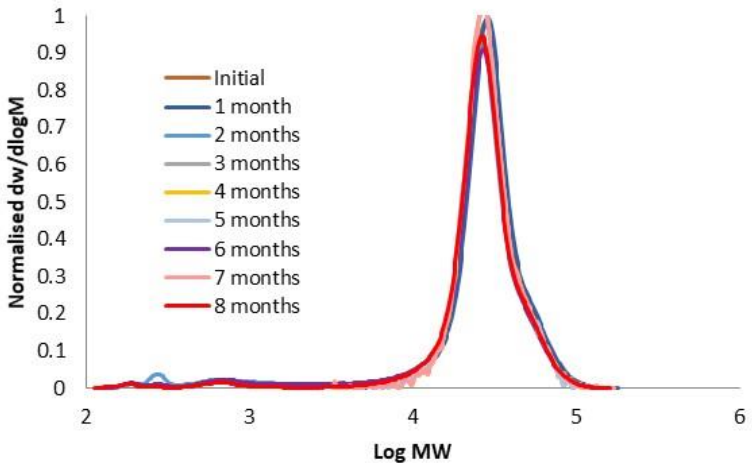

Figure 10.7: SEC characterisation of PLLA 100 particles without dye after degradation in Cleanzyme for 12 months

10.2 Complimentary Data for Chapter 4

10.2.1 PLLA 25 Particle Degradation and Release in Water

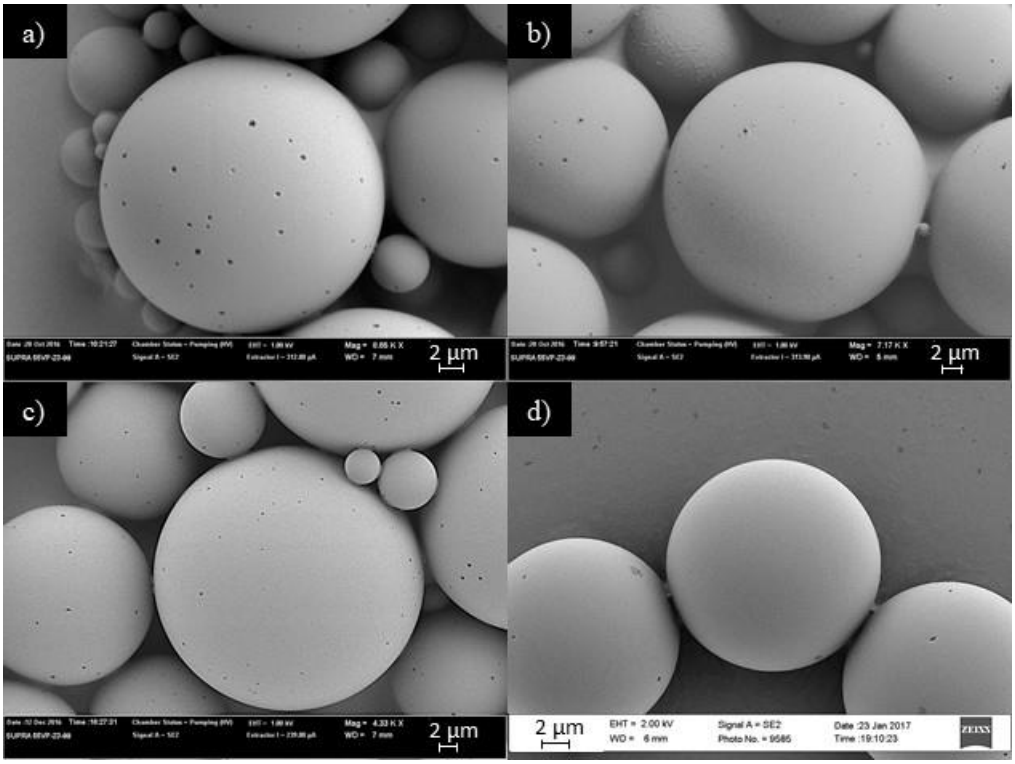

Figure 10.8: SEM characterisation of PLLA 25 particles after degradation in water for a) 0 months, b) 2 months, c) 4 months and d) 6 months

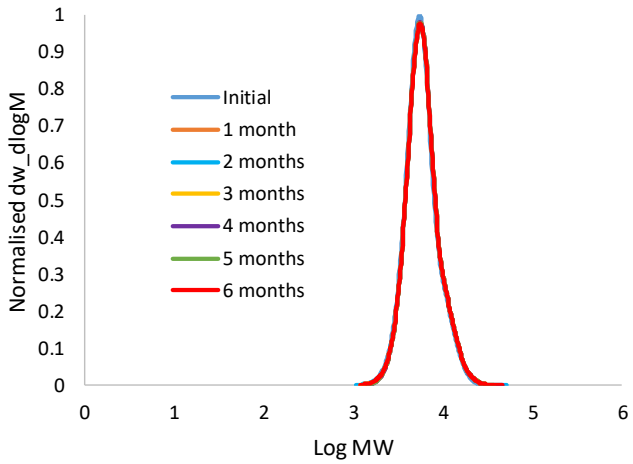

Figure 10.9: SEC characterisation of PLLA 25 particles after degradation in water for 6 months

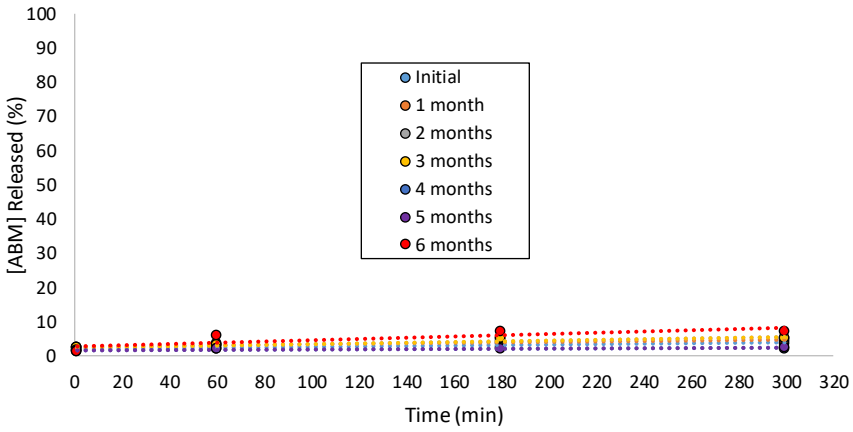

Figure 10.10: Characterisation of the change in [ABM] released into water/ethanol from PLLA 25 particles after degradation in water for 6 months

10.2.2 PLLA 250 Particle Degradation and Release in Water

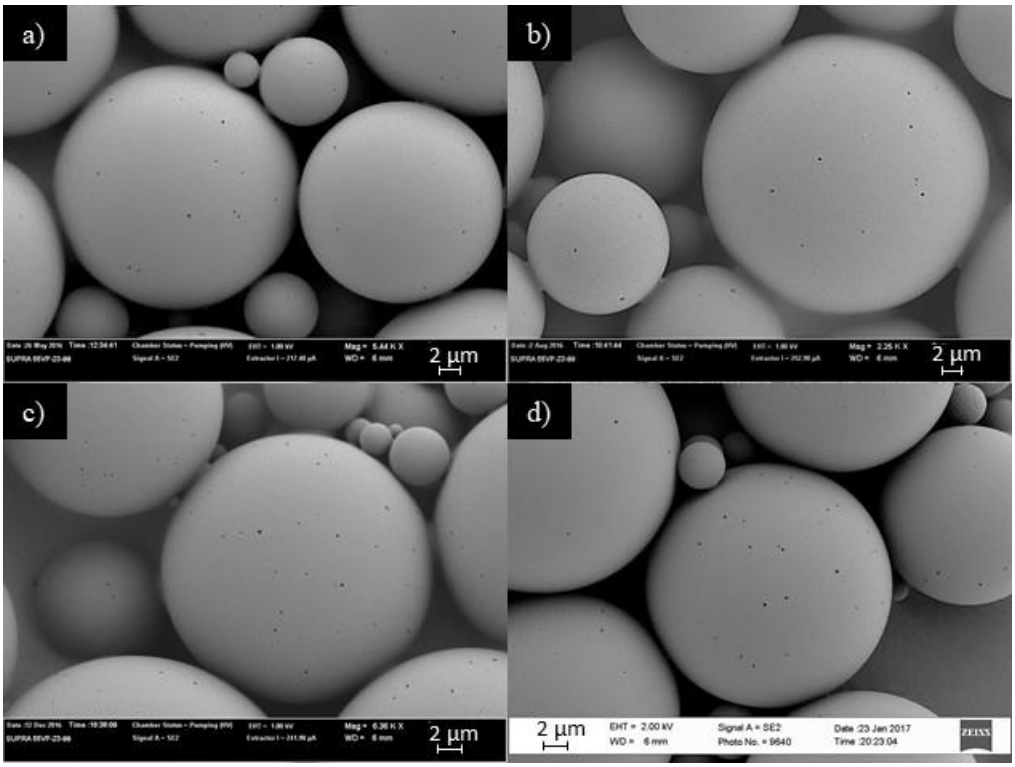

Figure 10.11: SEM characterisation of PLLA 250 particles after degradation in water for a) 0 months, b) 3 months, c) 6 months and d) 8 months

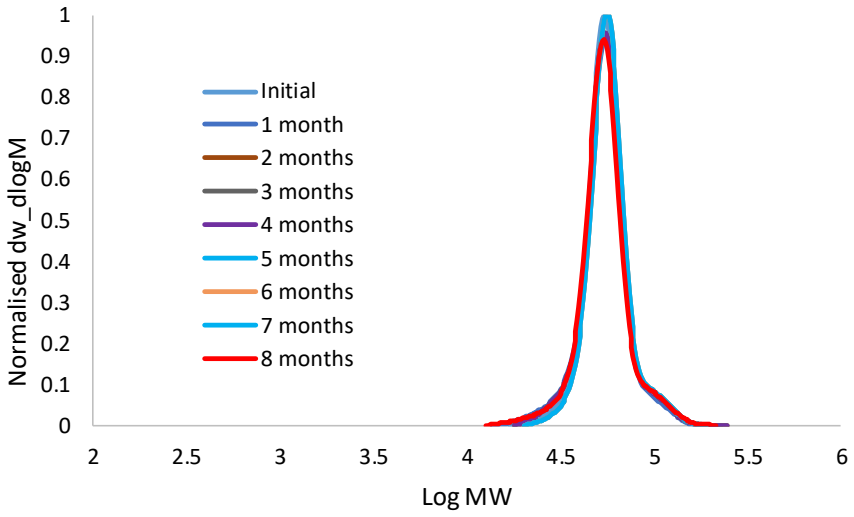

Figure 10.12: SEC characterisation of PLLA 250 particles after degradation in water for 8 months

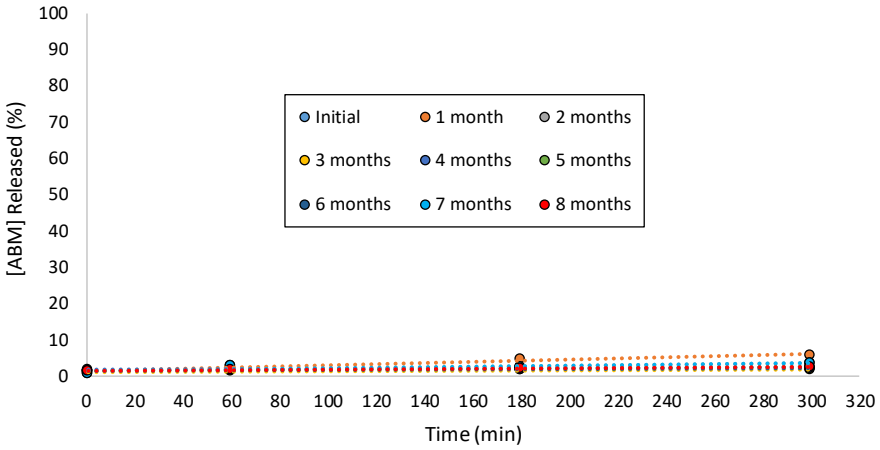

Figure 10.13: Characterisation of the change in [ABM] released into water/ethanol from PLLA 250 particles after degradation in water for 8 months

10.2.3 PDLLA 100 Particle Degradation and Release in Water

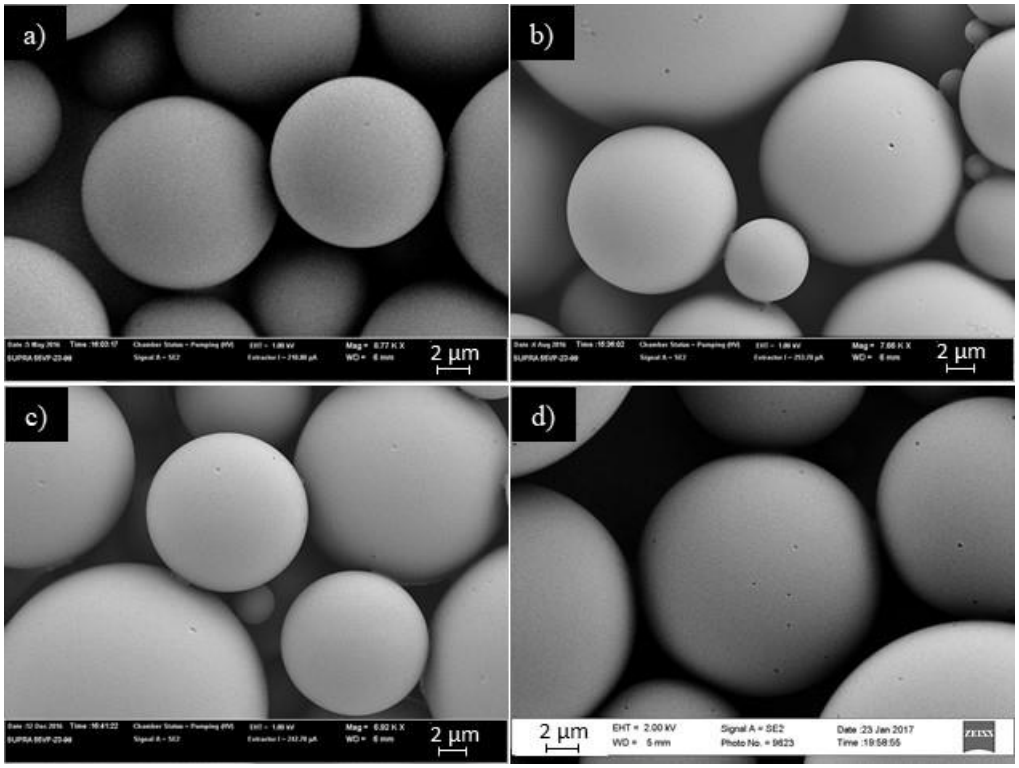

Figure 10.14: SEM characterisation of PDLLA 100 particles after degradation in water for a) 0 months, b) 3 months, c) 6 months and d) 8 months

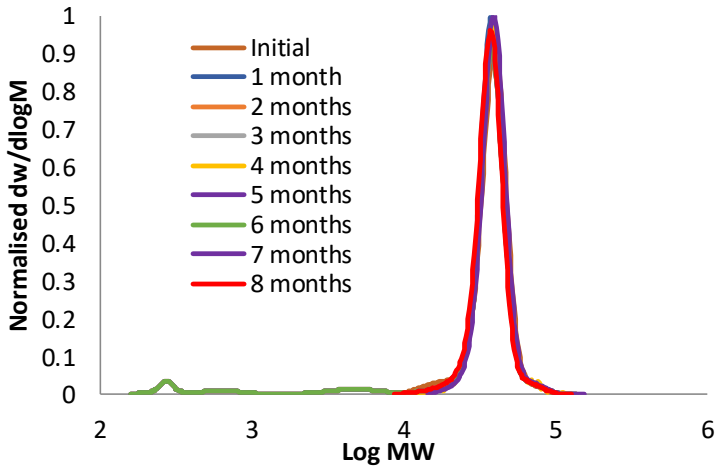

Figure 10.15: SEC characterisation of PDLLA 100 particles after degradation in water for 8 months

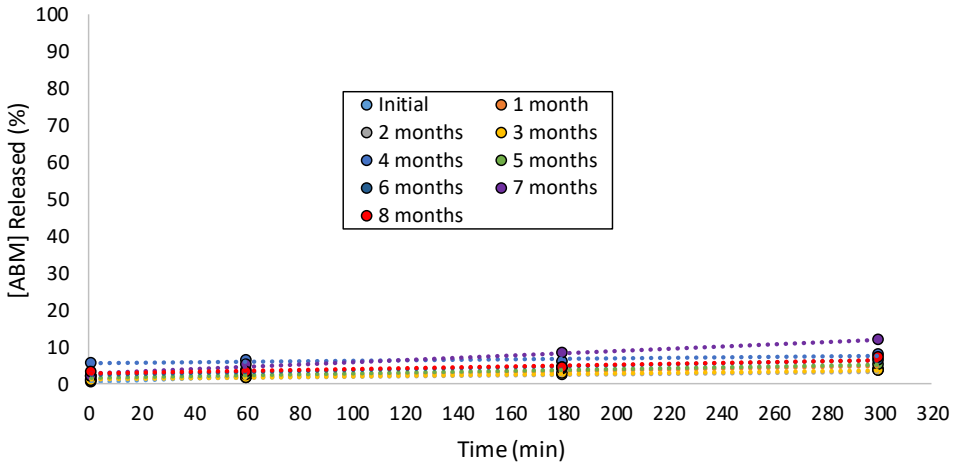

Figure 10.16: Characterisation of the change in [ABM] released into water/ethanol from PDLLA 100 particles after degradation in water for 8 months

10.2.4 PCL 100 Particle Degradation and Release in Water

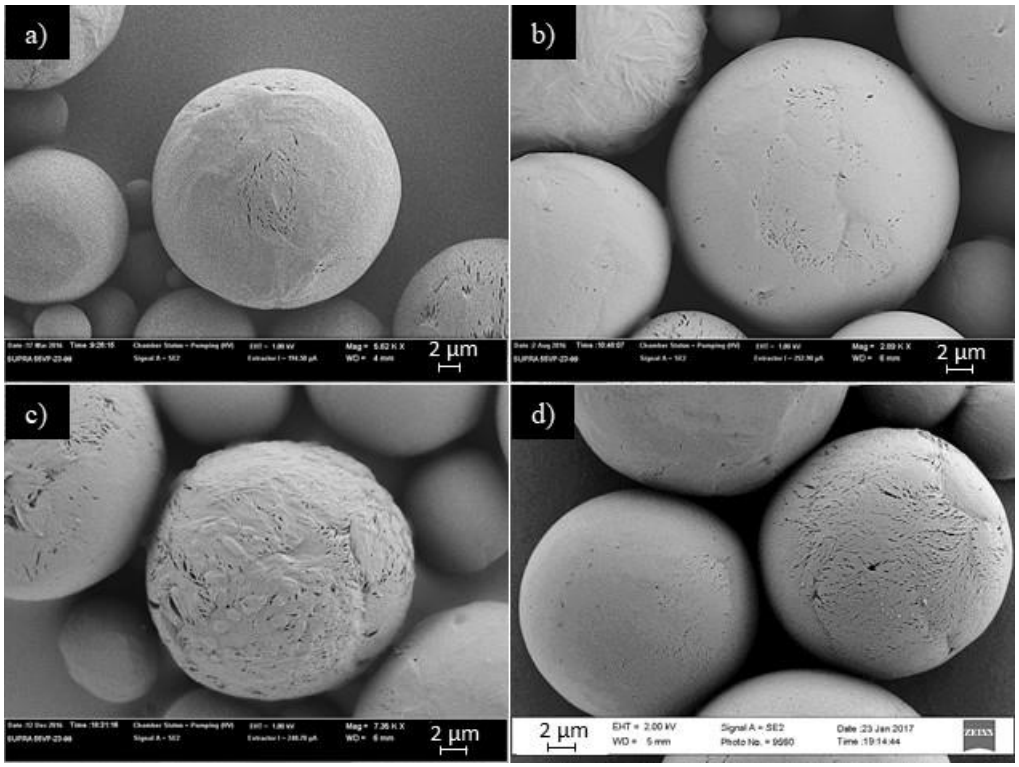

Figure 10.17: SEM characterisation of the change in particle morphology observed with PCL 100 after a) 0 months, b) 3 months, c) 6 months and d) 9 months in water

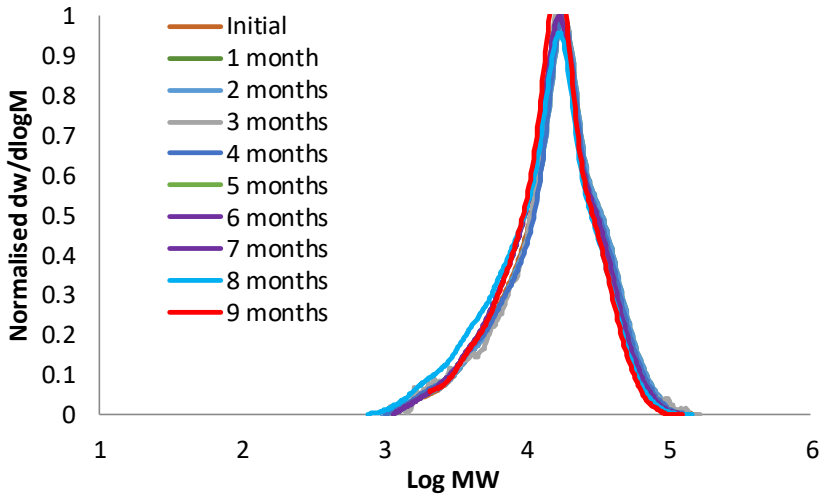

Figure 10.18: SEC characterisation of PCL 100 particles after degradation in water for 9 months

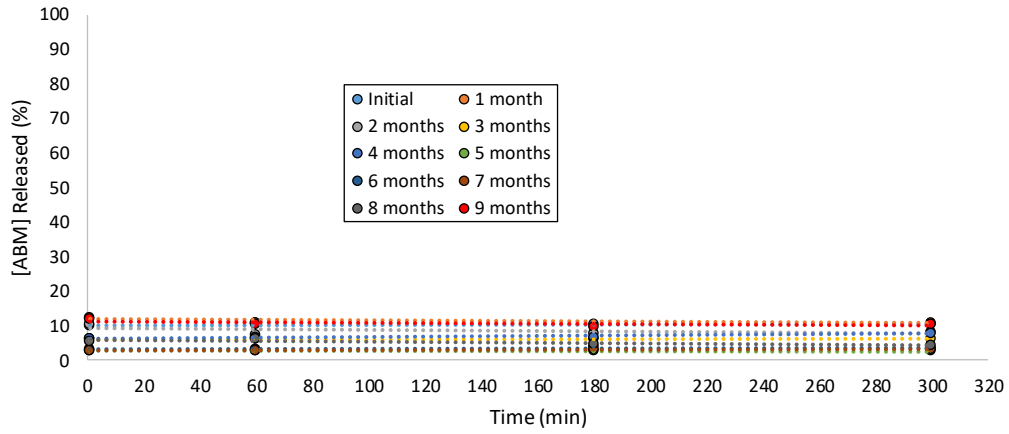

Figure 10.19: Characterisation of the change in [ABM] released into water/ethanol from PCL 100 particles after degradation in water for 9 months